

SINGLET AND TRIPLET EXCITONS IN ORGANIC AND ORGANOMETALLIC THIN
FILMS: DIFFUSION AND TRIPLET SENSITIZATION

By

JARRETT H. VELLA, JR.

A DISSERTATION PRESENTED TO THE GRADUATE SCHOOL
OF THE UNIVERSITY OF FLORIDA IN PARTIAL FULFILLMENT
OF THE REQUIREMENTS FOR THE DEGREE OF
DOCTOR OF PHILOSOPHY

UNIVERSITY OF FLORIDA

2009

© 2009 Jarrett H. Vella, Jr.

To my family and little Dolly

ACKNOWLEDGMENTS

Having spent close to nine years in school, the people who have helped me reach this point in my life are too numerous to mention. It is not possible to adequately thank all those who have helped me achieve my aspirations, but I'll try anyway: thank you.

I would like to foremost thank my parents and grandparents, Jarrett Sr. and Lou Ellen Vella, George and Louise Carpenter, for supporting me personally and financially throughout my undergraduate and graduate careers. Without their unconditional love and support, this accomplishment would not have been reached. To this day, my grandfather will still ask, "carbon still has a valence of four, right?"

I am also indebted to my advisor, Professor Kirk Schanze. He transformed me from a high-strung, slightly stressed first year graduate student to a calm(er), more professional, independently-thinking scientist. Through remarkable patience, he gave me the freedom to make mistakes, learn from them, and to perform experiments that more resemble a specialization in physical chemistry than in organic chemistry. To him I offer my sincere thanks and gratitude.

The members of my research group also deserve a large "thank you." Julia Keller was always a kind voice of support. Dr. Richard Farley was also helpful in many ways, as was Abby Shelton, the cuvette, TA and ordering overlord. Other current and former group members, Dr. Hui Jiang, Dr. Kye-Young Kim, Dr. Xiaoyoung Zhao, Lt. Col. Dr. John Peak (thanks for the desk), Seoung-Ho Lee, Jonathan Sommer, Enkyung Ji and everyone else deserve my greatest thanks.

I would also like to take time to thank my many collaborators. Dr. Jiangeng Xue and Jason Myers in the Department of Materials Science and Engineering were kind enough to vacuum-deposit acceptors onto what seemed to be endless supplies of thin films. Dr. Quentin Bricaud and Dr. John Reynolds were kind enough to allow me to include Quentin's polyfluorene work in

this dissertation. Special thanks go to Quentin for forcing me to finish the LbL project after having worked on it continuously for 3.5 years. In my group, I would like to thank Abby for giving me some of her benzothiazole iridium dimer and Julia for much appreciated help with synthesis. Dr. Ion Ghiviriga also gave many helpful NMR discussions. My committee members, Dr. John Reynolds, Dr. Valeria Kleiman, Dr. William Dolbier, Dr. Jiangeng Xue and Dr. Kirk Schanze, also have my gratitude for listening to me ramble on about thin films for hours at a time.

Lastly, I would like to acknowledge my chemistry department friends and those at the UF Swing Dancing Club, who helped me to discover awesome swing dancing (the Charleston), as well as Frank Sinatra. Mother Nancee and the other “chapelites” at the UF Chapel House (Episcopal) were also great, supportive friends. All of you will be missed.

TABLE OF CONTENTS

	<u>page</u>
ACKNOWLEDGMENTS	4
LIST OF TABLES	9
LIST OF FIGURES	10
ABSTRACT.....	15
CHAPTER	
1 INTRODUCTION	17
Organic Thin Films.....	17
Langmuir-Blodgett Films	17
Layer-by-Layer Self-Assembled Thin Films.....	19
Spin-Coated Thin Films	22
Thermally Evaporated Thin Films.....	23
Conjugated Polymers.....	24
Photophysical Processes of Conjugated Polymers	26
Exciton Diffusion.....	29
This Study	31
2 TRIPLET EXCITON DIFFUSION IN PLATINUM ACETYLIDE THIN FILMS	33
Introduction.....	33
Synthesis and Characterization.....	37
Results.....	42
Concentration-Based Quenching.....	43
Time of Flight Measurements	48
Discussion.....	51
The Concentration-Based Quenching Model	51
Time of Flight Validation	58
Experimental.....	60
Materials	60
Synthesis.....	61
Synthesis.....	62
Thin Film Preparation.....	63
Optical Characterization	64
Film Thickness Measurements	66
Time of Flight Curve Fitting Procedures.....	67
3 SINGLET EXCITON DIFFUSION IN LBL THIN FILMS	69
Introduction.....	69

Synthesis and Characterization.....	73
Results.....	77
LbL Films with Rigid Polyelectrolytes	77
LbL Films Using a Flexible Polyelectrolyte	83
The Source of the Aggregates	86
Time of Flight Measurements	89
Discussion.....	91
Mechanism of Film Deposition	91
Singlet Exciton Diffusion	94
Experimental.....	99
Materials	99
Layer-by-Layer Self Assembly	100
Film and Solution Characterization.....	101
Fluorescence Quenching	101
Film Thickness Calculations	102
Estimating L_D	103
4 TRIPLET SENSITIZATION OF PPESO3	105
Introduction.....	105
Synthesis and Characterization.....	111
Results.....	116
Titration with $\text{Ir}(\text{bt})_2(\text{bpy})\text{Cl}$	117
Titration with $\text{Ir}(\text{ppy})_2(\text{bpy})\text{Cl}$	120
Titration with $\text{Ir}(\text{hqx})_2(\text{bpy})\text{Cl}$	123
Discussion.....	125
Quenching Efficiency	125
Triplet Sensitization.....	130
Application to LbL Films	132
Experimental.....	134
Materials	134
Synthesis.....	134
Optical Titrations.....	136
5 CONCLUSION.....	138
Triplet Exciton Diffusion in Platinum Acetylide Thin Films	138
Singlet Exciton Diffusion in LbL Thin Films.....	139
Triplet Sensitization of PPESO3	141
APPENDIX	
A EXAMPLE CALCULATIONS FROM CHAPTER 2	143
Polymer Density	143
Thin-Film Acceptor Concentration.....	145
Concentration-Based Exciton Diffusion Coefficient.....	146

B	MASS SPECTRA OF CATIONIC IRIIDIUM DYES	148
C	NMR SPECTRA OF CATIONIC IRIIDIUM DYES	158
D	REPRESENTATIVE DECAYS OF pPtPh FILMS	165
	PCBM Blends	165
	C60 Bilayer Films	175
	PtTPP Blends	179
	PtTPP Bilayer Films	186
	LIST OF REFERENCES	192
	BIOGRAPHICAL SKETCH	202

LIST OF TABLES

<u>Table</u>	<u>page</u>
2-1 Summary of polymer characterization data.	41
2-2 Summary of the concentration- and time of flight (TOF)-based triplet exciton diffusion measurements for PCBM and PtTPP.	56
2-3 Singlet and triplet exciton diffusion literature data for spin-coated donor films.	61
3-1 Length of diffusion data obtained from fitting the ITO quenching data.	97
3-2 Singlet exciton diffusion literature data for organic films.	98
4-1 Literature examples of Iridium (III) dyes of the structure (C ^N) ₂ Ir(acac).	109
4-2 Photophysical characteristics of the cationic iridium dyes in methanol.	113
4-3 Summary of the PPESO3 quenching data by (C ^N) ₂ Ir(bpy)Cl dyes in methanol solution.	130

LIST OF FIGURES

<u>Figure</u>	<u>page</u>
1-1 Examples of amphiphilic polymers used for the Langmuir-Blodgett film deposition technique	18
1-2 The deposition process of Langmuir-Blodgett films. A) The down-stroke to form one monolayer. B) The upstroke to form two monolayers (one bilayer).....	19
1-3 Examples of polyelectrolyte structures used to create electrostatic and hydrogen bonded layer-by-layer self assembled thin films. ¹⁸⁻²¹	20
1-4 Schematic depiction of layer-by-layer self assembled thin films..	21
1-5 Schematic examples of conjugated polymers	26
1-6 Jablonski diagram describing the basic photophysical processes	27
2-1 Chemical structures for boron subphthalocyanine and platinum (II) octaethylporphine.....	34
2-2 Schematic description of a time of flight (TOF) experiment.....	36
2-3 The model platinum acetylide polymer, pPtPh, used in this study.	37
2-4 Synthesis of pPtPh using an AA + BB co-polymerization.	38
2-5 Synthesis of pPtPh using an AB asymmetric monomer.	39
2-6 Absorption and emission spectra for the polymers in degassed THF solution.	41
2-7 Chemical structures of the acceptors used for exciton diffusion studies	42
2-8 Example absorption and normalized emission spectra for spin-coated pPtPh films with 0.00 weight percent and 0.15 weight percent PCBM.	43
2-9 Fitted time correlated single photon counting decays for quenched pPtPh/PCBM films	44
2-10 Absorption and normalized emission spectra for pPtPh/PtTPP spin-coated films.	46
2-11 Thin film excitation spectra, monitored at the emission maximum of PtTPP/pPtPh films	46
2-12 Fitted time correlated single photon counting decays for quenched pPtPh/PtTPP films	48
2-13 Fitted time correlated single photon counting decays for pPtPh/C60 TOF experiments...	49

2-14	Fitted time correlated single photon counting decays for pPtPh PtTPP TOF experiments	50
2-15	Stern-Volmer plots for concentration-based pPtPh quenching	54
2-16	Hindered Access plots for concentration-based pPtPh quenching	56
2-17	Fitted TOF lifetime quenching data	59
2-18	Diagram describing the sample chamber configuration used to collect time correlated single photon counting decays	65
2-19	Thickness-absorption relationship for pPtPh films	67
3-1	Structures of the polyelectrolytes used for electrostatic layer-by-layer self assembly.	72
3-2	Synthesis of PPESO3	75
3-3	Absorption and emission spectra for PPESO3	76
3-4	Absorption and emission spectra for glass [PDDA/PPESO3] ₁₋₃₀ LbL films	78
3-5	Absorption and emission spectra for glass [PDDA/PPESO3] ₅₋₃₀ LbL films deposited from methanol	79
3-6	Absorption and emission spectra for quartz [PDDA/PPESO3] ₅₋₃₀ LbL films.	79
3-7	Absorption and emission spectra for glass [PAH/PPESO3] ₅₋₃₀ LbL films.	80
3-8	Absorption and emission spectra for glass [PDDA/PPECO2] ₅₋₃₀ LbL films	81
3-9	Absorption and emission spectra for glass [PPE4+/PPESO3] ₅₋₃₀ LbL films	81
3-10	Absorption and emission spectra for glass [PDDA/PPESO3] ₅₋₃₀ LbL films deposited from freshly synthesized PPESO3:	82
3-11	Tapping mode AFM images of glass [PDDA/PPESO3] ₅₋₃₀ LbL films	84
3-12	Absorption and emission spectra for pFl.	85
3-13	Time dependent absorption and emission spectra for PPESO3 aggregation in water.	87
3-14	Time dependent absorption and emission spectra for PPESO3 aggregation in methanol	88
3-15	Absorption and emission spectra for ITO [PDDA/PPESO3] ₁₋₃₀ LbL films	90
3-16	Maximum absorbance versus number of bilayers for glass [PDDA/pFl] films and glass [PDDA/PPESO3] films	92

3-17	Mechanism for aggregate formation in LbL films built electrostatically from conjugated polyelectrolytes.	93
3-18	Fluorescence quenching versus exciton diffusion distance for ITO [PDDA/PPESO3] LbL films.	96
3-19	Integrated fluorescence intensities versus the number of bilayers for glass [PDDA/PPESO3] films and ITO [PDDA/PPESO3] films.....	102
4-1	Examples of triplet sensitized systems from the literature.	104
4-2	Jablonski diagram describing donor-acceptor triplet sensitization.	106
4-3	Examples of triplet sensitized thin films from the literature.....	108
4-4	The cationic iridium dyes and anionic polymer to be used in this study	110
4-5	The synthesis of the cationic iridium dyes.....	111
4-6	Absorption and emission spectra in methanol for PPESO3 and the iridium dyes	112
4-7	Simplified Jablonski diagram of the photophysical processes involved in triplet-triplet transient absorption	114
4-8	Triplet-triplet transient absorption spectra in methanol.....	115
4-9	Absorption and emission spectra for the titration of a 4.61 μM solution of PPESO3 in methanol by $\text{Ir}(\text{bt})_2(\text{bpy})\text{Cl}$	116
4-10	Absorption and emission spectra for the titration of $\text{Ir}(\text{bt})_2(\text{bpy})\text{Cl}$ in methanol without PPESO3.	117
4-11	Triplet-triplet transient absorption spectra in methanol for 17.4 μM PPESO3. and 4.0 μM $\text{Ir}(\text{bt})_2(\text{bpy})\text{Cl}$ in 17.4 μM PPESO3.	119
4-12	Triplet-triplet transient decay at 734 nm for 17.4 μM PPESO3 in methanol titrated by $\text{Ir}(\text{bt})_2(\text{bpy})\text{Cl}$	120
4-13	Absorption and emission spectra for the titration of a 4.61 μM solution of PPESO3 in methanol by $\text{Ir}(\text{ppy})_2(\text{bpy})\text{Cl}$	121
4-14	Absorption and emission spectra for the titration of $\text{Ir}(\text{ppy})_2(\text{bpy})\text{Cl}$ in methanol without PPESO3.	122
4-15	Triplet-triplet transient decay at 734 nm for 17.4 μM PPESO3 in methanol titrated by $\text{Ir}(\text{ppy})_2(\text{bpy})\text{Cl}$	122

4-16	Absorption and emission spectra for the titration of a 4.61 μM solution of PPESO3 in methanol by $\text{Ir}(\text{hqx})_2(\text{bpy})\text{Cl}$	123
4-17	Absorption and emission spectra for the titration of $\text{Ir}(\text{hqx})_2(\text{bpy})\text{Cl}$ in methanol without PPESO3	124
4-18	Triplet-triplet transient decay at 734 nm for 19.1 μM PPESO3 in methanol titrated by $\text{Ir}(\text{hqx})_2(\text{bpy})\text{Cl}$	125
4-19	Stern-Volmer plots for 4.61 μM PPESO3 titrated in methanol.	128
4-22	Structure of BP-PPE- C_{18}	131
A-1	Chemical structure of the pPtPh repeat unit.	143
B-1	Full APCI-TOF mass spectrum of $\text{Ir}(\text{bt})_2(\text{bpy})^+$	149
B-2	Close-up view of the M^+ peak in the APCI-TOF mass spectrum of $\text{Ir}(\text{bt})_2(\text{bpy})^+$	150
B-3	Theoretical M^+ pattern for $\text{Ir}(\text{bt})_2(\text{bpy})^+$	151
B-4.	Full ESI-TOF mass spectrum of $\text{Ir}(\text{ppy})_2(\text{bpy})^+$	152
B-5	Close-up view of the M^+ peak in the ESI-TOF mass spectrum of $\text{Ir}(\text{ppy})_2(\text{bpy})^+$	153
B-6	Theoretical M^+ pattern for $\text{Ir}(\text{ppy})_2(\text{bpy})^+$	154
B-7	Full ESI-TOF mass spectrum of $\text{Ir}(\text{hqx})_2(\text{bpy})^+$	155
B-8	Close-up view of the M^+ peak in the ESI-TOF mass spectrum of $\text{Ir}(\text{hqx})_2(\text{bpy})^+$	156
B-9	Theoretical M^+ pattern for $\text{Ir}(\text{hqx})_2(\text{bpy})^+$	157
C-1	^1H NMR spectrum for $\text{Ir}(\text{bt})_2(\text{bpy})\text{PF}_6$ in acetonitrile- d_3 and dimethylsulfoxide- d_6	159
C-2	Expansion of the ^1H NMR spectrum for $\text{Ir}(\text{bt})_2(\text{bpy})\text{PF}_6$ in acetonitrile- d_3 and dimethylsulfoxide- d_6	160
C-3	^1H NMR spectrum for $\text{Ir}(\text{ppy})_2(\text{bpy})\text{PF}_6$ in acetonitrile- d_3	161
C-4	Expansion of the ^1H NMR spectrum for $\text{Ir}(\text{ppy})_2(\text{bpy})\text{PF}_6$ in acetonitrile- d_3	162
C-5.	^1H NMR spectrum for $\text{Ir}(\text{hqx})_2(\text{bpy})\text{Cl}$ in dimethylsulfoxide- d_6	163
C-6	Expansion of the ^1H NMR spectrum for $\text{Ir}(\text{hqx})_2(\text{bpy})\text{Cl}$ in dimethylsulfoxide- d_6	164
D-1	TCSPC decay of a pristine pPtPh film (y-axis units in log(counts per second)).	165
D-2	TCSPC decay for a 0.025 wt% (0.351 mM) PCBM/pPtPh film.	166

D-3	TCSPC decay for a 0.050 wt% (0.703 mM) PCBM/pPtPh film.	167
D-4	TCSPC decay for a 0.075 wt% (1.05 mM) PCBM/pPtPh film.	168
D-5	TCSPC decay for a 0.100 wt% (1.41 mM) PCBM/pPtPh film.	169
D-6	TCSPC decay for a 0.125 wt% (1.76 mM) PCBM/pPtPh film.	170
D-7	TCSPC decay for a 0.225 wt% (3.17 mM) PCBM/pPtPh film.	171
D-8	TCSPC decay for a 0.325 wt% (4.58 mM) PCBM/pPtPh film.	172
D-9	TCSPC decay for a 0.425 wt% (5.97 mM) PCBM/pPtPh film.	173
D-10	TCSPC decay for a 0.525 wt% (7.37mM) PCBM/pPtPh film.	174
D-11	TCSPC decay for C60 (40 nm) pPtPh (31.7 nm) bilayer film.....	175
D-12	TCSPC decay for C60 (40 nm) pPtPh (43.2 nm) bilayer film.....	176
D-13	TCSPC decay for C60 (40 nm) pPtPh (48.5 nm) bilayer film.....	177
D-14	TCSPC decay for C60 (40 nm) pPtPh (75.2 nm) bilayer film.....	178
D-15	TCSPC decay for a pristine pPtPh film.	179
D-16	TCSPC decay for a 0.022 wt% (0.351 mM) PtTPP/pPtPh film.	180
D-17	TCSPC decay for a 0.044 wt% (0.703 mM) PtTPP/pPtPh film.	181
D-18	TCSPC decay for a 0.11 wt% (1.76 mM) PtTPP/pPtPh film.	182
D-19	TCSPC decay for a 0.20 wt% (3.17 mM) PtTPP/pPtPh film.	183
D-20	TCSPC decay for a 0.29 wt% (4.58 mM) PtTPP/pPtPh film.	184
D-21	TCSPC decay for a 0.38 wt% (5.97 mM) PtTPP/pPtPh film.	185
D-22	TCSPC decay for PtTPP (40 nm) pPtPh (22.7 nm) bilayer film.	186
D-23	TCSPC decay for PtTPP (40 nm) pPtPh (24.3 nm) bilayer film.	187
D-24	TCSPC decay for PtTPP (40 nm) pPtPh (31.7 nm) bilayer film.	188
D-25	TCSPC decay for PtTPP (40 nm) pPtPh (46.7 nm) bilayer film.	189
D-26	TCSPC decay for PtTPP (40 nm) pPtPh (55.0 nm) bilayer film.	190
D-27	TCSPC decay for PtTPP (40 nm) pPtPh (65.0 nm) bilayer film.	191

Abstract of Dissertation Presented to the Graduate School
of the University of Florida in Partial Fulfillment of the
Requirements for the Degree of Doctor of Philosophy

SINGLET AND TRIPLET EXCITONS IN ORGANIC AND ORGANOMETALLIC THIN
FILMS: DIFFUSION AND TRIPLET SENSITIZATION

Jarrett H. Vella, Jr.

December 2009

Chair: Kirk Schanze

Major: Chemistry

Several organic thin films were constructed from optically active organic and organometallic polymers. Using standard photophysical measurement techniques, studies were performed to determine the ability of polymer-based singlet and triplet excitons to diffuse in organic thin films. This work was performed to provide a better understanding of the ability of polymers to efficiently function in organic-based electronic devices.

To study the ability of triplet excitons to diffuse in thin films, a platinum acetylide polymer was spin-coated with varying amounts of molecularly dissolved fullerene or porphyrin quenchers. A new model of exciton diffusion was derived where the concentration of acceptor molecules is used to calculate the exciton quenching rate constant; this is further related to the exciton diffusion coefficient through Fick's Law of Diffusion. The results were validated against time-of-flight experiments, where the same quenchers were thermally deposited onto variable-thickness, pristine films of spin-coated polymer. The effect of film thickness on exciton population was determined. The one dimensional model of exciton diffusion was applied to the results, enabling the calculation of the triplet exciton length of diffusion and diffusion coefficient. These findings validate the new diffusion model and indicate that polymer-based triplet excitons have substantially improved lengths of diffusion compared to small molecules.

The ability of singlet excitons to diffuse within thin organic films was studied using the electrostatic layer-by-layer self assembly technique. Films incorporating water-soluble conjugated polyelectrolytes were constructed. It was found that upon deposition, the polymers in the film aggregate. A mechanism of film aggregation was developed so that ways of preventing film aggregation could be identified. Films built on a quenching substrate enabled the estimation of the singlet exciton length of diffusion using the one dimensional exciton diffusion model. Because the films were aggregated, a decrease in the ability of singlet excitons to diffuse was found. Methods of improving the length of diffusion and avoiding film aggregation were identified.

Finally, a series of iridium-based triplet sensitizers were developed to sensitize the formation of triplets in layer-by-layer self assembled thin films of conjugated polyelectrolytes. This is one way of improving the exciton length of diffusion in layer-by-layer self assembled thin films. Fluorescence and transient absorption titrations of the polyelectrolyte solutions by the iridium sensitizers confirmed their ability to sensitize polyelectrolyte triplets. Methods of incorporating the sensitizers into layer-by-layer self assembled thin films were proposed.

CHAPTER 1 INTRODUCTION

Organic Thin Films

Generally speaking, an organic thin film can be described as a layer of carbon-based molecules coating an underlying material; accordingly, an organic thin film can range from a polymer spin-coated onto a glass slide to a layer of amphiphilic molecules covering a body of water. The concept of one material covering another is not new. In a letter to a colleague dated November 7, 1773, Benjamin Franklin described how Pliny observed fisherman pouring oil over the sides of their ships to calm the rough waters in which they were sailing.¹ Franklin went on to describe his contemporaries' accounts of pouring oil onto rough bodies of water to smooth them. Being a self described "experimental philosopher," this intrigued Franklin, who went on to perform one of the first film thickness observations:^{1,2}

I fetched out a cruet of oil, and dropt a little of it on the water. I saw it spread itself with surprising swiftness upon the surface...When put on water it spreads instantly many feet round, becoming so thin as to produce the prismatic colours, for a considerable space, and beyond them so much thinner, except in its effect of smoothing the waves at a much greater distance.

Langmuir-Blodgett Films

Had Benjamin Franklin lived another 144 years, he would have been familiar with the Langmuir-Blodgett technique (LB) of organic film deposition, developed by Irving Langmuir and Katharine Blodgett in the early part of the twentieth century.³ Two of the many examples of materials used for the LB technique are given in Figure 1-1.^{3,4} Films deposited using the LB technique are always made of amphiphilic molecules; that is, the molecules consist of a hydrophobic "tail" and a hydrophilic "head." For example, the long alkyl chain of molecule 1-1 in Figure 1-1 is the tail and the carboxylate group is the head. To construct LB films, the amphiphile is dissolved in a volatile, water insoluble solvent such as methylene chloride.

The solution is then poured onto a trough of water and when the solvent evaporates, there is a uniform film one molecule thick coating the subphase (water). Upon evaporation, the amphiphiles are vertically oriented on top of the subphase, with the polar heads extending into the subphase to maximize hydrophilic interactions. The nonpolar tails extend into the air to minimize hydrophobic interactions.^{5,6} The thin films are then deposited as shown in Figure 1-2.⁷

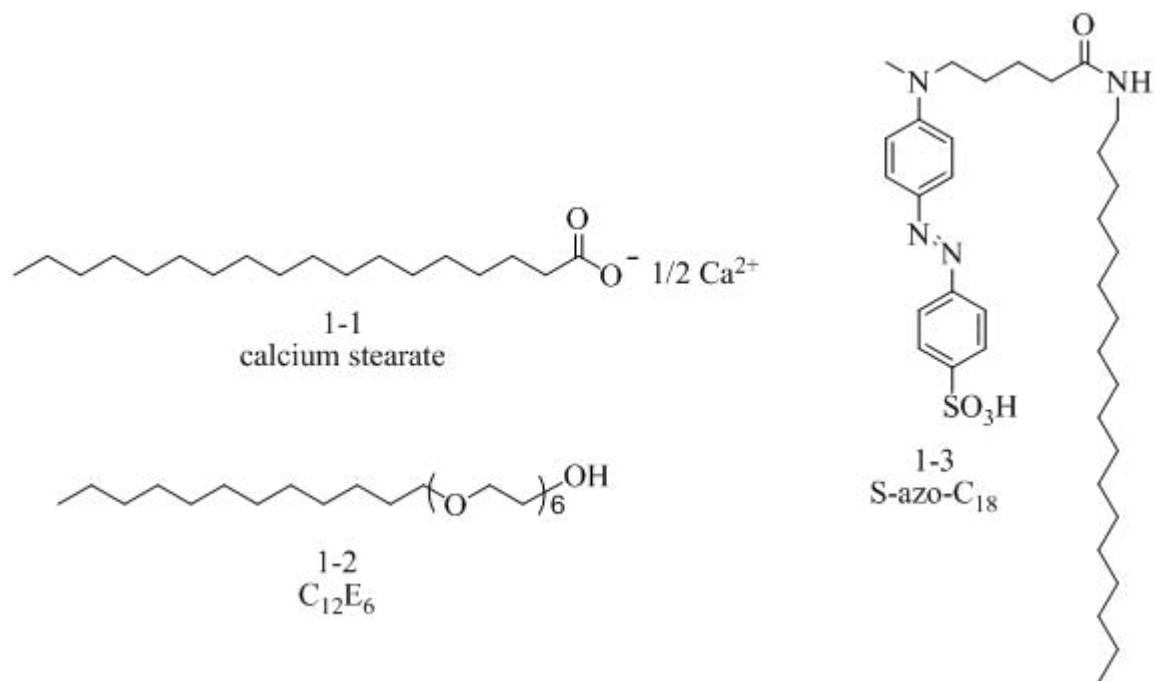


Figure 1-1. Examples of amphiphilic polymers used for the Langmuir-Blodgett film deposition technique.^{3,4}

The deposition process consists of a down-stroke followed by an up-stroke. In the down-stroke, the substrate is completely pushed through the amphiphilic layer and into the subphase. As a result of hydrophobic interactions and the surface tension of the amphiphilic layer, a film one molecule thick is deposited onto the substrate. During the up-stroke, surface tension and hydrophobic interactions deposit a second layer on the previous monolayer in a head-to-head fashion. Repeating this process allows for the control of film thickness.^{5,7} Using this technique, films for organic and organometallic magnets,⁵ light emitting devices,⁸ rectifiers,^{5,9} and for

nonlinear optical applications¹⁰ have been developed. There have also been investigations into the susceptibility of LB films towards nanotemplating.⁶

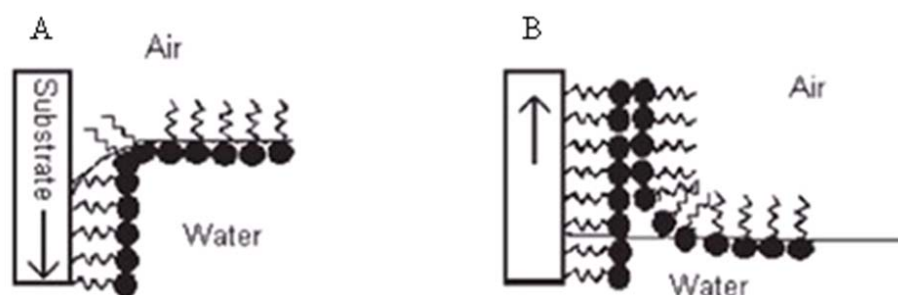



Figure 1-2. The deposition process of Langmuir-Blodgett films. A) The down-stroke to form one monolayer. B) The upstroke to form two monolayers (one bilayer). The amphiphiles are denoted as . Reproduced from McCullough and Regen⁷ with permission of The Royal Society of Chemistry. <http://dx.doi.org/10.1039/b410027c>.

X-ray reflectivity measurements on LB films built using hexaethylene glycol monododecylether (molecule 1-2 in Figure 1-1) have been performed to probe the organization and thickness of LB films.¹¹ In contrast to other types of organic thin films, LB films were found to be extremely organized and homogeneous. Analysis of the x-ray reflectivity data confirmed a bilayer structure to LB films similar to the model given in Figure 1-2; further analysis indicated that the films were less than 1 nm thick with a roughness of 3 Å. Atomic-scale atomic force microscopy (AFM) images provided further proof that LB films exist as highly ordered films, and it was estimated that the average vertical separation between individual molecular assemblies was about 6 Å.

Layer-by-Layer Self-Assembled Thin Films

Similar to Langmuir-Blodgett films are layer-by-layer (LbL) self-assembled thin films. Layer-by-layer self assembled films have been used for the creation of microcapsules,¹² for controlled chemical delivery,¹³ and for electronic applications.^{14,15} Instead of using surface tension and hydrophobic interactions to force insoluble molecules onto a substrate, most LbL films are deposited using aqueous solutions of polyelectrolytes. These materials are capable of

interacting with the substrate, and with each other, *via* electrostatic interactions¹⁶ or hydrogen bonding,¹⁷ among others. For most LbL applications, polyelectrolytes are polymers whose side groups contain ionized or ionizable moieties on each repeat unit. These moieties solubilize the organic component of the polymer in relatively polar solvents such as water. Examples of polyelectrolytes used for LbL films are shown in Figure 1-3.¹⁸⁻²¹ Note that many of the polyelectrolytes in Figure 1-3 that form hydrogen bonded LbL films (molecules 1-5, 1-6 and 1-10) are capable of forming electrostatic LbL films under different pH conditions.

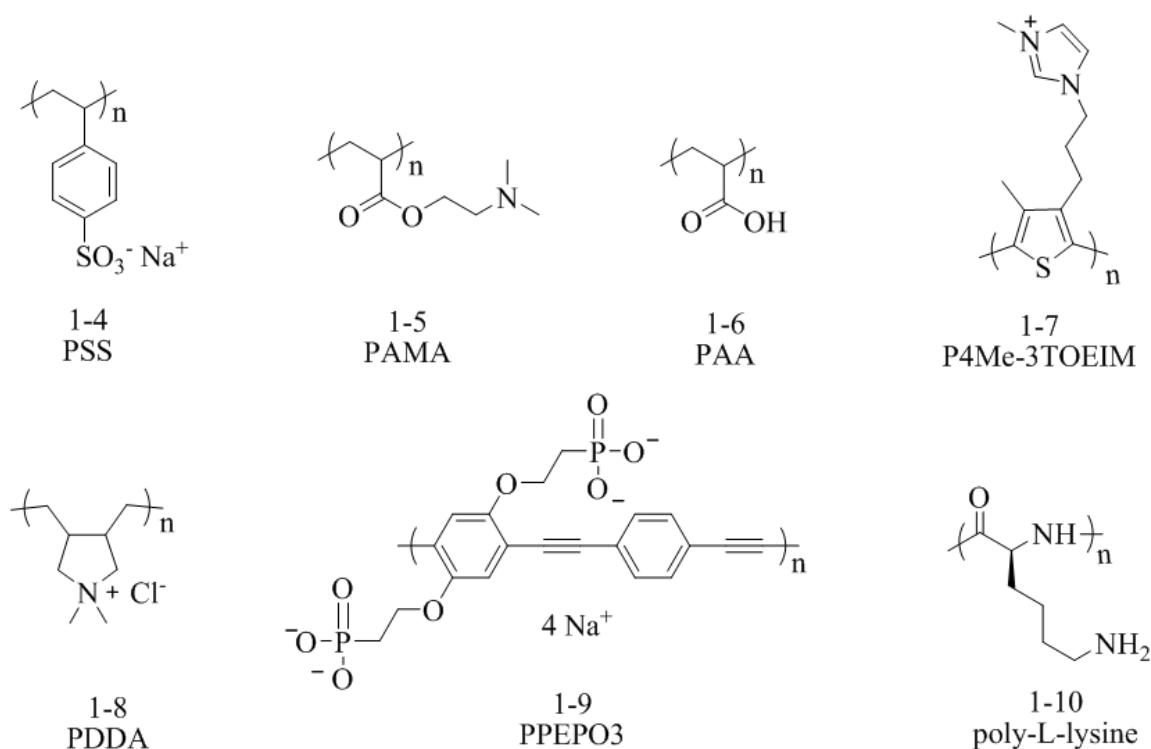


Figure 1-3. Examples of polyelectrolyte structures used to create electrostatic and hydrogen bonded layer-by-layer self assembled thin films.¹⁸⁻²¹

The typical LbL film is produced by alternately immersing a substrate into two different solutions of two different polyelectrolytes, capable of undergoing electrostatic binding or hydrogen bonding. The structure of an ideal electrostatic LbL film is given in Figure 1-4A, although it applies to a hydrogen bonded LbL film as well. Assuming the substrate is negatively

charged, immersion into a cationic polyelectrolyte would result in electrostatic binding with the polymer and the surface of the substrate, forming one layer. When the same substrate is immersed into a solution of anionic polyelectrolyte, the polymer will electrostatically bind to the cationic polymer, creating a second layer. This creates one bilayer that ideally has a lamellar-type structure.

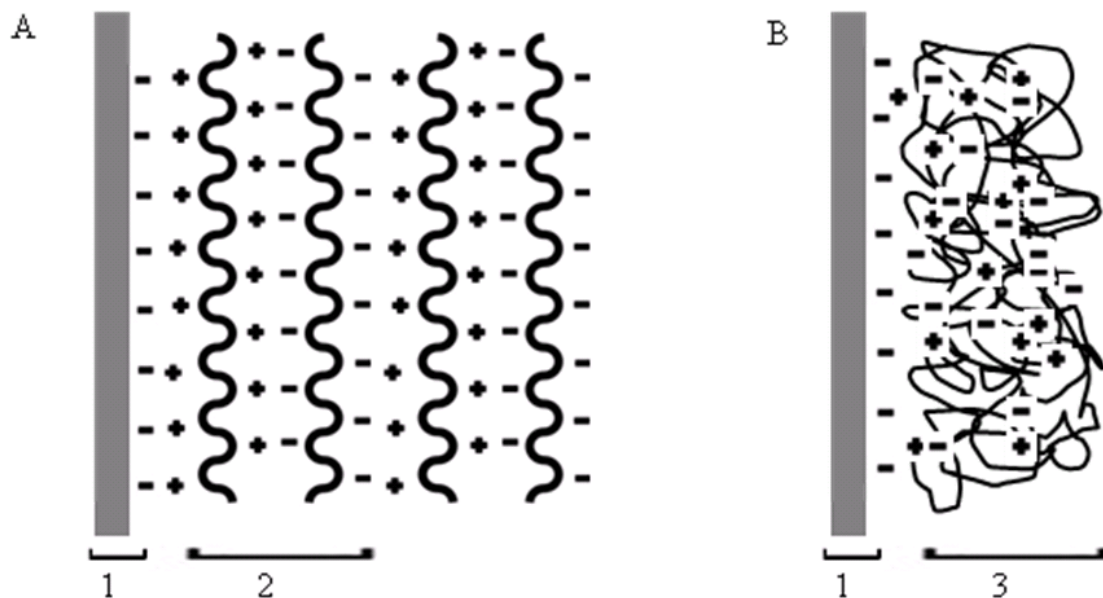


Figure 1-4. Schematic depiction of layer-by-layer self assembled thin films. A) The ideal, lamellar structure. B) The actual, interpenetrated structure. Component one represents the negatively charged substrate, component two describes one layer of polycation and one layer of polyanion (one bilayer) and component three describes a series of interpenetrated bilayers.

Unfortunately, there are a number of solid state interactions that disrupt the ideal structure of LbL films. When the internal structure of electrostatic and hydrogen bonded LbL films was probed using x-ray reflectivity and neutron reflectivity, there was a significant amount of layer intermixing found.²²⁻²⁵ The structure of a real LbL film is shown in Figure 1-4B, where it is not possible to differentiate one layer from another. The lack of a discrete structure in LbL films has been attributed to a number of factors, including the diffusion of polyelectrolytes within the film and layer interpenetration.^{21,24,25} Once deposited, a polyelectrolyte has the ability to diffuse in a

Brownian manner to the interior of the film and back to the outer surface.²¹ Lavallo and coworkers have measured the diffusion coefficient for a fluorescently labeled polypeptide in electrostatic polyelectrolyte LbL films.²¹ Using photobleaching techniques, the diffusion coefficient was estimated to be $0.05\text{--}1.0\ \mu\text{m}^2\text{--s}^{-1}$, which is much slower than the diffusion of polypeptides in high ionic strength solutions ($100\text{--}220\ \mu\text{m}^2\text{--s}^{-1}$).^{21,26} It has also been suggested that layer interpenetration also helps to destroy the lamellar structure of an ideal LbL film. When Sukhishvili studied the interior structure of hydrogen-bonded LbL films using neutron reflectivity, a higher degree of interpenetration was found than for electrostatically assembled films.²⁵ It was suggested that the need for electrostatic charge balance within the film partially hinders, but does not prevent, polyelectrolyte diffusion.

Spin-Coated Thin Films

Using the LbL approach, the thickness of films is governed by a host of conditions including pH, ionic strength, temperature, growth mechanism (hydrogen bonding or electrostatic), and number of substrate immersions, among others.^{19,27-30} By contrast, the thickness of an unannealed^{31,32} spin-coated film is governed by only three factors: solution viscosity, spin speed, and spin time.³³ When an organic thin film is constructed using the spin-coating technique, a concentrated polymer solution is placed on a substrate and rotated for up to a minute at speeds typically greater than 1 000 rotations per minute. The result is a smooth, uniform thin film.³³⁻³⁵ Organic thin films constructed using the spin-coating technique can be composed of small molecules or polymers,³⁶⁻³⁸ and have been used extensively, although not exclusively, for electronic applications.^{8,33,36-39}

The process of spin-coating a thin film has been extensively studied and modeled by several researchers; Budkowski has even authored a detailed study into the effects of casting

solvent and polymer solubility on the molecular organization of spin-coated films.^{35,40}

Regarding the mechanistic aspects of the spin-coating process, a three phase model has been developed.^{33,35} In the first phase, lasting for only a few seconds, as much as 90% of the initial solution volume is thrown off of the substrate. High speed photography of the first two revolutions in a spin-coating cycle indicates that the casting solution forms a series of arms emanating from the center of the casting solution. These arms contain a great portion of the casting volume and represent the first fraction of the solution to be thrown off of the substrate when rotation begins.³³ Through the next few seconds, the bulk of the film begins to form as the substrate rotates and the remaining solvent evaporates.³⁵

At the beginning of the second phase, the film is relatively thick, mainly owing to a rapid loss of solvent. This stage of film growth is characterized as interplay between centrifugal force and film viscosity. When stage two begins, the cast material is assumed to behave as a fluid where individual solute molecules of the cast material are able to slide past each other, driven by centrifugal force. Solute molecules behaving in this way are able to spread more evenly around the substrate, decreasing the film thickness. As the solvent continues to evaporate, the viscosity rises and begins to hinder spread the spread of solute molecules. In the third and final stage, the remaining solvent evaporates. While this occurs, the material is able spread just enough to minimize film thickness gradients. Ultimately, around 10% of the initial solvent volume is left in the film and must be removed during a separate drying sequence.³⁵

Thermally Evaporated Thin Films

In contrast to all of the thin film deposition techniques discussed so far, thermally evaporated thin films are unique; they are built without the use of solvents, consist mainly of either small molecules or metals, and are used for optical and electronic applications.⁴¹⁻⁴⁶ To construct organic thin films using thermal evaporation, the material is heated in a high vacuum

(10^{-6} Torr or lower) until sublimation occurs. The vaporized material diffuses vertically to a substrate positioned over the sublimation site. On this substrate, the vaporized molecules are allowed to deposit; during the process, a quartz crystal monitor measures the film's thickness and deposition rate.^{44,47,48}

Owing to its conductivity and ability to form ordered films, pentacene has been seen as a model deposition material; consequently, extensive studies, often involving x-ray reflectivity and x-ray diffraction, have been carried out using pentacene to study the growth and structure of thermally deposited organic films.⁴⁷⁻⁵⁶ There are three topologies/film structures that have been identified for thermally evaporated thin films: island (Volmer-Weber), layer-by-layer (Frank-van der Merwe), and layer plus island (Stranski-Krastanov), with layer plus island being preferred by organic films.^{47,49} Although there are a host of factors that differentiate the growth of organic from that of inorganic films,^{47,48} it is generally accepted that interactions between sample molecules with the substrate and with each other, as well as the deposition rate, temperature, and solid-state diffusion, govern the final structure of the deposited film.^{47-49,53-55}

Conjugated Polymers

With the current interest in conducting polymers and plastic technology, the synthesis and use of polymers has been thought of by many to be a twentieth century phenomenon; however, the first synthetic plastic was actually synthesized between 1862 and 1866 by Parkes and Hyatt. Their product, celluloid, is still in use today at movie theatres. Almost ten years later, Baumann decided to investigate the effects of sunlight on a substance identified in 1835 as vinyl chloride, but the actual mechanism for the formation of poly(vinyl chloride) was not discovered until 1916, by Klatte. Many other types of polymers soon followed, such as polyethylene (1933), poly(methyl methacrylate) (1933), nylon-6,6 (Carothers, 1935), poly(tetrafluoroethylene) (1938), polypropylene and polyethylene (Ziegler-Natta catalysis, 1953).⁵⁷

Until the mid-1970s, polymers had non-conjugated backbones; that is, the repeat units consisted mostly of single bonds. When π -bonds were present, there existed no long-range conjugation of the repeat units. This changed when Shirakawa, MacDiarmid, and Heeger developed polyacetylene (molecule 1-11, Figure 1-5). When exposed to halogen vapor, a remarkable increase in the room temperature conductivity was observed, making this the first electrically conducting polymer. Since then, the entire field of conducting polymers has blossomed.⁵⁷⁻⁵⁹

Generally speaking, most electrically conducting polymers belong to the larger class of conjugated polymers (CPs). In conjugated polymers, the π -cloud of one monomer is in conjugation with all other repeat units around it. This extended conjugation lowers the energy necessary to promote an electron from the highest occupied molecular orbital (HOMO) to the lowest unoccupied molecular orbital (LUMO) of the conjugated units. Absorption and emission of photons is thus able to occur in the near-ultraviolet (near-UV) through the near-infrared (near-IR) regions, about 300 nm-1000 nm. This range includes the visible spectrum of light, enabling conjugated polymers to be used for organic light-emitting devices and polymer-based solar cells, among other uses.⁶⁰⁻⁶³

Examples of conjugated polymers are shown in Figure 1-5.^{59,60,64-66} There are three main types of conjugated polymer backbones: those with single bonds, poly(arylene)s (PAs), those with double bonds, poly(arylene vinylene)s (PAVs), and those with triple bonds, poly(arylene ethynylene)s (PAEs). There is a plethora of different ring systems that have been used in CPs, such as benzene (Ph), pyridine (Py), thiophene (Th), fluorene (Fl), quinoline (Qn) and carbazole (Cbz). The solubility of conjugated polymers has been problematic from the beginning. Shirakawa, Heeger, and MacDiarmid quickly learned that polyacetylene is intractably insoluble

in just about every known solvent;^{58,59} as a result, CPs often contain long alkyl side groups extending from the backbone to solubilize the polymer in typical organic solvents.^{60,61,64,65,67} Interestingly, there are a few examples of ionic side groups, such as sulfonates, phosphonates, and various ammonium salts, that have been incorporated into the repeat units of conjugated polymers to render them soluble in solvents such as water and methanol.⁶⁸⁻⁷¹

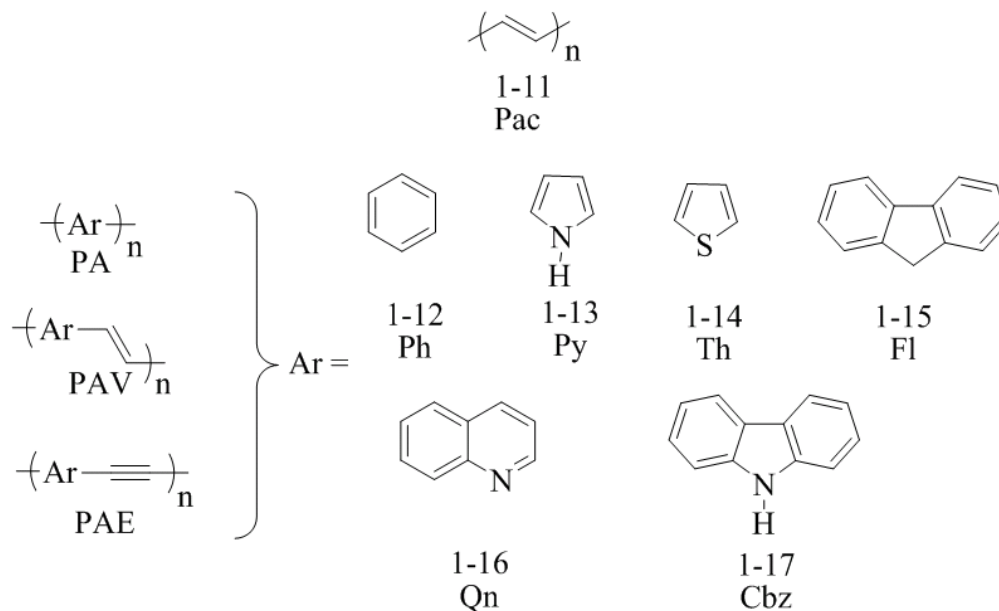


Figure 1-5. Schematic examples of conjugated polymers. The meanings of the abbreviations are given in the text.^{59,60,64-66}

Photophysical Processes of Conjugated Polymers

As previously mentioned, conjugated polymers are able to interact with light from the near-UV region through the near-IR region because of the extended π -cloud of the repeat units. But what happens to the conjugated polymer when it interacts with light? When an incident photon ($h\nu$) interacts with the polymer, there is a possibility that the photon will be absorbed by the material; however, this will only happen if Stark-Einstein law is followed. This law states that a photon will only be absorbed if its energy is equal to the amount of energy needed to promote a ground state electron to a higher energy level. The material will remain in a

photoexcited state for a length of time, τ , until the excess energy is lost. A molecule interacting with light in such a way is termed a *chromophore*.⁶³

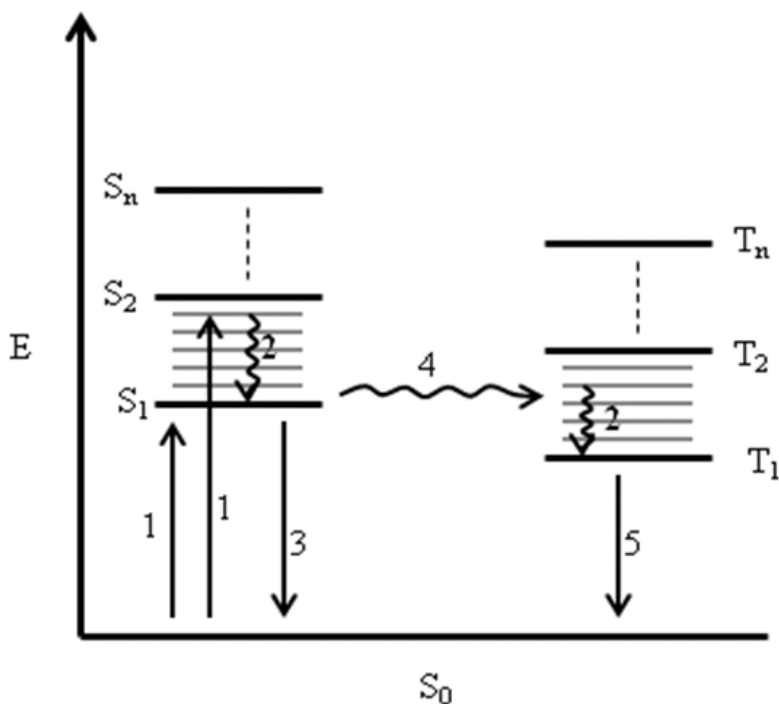


Figure 1-6. Jablonski diagram describing the basic photophysical processes: one, absorption; two, internal conversion; three, singlet decay; four, intersystem crossing; five, triplet decay. E represents system energy and S_0 represents the electronic ground state; S_{1-n} and T_{1-n} describe the singlet and triplet manifolds, respectively.

The intermolecular processes associated with the absorption of a photon by a chromophore are graphically illustrated in Figure 1-6.^{63,72} Initially in the electronic ground state, S_0 , the molecule absorbs a photon of appropriate energy, promoting the molecule to the first excited singlet state, S_1 (process 1). The process of absorption is very fast, with rates typically in the range of 10^{14} - 10^{16} s⁻¹. Depending on the photon's energy, the molecule can be excited to one of several vibrational levels within the S_1 state. When this occurs, the excess vibrational energy is lost as heat to the surroundings during internal conversion to the lowest vibrational energy level of S_1 (process 2). Chromophores also have higher energy singlet states, S_2 - S_n , that each contain their own set of distinct vibrational levels. These higher excited states are not accessible using

routine photoexcitation sources, and methods of attaining these energy levels are discussed in Chapter 4.^{63,72}

In the absence of external forces, there are a few fates awaiting the photoexcited molecule: decay to S_0 or intersystem crossing to the first excited triplet state, T_1 . Decay to S_0 can happen radiatively by fluorescence (process 3 in Figure 1-6), or nonradiatively by internal conversion. When fluorescence occurs, the photoexcited molecule returns to its original energy level; in the process, a photon of different energy than the one absorbed is emitted at rates of 10^8 - 10^{11} s⁻¹. The emitted photon will always have a lower energy than the absorbed photon because of vibrational relaxations that occur after the photoexcitation step (process 1). This energy difference is referred to as the *Stokes shift*. In addition to fluorescence, the singlet state can also decay nonradiatively, usually with rates of 10^{10} - 10^{11} s⁻¹. In this pathway, the energy of S_1 is lost solely through heat loss to the molecule's surroundings. The third fate of the singlet state is intersystem crossing (process 4). During intersystem crossing, the spin of the photoexcited electron "flips," adopting the same spin as the ground state electron that was not excited. This process happens relatively slowly, at rates of 10^6 - 10^8 s⁻¹ because this is a quantum mechanically forbidden process. For most organic molecules undergoing intersystem crossing, only the spin of the electron changes, without a corresponding change in orbital angular momentum. Momentum is thus not conserved, making this a forbidden process. One way around this problem is to incorporate heavy metals, such as platinum (Pt)⁷³ and iridium (Ir)⁷⁴ into the chromophore. Heavy metals facilitate spin-orbit coupling; that is, the spin and orbit momenta are quantum mechanically related, so a change in one induces a change in the other. In this way, intersystem crossing rates can be accelerated to $\geq 10^9$ s⁻¹.^{63,72}

Photoexcited molecules that have undergone intersystem crossing are termed *triplets*. As with singlets, triplets also undergo internal conversion (process 2) to the lowest vibrational state of the lowest energy triplet state, T_1 . As with the singlet states, there are higher triplet states (T_2 - T_n) available, but these are not populated using routine photoexcitation sources. The T_1 state can relax radiatively or nonradiatively. Radiative relaxation from the triplet state to S_0 is termed *phosphorescence* and has the lowest of all the photoexcited rates, 10 - 10^6 s⁻¹, because intersystem crossing must again occur so as not to violate the Exclusion Principle.^{63,72}

Exciton Diffusion

One application for conjugated polymers previously discussed involves using them as photo-active materials for thin films. In addition to undergoing all of the photophysical processes just described, photoexcited CPs in thin films are routinely involved in exciton diffusion, which is a process critical to the operation of organic electronic devices. When a conjugated polymer becomes photoexcited, the excitation energy can be delocalized over several repeat units of the polymer. A delocalized quantum of excitation energy in a conjugated polymer has been referred to as an *exciton*. Excitons are able to migrate not only within one polymer chain, but can migrate, or diffuse, over relatively long distances when CPs are used to make thin films. There are two general mechanisms by which excitons can diffuse in thin films: through Förster transfer or Dexter exchange.

Singlet excitons tend to diffuse within thin films *via* Förster transfer, mathematically described in Equation 1-1, where the rate of energy transfer between molecules, k_{ET} , is proportional to the electronic coupling, V , and inversely proportional to the sixth power of the distance between the two molecules, R_{DA} . The transition dipole moments of the donor (D) and acceptor (A) are denoted as μ_D and μ_A , respectively.

$$k_{ET} \propto V^2 = \frac{\mu_D^2 \mu_A^2}{R_{DA}^6} \quad (1-1)$$

When one polymer becomes photoexcited the orbital motions of the π -electrons change, causing a slight change in the distributions of electric charges within the molecule. This creates a temporary electric dipole in the photoexcited molecule. If two molecules are close enough, the temporary electric dipole of the photoexcited molecule can induce a dipole of equal magnitude in a second, ground state molecule. When the originally excited electron begins to relax, its energy can be transferred *via* this dipole-dipole interaction to the second, ground state molecule. This process results in the originally photoexcited molecule returning to the ground state without radiative relaxation, while the second molecule becomes excited without absorbing a photon; the originally photoexcited molecule is thus called the donor, while the second molecule is the acceptor. When Förster transfer occurs in a CP film, this mechanism allows the singlet excitation energy of a polymer to be transferred from one chain to another, a process known as *singlet exciton diffusion*.^{63,72}

The diffusion of triplet excitons within thin films mainly occurs by Dexter exchange, an intramolecular interchange of a donor's excited electron with an acceptor's ground-state electron. The very nature of the triplet prevents a Förster-type transfer mechanism from occurring. Triplets are formed when a photoexcited system undergoes intersystem crossing from a singlet. As depicted in Figure 1-6, this lowers the energy of the excited state while creating two electrons with the same spin. Furthermore, the formation of triplets in most organic molecules is a forbidden process, owing to nature's requirement of conserving electron momentum. The transfer of triplet energy between two molecules by a Förster-type mechanism would require that one, the donor triplet would have to sensitize the acceptor singlet (an energetically forbidden

process); and that two, the acceptor singlet would have to undergo intersystem crossing to the triplet (another forbidden process). These requirements rule out Förster transfer.

Dexter exchange is mathematically described as Equation 1-2. The rate of triplet exciton transfer is thus related to K, describing orbital interactions, the spectral overlap integral J, normalized to the excitation efficiency for the acceptor, an exponential dependence on the donor-acceptor distance, R_{DA} , and the sum of their Van der Waals radii, L.

$$k = KJ \exp\left(\frac{-2R_{DA}}{L}\right) \quad (1-2)$$

For small molecules, the exponential dependence on the donor-acceptor separation distance severely limits the effective range of Dexter transfer to about 5-10 Å, as compared to the average maximum distance of Förster transfer, about 100 Å. When *triplet exciton diffusion* occurs in a polymer film by Dexter exchange, the excitation energy is transferred *via* an electron hopping mechanism, where the excited electron of the donor is transferred to the LUMO of the acceptor, while an electron of opposite spin is transferred from the HOMO of the acceptor to the HOMO (with respect to the ground state) of the donor. As a result, the originally photoexcited molecule is in its ground state, while a previously ground state molecule is in a photoexcited state; all of this occurred without the absorption and re-emission of a photon.^{63,72}

This Study

The goal of this research is to examine singlet and triplet exciton diffusion in organic thin films made using an electrostatic layer-by-layer approach and using spin-coated films. Singlet exciton diffusion will be studied in LbL films using a poly(phenylene ethynylene) derivative, while a platinum acetylide polymer will be used to construct spin-coated films to study triplet exciton diffusion.

Chapter 2 contains a study of triplet exciton diffusion using spin-coated films of a platinum acetylide polymer. A new, simple approach to calculating the exciton diffusion coefficient will be presented that does not require the use of expensive film preparation equipment or the need for sophisticated mathematical modeling. These results will be validated against measurements made using traditional exciton time-of-flight techniques.

Chapter 3 describes the formation of LbL films using a series of water soluble polymers: the polyanions will be primarily poly(phenylene ethynylene) derivatives, while polycations will typically be of aliphatic nature. As mentioned earlier, LbL films can show a significant amount of polyelectrolyte aggregation, so attempts will be made to develop a mechanism by which CPE LbL films aggregate. The effects of film aggregation on the singlet exciton length of diffusion will then be studied using time-of-flight techniques.

Chapter 4 details the development of triplet sensitizers for use in electrostatic LbL films. A series of cationic iridium dyes will be synthesized. Using solution based optical techniques, the ability of the iridium dyes to sensitize anionic CPE triplets will be measured, and methods of incorporating the iridium dyes into electrostatic LbL films will be discussed within the context of triplet exciton diffusion in LbL films of CPEs. Chapter 5 will present a summary and prospectus on the described research.

CHAPTER 2

TRIPLET EXCITON DIFFUSION IN PLATINUM ACETYLIDE THIN FILMS

Introduction

An understanding of how excitons diffuse in thin polymer films is critical when designing organic electronic devices, such as organic photovoltaic cells (OPVs). In OPVs, sunlight excites a conjugated polymer, creating an exciton that diffuses throughout the device until it is ultimately converted into electricity. Because the triplet excited state of any molecule has a slower rate of decay (10^{-10} s⁻¹) as compared to the singlet state (10^8 - 10^{11} s⁻¹),⁶³ an OPV using triplet excitons should have a higher efficiency than one using singlets.⁷⁵

One potential drawback to using triplet materials for electronic devices is the mechanism of exciton diffusion. Singlet excitons diffuse *via* Förster transfer, which is a through-space transfer of excitation energy from an excited molecule (the donor) to a ground-state molecule (the acceptor); as such, Förster transfer is typically active over a relatively long distance (as much as 100 Å for small molecules). Although singlet excitons are short lived, the long distance over which their diffusion mechanism is active greatly enhances their diffusion coefficients. On the other hand, triplet excitons diffuse through Dexter exchange, a concerted transfer of an excited electron from the donor with a ground-state electron in the acceptor. Because a physical exchange of electrons occurs in triplet exciton diffusion, the distance over which this occurs is much smaller (a maximum of 10 Å for small molecules).^{63,72} Such a small interaction distance limits the overall distance an exciton can diffuse before it decays, greatly decreasing the diffusion coefficient. For example, boron subphthalocyanine (SubPc, molecule 2-1 in Figure 2-1) has a singlet exciton diffusion coefficient of 6.4×10^{-4} cm²-s⁻¹, while platinum octaethylporphine (PtOEP, molecule 2-2 in Figure 2-1) has a triplet exciton diffusion coefficient of 4.1×10^{-6} cm²-s⁻¹.⁷⁶ These are typical values of singlet- and triplet-exciton diffusion

coefficients. In non-crystalline systems,⁷⁷⁻⁷⁹ singlet exciton diffusion coefficients typically fall between 10^{-3} - 10^{-5} $\text{cm}^2\text{-s}^{-1}$, while triplet exciton diffusion coefficients are usually in the range of 10^{-8} - 10^{-11} $\text{cm}^2\text{-s}^{-1}$.^{76,80-87} Disparities in the diffusion coefficients for singlet and triplet excitons are mainly due to their different diffusion mechanisms.

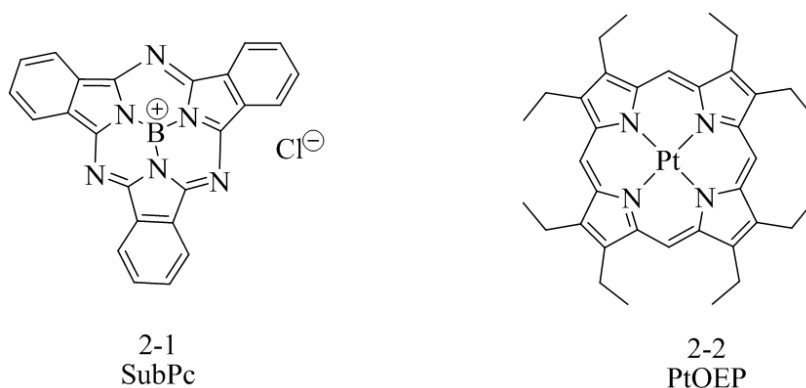


Figure 2-1. Chemical structures for boron subphthalocyanine and platinum (II) octaethylporphine.

A number of techniques to estimate exciton diffusion coefficients have been developed that employ transient decays,⁸⁰ photocurrent measurements,^{81,82} Monte Carlo simulations,⁸⁷ and time-of-flight experiments.⁸⁵ Yamamoto⁸⁰ used transient decays to observe triplet-triplet exciton annihilation in films containing benzophenone. A normal optical absorption spectrum measures absorbance as a function of wavelength, but a transient decay measures a molecule's excited state absorbance at one wavelength as a function of time. Since only one wavelength is monitored, the absorbance relates to the exciton population at any given time. Using this method, the triplet population (optical absorbance) of a system can be observed at any point in time. Yamamoto thus developed a rate expression relating the natural decay, the radius of exciton annihilation and the exciton diffusion coefficient to the concentration of benzophenone triplets. This expression and the measured decay were then used in a curve fitting procedure to obtain the diffusion coefficient.⁸⁰

Black⁸¹ and Wang⁸² both used photocurrent measurements to determine the exciton diffusion coefficients of a europium dye and an aluminum complex, respectively. In these experiments, OPVs were created by placing a film of either material between an electron donating electrode and an electron accepting electrode. When polychromatic light illuminates the film, excitons diffuse to the accepting electrode and inject an electron into the external circuit, creating an electrical current. The wavelength of the illumination source can then be varied to observe how the photocurrent is affected. The current is then be related to the thickness of the film and the light intensity to obtain the exciton diffusion coefficient.^{81,82}

Siebbeles⁸⁷ used Monte Carlo simulations (which are curiously named after the gambling mecca in Monoco) to simulate the diffusion of excitons in films constructed using a palladium porphyrin similar in structure to PtOEP (molecule 2-2, figure 2-1). Essentially, the photocurrent of the porphyrin film built on an electron accepting electrode was measured, and the data simulated using a Monte Carlo method where the excitons are assumed to randomly diffuse to the electrode; the exciton diffusion coefficient was included as one of the variables in the simulation.⁸⁷

One of the more popular methods of determining exciton diffusion coefficients is the time-of-flight (TOF) method, exemplified by Theander.⁸⁵ In this experiment, Theander constructed a layered film similar to Figure 2-2. On the substrate (C), a poly(thiophene) derivative, similar in structure to molecule 1-14 in Figure 1-5, was spin-coated to act as the donor (B). A layer of an electron accepting quencher (A) was then thermally deposited on top of the donor. When light illuminates the donor layer (B), the exciton is created and diffuses through the film by a “random walk” pathway, eventually reaching the exciton accepting (quenching) layer (A). If the thickness of the donor film, l , is too large, the exciton will relax before it is quenched; because the exciton

lifetime competes with the time necessary for exciton diffusion to occur, these measurements are termed “time-of-flight” experiments. The diffusion coefficient is then calculated using a mathematical model comparing the emission intensity of the unquenched donor film to that of the layered film.⁸⁵

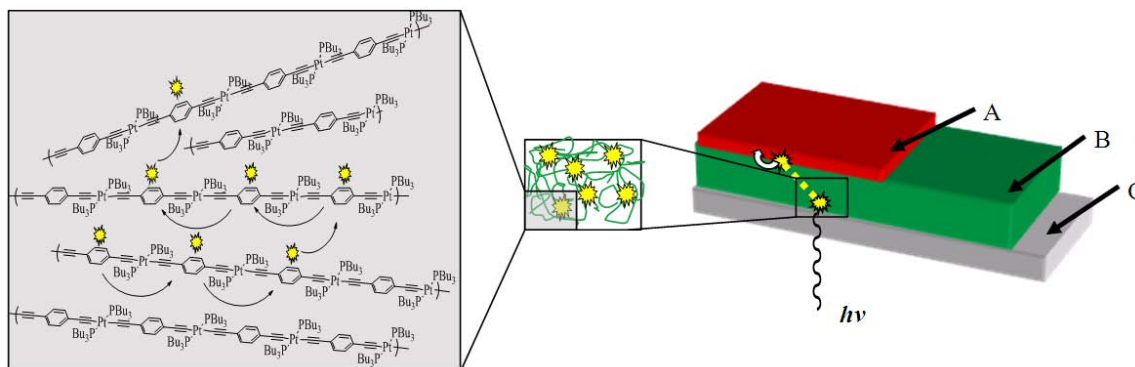


Figure 2-2. Schematic description of a time of flight (TOF) experiment. A) The vacuum-deposited acceptor layer. B) The spin-coated donor layer, consisting of pPtPh in this example. C) The substrate. $h\nu$ Represents the excitation light, - - - and represent exciton diffusion, \curvearrowright represents exciton quenching, and \star indicates an exciton.

While these studies are surely interesting to perform, most methods of calculating exciton diffusion coefficients have two major drawbacks: expensive, specialized equipment is often used, and sophisticated mathematical modeling is performed on the acquired data. For example, obtaining a transient decay spectrum requires an entire dedicated laboratory filled with lasers and other optical devices, while the measurement of photocurrents requires expensive electronic testing instrumentation. After the data is collected, differential equations or rate law derivations are necessary to arrive at an expression relating the exciton diffusion coefficient to some measurable parameter. Specialized computer routines could have to be written to employ a diffusion model. Clearly, a method to estimate exciton diffusion coefficients that is simple and uses basic instrumentation common to most conjugated polymer laboratories is needed.

The purpose of this study is to develop a simple, user-friendly method of estimating parameters related to exciton diffusion. A model platinum acetylide polymer, pPtPh, Figure 2-3, was synthesized to study its triplet diffusion coefficient. Incorporation of a platinum atom into the polymer repeat unit would increase the rate of singlet-triplet intersystem crossing. A simple mathematical model was developed to measure the triplet exciton diffusion coefficient of the platinum acetylide. In this model, a series of spin-coated films with differing amounts of added quencher are created. The relationship of exciton quenching to quencher concentration is examined, and standard, literature-based quenching models are used to analyze the results and calculate the diffusion coefficient. As a means of validating the model, two unrelated quenchers are used in two different experiments, and the results validated against the diffusion coefficients measured using literature-based time-of-flight techniques.

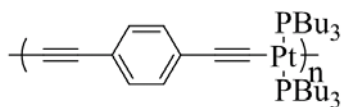


Figure 2-3. The model platinum acetylide polymer, pPtPh, used in this study.

Synthesis and Characterization

The platinum acetylide polymer, pPtPh, used in this study is not new to the literature. However, it was found during the course of investigation that the synthetic method used can greatly affect the defects present in the polymer backbone; therefore, the synthesis of pPtPh by two different methods will be discussed. In the first strategy, two symmetric monomers were reacted in an AA + BB co-polymerization to make pPtPh. In the second strategy, an asymmetric AB monomer was self-polymerized.^{75,88-90}

The first strategy is outlined in Figure 2-4 and uses two symmetric monomers in the polymerization. A Sonogashira reaction coupled 1,4-diiodobenzene **2-3** with (trimethylsilyl)acetylene **2-4** to produce trimethylsilyl-protected (TMS) 1,4-diethynylbenzene **2-**

5. Even though only two equivalents of TMS-acetylene **2-4** were stoichiometrically needed, the volatility of TMS-acetylene necessitated the use of four equivalents. After stirring overnight at room temperature, **2-5** was afforded in a 60% yield. In a separate step before polymerization, **2-5** was deprotected with tetrabutylammonium fluoride (TBAF) for twenty minutes at room temperature, giving diethynylbenzene, **2-9**, in a 75% yield. The second monomer, *trans*-bis(tributylphosphino)platinum (II) chloride, **2-8**, was synthesized by a ligand exchange between platinate **2-6** and two equivalents of tributylphosphine, **2-7**. Under Hagihara conditions, **2-8** reacted with **2-9** overnight in argon outgassed diisopropylamine (DIPAM) and dichloromethane (DCM). Polymer **2-10** was thus obtained in 33% yield (with respect to the repeat unit).

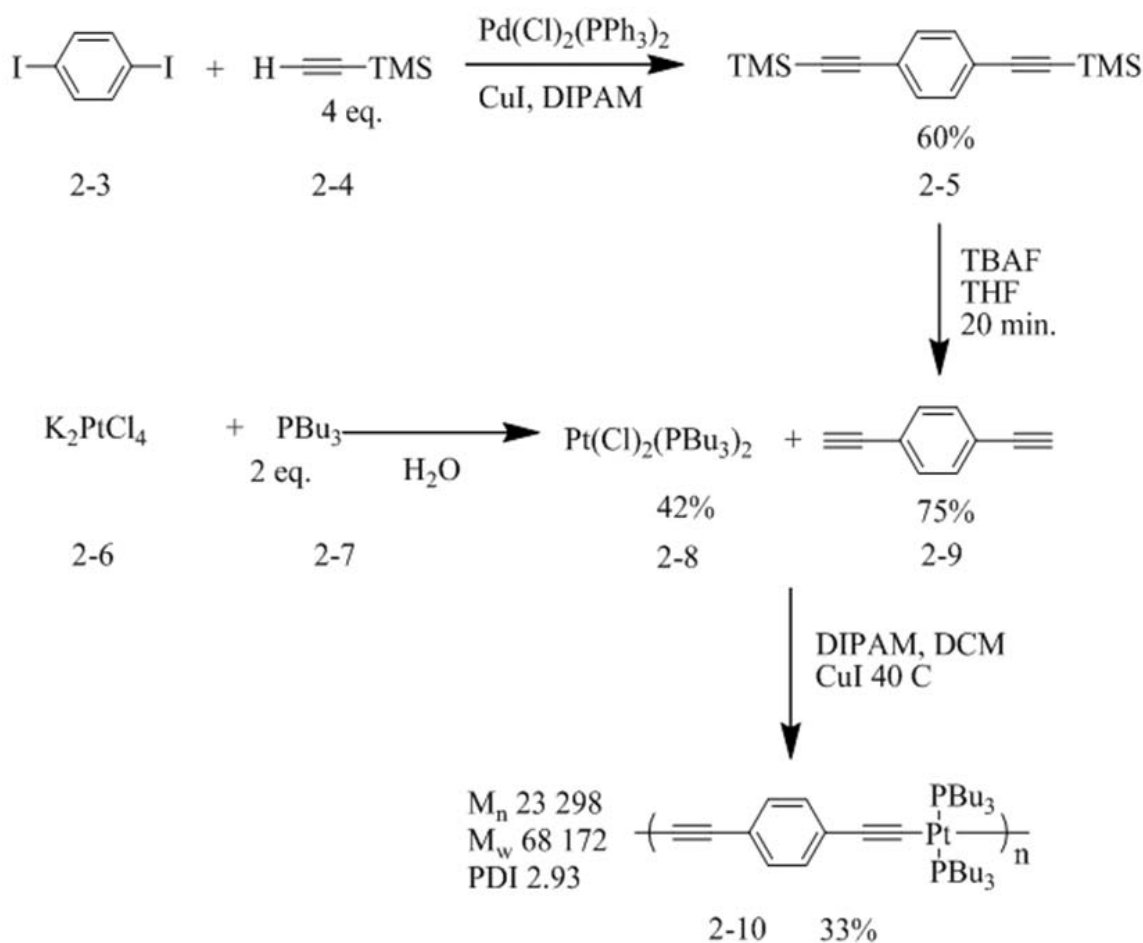


Figure 2-4. Synthesis of pPtPh using an AA + BB co-polymerization. The polymer was prepared from adaptations of the literature procedures.^{88,90}

A second strategy for synthesizing pPtPh is given in Figure 2-5. To begin, diiodobenzene, **2-3**, was subjected to a one pot Sonogashira coupling between propargyl alcohol **2-12** and (triisopropylsilyl)acetylene (TIPS-acetylene), **2-13**, giving asymmetrically protected diethynylbenzene, **2-14**, in a 63% yield. The propargyl alcohol protecting group was selectively removed through reaction with manganese dioxide and potassium hydroxide to give **2-15** in a 50% yield. Following a Hagihara reaction with platinum complex **2-8**, the TIPS-protected monomer **2-15** was then deprotected *in situ* with TBAF and polymerized overnight to give polymer **2-17** in high yield.

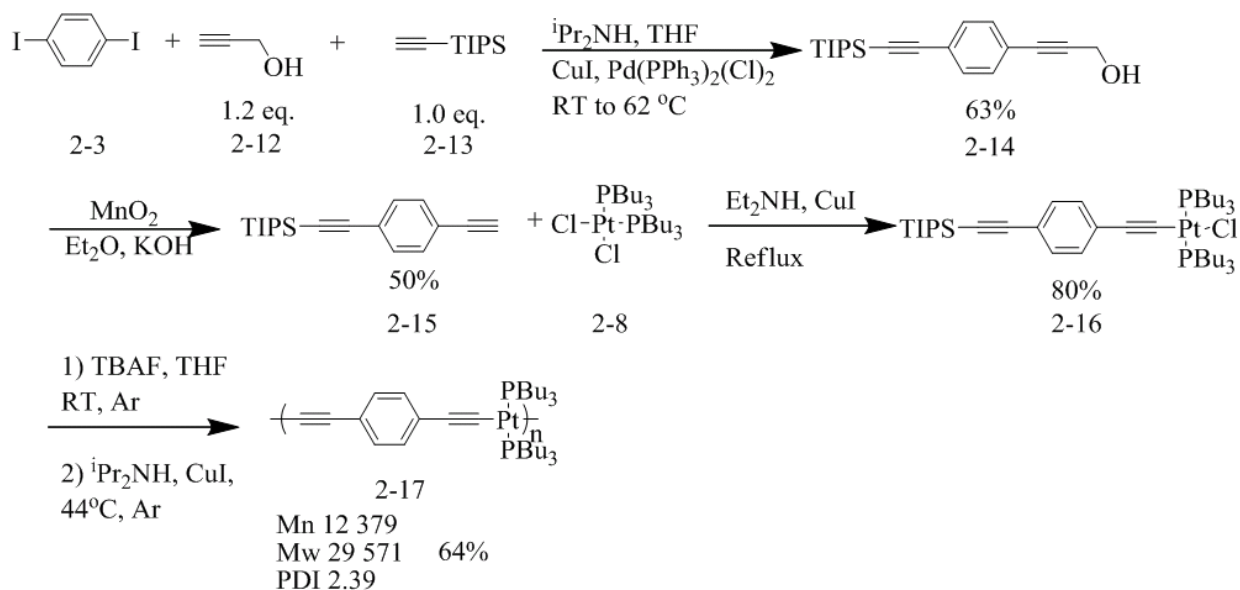


Figure 2-5. Synthesis of pPtPh using an AB asymmetric monomer. All materials except the polymer were synthesized according to the literature.⁹⁰

Both polymers were characterized by ultraviolet-visible absorption (UV-VIS) and photoluminescence spectroscopies, as well as by gel permeation chromatography (GPC). The UV-VIS and emission spectra for both polymers in degassed tetrahydrofuran (THF) is given in Figure 2-6 and the results are summarized in Table 2-1. The absorption and emission spectra in tetrahydrofuran (THF) for polymer **2-10**, created using and AA + BB co-polymerization, are shown in Figure 2-6A, while the absorption and emission spectra in THF for polymer **2-17**,

synthesized from the AB monomer, are shown in Figure 2-6B. Compared to **2-17**, the absorption spectrum of **2-10** (Figure 2-6A) features a blue-shifted absorbance maximum (376 nm and 372 nm, respectively) and the spectrum is slightly broader. Examining the emission spectra, there are two noticeable differences. Firstly, the fluorescence peak at 390 nm for **2-10** (Figure 2-6A) has a sharp, narrow shoulder near 410 nm. The fluorescence of **2-17** (Figure 2-6B) is similar in energy, yet has a broader, less intense shoulder near 425 nm. The second and most obvious differences between the two spectra are the phosphorescence peaks. Compared to **2-17** (Figure 2-6B), the phosphorescence shoulder of **2-10** (Figure 2-6A) is significantly broader.

The difference in the spectra suggest butadiyne defects in the backbone of polymer **2-10**, as illustrated in Figure 2-6C. The butadiyne structure is shown in **2-19** and is formed through homo-coupling of 1,4-diethynylbenzene, **2-9**. Polymer **2-18** can be assumed to be defect free because the asymmetric monomer would limit the formation of butadiyne defects to one per polymer chain. The photophysical properties of platinum acetylides containing butadiyne moieties have been studied in detail.⁹¹⁻⁹³ Materials featuring the butadiyne moiety are defined by an emission spectrum of very sharp and narrow peaks throughout the visible region.^{92,93} The sharp peak near 410 nm in Figure 2-6A and the broad phosphorescence shoulder could be the result of butadiyne defects in the polymer backbone. It has also been shown that the Pt-C bond distance decreases as the number of butadiyne units in a molecule increases.⁹¹ Assuming that polymer **2-18** has almost no butadiyne defects and **2-19** has many, the defects in the latter would slightly decrease the average Pt-C bond distance. Presumably, a smaller Pt-C bond distance would increase the amount of overlap between Pt d-orbitals and C p-orbitals.⁹⁴ This would increase the amount of orbital mixing, increasing the HOMO-LUMO energy gap, thus increasing the S_0 - S_1 transition energy of **2-19**. Because it is now assumed that any polymer made using two

symmetric monomers would have backbone defects, all of the exciton diffusion studies were done on the defect-free polymer, made using the self-polymerization route (Figure 2-5).

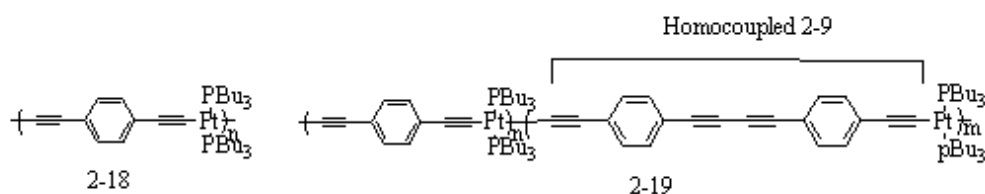
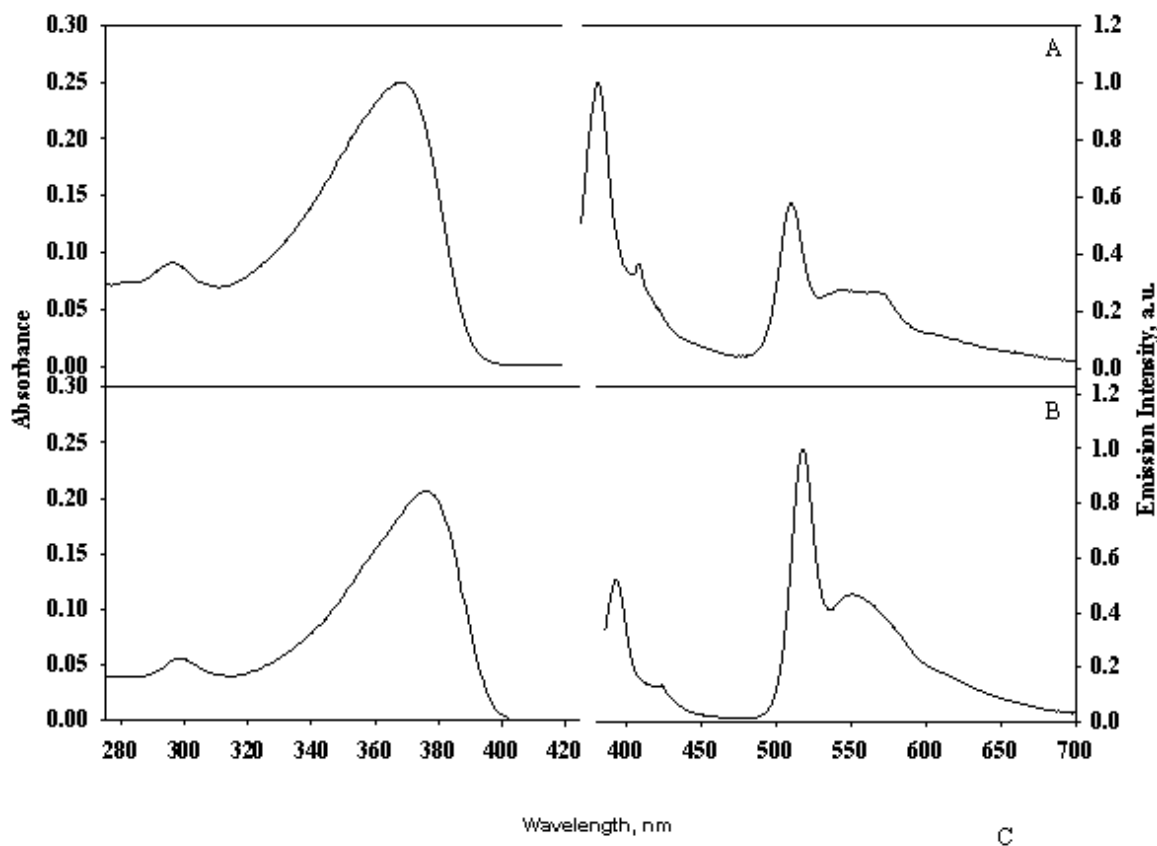


Figure 2-6. Absorption and emission spectra for the polymers in degassed THF solution. A) pPtPh synthesized from diethynylbenzene and bis(tributylphosphino)platinum(II) chloride. B) pPtPh synthesized from one asymmetric monomer. C). Proposed structures for the polymer giving spectrum A (**2-19**) and spectrum B (**2-18**).

Table 2-1. Summary of polymer characterization data.

Polymer	M _N	M _W	PDI	λ _{max} ^A	λ _{max} ^F	λ _{max} ^P
2-10	23 298	68 172	2.93	372	390	515
2-17	12 379	29 571	2.39	376	391	516

Results

To calculate the triplet exciton diffusion coefficient for pPtPh films, a simple model was developed that relates the quenching rate constant of triplet excitons to their diffusion coefficient. This is a model based on quencher concentration that will be described in the discussion section. For this model to work, the effect of quencher concentration on the exciton quenching in the film must be ascertained. To do so, a series of pPtPh films containing varying quencher concentrations were spin-coated. Assuming that the quenchers become dissolved in the polymer film and that the ratio of quencher-to-polymer repeat units does not change upon spin-coating, the effects of the amount of quencher on the triplet exciton concentration can be determined. To ensure reproducibility, a set of films using a known electron accepting quencher, phenyl[C61]butyric acid methyl ester (PCBM, a fullerene derivative) were made. These results were compared to a second set of films made using platinum tetraphenylporphyrin (PtTPP), a quencher assumed to accept energy. The structures of the quenchers are given in Figure 2-7.

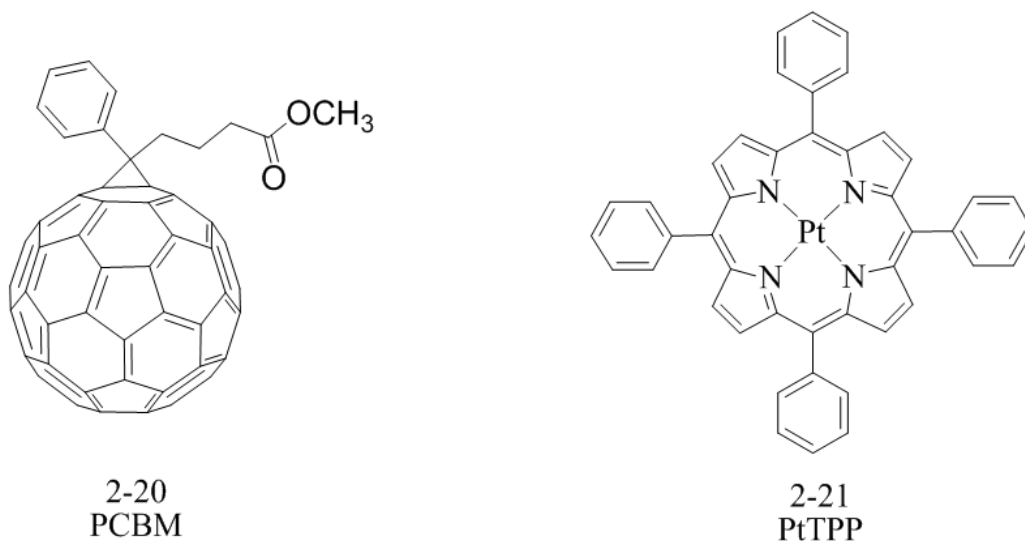


Figure 2-7. Chemical structures of the acceptors used for exciton diffusion studies: phenyl[C61]butyric acid methylester (PCBM, **2-20**) and platinum tetraphenylporphine (PtTPP, **2-21**).

Concentration-Based Quenching

The electron accepting ability of fullerenes, and in particular PCBM, has been widely studied.⁹⁵⁻⁹⁸ When PCBM accepts an electron from a donor, a charge separated pair is formed; that is, the donor, absent one electron, becomes a radical cation and the acceptor (PCBM), with one extra electron, becomes a radical anion. Indeed, this charge separated state has been directly observed in a solution of PCBM with a platinum acetylide polymer.⁹⁸ Initially, it was hoped that phosphorescence intensity quenching could be observed in spin-coated films containing varying amounts of PCBM, as exemplified in Figure 2-8. The absorption spectra of the thin films are broad, with maxima centered near 380 nm. When the air-saturated emission spectra of the films are taken, intense phosphorescence near 515 nm can be clearly seen. This suggests that the films' oxygen permeability is low. When 0.15 weight percent (wt%) PCBM was added to the film, an increase in the phosphorescence intensity was observed, likely due to an increase in the film's absorbance (film thickness). Upon addition of PCBM, the viscosity of the casting solution increased, resulting in a thicker film. This effect was observed over every PCBM concentration employed, and efforts to compensate for this effect failed.

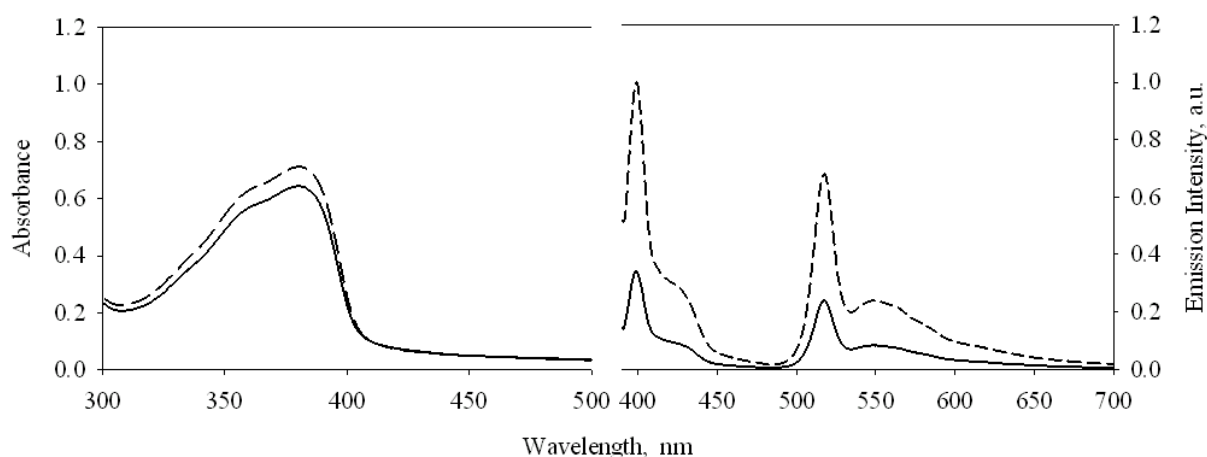


Figure 2-8. Example absorption and normalized emission spectra for spin-coated pPtPh films with 0.00 weight percent (—) and 0.15 weight percent (— —) PCBM.

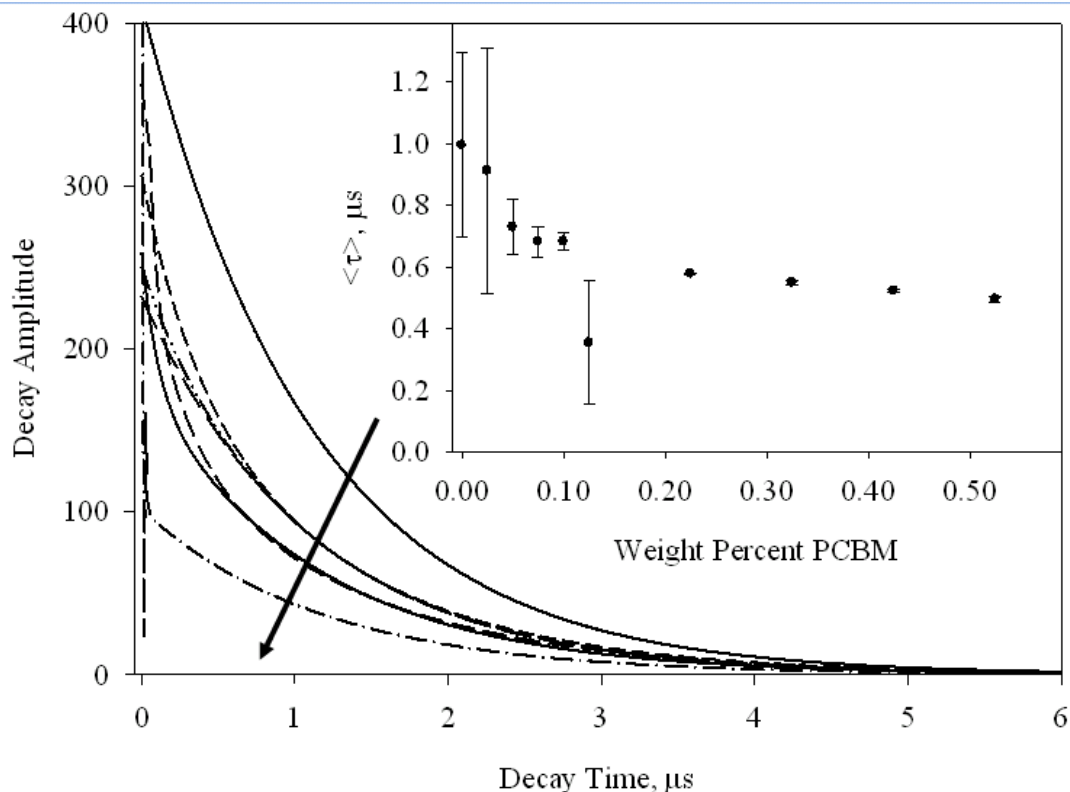


Figure 2-9. Fitted time correlated single photon counting decays for quenched pPtPh/PCBM films, in order of increasing decay area: 0.125 wt%, 0.525 wt%, 0.225 wt%, 0.100 wt%, 0.075 wt%, 0.05 wt%, and 0.00 wt% PCBM. The error bars represent the standard deviation of the average pPtPh triplet lifetime.

Unlike photoluminescence measurements, exciton lifetime studies are not affected by changes in film thickness. Lifetime measurements were carried out using the time correlated single photon counting technique (TCSPC), details of which can be found elsewhere.⁹⁹ As discussed in the experimental section, the triplet pPtPh lifetime for each film was calculated by using the integrated first order rate law to model the experimentally collected phosphorescence decays. The decay of a pristine pPtPh film was best modeled as a single exponential decay, and its triplet lifetime was found to be 0.996 μs . As evident in Figure 2-9, the amplitude of the phosphorescence decays decreased as the PCBM concentration increased. This suggests that as the quencher concentration increases, more pPtPh triplets are quenched. As the PCBM concentration increases from 0.025 wt% to 0.525 wt%, the triplet lifetimes decreased to 0.49 μs .

An interesting, out-of-sequence point was found at 0.125 wt% PCBM, suggesting this concentration to be a point of maximum solubility for the quencher.¹⁰⁰ This point was reproducible. Obviously being an anomalous point, this lifetime was omitted from subsequent diffusion calculations. Large deviations in the mean pPtPh lifetimes were observed, mainly due to changes in quencher solubility during the spin-coating process. Accordingly, all films, both pristine and quenched, were prepared in triplicate. Three separate lifetimes were thus obtained for three separate films at each PCBM concentration. The lifetimes were averaged and are summarized in the inset of Figure 2-9. The error bars represent the range of lifetimes measured for each quencher concentration.

To reproduce the data obtained using PCBM, a series of spin-coated films using PtTPP as an energy accepting quencher were studied. Metalloporphyrins such as PtTPP are ideally suited as energy transfer quenchers because they feature multiple absorption peaks and relatively low energy excited states.¹⁰¹ Example absorption and emission spectra for pPtPh films containing PtTPP are shown in Figure 2-10. Upon addition of PtTPP, the absorption spectrum of pPtPh is not strongly affected, with its absorption maximum remaining at 380 nm. The thin film absorbance of PtTPP features a Souret band near 425 nm and a Q-band absorption near 510 nm.¹⁰¹ Most importantly, there is minimal PtTPP absorbance at the pPtPh maximum, the implications of which will be discussed shortly. In the air-saturated emission spectrum of the PtTPP-containing pPtPh film, there is a peak near 660 nm corresponding to emission of the porphyrin. The emission spectra of the films were acquired by exciting the film at the absorbance maximum of pPtPh. Because there is not much absorption by PtTPP at this wavelength, the increase of this peak is probably due to energy transfer from pPtPh to PtTPP.

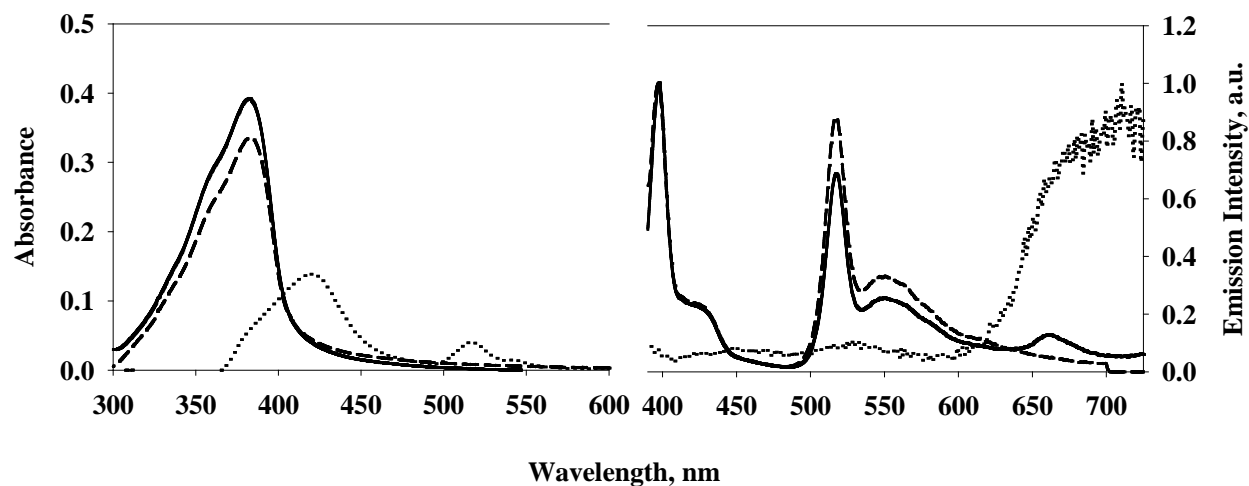


Figure 2-10. Absorption and normalized emission spectra for pPtPh/PtTPP spin-coated films: (—) 0.00 wt%, (— —) 0.38 wt% PtTPP, and (···) pristine PtTPP. All films were excited at the absorbance maximum for pPtPh, 380 nm.

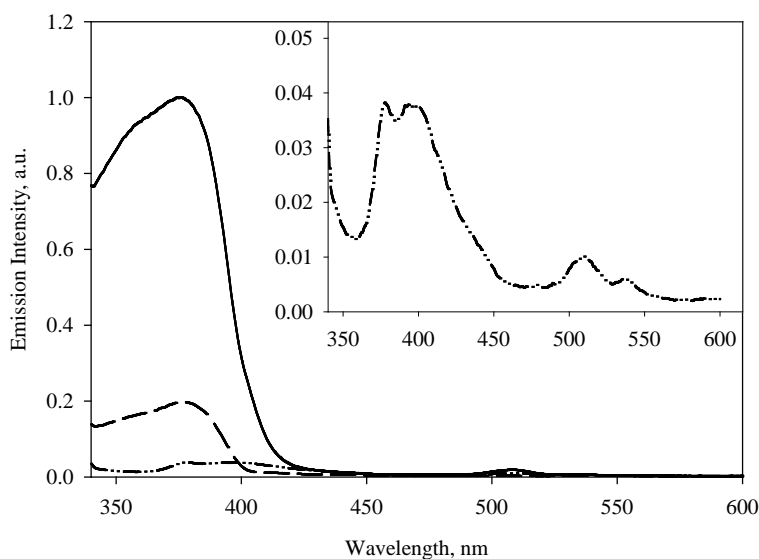


Figure 2-11. Thin film excitation spectra, monitored at the emission maximum of PtTPP, 660 nm: (—) 0.38 wt% PtTPP, (— —) pristine pPtPh, and (— · —), pristine PtTPP. The optical densities for each film can be found in Figure 2-10.

Energy transfer quenching from pPtPh to PtTPP is confirmed by the thin film excitation spectra in Figure 2-11. An excitation spectrum is essentially an optical absorption spectrum, except the fluorescence at one wavelength is monitored, rather than the optical transmission of the sample. In this experiment the emission at 660 nm, corresponding to the fluorescence maximum of PtTPP, was monitored. As shown in Figure 2-11, there is a substantial boost to the emission intensity when 0.38 wt% PtTPP is added to pPtPh. The lineshape of the quenched film closely resembles that of pristine pPtPh, which is significantly different than the excitation spectrum of PtTPP. The intensity boost upon addition of PtTPP to pPtPh, coupled with the similarities between the lineshapes of pristine pPtPh and PtTPP-containing pPtPh films, indicates that excitation energy is being transferred from pPtPh to PtTPP, which then radiatively relaxes.

As with PCBM, quantitative quenching information could not be gleaned from the emission quenching of pPtPh with PtTPP, so lifetime decays were again obtained (Figure 2-12). As the weight percent of PtTPP in pPtPh films increases from 0.022-0.38 wt%, the lifetime of the polymer decreases from 1.2 μ s to 0.78 μ s. Large deviations were again observed in the mean pPtPh lifetimes due to changes in PtTPP solubility during spin-coating, so the inset of Figure 2-12 again shows the average lifetime of three films at each quencher concentration. Upon first inspection, it would seem that the PtTPP quenching data do not reproduce the PCBM quenching data; that is, the final lifetime of PtTPP-quenched films is significantly higher than the final lifetime of the PCBM-quenched films. If one considers the lifetimes of the pristine pPtPh films in Figure 2-9 (0.996 μ s) and Figure 2-12 (1.2 μ s), the differences between the pristine and final, quenched lifetimes are approximately equal. As shown later, similar exciton diffusion coefficients can thus be expected for pPtPh films quenched by PCBM and PtTPP.

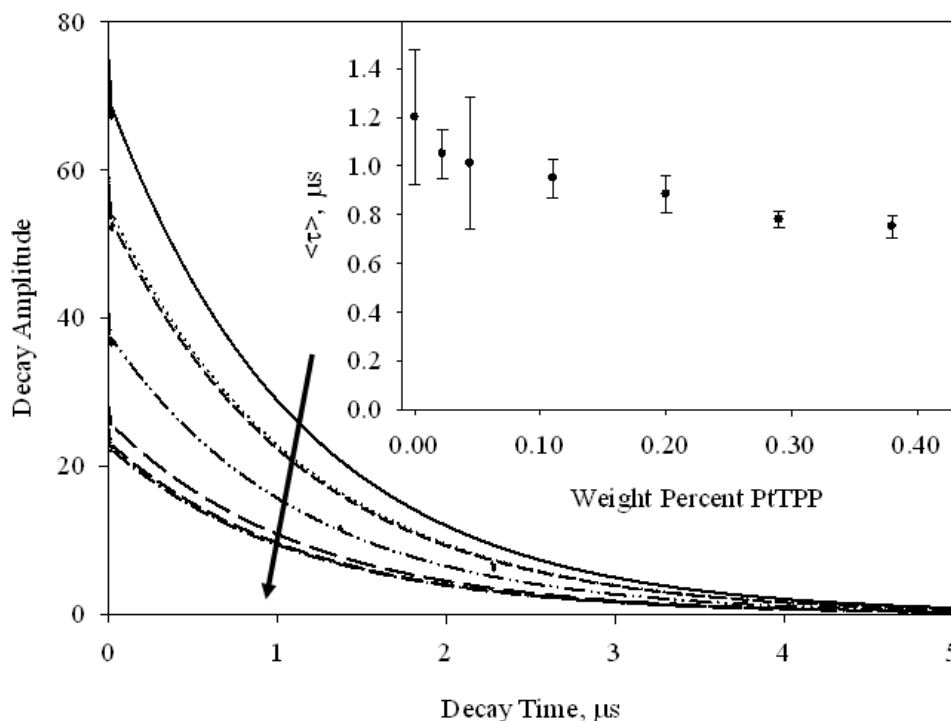


Figure 2-12. Fitted time correlated single photon counting decays for quenched pPtPh/PtTPP films, in order of decreasing decay area: 0.00 wt%, 0.022 wt%, 0.044 wt%, 0.11 wt%, 0.20 wt%, 0.29 wt%, and 0.38 wt% PtTPP. The error bars represent the standard deviation of the average pPtPh triplet lifetime.

Time of Flight Measurements

Exciton diffusion coefficients for pPtPh determined from the concentration-based quenching data will be from a new, untried method. To validate and compare the results with the literature, time-of-flight (TOF) measurements were conducted. In TOF measurements, an acceptor layer of constant thickness is thermally evaporated onto several spin-coated donor films of varying thicknesses. As described in Figure 2-2, a photon is absorbed by the donor layer, producing an exciton. In these experiments, an increase of donor film thickness results in less exciton quenching because fewer excitons can diffuse to the quenching layer before they relax. Using mathematical models described in the discussion section, a comparison of film thickness to exciton quenching enables estimation of the exciton diffusion coefficient for the donor layer. Here, the donor layer is pPtPh and the accepting/quenching layer consists of either C60 or

PtTPP. The pPtPh film thicknesses were indirectly determined using step-height atomic force microscopy as discussed in the experimental section.

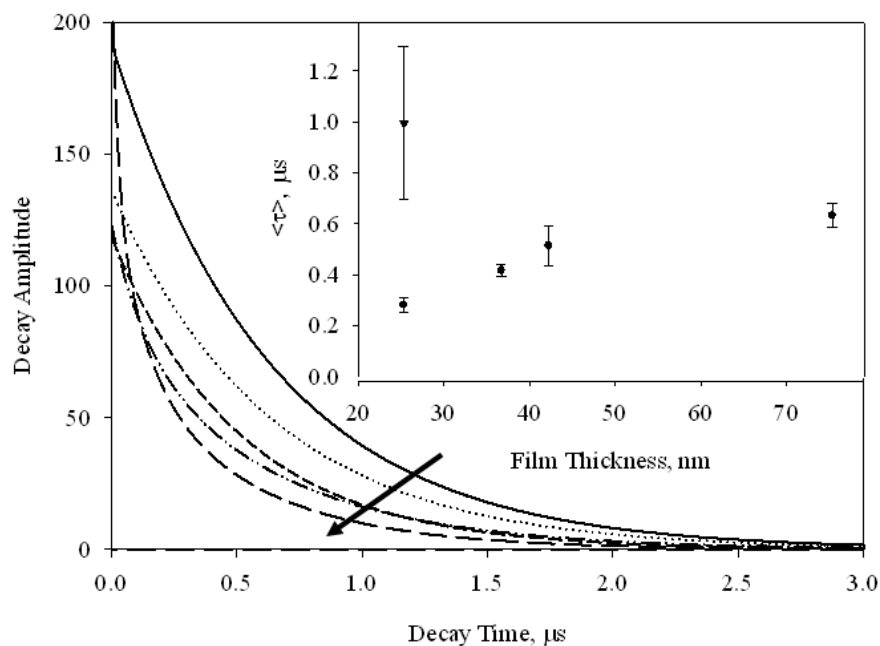


Figure 2-13. Fitted time correlated single photon counting decays for pPtPh/C60 TOF experiments, in order of decreasing decay area: unquenched pPtPh, 75.3 nm, 42.2 nm, 36.7 nm, and 25.3 nm pPtPh layers. The error bars represent the standard deviation of the average pPtPh triplet lifetime.

A summary of the TOF experiments for variable thickness pPtPh films quenched with a 40 nm layer of deposited C60 is given in Figure 2-13. Like PCBM, C60 is also a well-known electron accepting quencher; however, the thermal evaporation of PCBM was not possible, so C60 was evaporated in its place. When the pPtPh film thickness is 25.3 nm, a significant reduction in triplet lifetime occurs that suggests very efficient quenching. As the donor thickness increases to 75.3 nm, the triplet lifetime partially recovers, with changes in lifetimes appearing to stabilize by this point. A direct comparison of this data with those in Figure 2-9 is not possible because they are obtained using two different theoretical models; however the range of lifetimes suggest that it will be possible to obtain triplet exciton diffusion coefficients from these data.

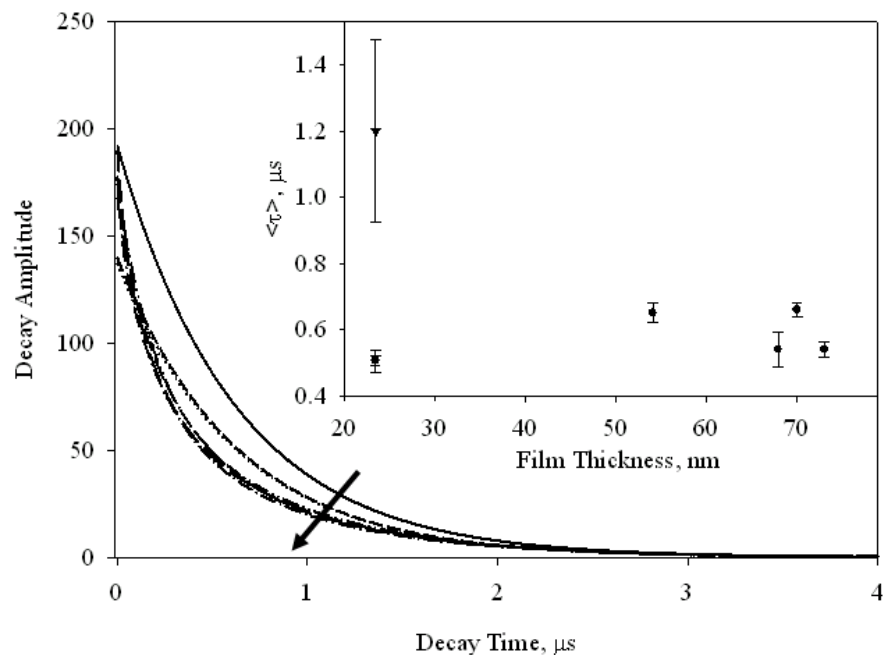


Figure 2-14. Fitted time correlated single photon counting decays for pPtPh/PtTPP TOF experiments, in order of decreasing decay area: unquenched pPtPh, 54.1 nm, 70.1 nm, 73.1 nm, 68 nm, 23.3 nm, and 23.4 nm pPtPh layers. The error bars represent the standard deviation of the average pPtPh triplet lifetime.

Similar to the concentration-based experiments, TOF measurements using PtTPP as a quencher were taken to reproduce the C60 TOF results. The results are given in Figure 2-14. Even though the pPtPh film thickness varies from 23.4 nm-73.1 nm, there is no discernable change in triplet exciton quenching with donor film thickness. Thin film excitation spectra in Figure 2-11 prove beyond a doubt that PtTPP is able to quench pPtPh films *via* energy transfer. So why, then, are the pPtPh triplet lifetimes unaffected by changing the donor film thickness? The answer lies in the polarities of pPtPh and PtTPP. Being essentially made up of carbon and hydrogen atoms, pPtPh can be assumed to be relatively nonpolar; on the other hand, PtTPP has a distinct outer region of only carbon atoms and a center filled with platinum and nitrogen atoms. This would impart polar characteristics to PtTPP. When evaporated onto pPtPh, the differences in polarities could be causing a de-wetting of PtTPP from the pPtPh surface. The result is an

uneven, island or layer-plus-island topology for the acceptor film (see Chapter 1) that results in uneven pPtPh triplet exciton quenching.

Discussion

The Concentration-Based Quenching Model

There are a variety of models describing donor-acceptor exciton quenching in solutions, such as the Perrin, Stern-Volmer, and Hindered Access models.^{72,102} In all of these models, the rate constant of exciton quenching, k_q , is related to the concentration of quencher and a quenching parameter unique to each model. Fitting the experimental data to the model enables calculation of k_q . These experiments are typically done by adding an acceptor volume of known concentration to a donor solution. When dealing with solutions, calculating the concentration of acceptor is an easy task. To determine the triplet exciton diffusion coefficient of a thin film, solution-based quenching models will be applied to a series of spin-coated films with different amounts of added quencher.

For these models to be applicable to thin films, there are several conditions that must be met. The spin-coated films were constructed from a casting solution with a known amount of polymer and a known amount of quencher. It is assumed that upon spin-coating, the ratio of donor-to-acceptor does not change. The effects of donor/acceptor phase separation are also assumed to be minimal. Multiple studies have suggested that in spin-coated films made from a mixture of different components, the materials can separate into mutually exclusive domains.¹⁰³⁻

¹⁰⁷ For example, polymer films containing large amounts PCBM have been shown to form regions of only PCBM and regions of only polymer.^{103,104,107} This phase separation effect has been observed at very high (e.g., 80 wt%) PCBM concentrations and has been attributed to a number of factors, including PCBM solubility in the polymer, solvent evaporation-induced crystallization, and annealing-promoted diffusion.^{103,104,107} Although donor-acceptor solubility in

pPtPh/PCBM and pPtPh/PtTPP films could be an issue, the films have less than 1.0 wt% acceptor, are not annealed, and are cast from a fast-evaporating solvent (methylene chloride).¹⁰⁷ All of these conditions would favor the formation of a uniformly dispersed acceptor in the donor matrix. Finally, for the concentration-based, solution quenching models to be applicable, there must be a method of determining the acceptor's molar concentration. Accordingly, it will be assumed that the acceptor is "dissolved" in the donor matrix, viewed as the "solvent." Thus, knowledge of the volume of polymer in the film will enable the calculation of the acceptor's molar concentration.

Density (ρ) relates a substance's mass (m) to its volume (v), as shown in Equation 2-1.

$$\rho = \frac{m}{v} \quad (2-1)$$

The polymer's density can be used to relate the mass dissolved in the casting solution to the volume of polymer dissolved in the casting solution. Because the volume of polymer is known, the concentration of acceptor with respect to the polymer volume can be calculated for the casting solution. It is assumed that the donor-to-acceptor ratio in the casting solution is equal to that of the thin film, so the acceptor concentration of the casting solution is equal to the acceptor concentration of the spin-coated film.

Fortunately, Albert and Malone developed a highly accurate method of calculating the density of polymers based on a group increment method.¹⁰⁸ When compared to the experimentally determined density of various polymers, this method is accurate to within 90% of each measured value. The calculated density, ρ , is a product of the a_1 constant and the ratio of the repeat unit molecular weight, M_{ru} , and the repeat unit parachor, P_{ru} , as shown in Equation 2-2.¹⁰⁸

$$\rho = a_1 \frac{M_{ru}}{P_{ru}} \quad (2-2)$$

The parachor is a value that relates atomic mass to atomic volume and has been shown to be relatively independent of temperature. It is calculated using Equation 2-3, where γ is the liquid surface tension and V_m is the molar volume.¹⁰⁸⁻¹¹⁰

$$P = V_m \sqrt[4]{\gamma} \quad (2-3)$$

Each atom, bond, and electron has a corresponding parachor, and there exist tables enabling one to calculate the parachor for an entire molecule.¹⁰⁹ For example, the parachor for ethylene ($\text{CH}_2=\text{CH}_2$) would be the summation of the parachors for two carbons, four hydrogens, and one double bond. The parachors for single bonds are included in those of atoms.

The a_1 constant is the ratio of a molecule's parachor to its molar volume (Equation 2-4), and introduces volume to the density calculation.¹⁰⁸ As with the parachor, the molar volume of a molecule can also be estimated using group increment methods.¹¹¹

$$a_1 = \frac{P}{V_m} \quad (2-4)$$

Applying this method to pPtPh, the density of the polymer is estimated to be $1.28 \text{ g}\cdot\text{cm}^{-3}$, a value just slightly higher than the density of most polymers ($\sim 1.0 \text{ g}\cdot\text{cm}^{-3}$).¹⁰⁸ The pPtPh density calculation can be found in Appendix A. It is important to note that the parachors for heavy transition metals (to the author's knowledge) do not exist, so the parachor of platinum was calculated using Equation 2-3 to be $10.628 \text{ cm}^3\cdot\text{mol}^{-1} \text{ N}\cdot\text{m}^{-1}$.^{112,113}

Using the estimated density of pPtPh, the molar concentrations of PCBM and PtTPP in the spin-coated films can be calculated. In the thin-film solution-based quenching model, it is assumed that the donor becomes photoexcited, the exciton diffuses to the acceptor, at which time the exciton is quenched. One of the standard solution-based, diffusional quenching models is the

Stern-Volmer model, described by Equation 2-5, where I_0 is the initial, unquenched emission intensity, I is the quenched emission intensity, K_{SV} is the Stern-Volmer constant and $[Q]$ is the quencher concentration. Lifetime quenching often gives the same information as intensity quenching, so lifetimes are occasionally used in the Stern-Volmer equation instead of the intensities.^{72,98,102}

$$\frac{I_0}{I} = 1 + K_{SV}[Q] \quad (2-5)$$

The Stern-Volmer constant is further related to the quenching rate constant, k_q , and the unquenched lifetime of the donor, τ , by Equation 2-6.

$$K_{SV} = k_q \tau \quad (2-6)$$

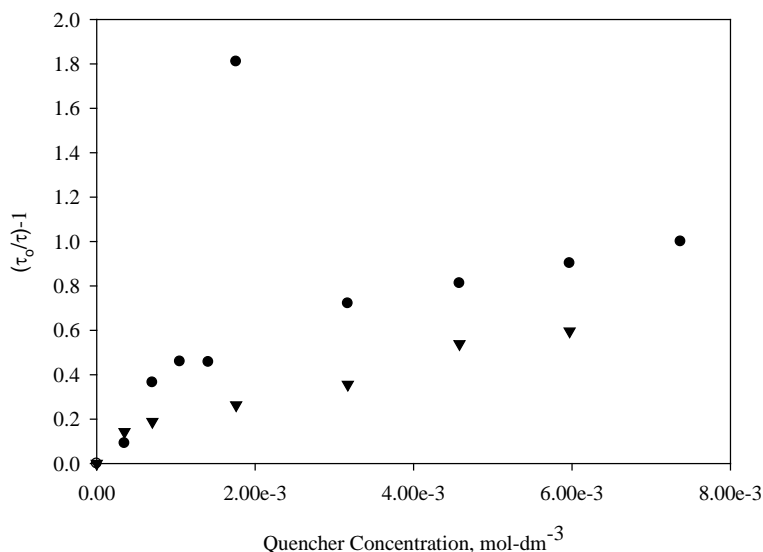


Figure 2-15. Stern-Volmer plots for concentration-based pPtPh quenching by PCBM (circles) and PtTPP (triangles).

Stern-Volmer plots for spin-coated pPtPh films, quenched either by PCBM or PtTPP, are given in Figure 2-15. When the Stern-Volmer model applies to a donor-acceptor system, a linear relationship is shown between quencher concentration and the quenching metric on the y-axis. As evident for both systems, the plots are not linear and appear to rise asymptotically to a

maximum. Such deviation from linearity in Stern-Volmer plots is not unprecedented. Webber observed such an occurrence while studying the tantalum-mediated quenching of anthracene-labeled polymers.¹⁰² A nonlinear Stern-Volmer plot does not suggest the absence of exciton diffusion; rather, it suggests that there is a combination of exciton diffusion and some other force at work. Webber's solution to this problem was to use the Hindered Access model, given by Equation 2-7.¹⁰² The hindered access model is still a diffusional quenching model, as the Stern-Volmer constant is present in the mathematical description. However, the model assumes that in the system, there is a fraction of chromophore that is not able to be quenched and a fraction of chromophore that can be quenched, giving rise to the fraction of accessible chromophore, f_a .

$$\frac{I_0}{I_0 - I} = \frac{1}{f_a} + \frac{1}{K_{SV} f_a [Q]} \quad (2-7)$$

A plot of the quenching metric, again using either intensity or lifetime values, versus the reciprocal of the acceptor concentration will produce a linear plot if the model applies. It then follows that f_a is the inverse of the y-intercept and K_{SV} is the y-intercept divided by the slope, calculated using a linear regression fit of the data.¹⁰² As evident in Figure 2-16, the Hindered Access model describes the spin-coated films' quenching data well, in agreement with Webber's precedent.

The results are summarized in Table 2-2. Both quenchers, PCBM and PtTPP have similar Stern-Volmer constants and high quenching rate constants, indicating that the diffusion coefficients measured for these systems should be similar. This occurs through a mechanism whereby the excitons produced on a polymer chain diffuse in a random-walk pattern to the fixed-location acceptor, whereupon quenching occurs.¹¹⁴

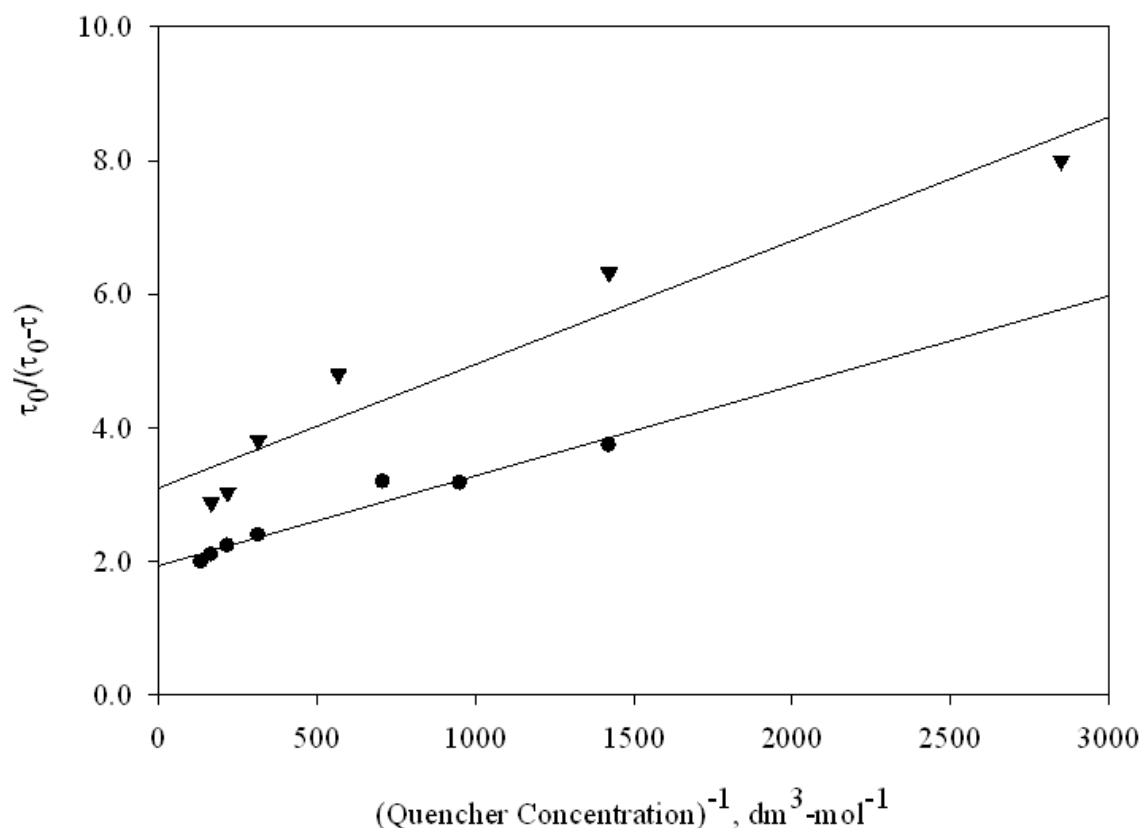


Figure 2-16. Hindered Access plots for concentration-based pPtPh quenching by PCBM (circles) and PtTPP (triangles). Data points for PCBM at 0.351 mM (2846 M⁻¹) and 1.76 mM (568 M⁻¹) have been omitted because they lie significantly outside the range of data.

Table 2-2. Summary of the concentration- and time of flight (TOF)-based triplet exciton diffusion measurements.

Quencher	Film type ^a	K _{SV} (M ⁻¹)	k _q (10 ⁹ M ⁻¹ ·s ⁻¹)	D (10 ⁻⁶ cm ² ·s ⁻¹)	L _D (nm)	f _a
PCBM	Blend	1,486	1.49	4.96	22.2	0.517
PtTPP	Blend	1,675	1.39	4.59	23.5	0.323
C60	Bilayer	N/A	N/A	7.70	27.7	N/A

Notes: ^a“Blend” refers to spin-coated films and “Bilayer” refers to TOF experiments.

Kinetically speaking, the quenching rate constant is a bimolecular, second-order process. Exciton quenching with a donor and acceptor cannot occur unless one entity diffuses to the other. The resulting collision can result in an exciton quenching reaction. From Fick’s First Law of Diffusion, Benson derived a relation describing the collision frequency of the two entities to the the diffusion coefficient.¹¹⁵ This is given by Equation 2-8, where Z’_{AB} is the collision frequency

($M^{-1}\cdot s^{-1}$), r_{AB} is the reactive radius of the two entities A and B, D_{AB} is the diffusion coefficient and N_{AV} is Avagadro's number. For energy transfer reactions such as the Dexter mechanism, r_{AB} is typically assumed to be 4 Å.¹¹⁵

$$Z'_{AB} = \frac{4\pi r_{AB} D_{AB} N_{AV}}{1000} \quad (2-8)$$

Both the quenching rate constant and the collision frequency describe a kinetically second order process; that is, they both describe the number of effective collisions as a function of molar concentration and time. The collision frequency is statistically related to the rate constant, k , through Equation 2-9, where P is the probability that a reaction occurs when A and B collide.

$$k = PZ \quad (2-9)$$

Assuming that every exciton diffusing to an acceptor is quenched, $P = 1$. It follows that the collision frequency is equal to the quenching rate constant. Substituting the experimentally calculated k_q for Z'_{AB} and rearranging Equation 2-8 for D , the triplet exciton diffusion coefficients are obtained and are given in Table 2-2. An example calculation using Equation 2-8 is given in Appendix A. Using two different quenchers that operate using two different quenching mechanisms, a reproducible triplet diffusion coefficient of $10^{-6} \text{ cm}^2\cdot\text{s}^{-1}$ is obtained. Given this value and the lifetime of the pristine film, one can further calculate the average distance traveled by triplet excitons to the acceptor sites, using Equation 2-10.⁸⁴

$$L_D = \sqrt{D\tau} \quad (2-10)$$

In this relationship, L_D is the average exciton length of diffusion, D is the exciton diffusion coefficient and τ is the unquenched exciton lifetime. Also given in Table 2-2, the lengths of diffusion for pPtPh/(PCBM or PtTPP) spin-coated films are relatively long. If confirmed by the time of flight experiments, the high diffusion coefficients and lengths of diffusion would represent a substantial improvement to existing parameters in the literature.^{76,80,81,83,87}

Time of Flight Validation

Applying concentration-based quenching models to calculate exciton diffusion parameters represents a method new to the literature. To validate this method, time of flight measurements were carried out on films of variable thickness pPtPh with a 40 nm thick layer of either C60 or PtTPP vacuum-deposited on top. In these experiments, the exciton is produced when the donor layer absorbs a photon, creating an exciton, which diffuses to the acceptor layer and is quenched. By performing quenching measurements using several films of variable thickness, the effect of film thickness on exciton quenching can be determined. Mikhnenko used the one dimensional continuity model (Equation 2-11) to describe the fate of the excitons.⁸⁴

$$\frac{\partial n(x,t)}{\partial t} = -\frac{n(x,t)}{\tau} + D \frac{\partial^2 n(x,t)}{\partial x^2} - S(x)n(x,t) + G(x,t) \quad (2-11)$$

This model describes the fate of every exciton in a film. It is referred to as one dimensional because the excitons are assumed to only diffuse in one direction, from the point-of-excitation to the point-of-quenching. The first term describes all the natural decay processes of the exciton, such as luminescence and nonradiative decay. The second term describes exciton diffusion within the film, while the third term describes exciton quenching and the fourth, exciton formation.^{84,85} From this equation, Mikhnenko derived a simple expression relating exciton quenching, $Q(L)$, to the film thickness, L , and average exciton length of diffusion, L_D , for TOF experiments (Equation 2-12).⁸⁴

$$Q(L, L_D) = \frac{L_D}{L} \tanh\left(\frac{L}{L_D}\right) \quad (2-12)$$

Using Equation 2-12, L_D is assumed to be the only variable, with $Q(L)$ and L being calculated from experimental data (see the experimental section). A nonlinear regression is thus performed,

treating L_D as a variable. Once L_D is known, Equation 2-10 can be applied to calculate the diffusion coefficient, since τ and L_D are known.

The curve fitting process applied to the experimentally obtained TOF data for pPtPh|(C60 or PtTPP) films is shown in Figure 2-17, with the results summarized in Table 2-2. For quenching by C60 (Figure 2-17A), the procedure produced an excellent fit with a diffusion coefficient similar in magnitude to those obtained from the concentration-based PCBM and PtTPP values, about $10^{-6} \text{ cm}^2 \cdot \text{s}^{-1}$. However, the model failed for the TOF data with PtTPP. This was not unexpected, as the exciton decays in Figure 2-14 did not show much variation with film thickness.

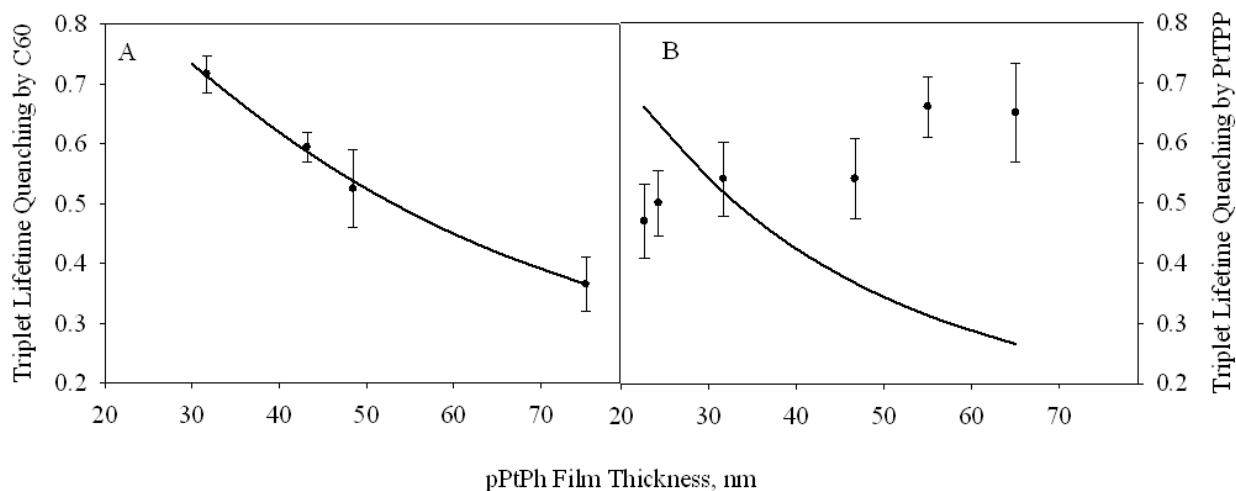


Figure 2-17. Fitted TOF lifetime quenching data. A) pPtPh/C60 TOF experiments. B) pPtPh/PtTPP TOF experiments. The solid, fitted lines are produced using Equation 2-12 and the circles represent experimental measurements calculated using Equation 2-14. Error bars represent the range of lifetimes measured for each film thickness.

The PtTPP TOF data notwithstanding, the C60 TOF data affords D and L_D values similar to those obtained from concentration-based PCBM and PtTPP quenching of pPtPh. This indicates that the simpler mathematical model developed herein is a valid method to estimate exciton diffusion parameters in thin films. Both models gave triplet exciton diffusion and length of diffusion values significantly higher than the majority of the literature, as summarized in

Table 2-3. Most triplet diffusion coefficients in the literature have been measured using small molecules, where there is no substantial contribution from intermolecular diffusion to the bulk exciton diffusion coefficient. In a polymer, the exciton can diffuse not only intramolecularly, but also along the polymer chain. Since intermolecular rates are always faster than intramolecular rates, the triplet exciton diffusion coefficient is greatly enhanced. These factors suggest that if polymers capable of forming high amounts of triplet excitons are used to create organic electronic devices, the longer exciton lifetime and long length of exciton diffusion have the potential to greatly enhance the performance of these devices.

Experimental

Materials

Dipotassium tetrachloroplatinate and dichloro-bis(triphenylphosphine) palladium (II) were purchased from Strem, as was (trimethylsilyl)acetylene, propargyl alcohol, and (triisopropylsilyl)acetylene. All other chemicals were purchased either from Fisher or Sigma-Aldrich. 1,4-Diethynylbenzene was synthesized according to a previously published method,¹¹⁶ and pPtPh **2-10** was prepared from a modification of a procedure described by Friend *et.al.*⁸⁸ Monomer **2-16** was synthesized by a literature procedure.⁹⁰ Borosilicate glass slides were purchased from Corning. Gel permeation chromatography (GPC) was performed by eluting a tetrahydrofuran (THF) solution of the polymer through two PL-Gel 5 Mixed D columns pressurized by a Rainin Dynamax SD-200 solvent pump. Polymer elution was spectroscopically monitored using a UV detector set to a wavelength where the polymer absorbs, and molecular weight calculations were performed using Polymer Laboratories PL software against a polystyrene standard. All solvents used were of HPLC grade. Nuclear magnetic resonance (NMR) spectra were recorded on a VXR-300 instrument and chemical shifts are reported downfield from an internal tetramethylsilane (TMS) standard.

Table 2-3. Singlet and triplet exciton diffusion literature data for spin-coated donor films.

Material	Exciton multiplicity ^a	D /10 ⁻⁶ cm ² -s ⁻¹	L _D (Å)	Reference
PEOPT	S	4500	47	85
MDMO-PPV	S	3200	45	84
PPP	S	4300	110	117
DIP ^C	S	5000	1000	77
Pent ^C	S	500	---	79
NPD	S	700	51	76
SubPC	S	640	80	76
PTCDA	S	3400	104	76
TnBuPP	S	2500	220	118
Alq ₃	S	12	200	76,119
Alq ₃	T	0.08	140	120
pPtPh	T	4.59-7.70	222-277	This work
PtOEP	T	0.06-4.1	130-180	76
BP	T	0.00001-0.5	---	80
PdTPPC	T	0.00008	---	87
CBP	T	0.014	---	83
Eu-DM	T	---	250	81
PTCDA	T	---	880	121
Ir-G1	T	0.40	100	122
Ir-Carb	T	0.060	60	122
Ir-G2	T	0.008	20	122
Ru(bpy) ₃ (Cl) ₂ ^C	T	9.0	---	78
Pent ^C	T	1350	---	79

Notes: ^aS=singlet, T=triplet; ^CThe data presented is for the organic crystal;---, data not reported; PEOPT, poly-3-(trioxaoctylphenyl)thiophenes; MDMO-PPV, poly-(2-methyl-5-(3',7'-dimethyloctyloxy)-p-phenylenevinylene; Alq₃,tris-(8-hydroxyquinoline) aluminum; NPD, N,N'-diphenyl-N,N'-bis(1-naphthyl-1,1'-biphenyl-4,4'' diamine; SubPC, boron subphthalocyanine; PTCDA, 3,4,9,10-perylenetetracarboxylic dianhydride; TnBuPP, tetra-(4-n-butylphenyl)porphyrin; DIP, diindenoperylene; PtOEP, platinum (II) octaethylporphine; BP, benzophenone; Ir-G1 and Ir-G2, dendrimeric tris-(2-phenylpyridine) iridium complexes; Ir-carb, dendrimeric tris(3',3'-dicarbazolyl-2-phenylpyridine) iridium complex; Pent, pentacene; PPP, poly(para-phenylene).

Synthesis

Polymer 2-10. 1,4-Diethynylbenzene (25.1 mg, 0.20 mmol) and platinum complex 2-8 (134.2 mg, 0.20 mmol) were dissolved in a 1:5 mixture of methylene chloride:diisopropylamine (6 mL total) in a Schlenk flask. The solution was outgassed with argon for 30 min, after which time CuI (5.3 mg, 0.028 mmol) was added. The previously clear solution immediately formed a

white precipitate upon CuI addition. The polymerization was allowed to proceed for 24 hr under argon at 40 °C , at which time the reaction was filtered through a bed of Celite 545 and washed with methylene chloride (DCM). The solvent was evaporated and the residue redissolved in minimal DCM. The polymer was precipitated from a large excess of methanol and filtered to give pPtPh (48 mg, 33%). A second precipitation was not performed because of the low yield of the reaction. The polymer was then characterized by GPC , optical absorption/emission spectra and by NMR. ¹H NMR (CDCl₃, 300 MHz): 0.91 (s, 18H), 1.42-1.56 (m, 25H), 2.10 (s, 11H), 7.09 (s, 4H). ³¹P NMR (CDCl₃, 120 MHz): 3.95 (t, 2357 Hz).

Synthesis

Polymer 2-17. Monomer **2-16** (250 mg, 0.272 mmol) was dissolved in a 7:2 mixture of diisopropylamine:THF (9 mL) in a Schlenk flask. The solution was degassed over 5 freeze-pump-thaw cycles. The flask was backfilled with dry argon and tetrabutylammonium fluoride (0.144 g, 0.54 mmol) was added *via* syringe. A white precipitate immediately formed from the yellow-colored solution. The reaction was stirred at room temperature for about 40 min, at which time a TLC with 1:4 hexanes:DCM revealed total consumption of **2-16**. Copper (I) iodide (2.8 mg, 0.015 mmol) was then added and the reaction heated to 44 °C. After stirring overnight, it was noticed that the polymerization reaction formed a neon-yellow suspension. The reaction was poured into an excess of methanol, precipitating the polymer as yellow fibers. The precipitate was filtered using a 2.5 µm glass fiber filter pad and redissolved in THF. The solution was reprecipitated into an excess of methanol and filtered using a glass fiber filter pad. The yellow fibers were once again redissolved in THF, precipitated from methanol, and filtered for a third and final time. After the final precipitation, the polymer was dried under a vacuum at room temperature overnight to give pPtPh (126 mg, 64%). The polymer was characterized by GPC,

UV-VIS/emission and by NMR. ^1H NMR (CDCl_3 , 300 MHz): 0.91 (t, 18H), 1.44 (q, 24H), 2.12 (m, 8H), 7.09 (s, 4H). ^{31}P NMR (CDCl_3 , 120 MHz): 3.96 (t, 2360 Hz).

Thin Film Preparation

Glass slides were cut into 1.2×2.5 cm rectangles using a glass scribe. Slides this size are the maximum size that will fit inside a standard 1 cm² fluorescence cuvette. Each slide was hand polished using a Kimwipe until no visible contaminant films were visible to the naked eye. The slides were then placed in a custom made slide holder and sonicated for 10 min each in sodium dodecylsulfate (SDS)/water, water, acetone, then isopropanol. All water used was purified to a resistivity of 18.2 M Ω using a Millipore Simplicity water purification system. Each slide was dried using filtered, compressed air and covered before use.

Each spin-coated film was prepared in triplicate using the procedure below. The photophysical measurements of all three films were averaged without eliminating any data points. This procedure was used to make seven sets of three slides using seven different acceptor concentrations. Glass vials, approximate volume three milliliters, were arranged in seven vertical columns, with each column containing three vials. A methylene chloride (DCM) solution of pPtPh **2-17** with a concentration of 20.2 g·L⁻¹ was dispensed into each vial in 20 μL aliquots using a precision glass syringe. A dilute (<0.02 g·L⁻¹) solution of acceptor in DCM was added, using a precision glass syringe, to each vial in pre-determined aliquots. Each volume increment was not less than 15 μL to ensure reproducibility of the quencher concentration. To ensure reproducible film thicknesses and complete slide coverage, the solvent in each vial was allowed to evaporate under ambient conditions. Immediately before spin-coating, the solution was redissolved in 100 μL DCM. A slide was placed on a spin-coater set to rotate at 1000 rotations per minute for 9.0 sec. After ensuring the slide was properly affixed to the spin-coater,

all of the redissolved DCM solution was transferred to the slide. The film was spin-coated and allowed to dry in the dark under a vacuum overnight before any measurements were made.

Thin films for TOF measurements were made using a similar technique with anhydrous DCM degassed using four cycles of freeze-pump-thaw. The pPtPh films were spin-coated inside an argon atmosphere glovebox. C60 and PtTPP films 400 Å thick were deposited at a rate of 2 Å-s⁻¹ in a high vacuum (<10⁻⁶ Torr) by Jason Myers of Dr. Jiangeng Xue's group in the University of Florida Department of Materials Science and Engineering.

Optical Characterization

Ultraviolet-visible absorption spectra were acquired using a Varian-Carey 50 Bio spectrophotometer. Photoluminescence measurements were performed on a Jobin-Yvon Fluorolog 3 spectrophotometer. All absorption spectra were carried out in standard 1 cm² cuvettes. The emission spectra of thin films were done in THF solutions outgassed by argon for at least 20 min. For thin films, the fluorimeter was fitted with a custom made slide holder that positioned the slide perpendicular to the excitation beam, and all thin film data was gathered with the instrument in front face mode. This detection geometry was necessary to prevent the detection of evanescent light. All absorption and emission measurements were taken three times per film and averaged.

Phosphorescence lifetimes were obtained using the time correlated single photon counting technique (TCSPC) with a PicoQuant FluoTime 100 Compact Fluorescence Lifetime Spectrophotometer. Excitation was achieved using a UV pulsed diode laser (λ_{max} 375 nm, P <10 mW). The laser was pulsed using an external BK Precision 4011A 5 HMz function generator. Decays were obtained from air saturated films using PicoQuant PicoHarp software. All decays were observed near the phosphorescence maximum using a bandpass filter (CWL 550

nm, FWHM 70 nm). Indirect excitation of the bandpass filter was minimized, not eliminated, using the setup described in Figure 2-18. The slide was placed in a square fluorescence cuvette (C) with the film facing the detector. In this setup, the excitation light, B, is reflected to the walls of the sample chamber (A), or transmitted through the slide, E. The phosphorescence, F, was first passed through a 450 nm long pass filter, G, to further remove scattered excitation light and most pPtPh fluorescence. It was then passed through a 550 ± 35 nm bandpass filter and into the detector.

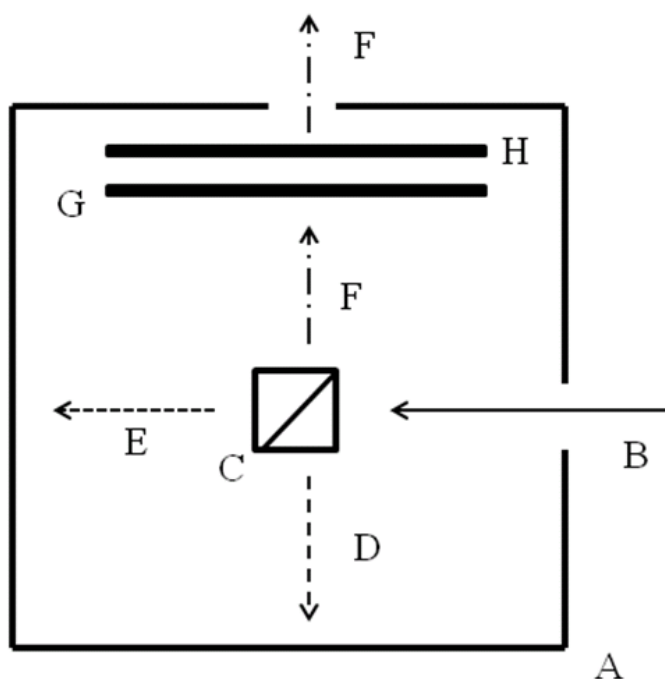


Figure 2-18. Diagram describing the sample chamber configuration used to collect time correlated single photon counting decays. A) The walls of the sample chamber. B) The excitation light. C) A standard fluorescence cuvette with sample film. D) Reflected excitation light. E) Transmitted excitation light. F) Phosphorescence entering the detection optics. G) A 450 nm long pass filter. H) A 550 ± 35 nm bandpass filter.

Triplet lifetimes were calculated using PicoQuant FluoFit software. No scattering sample was used because the decays were significantly longer than the instrument response. Residual emission from the filters or glass substrate was still detected, so all curve fitting began 20 ns after

time zero to negate this emission. The “tailfit” curve-fitting model (Equation 2-13) was used to estimate the triplet lifetimes, where $I(t)$ is the number of counts at a given time, t , A is the pre-exponential factor and τ is the excited state lifetime.¹²³

$$I(t) = \sum_{i=1}^n A_i e^{-\frac{t}{\tau_i}} \quad (2-13)$$

The number of exponentials of the fit, n , representing different components of the average lifetime, were systematically increased until the error estimation parameter, reduced chi-squared, was $0.8 \leq \chi^2_{\text{red}} \leq 1.8$. A χ^2_{red} value of 1.0 is optimal and represents the minimum amount of error. Pristine pPtPh films were adequately characterized with a single exponential model. It was found that as the amount of pPtPh triplet quenching increased, the number of exponential terms needed to fit the decay data increased. When a multi-exponential model was used to fit the data, the average triplet lifetime was calculated by weighting the component lifetime by its amplitude at time zero, the so-called “amplitude weighted” average lifetime.

Film Thickness Measurements

Step-height atomic force microscopy (AFM) was used to create film thickness calibration plots for the donor layer thickness in TOF measurements. Four sets of three films were spin-coated using the previously described procedure, except no acceptor was added to the casting solution; instead, equal aliquots of the pPtPh solution were added to all twelve vials. Films with a range of film thicknesses were achieved by adding increasing amounts of DCM to each set of casting solutions. Three films were spin-coated from equal concentration casting solutions and their absorption spectra recorded. A razor was lightly run across the middle of each film to create a slit along the long axis of the substrate. Using a Veeco diInova AFM in tapping mode, one $1600 \mu\text{m}^2$ image containing the razor slit and the polymer film was obtained. For each film,

three such images were taken every 0.33 inches apart. From each image there were three randomly selected scan lines. For each scan line, the change in z-scale from the bottom of the slit to the top of the polymer film was taken to be the film thickness of that area. In all, each individual film had nine thickness measurements made. These thicknesses were averaged and plotted versus the average absorbance for each film. A sample calibration plot is shown in Figure 2-19. To determine the donor layer thickness for TOF measurements, a section of pristine film was identified and its absorption measured. Using Figure 2-19, the slope of the calibration plot was used to calculate the film thickness from the optical absorbance of the film.

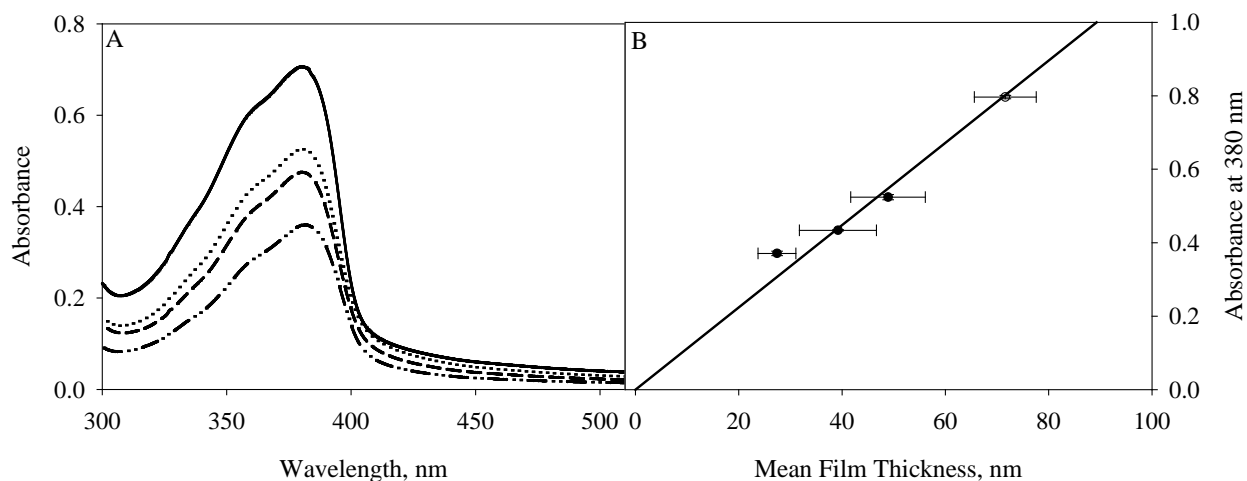


Figure 2-19. Thickness-absorption relationship for pPtPh films. A) Optical absorption spectra for variable thickness, pristine pPtPh films. B) Their corresponding thickness determined by step height atomic force microscopy. Vertical and horizontal error bars represent the ranges of absorbance and film thickness, respectively, measured for each set of three films.

Time of Flight Curve Fitting Procedures

MatLab M-Files were written to calculate L_D from the TOF data. Equation 2-10 can be used to convert L_D to D . The texts of the M-Files are given below. Copying these into the M-file editor of MatLab will enable their use. To use them, calculate the lifetime quenching using Equation 2-14, where Q is the lifetime quenching, τ_0 is the lifetime of an unquenched film and τ

is the lifetime of a quenched film. This data is entered into the command line in the following form $Q=[\text{value 1 value 2} \dots \text{value n}]$. Next, enter the thicknesses of the films in the following manner: $L=[\text{value 1 value2} \dots \text{value n}]$, with each thickness in nanometer units. In Matlab parlance, the Q and L data should be entered as *column vectors*.

$$Q=1-\frac{\tau}{\tau_0} \quad (2-14)$$

After the data has been entered, issue the command `quenching(Q,L)` to estimate the exciton length of diffusion. Here is the text of this M-File.

```
function QuenchEff=quenching(Q,L)
% This computes the length of diffusion, Ld, given the percent quenching Q
% and the film thickness L. Enter the experimental data as column vectors
% (1-by-xx). Use this function by typing quenching(Q,L) in the command line
% after the variables are entered. Equation from J. Phys. Chem. B. 2009, 113, 9104.
x=L';
y=Q';
f=fittype('(Ld/L*tanh(L/(Ld)))','independent','L','coefficients','Ld');
QuenchEff=fit(x,y,f);
```

Next, enter the returned value of L_D using the command, `Ld=value` and call the next M-File by entering `plotQuenchEff(Q,L,Ld)`. This will return an estimate of the quenching data using the fitted L_D .

```
function Qpredict=plotQuenchEff(Q,L,Ld)
% This predicts the quenching efficiency, Qpredict, given the quenching Q,
% film thickness L, and Length of Diffusion, Ld. Type plotQuenchEff(Q,L,Ld)
% in the command line to use this function. To calculate the error,
% type [h,p,stats]=chi2gof(ans,'expected',Q) in the command line. A
% chi2stat=0 is optimal.
Qpredict=(Ld./L.*tanh(L./(Ld)));
plot(L,Q,'o',L,Qpredict,'-');
```


CHAPTER 3 SINGLET EXCITON DIFFUSION IN LBL THIN FILMS

Introduction

Among the methods of constructing organic thin films, such as the Langmuir-Blodgett, spin-coating, and thermal deposition methods, layer-by-layer self assembly (LbL) is by far the simplest and least expensive. Films are constructed using the LbL method by alternately immersing a substrate into beakers containing water-soluble electrolytes.¹²⁴ These polymers are capable of noncovalently interacting with each other through hydrogen bonds or electrostatic interactions, for example.^{16,17} Control of film thickness depends on a number of factors,^{19,27,125-128} chief among them being the number of dipping cycles; for thick films, use a large number of dipping cycles and for thinner films, use fewer dipping cycles. Films built with the LbL technique can have thicknesses anywhere from less than 2 nm to more than 45 nm.^{24,129} Figure 1-3¹⁸⁻²¹ gives a few examples of polyelectrolytes used for LbL deposition; molecules 1-5, 1-6, and 1-10 can form hydrogen bonded films depending on the solution pH, while the rest can form electrostatic films. As mentioned in Chapter 1, LbL films have applications ranging from the biochemical to the electronic.¹³⁻¹⁵

Two mechanisms of LbL film growth have been identified. Lavallo suggested a non-linear relationship between bilayer number and film thickness,²¹ while Furlong studied a mechanism that involves a linear relationship between the two.²⁹ Although not the sole factor, Lavallo suggested that the relationship of bilayer number to film thickness is governed mainly by the ability of polyelectrolytes to diffuse within the thin film. Using a technique called fluorescence recovery after pattern photobleaching (FRAPP), Lavallo measured the interlayer diffusion coefficient of charged biological polyelectrolytes in an electrostatic LbL film to be $0.05\text{-}1.0\text{ }\mu\text{m}^2\text{-s}^{-1}$.²¹ By monitoring the changes in an electrostatic LbL film using neutron reflectivity,

Schlenoff estimated the interlayer diffusion coefficient of charged synthetic polyelectrolytes to be $10^{-9} \mu\text{m}^2\text{-s}^{-1}$.¹³⁰ Lavalle studied LbL films built with biological polymers, while Schlenoff used synthetic polyelectrolytes, such as PDDA and PSS. On the basis of these measurements and others, Salomäki suggested biological molecules provide for a non-linear mechanism and synthetic polymers deposit with a linear mechanism.²⁸

The exponential buildup mechanism is governed by polyelectrolyte diffusion. Once deposited, a polyelectrolyte can diffuse into the interior of the film, allowing additional electrolyte to deposit in its place. During the deposition of the next polyelectrolyte, material is deposited on the outer layer, allowing the mobile electrolyte to re-diffuse to the outer layer of the film. This allows more polyelectrolyte to deposit on the film's surface. As the number of deposition cycles increases, the magnitude of this effect grows, resulting in a non-linear buildup of film thickness. If polyelectrolyte diffusion in the film is limited, a linear relationship between bilayer number and film thickness will develop.^{21,29}

In an effort to provide a satisfactory explanation as to why two layer buildup mechanisms exist for LbL films, Salomäki developed the β -parameter.²⁸ This parameter governs the magnitude of the film thickness increment for each polyelectrolyte layer. Qualitatively, β is a measure of the ability of polyelectrolytes to diffuse within a thin film; when the interlayer diffusion coefficient is high, so too will be β . This model suggests that all LbL films will tend to grow according to the exponential model, but the growth will be linear whenever interlayer diffusion is very slow.²⁸

As this discussion of interlayer polyelectrolyte diffusion might suggest, the actual structure of polyelectrolyte LbL films features a high degree of layer disorder; that is, polyelectrolyte diffusion (no matter how small) drives the ability of adjacent layers to mix (interpenetrate) with

previously deposited layers.^{24,128,131} This can result in a highly entangled mass of polymer, as shown in Figure 1-4B. The lack of long-range structural order has been studied with x-ray and neutron reflectometry.²²⁻²⁵ Reflectometry measurements such as these provide a way of probing the internal structure of thin films. In general, each change in film composition generates a new wave interference; analysis of these interference patterns gives insights into the degree of structural order in the film.²³ For most LbL systems studied, a lack of significant long-range structural order in the films was found, with some studies suggesting that polyelectrolyte interlayer diffusion disrupts structural order in the LbL film.^{24,25}

Studies where photo-active materials have been used as polyelectrolytes in building LbL films exemplify the effects of layer interpenetration. Electrostatic LbL films built using an anionic polythiophene (similar to molecule 1-14, Figure 1-5) and also using an anionic quinoline derivative (like molecule 1-16) with nonconjugated, cationic polymers as counterions, exhibited a systematic, linear decrease in photoluminescence intensity as the number of bilayers increased.^{132,133} In both cases, the thicknesses of the films were found to increase after each deposition cycle. Each cycle deposited more chromophore onto the film; a higher amount of chromophore should give a higher amount of photoluminescence. The observed decreases in photoluminescence intensities were attributed to the formation of aggregates between conjugated molecules. When conjugated molecules aggregate, the π -electron system of one molecule interacts with that of a second molecule to form a π -complex; a distinguishing feature of aggregates is a characteristic increase in the rate of nonradiative decay that lowers the intensity of photoluminescence.⁷² Aggregation in LbL films built from conjugated polyelectrolytes has been directly observed in atomic force microscopy (AFM) images.^{18,20,133,134}

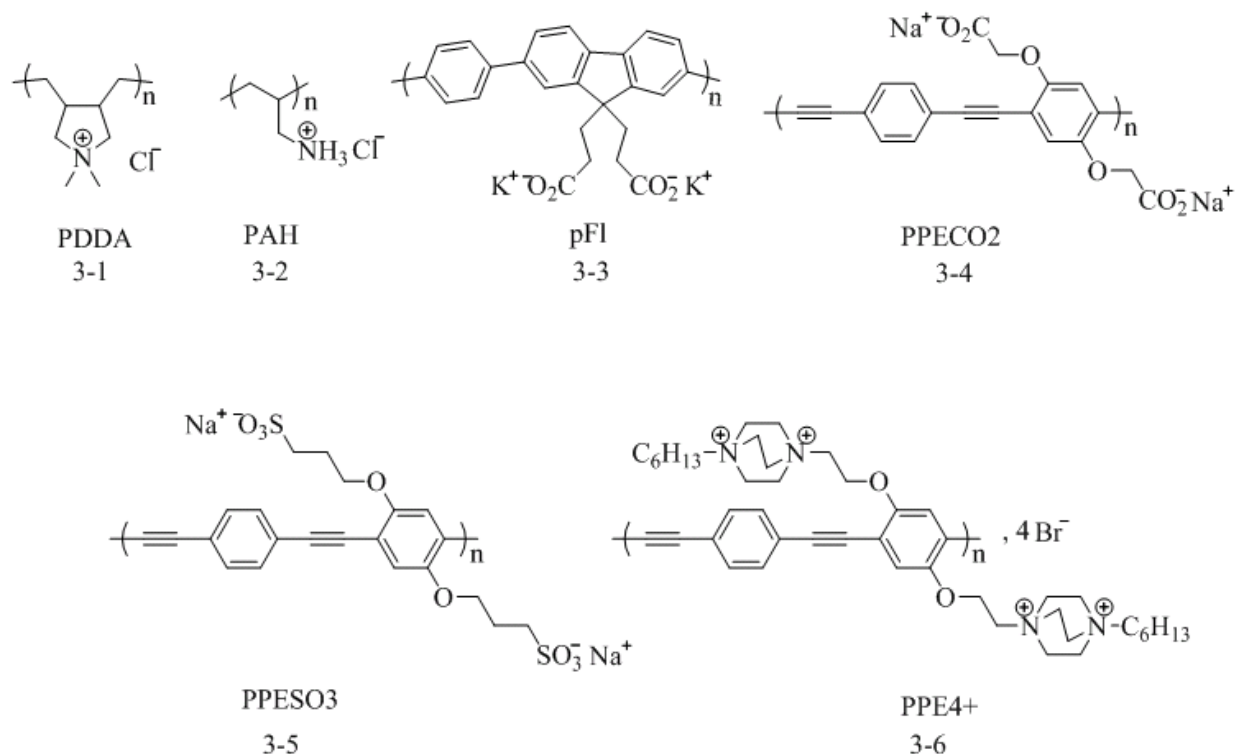


Figure 3-1. Structures of the polyelectrolytes used for electrostatic layer-by-layer self assembly.

The purpose of this study is three fold: to further probe the ability of conjugated polymers (CPs) to aggregate in LbL films, to develop a mechanism of CP aggregation, and to study the effects of CP aggregation on exciton diffusion in LbL films. To accomplish the first goal, the series of conjugated polyelectrolytes in Figure 3-1 will be used to construct electrostatic LbL films. The rigid, inflexible poly(phenylene ethynylene)s, exemplified by polymers 3-4, 3-5, and 3-6 will be used, as well as a rotationally flexible polyfluorene, exemplified by the water soluble polymer 3-3. The aliphatic polymers PDDA (3-1) and PAH (3-2) will be used as counter-polyelectrolytes. A mechanism of CP aggregation in LbL films will be established in order to further understand the formation of LbL films using CPs and to provide insight into how the aggregation can be disrupted. Lastly, the effects of film aggregation on exciton diffusion will be studied using time-of-flight techniques similar to those discussed in Chapter 2.

Synthesis and Characterization

The polymers poly(phenylene ethynylene carboxylate) [PPECO2], (3-4, Figure 3-1) and poly(phenylene ethynylene diazobicyclobutane) [PPE4+], (3-6, Figure 3-1) were made by Dr. Katsu Ogawa according to literature procedures.^{71,135} Dr. Bob Brookins and Dr. Quentin Bricaud prepared polyfluorene carboxylate [pFl] (3-3, Figure 3-1) according to the published procedure.¹³⁶ The aliphatic polyelectrolytes poly(diallyldimethylammonium chloride) [PDDA] (3-1, Figure 3-1) and poly(allylamine hydrochloride) [PAH] (3-2, Figure 3-1) are commercially available and used as received. The polymer poly(phenylene ethynylene sulfonate) [PPESO3], (3-5, Figure 3-1) was synthesized according to the published procedures, but since two ways to make PPESO3 were studied, the synthesis will now be discussed.^{116,137}

The synthetic scheme for PPESO3 is given in Figure 3-2. The polymer **3-5** was prepared using a Sonogashira polymerization between two symmetric monomers, 1,4-diethynylbenzene **3-10** and sulfonate monomer **3-11**. 1,4-Diethynylbenzene **3-10** was synthesized from a tetrabutylammonium fluoride (TBAF)-mediated deprotection of the trimethylsilyl (TMS)-protected monomer, **3-9** in 75% yield. This deprotection was typically performed immediately before polymerization and in a separate step, to prevent the monomer from decomposing. The TMS-protected diethynylbenzene **3-9** was prepared *via* the Sonogashira reaction between 1,4-diiodobenzene **3-7** and four equivalents of TMS-acetylene, **3-8**. Although only two equivalents of **3-8** are stoichiometrically needed, the volatility of the material necessitates the use of four equivalents.¹¹⁶

The sulfonate monomer **3-11** was synthesized in two ways, also depicted in Figure 3-2. In the first method developed by Schanze,¹¹⁶ para-dimethoxybenzene **3-12** was iodinated overnight in a refluxing mixture of sulfuric acid, acetic acid and water to afford **3-13** in a 49% yield after recrystallization from ethanol. The methoxy groups were removed through a reaction with boron

tribromide (BBr_3) at room temperature to afford diiodohydroquinone **3-14** as a neat product in 50% yield. The sulfonate monomer **3-11** was then synthesized through a ring-opening reaction with 1,3-propane sultone in a 94% yield.

The second synthesis of sulfonate monomer **3-11** was developed by Jin in 2006 as a “novel route” to the polymer, based on Schanze’s 2002 procedure.¹³⁷ In this method, 1,4-dihydroquinone **3-15** first underwent a ring-opening reaction with 1,4-propanesultone to give material **3-16** in a quantitative yield with no purification necessary; the product selectively precipitated from the reaction solution as it formed. This material was then subjected to iodination conditions nearly identical to that for **3-13**, affording the sulfonate monomer **3-11** in a 70% yield. This material also selectively precipitated from the reaction mixture as it formed, and no additional purification was necessary.

After synthesizing sulfonate monomer **3-11** using both procedures, it was determined that Jin’s procedure is the easiest procedure of the two. The first procedure requires the use of concentrated sulfuric and acetic acids that are refluxed overnight. To state the obvious, this is a very caustic mixture; furthermore, when a reaction containing iodine is refluxed, the reflux condenser can become clogged with sublimed iodine, possibly causing an explosion. The BBr_3 step to synthesize intermediate **3-14** is also dangerous. Boron tribromide is extremely sensitive to water, and forms hydrogen bromide gas as a decomposition product. This water sensitivity can greatly affect the yield of the reaction. The addition of BBr_3 to the reaction solution is very exothermic and even at dry ice/acetone temperatures, a rapid buildup of pressure in the reaction flask can form if the reactant is added too quickly.

Jin's procedure, on the other hand, starts directly with dihydroquinone, the deprotected version of dimethoxybenzene. Dihydroquinone is commercially available, and beginning with this starting material eliminates the BBr_3 reaction. The sulfonate material **3-16** also precipitates from the reaction mixture as it forms; in the workup, one only has to filter the reaction and wash with a little dioxane to give the neat product in a quantitative yield. The iodination step of this material does require heat, but not refluxing temperatures, decreasing the potential for an explosion. The sulfonate monomer **3-11** also precipitates as it forms, with only a little iodine as an impurity that can be easily removed. This is in contrast to the workup of **3-13**, which is almost insoluble in ethanol and other solvents; this material also cannot be separated using column chromatography due to its similar polarity to dimethoxybenzene **3-12**.

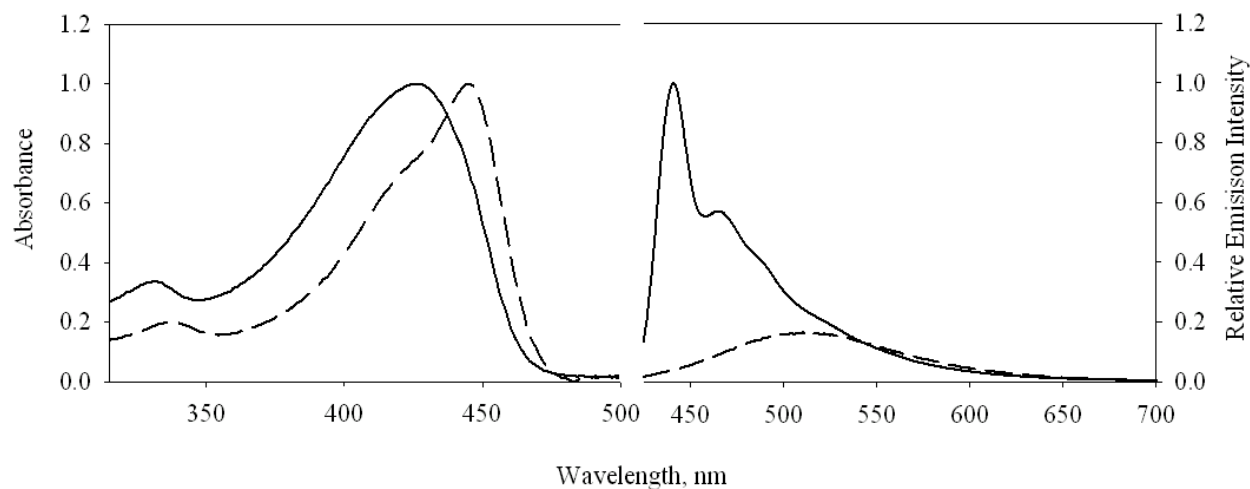


Figure 3-3. Absorption and emission spectra for PPESO3 in methanol (—) and water (---).

The polymer was mainly characterized by its solution optical absorption and emission spectra, as the solution photophysics of water-soluble CPs such as PPESO3 are very well understood.^{71,138} In addition, the polymerization reaction became extremely viscous with a strong, yellow color. Precipitating a sample of the reaction into acetone produced bright yellow-green fibers; these observations indicated that the monomers polymerized; had only oligomers

formed, the reaction would have formed a dust-like precipitate in acetone. The ultra-violet-visible absorption (UV-VIS) and photoluminescence (PL) spectra of the polymer in methanol and in water are shown in Figure 3-3. Both absorption spectra feature a π - π^* transition in the near-UV region, with the absorption maximum for the polymer in water red shifted by almost 25 nm from that of the polymer in methanol. The fluorescence of PPESO3 in methanol is centered near 450 nm and features two well defined, vibronic peaks. By contrast, the fluorescence spectrum of the polymer in water is broad, smooth and red-shifted from the PL spectrum in methanol by almost 100 nm.

The observed changes in the optical spectra have been attributed to aggregation of the polymer. The polymer is essentially an amphiphile: the backbone is nonpolar with polar sulfonate side groups that extend into the solvent, solubilizing the polymer. When dissolved in water, the rigid, relatively nonpolar, π -conjugated polymer backbones of several polymer chains undergo π - π stacking to minimize hydrophobic interactions. The sulfonate groups, being highly polarized, extend into the water to maximize hydrophilic interactions. When the resulting multi-polymer complex becomes photoexcited, excitation energy is able to be shared between multiple polymer chains, creating an excimer.¹³⁸ The emission spectra of excimers are characterized as being very broad, featureless, and with a low intensity, just like the PL spectrum of PPESO3 in water.⁷²

Results

LbL Films with Rigid Polyelectrolytes

For the purposes of LbL work, one bilayer is defined as one layer of a polycation and one layer of a polyanion. Using PDDA as a polycation and PPESO3 as a polyanion, LbL films on glass ranging from one to thirty bilayers in thickness were deposited from 0.10 mM solutions of both polyelectrolytes. The absorption and emission spectra for these films,

glass/[PDDA/PPESO3]₁₋₃₀, are given in Figure 3-4. Their absorption spectra feature a broad absorption maximum near 420 nm that appears constant throughout the range of bilayers studied. The absorbance of the films, although low, are observed to rise as the number of bilayers increases. For LbL films, a higher absorbance corresponds to a greater film thickness, as each added bilayer adds one more layer of chromophore to the film.

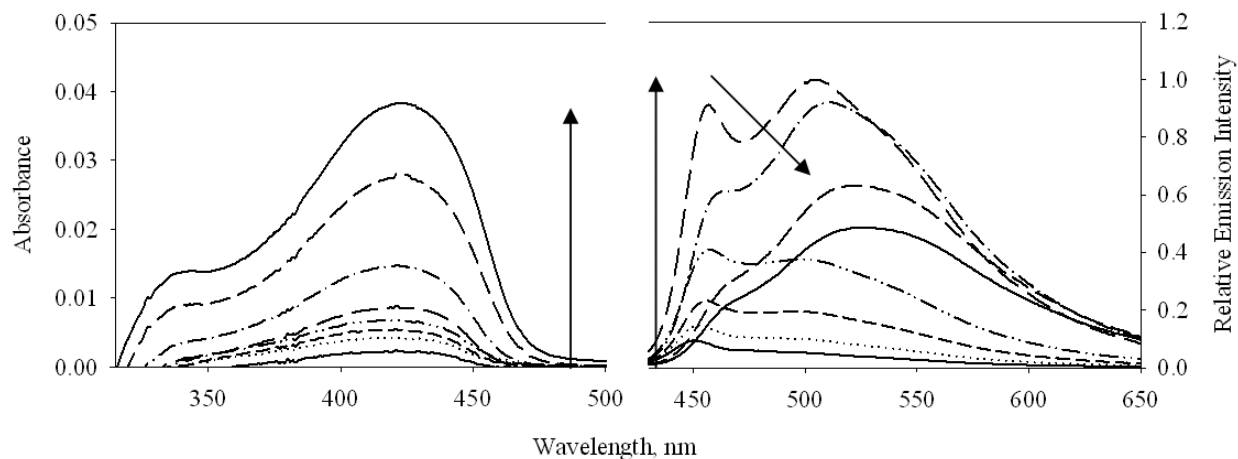


Figure 3-4. Absorption and emission spectra for glass/[PDDA/PPESO3]₁₋₃₀ LbL films: 1 bilayer (—), 2 bilayers (···), 3 bilayers (— —), 4 bilayers (— · —), 5 bilayers (— — —), 10 bilayers (— · —), 20 bilayers (— —), and 30 bilayers (—).

Unlike the absorption spectra, the fluorescence spectra of glass/[PDDA/PPESO3]₁₋₃₀ films are quite complicated. From one to five bilayers, the emission intensity of the films increase, followed by a decrease from ten to thirty bilayers. The PL spectra from one to five bilayers feature a narrow emission maximum near 450 nm. As the film thicknesses increase, a peak near 525 nm appears. This peak is significantly broader than the peak at 450 nm and is also smooth. As the number of bilayers increases to five, the intensity of both peaks reaches a maximum. After five bilayers, the peak at 450 nm begins to decrease in intensity; by thirty bilayers, this peak is almost completely gone, leaving the smooth, broad red-shifted peak at 525 nm. These data taken in conjunction with effects of solvent on the emission of PPESO3 (Figure 3-3) suggest that the polymer is able to form π -complexes in the LbL films. The complexes are

manifested in the fluorescence spectra as an excimer emission near 525 nm. As the number of bilayers increases, so too does the amount of PPESO3 added; the increasing amount of PPESO3 enables the formation of increasingly large aggregates that dominate the films' emission at high numbers of bilayers.

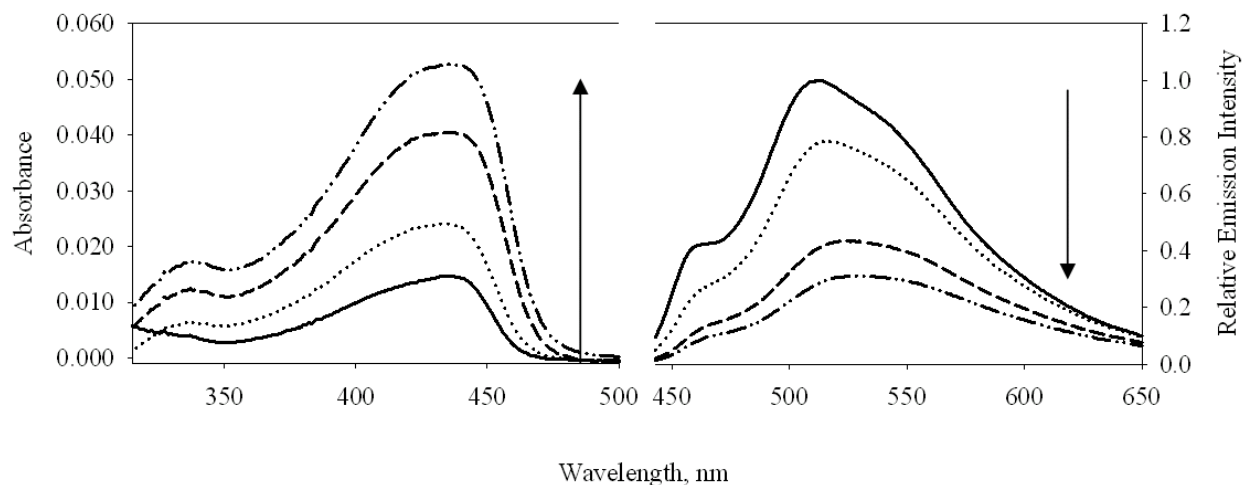


Figure 3-5. Absorption and emission spectra for glass/[PDDA/PPESO3]₅₋₃₀ LbL films deposited from methanol: 5 bilayers (—), 10 bilayers (···), 20 bilayers (— —), and 30 bilayers (— · —).

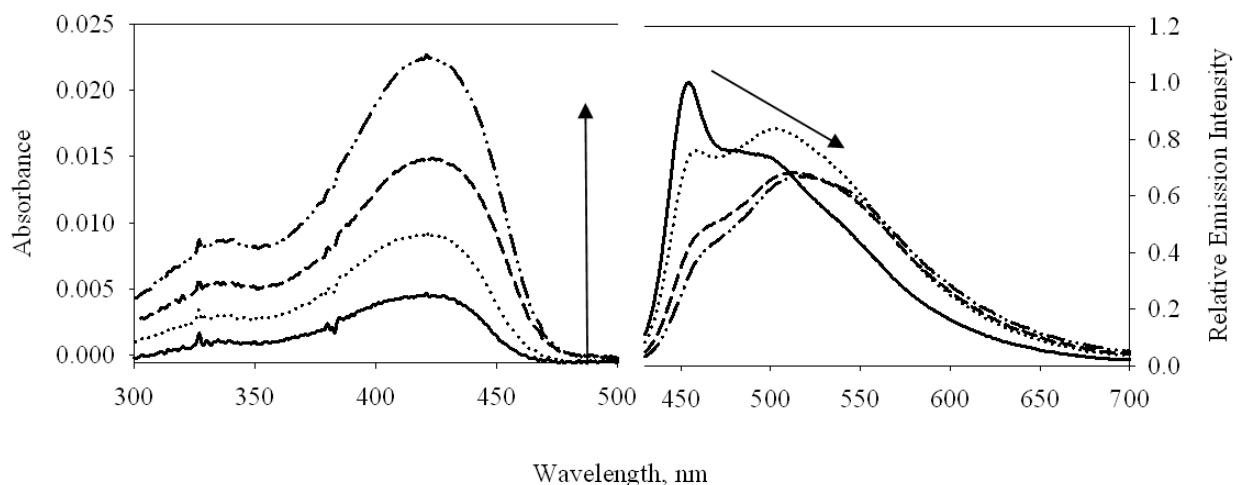


Figure 3-6. Absorption and emission spectra for quartz/[PDDA/PPESO3]₅₋₃₀ LbL films: 5 bilayers (—), 10 bilayers (···), 20 bilayers (— —), and 30 bilayers (— · —).

To test if these observations are unique to LbL films of the structure glass|[PDDA/PPESO3]₁₋₃₀, a series of systematically varied LbL films were also studied by absorption and fluorescence spectroscopies. The films in Figure 3-4 were deposited from water, a solvent known to induce aggregation of PPESO3. By contrast, the polymer is less aggregated in methanol, so glass|[PDDA/PPESO3]₅₋₃₀ films were deposited from methanol. The results are shown in Figure 3-5. These films show the same pattern: absorbance increases with the bilayer number, while the fluorescence spectra broaden and decrease in intensity. Changing the substrate from glass to quartz yielded similar results (Figure 3-6), as did several polyelectrolyte variations (Figures 3-7, 3-8, and 3-9). The age of the PPESO3 solution was also not an issue, as shown in Figure 3-10, which depicts the optical spectra of glass|[PDDA/PPESO3]₅₋₃₀ films made using freshly synthesized PPESO3. These observations indicate that the aggregation of rigid-rod CPs in LbL films occurs regardless of electrolyte combination, solvent, or substrate employed.

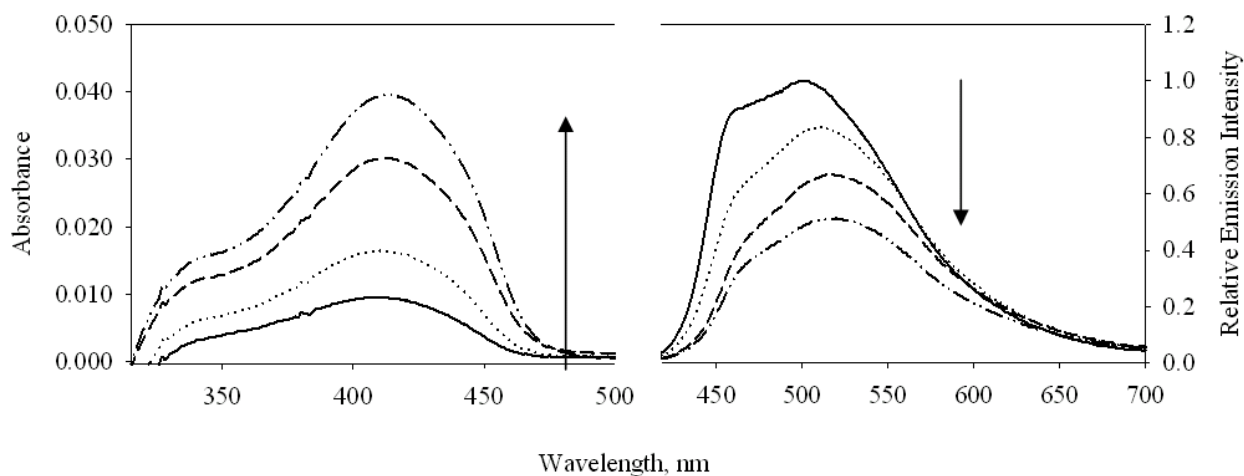


Figure 3-7. Absorption and emission spectra for glass|[PAH/PPESO3]₅₋₃₀ LbL films: 5 bilayers (—), 10 bilayers (···), 20 bilayers (— —), and 30 bilayers (— · —).

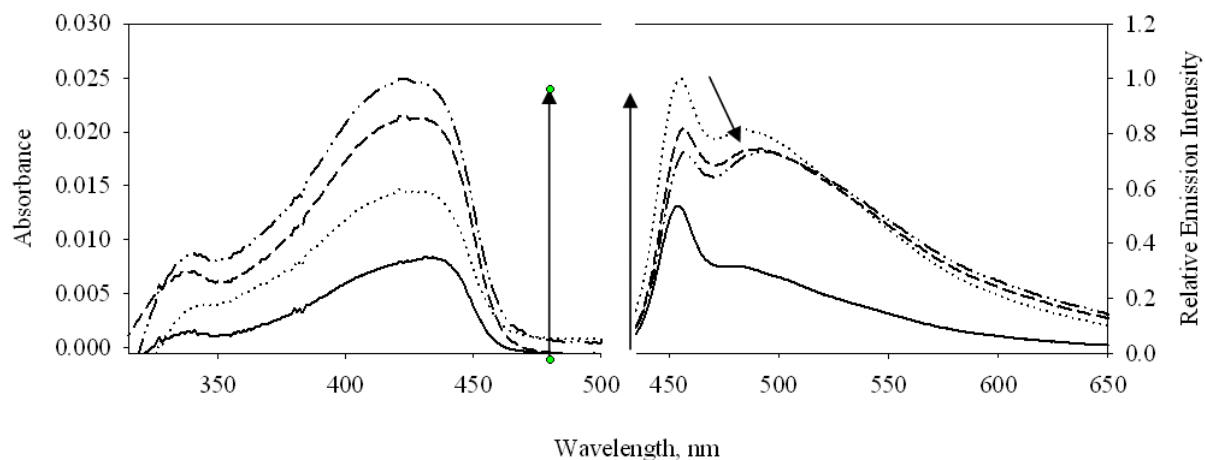


Figure 3-8. Absorption and emission spectra for glass[PDDA/PPECO2]₅₋₃₀ LbL films: 5 bilayers (—), 10 bilayers (···), 20 bilayers (---), and 30 bilayers (—·—).

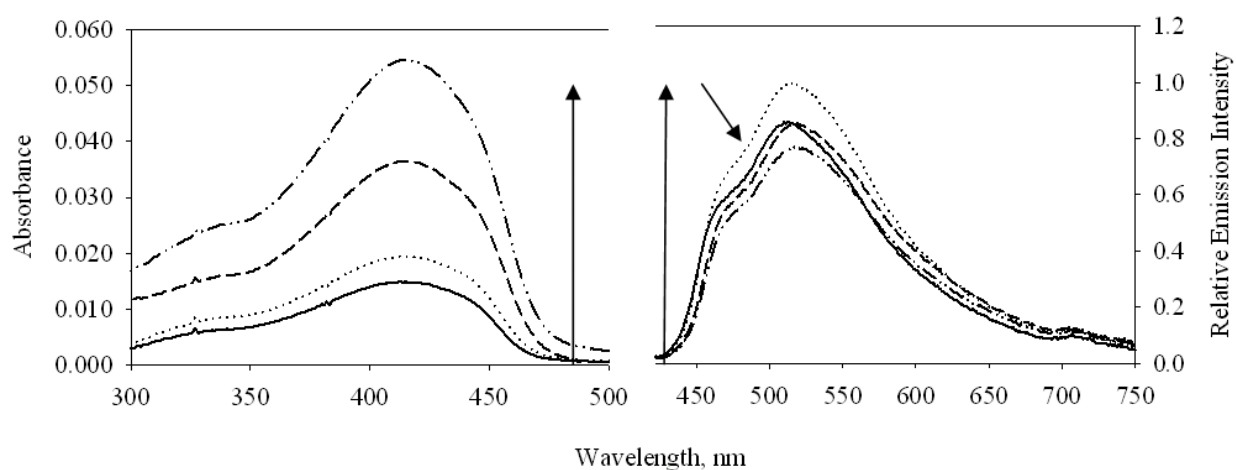


Figure 3-9. Absorption and emission spectra for glass[PPE4+/PPESO3]₅₋₃₀ LbL films: 5 bilayers (—), 10 bilayers (···), 20 bilayers (---), and 30 bilayers (—·—).

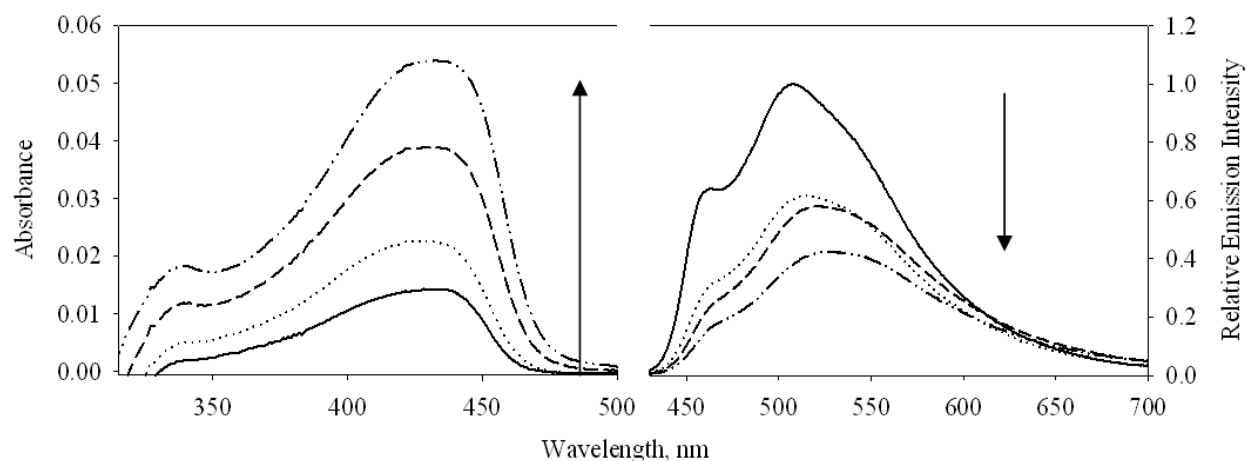


Figure 3-10. Absorption and emission spectra for glass/[PDDA/PPESO3]₅₋₃₀ LbL films deposited from freshly synthesized PPESO3: 5 bilayers (—), 10 bilayers (···), 20 bilayers (---), and 30 bilayers (-·-·).

If these LbL films are becoming increasingly aggregated as the number of bilayers increase, these aggregates should be able to be observed using tapping mode atomic force microscopy (AFM). As shown in Figure 3-11, glass/[PDDA/PPESO3]₅₋₃₀ LbL films do indeed show increased aggregation with increased numbers of bilayers. At five bilayers, the films are relatively flat with more or less interconnected domains of polyelectrolyte assemblies. The films appear to be slightly aggregated, as suggested by the presence of a few individual, round clumps of material. The mostly smooth appearance of this film, indicated by the small observed variation in the image's z-scale, would seem to suggest a mixture of unaggregated and aggregated polyelectrolyte. This is also suggested by the fluorescence spectra in Figure 3-4. The image of a ten bilayer film shows that the mostly interconnected polyelectrolyte assemblies of the five bilayer film are becoming more defined, with clear boundaries visible for the aggregated domains. The z-scale variation also increases from the five bilayer film, suggesting that these films are more aggregated than the five bilayer films. A sea of well defined, round aggregates only a few nanometers in size is plainly seen in the image of a twenty bilayer film. There is also a greater variation in the image's z-scale, suggesting a rougher film. For the thirty

bilayer film, the aggregates have become larger in size and the z-scale variation has increased, suggesting an even rougher film. The AFM images suggest that as the number of bilayers increase, LbL films using rigid rod CPs become increasingly aggregated. This further lends evidence to the hypothesis that CP aggregation in the film is the cause of the decreased PL intensities of Figures 3-4-3-10. Other researchers studying LbL films built from conjugated polyelectrolytes have used similar AFM results to explain the decrease in PL intensity they observed at high numbers of bilayers.^{132,134}

LbL Films Using a Flexible Polyelectrolyte

Just as with PPESO3 and other poly(phenylene ethynylene)s, pFl (3-3, Figure 3-1) also has solvent-dependent absorption and emission spectra, demonstrated in Figure 3-12A. When dissolved in tetrahydrofuran (THF), the UV-VIS spectrum is broader than when the polymer is dissolved in methanol or water. In addition, the fluorescence maximum of pFl in THF is red-shifted by almost 25 nm, compared to the fluorescence maxima of pFl in methanol and water. The red-shifting of the polymer's emission maximum in THF, as well as its broadened absorption spectrum, indicate that THF is a poor solvent for pFl. These changes are likely due to the formation of pFl aggregates and not because of solvent effects on the 0-0 transition energy.⁷² Aggregates of polyfluorene would not be manifested through excimer emission. In polyfluorenes, the sigma bonded backbone allows aromatic moieties in the repeat units to rotate. This rotation has been demonstrated to cause polyfluorenes to form sheet-like complexes where the torsion angle of the repeat units causes the aggregated polymers to pack less efficiently, preventing the formation of excimers.^{72,139,140} Rather, the only manifestation of the aggregate is a lowering of the excited state energy of the polymer.⁷²

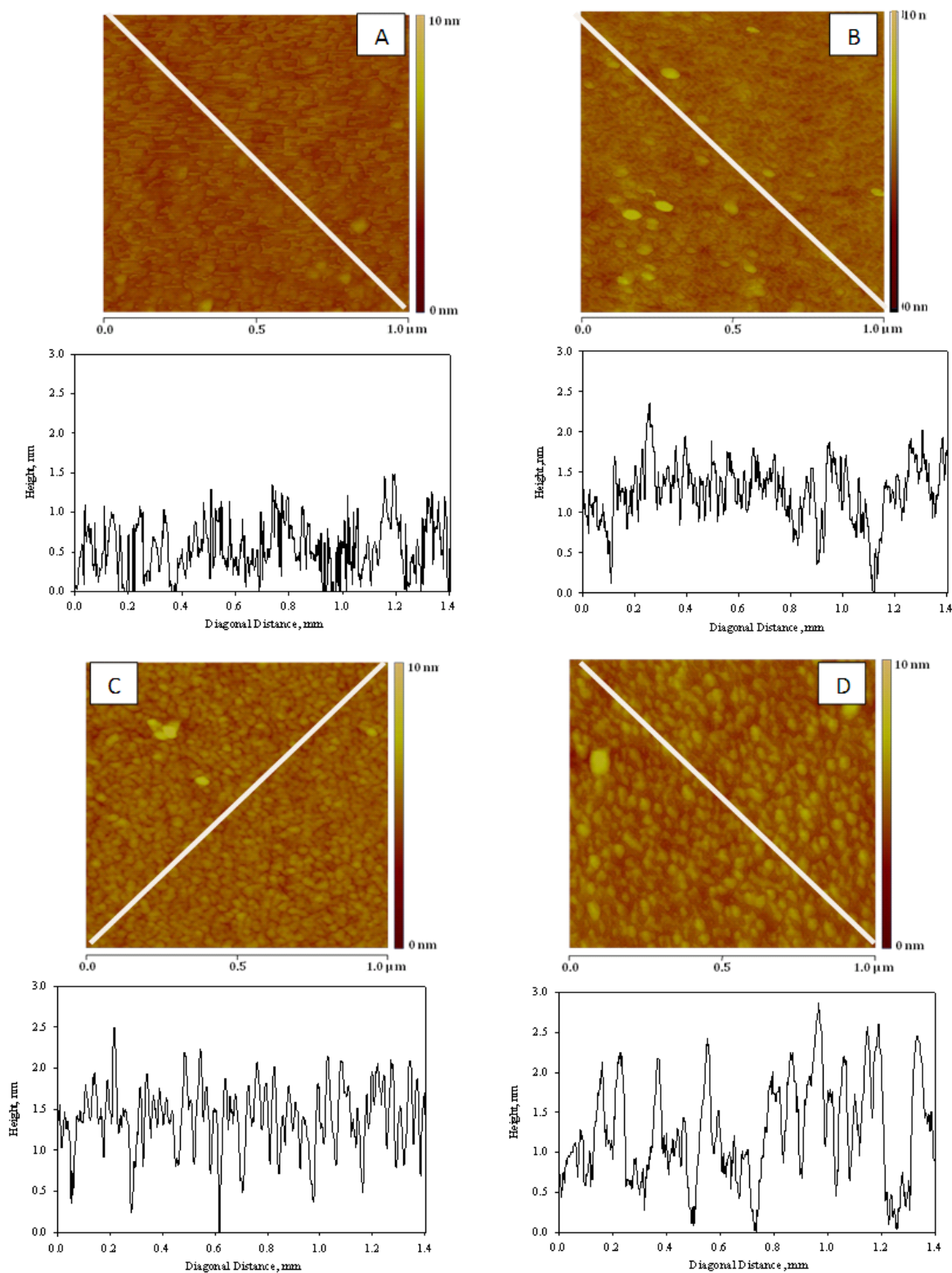


Figure 3-11. Tapping mode AFM images of glass/[PDDA/PPESO3]₅₋₃₀ LbL films. A) 5 bilayers (roughness 0.365 nm). B) 10 Bilayers (roughness 0.410 nm). C) 20 Bilayers (roughness 0.471nm). D) 30 Bilayers (roughness 0.598 nm).

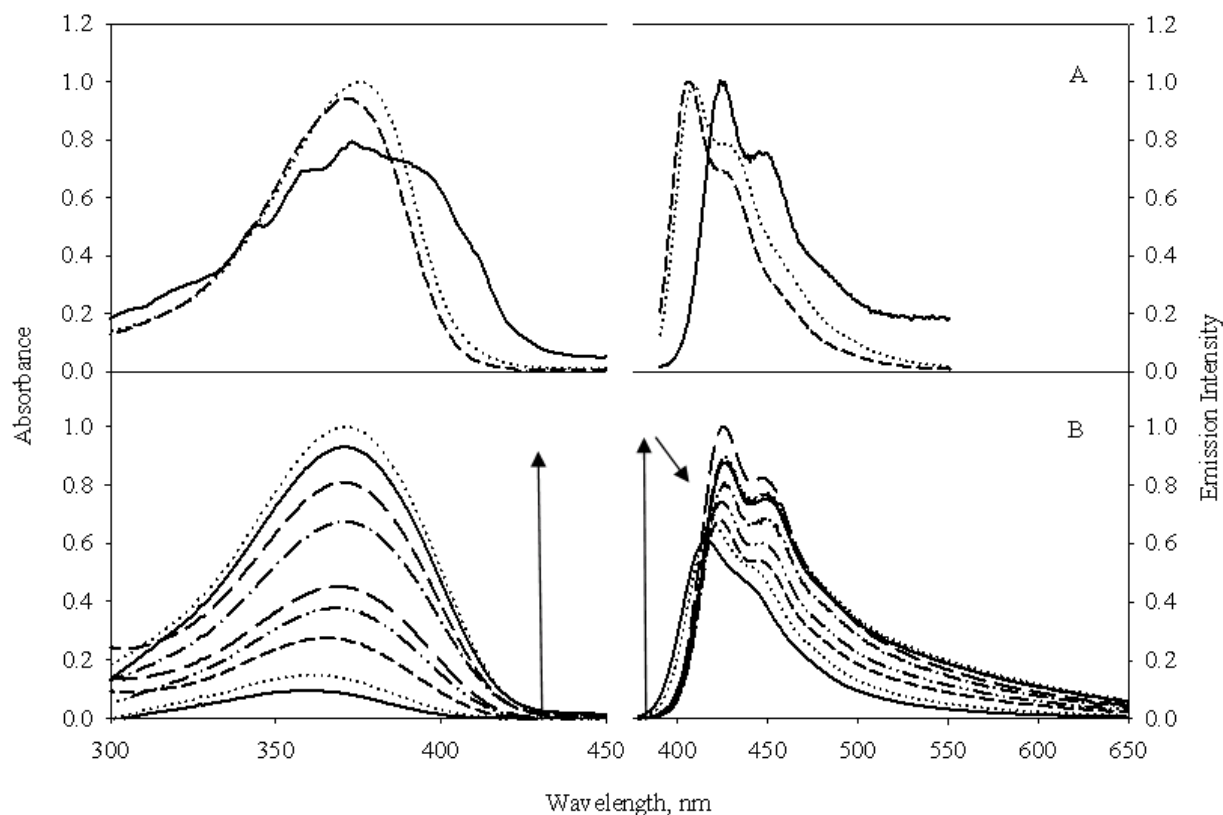


Figure 3-12. Absorption and emission spectra for pFl. A) pFl in water (---), methanol (···), and THF (—). B) glass/[PDDA/pFl]₂₋₃₀ LbL films: 2 bilayers (—), 4 bilayers (···), 6 bilayers (---), 8 bilayers (— · —), 10 bilayers (— —), 15 bilayers (— · —), 20 bilayers (— · —), 25 bilayers (— · —), and 30 bilayers (···).

When LbL films are made from 0.10 mM solutions of pFl and PDDA in water, the results in Figure 3-12B are obtained. From two through thirty bilayers, the absorbance of each film systematically increases, along with a slight red shift in the absorbance maximum. The emission spectra of the films increases as expected from two through ten bilayers. After two bilayers, a slight red-shift in the fluorescence maximum is observed that remains constant throughout all of the films. From fifteen to thirty bilayers, the fluorescence intensity begins to decrease. These observations are consistent with the aggregation of pFl in LbL films. Initially, the aggregates are only manifested as a red-shifting of the fluorescence maximum. The fluorescence intensity continues to increase, suggesting that the extent of aggregation is minimal. After ten bilayers the

aggregation increases, causing an increase in the rate of non-radiative pFl decay that lowers the fluorescence intensities of the films.⁷²

The Source of the Aggregates

It has been shown that CPs can aggregate in solution (Figures 3-3 and 3-12A), depending on the solvent. For poly(phenylene ethynylene)s, water has been shown to be a so-called “poor” solvent: one that allows the polymer to aggregate.¹³⁸ Since most of the LbL films discussed have been deposited using aqueous polyelectrolyte solutions, the possibility exists that polymer aggregates, formed in solution, deposit directly onto the film. Along this line, a thirty bilayer film will be strongly aggregated because it has been exposed to the deposition solutions longer, allowing more aggregates to deposit than in any other film. The AFM data in Figure 3-11 clearly indicate that the size of the aggregates in LbL films grow in size with time. If the aggregates are deposited solely from solution, the size of the aggregates in the deposition solution should also grow with time.

To determine if the aggregates are deposited from the deposition solutions, separate, time-dependent, room temperature aggregation studies were performed on PPESO3 dissolved in water and in methanol. At the beginning of the experiments, the stock solution of PPESO3 was diluted to 0.10 mM. An aliquot of this stock solution was obtained and its solution absorption and emission spectra recorded. Since this aliquot was taken from a freshly diluted deposition solution, this aliquot was defined as the time zero solution sample. A five bilayer film was then deposited onto glass with PDDA acting as a counter-ion. This film was deposited from freshly diluted deposition solutions, so the spectra of this film were defined as the time zero film sample. Afterwards, both the PPESO3 and PDDA deposition solutions were left standing at room temperature for a total of 32 hours. Every 8 hours during this period, an aliquot of the PPESO3 solution was taken, and its absorption and emission spectra recorded. Additionally, a five-

bilayer glass|[PDDA/PPESO3] film was constructed every 8 hours from the deposition solutions. By monitoring the changes in the solution absorption and emission spectra of PPESO3 over time, any changes in the extent of solution aggregation can be observed. Similarly, by monitoring the absorption and emission spectra of PPESO3 in an LbL film where it is the only chromophore, the extent of aggregation in the film as a function of deposition solution age can be determined.

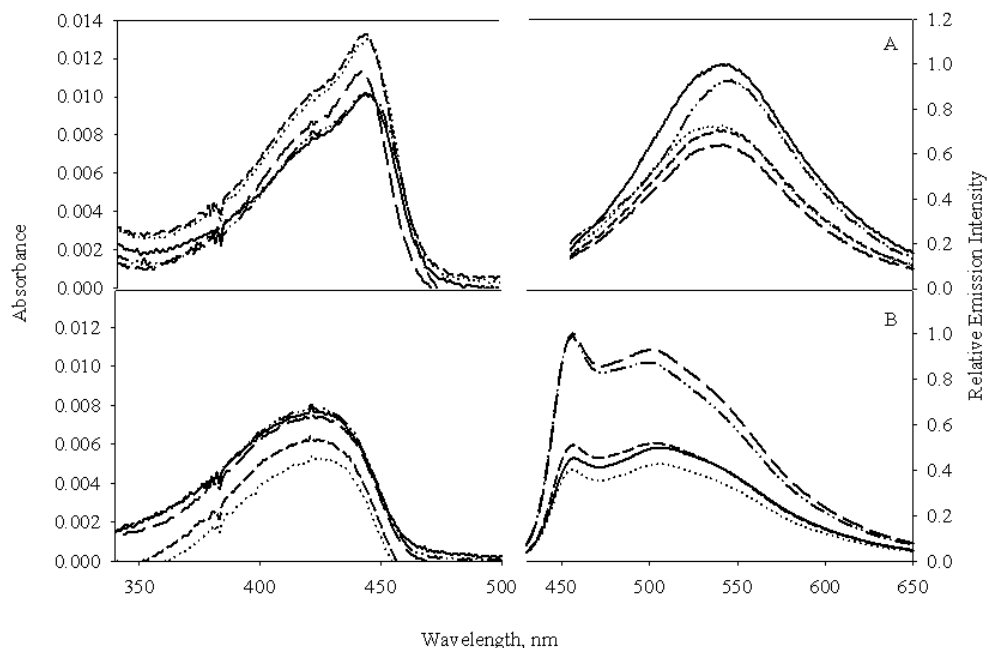


Figure 3-13. Time dependent absorption and emission spectra for PPESO3 aggregation in water. A) The PPESO3 deposition solution after 0 hours (—), 8 hours (···), 16 hours (---), 24 hours (— · —), and 32 hours (— —) at room temperature. B) A 5 bilayer glass|[PDDA/PPESO3] LbL film after 0 hours (—), 8 hours (···), 16 hours (---), 24 hours (— · —), and 32 hours (— —) at room temperature.

The results for the time dependent aggregation study for PPESO3 in water are shown in Figure 3-13. The solution absorption spectra (Figure 3-13A) feature a π - π^* transition centered near 450 nm, while the emission spectra are broad and featureless with maxima located around 550 nm. These spectra indicate that PPESO3 is almost completely aggregated in the aqueous deposition solution. Close inspection of Figure 3-13A will further reveal that there is no real correlation between the time that the deposition solution spent at room temperature and the

extent of PPESO3 aggregation; the intensity of the fluorescence and absorption spectra randomly fluctuate with time. If the sizes of the polymer aggregates were growing with time, the intensity of the emission spectra should decrease with time: as the sizes of the aggregates grow, the rate of non-radiative decay increases, decreasing the fluorescence quantum yield. Such is not the case, indicating that the sizes of PPESO3 aggregates in solution vary little over time.

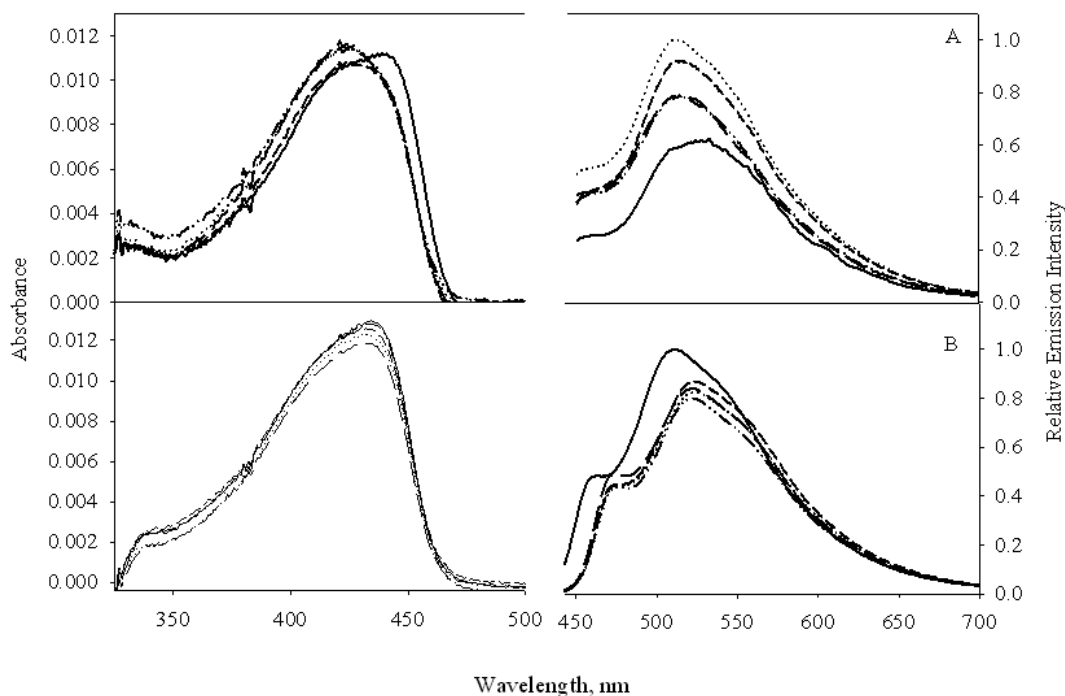


Figure 3-14. Time dependent absorption and emission spectra for PPESO3 aggregation in methanol. A) The PPESO3 deposition solution after 0 hours (—), 8 hours (···), 16 hours (---), 24 hours (----), and 32 hours (— · —) at room temperature. B) A 5 bilayer glass/[PDDA/PPESO3] LbL film after 0 hours (—), 8 hours (···), 16 hours (---), 24 hours (----), and 32 hours (— · —) at room temperature.

The absorption and emission spectra over time for a five bilayer glass/[PDDA/PPESO3] LbL film are shown in Figure 3-13B. The absorption spectra are rather broad with a maximum centered close to 425 nm. The emission spectra feature a narrow peak near 450 nm and a much broader peak around 515 nm. From earlier experiments, it has been established that the peak at 450 nm corresponds to unaggregated polymer, while the peak at 515 nm corresponds to aggregated PPESO3. Although there is an increase in the fluorescence intensity with time, the

intensity ratios of the peak at 450 nm to the peak at 515 nm appear relatively constant. This would suggest that the extent of PPESO3 aggregation in an LbL film is constant over time. If these aggregates are solely deposited from solution, the extent of aggregation in the five bilayer sample films should also increase with time, manifested as lower intensity emission spectra. This is not the case, indicating that the source of increasingly large aggregates in the LbL films is not from the deposition solutions.

Repeating these time-dependent aggregation experiments with the polymers dissolved in methanol gives the same results, as shown in Figure 3-14. The time-dependent methanol solution spectra (Figure 3-14A) show no change in either the extent of aggregation or in the size of the aggregates with time. More importantly, the time-dependent emission spectra (Figure 3-14B) of five bilayer glass|[PDDA/PPESO3] films deposited from methanol show a significant amount of aggregation that is very constant over time. It has been shown (Figure 3-3) that methanol does not allow PPESO3 to appreciably aggregate in solution. Thus it is not possible for any meaningful aggregates to be deposited directly from a methanol deposition solution. It follows that the film itself is the source of the aggregation, possibly through a rearrangement of the polyelectrolytes post-deposition, as has been suggested by Johal.¹⁴¹

Time of Flight Measurements

The theory of time-of-flight (TOF) measurements is discussed extensively in Chapter 2 and will not be explained in detail here. Essentially, TOF measurements are a way of determining the ability of excitons to diffuse within a thin film by layering an acceptor (exciton quenching) layer on top of an exciton donating (polymer) layer, typically on a glass substrate (see Figure 2-2). The magnitude of exciton quenching as a function of donor layer thickness is measured. By applying mathematical models to the quenching data obtained, the exciton diffusion coefficient, D , and the mean exciton length of diffusion, L_D , can be obtained.⁸⁴

For LbL films, TOF measurements will be carried out using indium-tin oxide (ITO) as an electron-accepting quencher with [PDDA/PPESO3] bilayers acting as a donor. In organic electronic applications, ITO is routinely used as a hole injector; in other words, it is used to accept electrons from excited organic donors as part of an electrical circuit.¹⁴² The surface of ITO can be regarded as a combination of positively charged metal atoms and negatively charged oxygen atoms, making ITO a versatile substrate for electrostatic LbL films.^{142,143} A series of glass|ITO|[PDDA/PPESO3] LbL films one through thirty bilayers thick were constructed. In these films, PPESO3 became photoexcited. Lacking metal atoms to promote intersystem crossing, the PPESO3 excitons were mainly singlets. They diffused throughout the film *via* Förster transfer. Upon reaching the first bilayer (built directly on ITO), the excitons were quenched by electron transfer to ITO. The effect of bilayer number (film thickness) on the fluorescence intensity of each film was measured, and the results are shown in Figure 3-15.

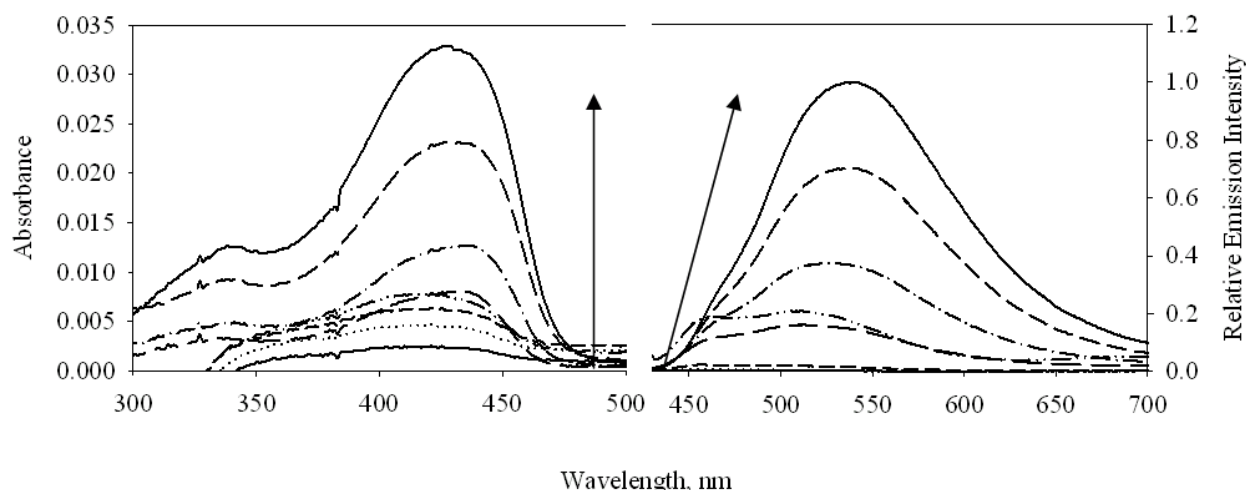


Figure 3-15. Absorption and emission spectra for ITO|[PDDA/PPESO3]₁₋₃₀ LbL films: 1 bilayer (—), 2 bilayers (···), 3 bilayers (---), 4 bilayers (— —), 5 bilayers (— · —), 10 bilayers (— · — ·), 20 bilayers (— · — · —), and 30 bilayers (— · — · — ·).

The absorption spectra show increasing absorbance with increasing numbers of bilayers, indicating a systematic increase in film thickness. The fluorescence spectra for

glass|ITO|[PDDA/PPESO3] films one, two and three bilayers thick are extremely weak, indicating a substantial amount of exciton quenching. The fluorescence intensity jumps at four bilayers and increases thereafter. The sudden, drastic increase in the fluorescence intensity from three to four bilayers indicates that films of this thickness could be the upper limit of PPESO3 singlet exciton diffusion in LbL films; after three bilayers, the lifetime of the singlet exciton is shorter than the time necessary for it to diffuse to the quenching layer. The shapes of the fluorescence spectra also change. For films of five or fewer bilayers, the films are a combination of unaggregated and aggregated polymers, indicated by the transitions at 450 nm and 515 nm, respectively. After five bilayers, the films become increasingly aggregated and by thirty bilayers, the fluorescence of the films is dominated by excimer emission.

Discussion

Mechanism of Film Deposition

Layer-by-layer self assembled thin films can exhibit either linear or nonlinear film growth. When interlayer polyelectrolyte diffusion is sufficiently high, polymers can deposit and diffuse to the interior of the film, allowing more electrolyte to deposit in its place. During deposition of the counter-polyelectrolyte, the polymer is able to re-diffuse to the outermost layer. This increases the amount of counter-electrolyte deposited, resulting in a nonlinear film thickness buildup.^{21,28,29}

Analysis of the maximum absorbance versus bilayer number for glass|[PDDA/(pFl or PPESO3)] indicates that these films exhibit a linear growth mechanism, as shown in Figure 3-16. The data can be fit reasonably well using a standard linear regression. The linear buildup mechanism suggested by Figure 3-16 suggests that interlayer polyelectrolyte diffusion in these LbL films is very small, perhaps on the order of $10^{-9} \mu\text{m}^2\text{-s}^{-1}$.¹³⁰ Strong electrostatic interactions and film aggregation are possible causes for the linear buildup model. Films where the nonlinear

buildup mechanism was found to predominate were primarily biological in nature, consisting of polymers such as proteins and carbohydrates.^{21,28,29} Proteins are widely known for the unique conformations they form. These conformations could be screening the charges of the polymers, lessening the number of charges available for electrostatic self assembly and decreasing the strength of the ionic bonds thus formed. Weaker electrostatic bonds would result in an increased ability for the polymers to diffuse within the film. By contrast, π -conjugated polymers have a significantly lower ability to rotate and fold on themselves, creating much stronger ionic bonds. Furthermore, the polymers have been shown to undergo π -stacking in the solid state. These macromolecular aggregates can be expected to have a very low diffusion coefficient, making the possibility of interlayer diffusion even less likely.

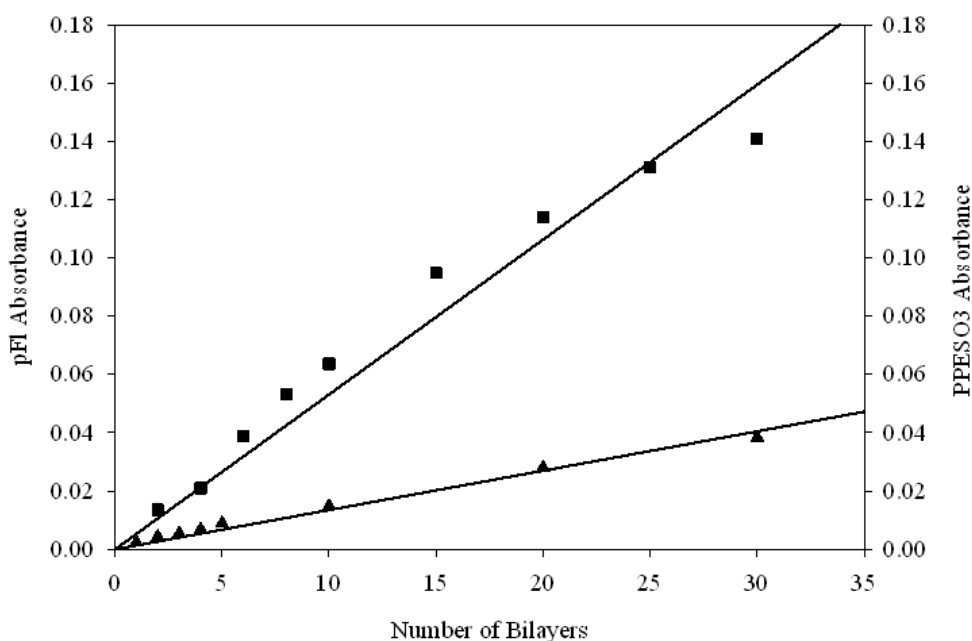


Figure 3-16. Maximum absorbance versus number of bilayers for glass|[PDDA/pFl] films (rectangles) and glass|[PDDA/PPESO3] films (triangles). The solid lines are fits from a linear regression.

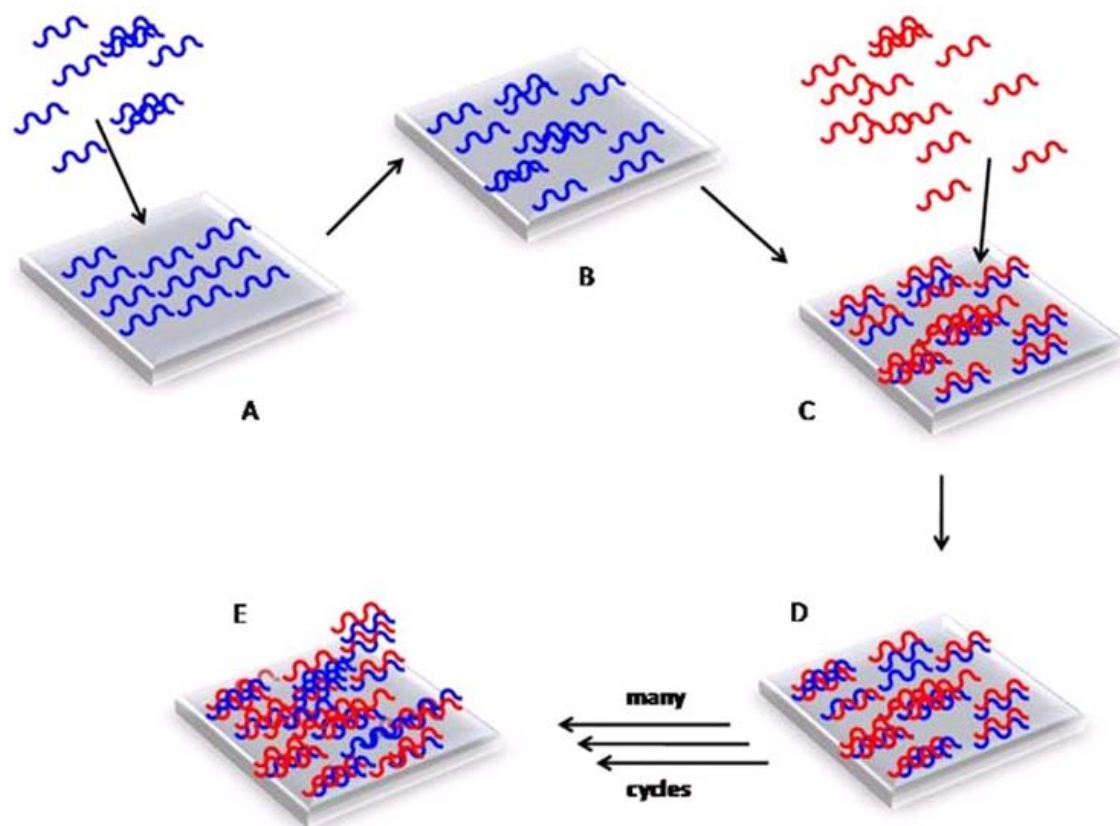


Figure 3-17. Mechanism for aggregate formation in LbL films built electrostatically from conjugated polyelectrolytes. A) Layer deposition. B) Polyelectrolyte aggregation *via* interpenetration, diffusion and π -stacking of the polyelectrolytes. C) Second layer deposition. D) Polyelectrolyte aggregation. E) A mostly aggregated film after many bilayer depositions.

Fluorescence spectra and AFM images of a variety of multilayer films (Figures 3-4 through 3-12) indicated that LbL films of CPs become increasingly aggregated as the number of bilayers grows. Time dependent aggregation studies of the films and deposition solutions (Figures 3-13 and 3-14) demonstrated that the aggregates form primarily in the film post deposition. Such a mechanism has been suggested for the LbL deposition of poly(ethyleneimmonium chloride) and poly(styrene sulfonate) by M.S. Johal.¹⁴¹ Using dual beam polarization interferometry, a technique that allows for real-time measurement of the refractive index and thickness of thin films, Johal found that both polyelectrolytes deposit in their coiled, solution conformations onto the film, whereupon they flatten out and interpenetrate

into the bulk of the film. A similar mechanism for the aggregation of LbL films constructed using CPs is now proposed that accounts for their unique features, such as π -stacking.

This mechanism is graphically depicted in Figure 3-17. In step A, the first polyelectrolyte deposits onto the substrate, either as individual polymer chains or as relatively constantly-sized aggregates. They deposit in a manner so as to provide for complete charge reversal of the film's outermost layer.^{126,127} In step B, the deposited polyelectrolytes rearrange, minimizing hydrophobic interactions while simultaneously maximizing π - π stacking, electrostatic, and hydrophilic interactions. The net result of step B is a general lowering in the overall energy of the thin film. In step C, the counter polyelectrolyte deposits in a manner similar to step A, followed by rearrangement and aggregation in step D. The process then repeats for additional deposition cycles. For small numbers of bilayers, the flat topology of the substrate could influence the extent of film aggregation, resulting in some unaggregated polyelectrolytes, as has been suggested by Voegel.³⁰ For large numbers of bilayers, there is no significant effect of substrate topology on that of the film, as each additional layer is deposited on the previous electrolyte, not on the substrate. The result is step E in Figure 3-17: a completely aggregated film, devoid of long-range structural order.

Singlet Exciton Diffusion

A direct method of measuring the ability of excitons to diffuse within thin, conjugated polymer films uses time of flight techniques. In these measurements, an exciton produced in the donor layer is assumed to diffuse from the point of photoexcitation to the quenching/accepting layer. Because the exciton is assumed to diffuse only from the point of generation to the point of quenching, the diffusion is assumed to be one dimensional and can be modeled using the one dimensional continuity equation, Equation 2-11.

$$\frac{\partial n(x,t)}{\partial t} = -\frac{n(x,t)}{\tau} + D \frac{\partial^2 n(x,t)}{\partial x^2} - S(x)n(x,t) + G(x,t) \quad (2-11)$$

This equation was described in detail in Chapter 2 and will not be greatly discussed here. This model describes the time evolution of excitons in space, governed by their natural radiative and non-radiative decays (the first term), their diffusion (the second term), their quenching interactions (the third term), and their generation (the fourth term). From this model, Mikhnenko developed Equation 2-12, which relates the magnitude of exciton quenching, $Q(L)$, to the thickness of the donor layer, L , and the length of diffusion, L_D , in TOF measurements.⁸⁴ Application of Equation 2-12 is simple; construct a plot of $Q(L)$ versus L and use a nonlinear curve fitting procedure to fit L_D to the experimental data, $Q(L)$ and L . The film thickness can be given in bilayers or in nanometers. The thicknesses of the LbL films were calculated using the procedure described in the experimental section.

$$Q(L, L_D) = \frac{L_D}{L} \tanh\left(\frac{L}{L_D}\right) \quad (2-12)$$

The exciton diffusion coefficient, D , can be related to L_D and the unquenched lifetime, τ , of the film using Equation 2-10.

$$L_D = \sqrt{D\tau} \quad (2-10)$$

By assuming that the fluorescence of LbL films built on glass is not quenched, the magnitude of fluorescence quenching for films on ITO can be calculated using the procedure given in the experimental section. Using this procedure, Figure 3-18 is obtained. As suggested by the fluorescence spectra of the films on ITO (Figure 3-15), there is almost a quantitative quenching of singlet PPESO3 excitons from one to three bilayers. This indicates that every exciton generated in the first three bilayers is able to diffuse to the ITO layer and be quenched before they naturally decay. After three bilayers, the quenching decreases and ultimately

recovers by twenty bilayers. The quenching data of the ITO films indicate that the maximum distance a singlet exciton can travel in glass/[PDDA/PPESO3] LbL films is around three bilayers. Any exciton generated in a film greater than three bilayers thick will not be able to completely diffuse to ITO within its lifetime. These excitons fluoresce, which decreases the fluorescence quenching. As more PPESO3 is added, more excitons fluoresce. By twenty bilayers, more excitons are fluorescing than are being quenched. At this film thickness, the emission of the film is said to have recovered. Attempts at measuring the fluorescence lifetimes of the films failed, preventing the calculation of the exciton diffusion coefficient.

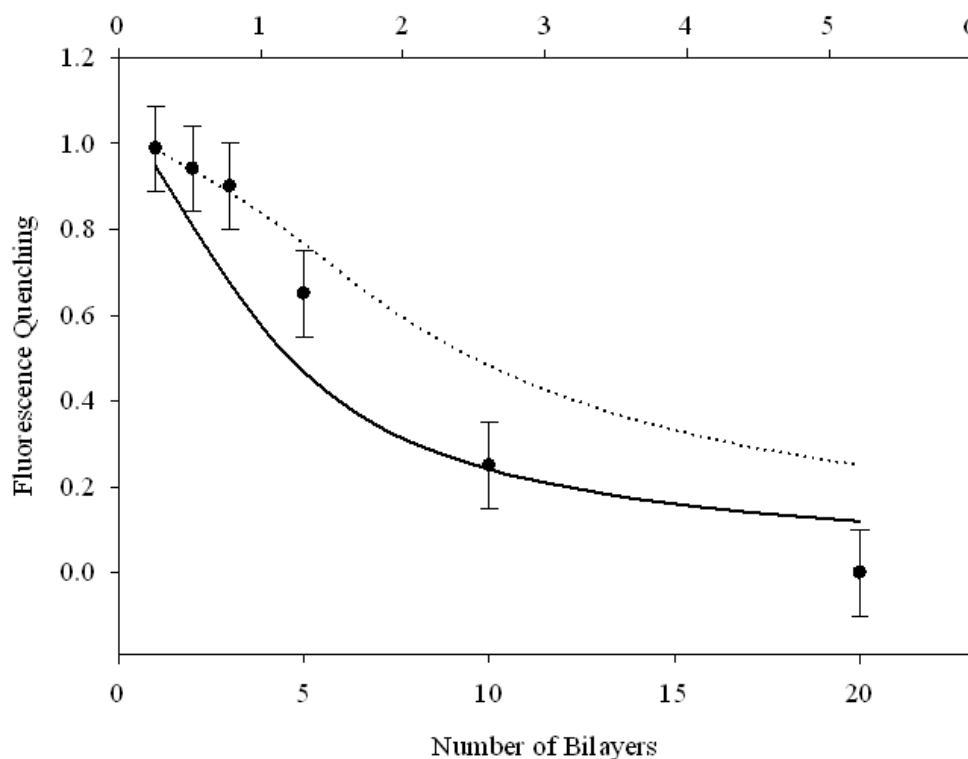


Figure 3-18. Fluorescence quenching versus exciton diffusion distance for ITO/[PDDA/PPESO3] LbL films. The circles represent the experimentally calculated fluorescence quenching, calculated using Equation 3-1. Equation 2-12 was used to produce the fitted lines by including the whole range of film thicknesses (solid line) or only the first three films (broken line). The film thickness in nanometers was calculated using Equation 3-4. Being an substantial outlier, the four-bilayer film has been omitted.

Table 3-1. Length of diffusion data obtained from fitting the ITO quenching data to Equation 2-12.

Entry	L_D	L_D units ^a	Fitted points	χ^2
1	2.4	BL	6	4.74
2	0.969	nm	6	4.74
3	5.0	BL	3	0.014
4	2.12	nm	3	0.014

Notes: ^aBL=bilayers, nm=nanometers.

The average length of diffusion for the excitons in the LbL films can be estimated by fitting Equation 2-12 to the data in Figure 3-18. The results of the fitting procedure are summarized in Table 3-1. When the thickness of all five films is included in the fit, there is a poor correlation between the predicted and experimental data. Mikhnenko's model was developed for TOF measurements of spin-coated films, which are typically smooth, in contrast to LbL films, which can be very rough due to aggregation. Strong evidence has been given in this work indicating that at five bilayers, an LbL film can be aggregated. As a film five bilayers thick is deposited, the film becomes so aggregated that some PPESO3 excitons diffuse to an aggregate before they diffuse to the ITO quenching layer. As a result, the excitons are trapped within polyelectrolyte aggregates; they diffuse within the aggregate until relaxation occurs. In effect, the aggregates become exciton traps that significantly hinder exciton diffusion, decreasing the accuracy of the exciton diffusion model.

Eliminating all data points in Figure 3-18 except the first three gives a much better fit, although using only three data points to obtain quantitative results imparts a degree of dubiousness to any conclusions. Films three bilayers thick or less can be expected to be more homogeneous than a thicker film; thus, the extent of aggregation in these films is small enough such that the probability of an exciton becoming trapped within an aggregate is lowered. This enhances the ability of excitons to diffuse within the film; as a result, the only major impedances to exciton

quenching are film thickness and exciton lifetime, which the model assumes are the only factors governing exciton quenching. Using Equation 2-12, the estimated singlet exciton length of diffusion for these films is 5.0 bilayers, or 2.12 nm. The L_D value of 2.12 nm (5.0 bilayers) is in rough agreement with the observed decrease in fluorescence quenching that occurs after three bilayers. This imparts a degree of certainty to the three-point data fit. The measured value of L_D , 2.12 nm, is lower than literature values for singlet exciton lengths of diffusion (Table 3-2), indicating that there are enough aggregates present in a three bilayer film to trap excitons, shortening the value of L_D .

Table 3-2. Singlet exciton diffusion literature data for organic films.

Material	Exciton multiplicity ^a	$D/10^{-3} \text{ cm}^2\text{-s}^{-1}$	L_D (Å)	Reference
PPESO3	S	---	21.2	This work
PEOPT	S	4.50	47	85
MDMO-PPV	S	3.20	45	84
PPP	S	4.30	110	117
DIP ^C	S	5.00	1000	77
NPD	S	0.70	51	76
SubPC	S	0.64	80	76
PTCDA	S	3.40	104	76
TnBuPP	S	2.5	220	118
Alq ₃	S	0.012	200	76,119

Notes: This table is adapted from Table 2-3 in Chapter 2 of this dissertation. ^aS=singlet ^C The data presented is for the organic crystal; ---, data not reported; PEOPT, poly-3-(trioxaoctylphenyl)thiophene; MDMO-PPV, poly-(2-methyl-5-(3',7'-dimethyloctyloxy)-p-phenylenevinylene; Alq₃, tris-(8-hydroxyquinoline) aluminum; NPD, N,N'-diphenyl-N,N'-bis(1-naphthyl-1,1'-biphenyl-4,4'' diamine; DIP, diindenoperylene; PPP, poly(para-phenylene); SubPC, boron subphthalocyanine; PTCDA, 3,4,9,10-perylenetetracarboxylic dianhydride; TnBuPP, tetra-(4-n-butylphenyl)porphyrin.

The value of L_D for LbL films obviously needs to be improved if LbL films are ever to be used for efficiently functioning devices. For example an organic solar cell made using the layer-by-layer method functioned very poorly, with a maximum overall solar efficiency of 0.04%.¹⁵ Finding a way to prevent the aggregation of LbL films could provide a means of increasing the

value of L_D and the efficiency of devices made by this method. One promising route of investigation incorporates layered double hydroxides (LDHs) into LbL films.¹⁴⁴⁻¹⁴⁷ These inorganic materials are essentially two layers of cationic metals, such as Mg^{2+} and Al^{3+} with small, inorganic anions binding one metal to the other, forming a large, rigid molecular sheet. The surfaces of LDHs feature a combination of positively charged metals and hydroxyl groups that are able to interact with charged polyelectrolytes. The preparation of LDHs is very simple; just dissolve the metal salts in water, reflux the solution and collect the precipitate.^{144,145,147} When Lu and Evans built electrostatic LbL films using poly(para-phenylene sulfonate) and a LDH with Mg^{2+} and Al^{3+} , the polymer's fluorescence intensity increased with the number of bilayers, contrary to most literature examples of LbL films built using charged CPs.¹⁴⁴ It has been suggested by several researchers that when incorporated into LbL films, LDHs are so rigid and immovable that they prevent most layer interpenetration of the organic polyelectrolytes.¹⁴⁴⁻¹⁴⁷ Alternatively, the inherently low length of diffusion for singlet excitons can be increased if they can be converted into triplets. As demonstrated in Chapter 2, triplet excitons have greatly enhanced lengths of diffusion. The proceeding chapter describes the development of heavy metal dyes for LbL films that are able to promote the formation of PPESO3 triplets.

Experimental

Materials

All monomers and polymers were synthesized according to the literature procedures.^{116,136,137} All experiments involving pFl were performed by Dr. Bob Brookins or Dr. Quentin Bricaud. Starting materials, PDDA and PAH were purchased from Fischer or Sigma-Aldrich and palladium catalysts were bought from Strem. All materials were used as received. All water used was purified to a resistance of 18.2 MΩ using a Millipore Milli-Q system. Methanol and any other solvents were of HPLC grade and used as received. Borosilicate glass

slides were purchased from Corning and quartz slides were obtained from Prism Research Glass (Raleigh, NC). Indium-tin oxide slides were bought with a sheet resistance of 8-10 Ω per square inch from Delta Technologies. Clear silicone glue was purchased from DAP and cured according to the package directions.

Layer-by-Layer Self Assembly

Glass and quartz slides measuring 5 cm \times 2.5 cm were cleaned according to the procedure given in Chapter 2. Indium-tin oxide slides were sonicated only (Chapter 2) and subjected to 20 minutes of oxygen plasma cleaning before use. Since the ITO slides only had the acceptor coated only one side, it was necessary to prevent polyelectrolytes from depositing on the uncoated side. A small amount of clear silicon glue was applied along the outer perimeter of the uncoated side of the ITO substrates. A glass slide was then affixed to the ITO slide and the glue allowed to cure overnight. After LbL deposition, the two slides were separated with a razor, leaving an area in the middle of the ITO slide that only had polyelectrolyte on the ITO side. Spectroscopic measurements were performed on this area.

Layer-by-layer deposition was performed using a Nanostrata StratoSequence IV robot (Nanostrata, Tallahassee, FL). All deposition solutions were approximately 0.10 mM in concentration. The solution pH was unadjusted, and all depositions were done from water unless otherwise noted. When not in use, the deposition solutions were stored in a refrigerator and allowed to warm to room temperature before deposition began. The substrates were first deposited in the cationic polyelectrolyte solution for 10 min, after which time three separate rinsing steps of 3 min, 1 min and 1 min were respectively performed, always with fresh rinsing solvent. The substrate was then immersed into the anionic polyelectrolyte solution for 10 min and the rinsing sequence repeated. For the deposition and rinsing steps, the substrates were mechanically rotated. Films were gently dried in a stream of filtered, compressed air after each

deposition session was complete, but not between individual layers. The coated substrates were stored under a room temperature, dark vacuum when not being used. Before any measurements on the slides were made, the films were allowed to dry overnight in a dark, room temperature vacuum.

Film and Solution Characterization

All absorption measurements were carried out on a Perkin-Elmer Lambda 25 spectrophotometer. A clean substrate was used as the absorption blank. For measurements on ITO, it is recommended to use a glass blank, not an ITO blank, to minimize background interference. Fluorescence measurements were recorded on a Jobin-Yvon Fluorolog-3 fluorimeter in front-face mode for films and right-angle mode for solutions. All optical measurements were carried out on four separate areas of each film. The spectra were then averaged without regard to spectral intensity or absorbance maximum to better represent the heterogeneity of the films. Atomic force microscopy images were obtained using a Veeco diInova microscope in tapping mode with the assistance of Dr. Quentin Bricaud.

Fluorescence Quenching

The magnitude of fluorescence quenching of PPESO3 multilayer films on ITO was calculated with respect to the unquenched fluorescence intensity of PPESO3 on a glass substrate using Equation 3-1, where Q is the quenching magnitude, $I_{q,x}$ is the integrated fluorescence intensity of a film x bilayers thick on ITO, and $I_{o,x}$ is the integrated fluorescence intensity of a film x bilayers thick on glass. For reasons discussed below, the integrated fluorescence intensities of the films were normalized to their fractions of light absorbed, Equation 3-2.

$$Q=1-\left(\frac{I_{q,x}}{I_{o,x}}\right)\left(\frac{1-10^{-A_{o,x}^{420}}}{1-10^{-A_{q,x}^{420}}}\right) \quad (3-1)$$

The integrated fluorescence intensities of the LbL films on glass and on ITO, uncorrected for differences in film thickness, are given in Figure 3-19. Inspection of the absorption spectra for the unquenched and quenched films (Figures 3-4 and 3-15, respectively) reveals that ITO adsorbs less polyelectrolytes than does glass, resulting in a lower absorption for the ITO films. To compensate for these for differences in adsorbed material between the two substrates, the integrated fluorescence intensities used in Equation 3-1 were divided by the fraction of light absorbed, $F_{hv,abs}$, (Equation 3-2) for each film. The variable A^{420} stands for the absorbance at 420 nm of each film. This corresponds to the excitation wavelength used for fluorescence measurements on ITO and glass substrates.

$$F_{hv,abs} = 1 - 10^{-A^{420}} \quad (3-2)$$

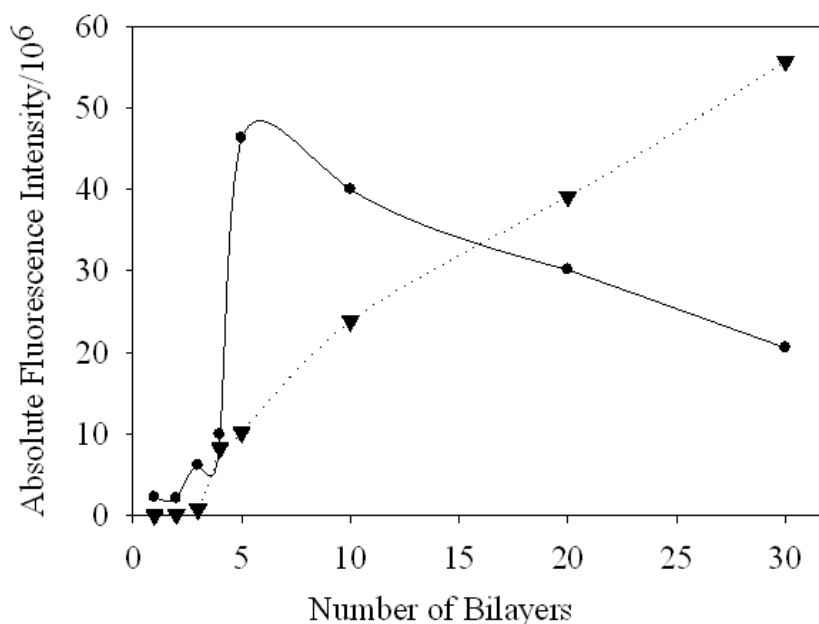


Figure 3-19. Integrated fluorescence intensities versus the number of bilayers for glass/[PDDA/PPESO3] films (circles) and ITO/[PDDA/PPESO3] films (triangles).

Film Thickness Calculations

The thicknesses of the LbL films on ITO were calculated using the procedure developed by Bergstedt because the films were too thin for step-height AFM.¹⁴⁸ The Beer-Lambert Law

relates the optical absorbance, A , to the pathlength, l , the concentration, c , and the molar absorptivity, ϵ , as shown in Equation 3-3.

$$A = \epsilon lc \quad (3-3)$$

In a thin film, the molar absorptivity of the chromophore is assumed to be equal to the molar absorptivity in solution and the concentration is assumed to be the polymer density ($\sim 1.0 \text{ g-cm}^{-3}$; see Chapter 2). The product of the concentration and film thickness can be combined into one term, the surface coverage, Γ (units: mol-cm^{-2}), Equation 3-4.

$$\Gamma = cl = \frac{A_{\max}}{\epsilon} \quad (3-4)$$

By calculating Γ from the maximum absorbance and molar absorptivity, the optical pathlength (film thickness) can be determined using the assumed concentration. To convert the concentration from g-cm^{-3} to mol-cm^{-3} , it was assumed that the molar mass increment of each bilayer is the formula weight of one PDDA and one PPESO3 repeat unit.

Estimating L_D

See the experimental section of Chapter 2.

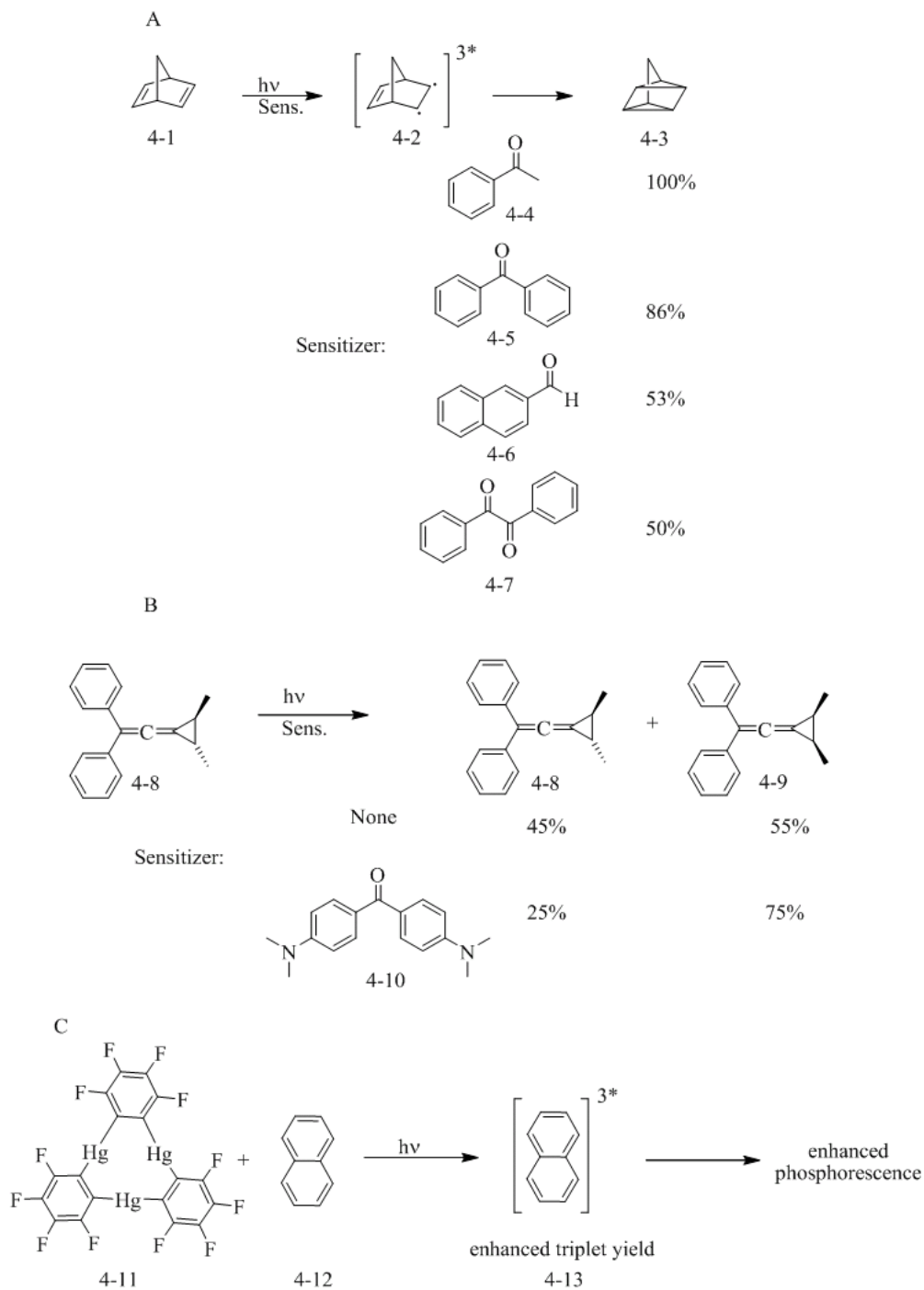


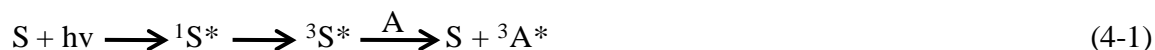
Figure 4-1. Examples of triplet sensitized systems from the literature. A) The sensitized synthesis of [2.2.1.0.0]quadricycloheptane from norbornadiene.¹⁴⁹ B) The photosensitized isomerization of *trans*-2,3-dimethyl-1-(2',2'-diphenylvinylidene)cyclopropane.¹⁵⁰ C) The triplet sensitization of naphthalene by a mercury trimer.¹⁵¹

CHAPTER 4

TRIPLET SENSITIZATION OF PPESO3

Introduction

Triplet sensitization of organic molecules has traditionally been the purview of synthetic organic chemists.^{149,150,152-155} When an organic molecule absorbs light, a singlet excited state is created, as discussed in Chapter 1. The weak spin-orbit coupling of electrons in some organic molecules prevents efficient intersystem crossing from the singlet state to the triplet state. A triplet molecule exists for a longer period of time than does a singlet; from a synthetic perspective, singlets decrease the yields of reactions utilizing photochemically generated excited states, among other things. A solution to this problem is to add molecules such as ketones that have high rates of intersystem crossing to the reaction mixture, as given by Equation 4-1.



Upon irradiation, these molecules, called sensitizers (S), become photoexcited, generating triplets and becoming a triplet donor. When this molecule collides with a molecule of starting material, called the acceptor (A), Dexter exchange occurs, producing a triplet acceptor and a ground state sensitizer. The acceptor can then undergo the desired reaction in the triplet excited state, generating the product with enhanced yields. Examples of triplet sensitization are given in Figure 4-1A,B.^{72,149,150} The ability of excited triplet donors to form excited state triplets from ground state acceptors has been proven using multiple techniques.^{156,157}

More recently, triplet sensitization has been expanded to include photophysical studies. For example, Ramamurthy demonstrated that when naphthalene was incorporated into a zeolite featuring Li^+ , only naphthalene fluorescence was observed. However, when Rb^+ and Cs^+ were present in the zeolite, strong naphthalene phosphorescence was observed. It was postulated that upon complexation with naphthalene, the heavier Rb^+ and Cs^+ atoms promoted intersystem

crossing of naphthalene singlets through the external heavy atom effect.¹⁵⁸ Omary¹⁵⁹ and Gabbai¹⁵¹ both demonstrated the ability of heavy metal-arene complexes such as molecule 4-11 in Figure 4-1, to induce phosphorescence of naphthalene, also through the external heavy atom effect. In every case, the naphthalene was selectively excited and addition of the heavy metal induced phosphorescence.

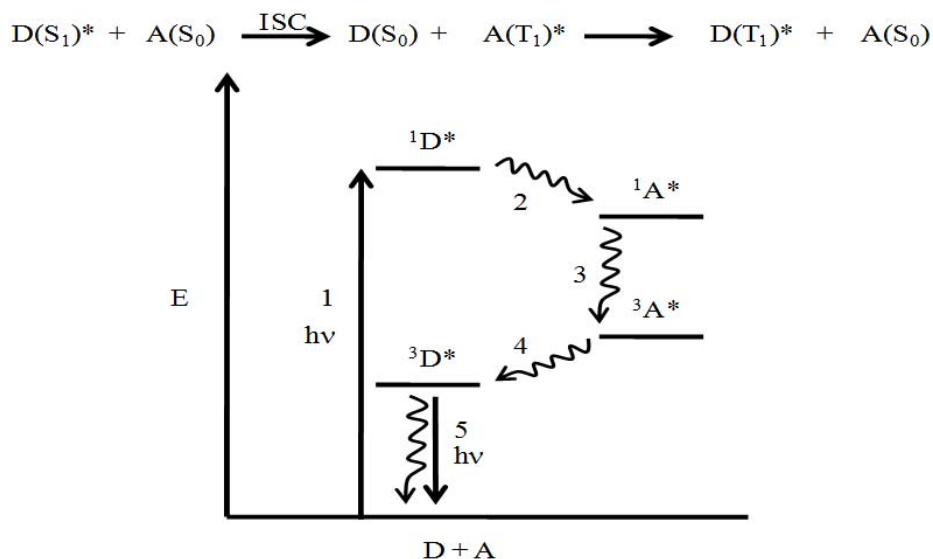


Figure 4-2. Jablonski diagram describing donor-acceptor triplet sensitization. One, photoexcitation of the donor, D; two, Förster transfer of singlet excitation energy from D to the acceptor, A; three, intersystem crossing of the acceptor; four, Dexter exchange of the acceptor's triplet excitation energy with the ground-state donor (back energy transfer); five, triplet decay of the donor. Adapted from Turro.⁷²

One possible mechanism for the triplet sensitization of naphthalene by external heavy metals is given in Figure 4-2.⁷² Step one involves excitation of the donor, D, (naphthalene, for example) to the S_1 state. When the ground state acceptor, A, (a heavy metal, for example), is added to the solution, the acceptor quenches the singlet state of the donor (step 2). In Figure 4-2, singlet quenching by Förster transfer is shown. The acceptor is now in the singlet excited state, with the donor in the ground state. The acceptor contains the heavy metal which promotes rapid intersystem crossing to the triplet excited state (step 3). In step four, the triplet acceptor undergoes Dexter exchange with the ground state donor. This corresponds to the actual triplet

sensitization process. As a result, the acceptor is again in the ground state, while the donor is in the triplet excited state. The donor can then undergo triplet decay to the ground state (step 5).

The ability of heavy metal containing acceptors to sensitize donor triplets is not limited to solutions, but also has been demonstrated to occur in thin organic films to be used for electronic applications.¹⁶⁰⁻¹⁶² For example, when 5% tris(2-phenylpyridine) iridium (III) [Ir(ppy)₃] was doped into a film of N,N'-bis(phenyl)-benzidine [NPD], as shown in Figure 4-3A,¹⁶⁰ the NPD exciton length of diffusion almost doubled from 6.5 nm in the pristine NPD film to 11.8 nm in the doped film. In this film, the NPD became photoexcited; the singlet exciton diffused to an iridium molecule, whereupon NPD triplet sensitization occurred as described in Figure 4-2. The NPD triplets then diffused throughout the film. As described in Chapter 2, the lifetime of a triplet exciton is greater than that of a singlet; this enables the triplet exciton to diffuse over a much larger distance than can a singlet exciton in the same film.

The triplet sensitizers Figure 4-3 are an example of a much larger class of conjugated organometallic iridium dyes. As seen in Table 4-1,^{44,163,164} Ir³⁺ dyes have triplet energies corresponding to wavelengths throughout the visible region and into the near-infrared region. The iridium atom induces strong intersystem crossing of the organic ligand through the heavy atom effect, producing triplets with lifetimes in the microsecond range. These complexes have low-to-moderate phosphorescence quantum yields and can be neutral or positively charged.^{44,163-166} These qualities, especially the broad range of triplet energies and long triplet lifetimes, make iridium dyes well suited for triplet sensitization. For triplet sensitization to occur, the triplet state of the sensitizer needs to be lower in energy than the donor singlet state, yet higher in energy than the expected donor triplet state. This ensures an exothermic transfer of excitation energy and maximum sensitization efficiency.

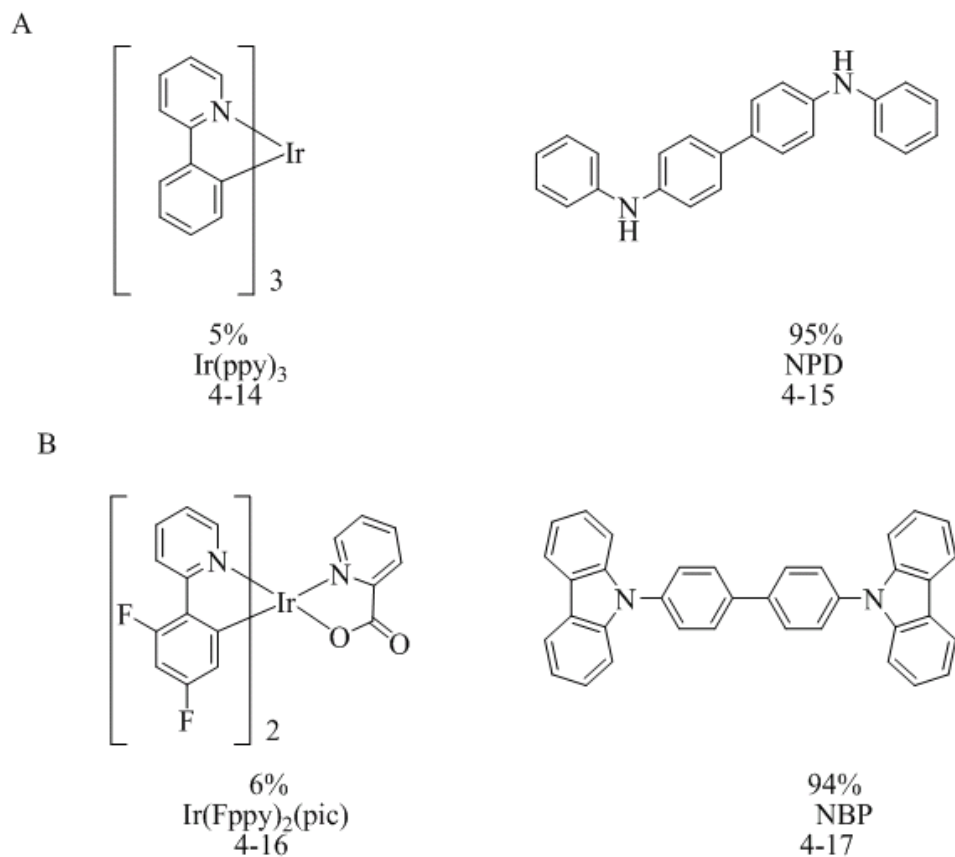
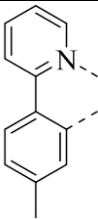
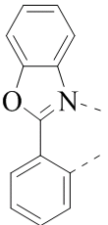
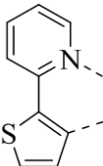
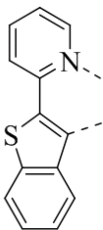
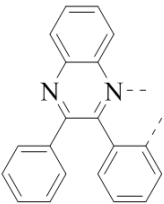
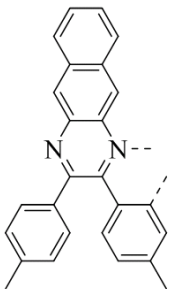


Figure 4-3. Examples of triplet sensitized thin films from the literature. A) Tris(2-phenylpyridinato-N,C^{2'}) iridium (III)/N,N'-bis(phenyl)-benzidine.¹⁶⁰ B) Bis(4,6-difluorophenyl)pyridinato-N,C^{2'}) iridium (III) picolinate/4,4'-N,N' dicarbazole-biphenyl.¹⁶¹

Table 4-1. Literature examples of Iridium (III) dyes of the structure (C^N)₂Ir(acac).^{44,163,164}

Entry	C ^N	Abbreviation	$\lambda_{\text{max}}^{\text{P}}$, nm	τ_{P} , μs	Φ_{P}
1		tpy	512	3.1	0.31
2		bo	525	1.1	0.25
3		thp	562	5.3	0.10
4		btp	612	5.8	0.21
5		hqx	670	---	0.50
6		dtbq	904	0.29	0.022

Notes: acac, acetylacetonate; ---, not available; tpy, 2-(4-tolyl)pyridine; bo, 2-phenylbenzoxazole; thp, 2-(2'-thienyl)pyridine; btp, 2-(2'-benzothienyl)pyridine; hqx, 2,3-diphenylquinoxaline; dtbq, di-*p*-tolylbenzo[g]quinoxaline.

In this study, a series of cationic Ir^{3+} dyes were developed to act as triplet sensitizers for PPESO3. Their structures are shown in Figure 4-4. The synthesis and photophysical properties of the dyes will be discussed. Their ability to sensitize PPESO3 triplets will be determined using solution-based fluorimetry and transient absorption measurements; methods of incorporating these dyes into LbL films will be proposed. It is hoped that by employing triplet sensitizers in PPESO3 LbL films, the low PPESO3 exciton length of diffusion will be enhanced. By varying the triplet energy of the iridium dyes, it is hoped that the triplet energy of PPESO3 can be estimated by examining each dye's ability to sensitize PPESO3 triplets.

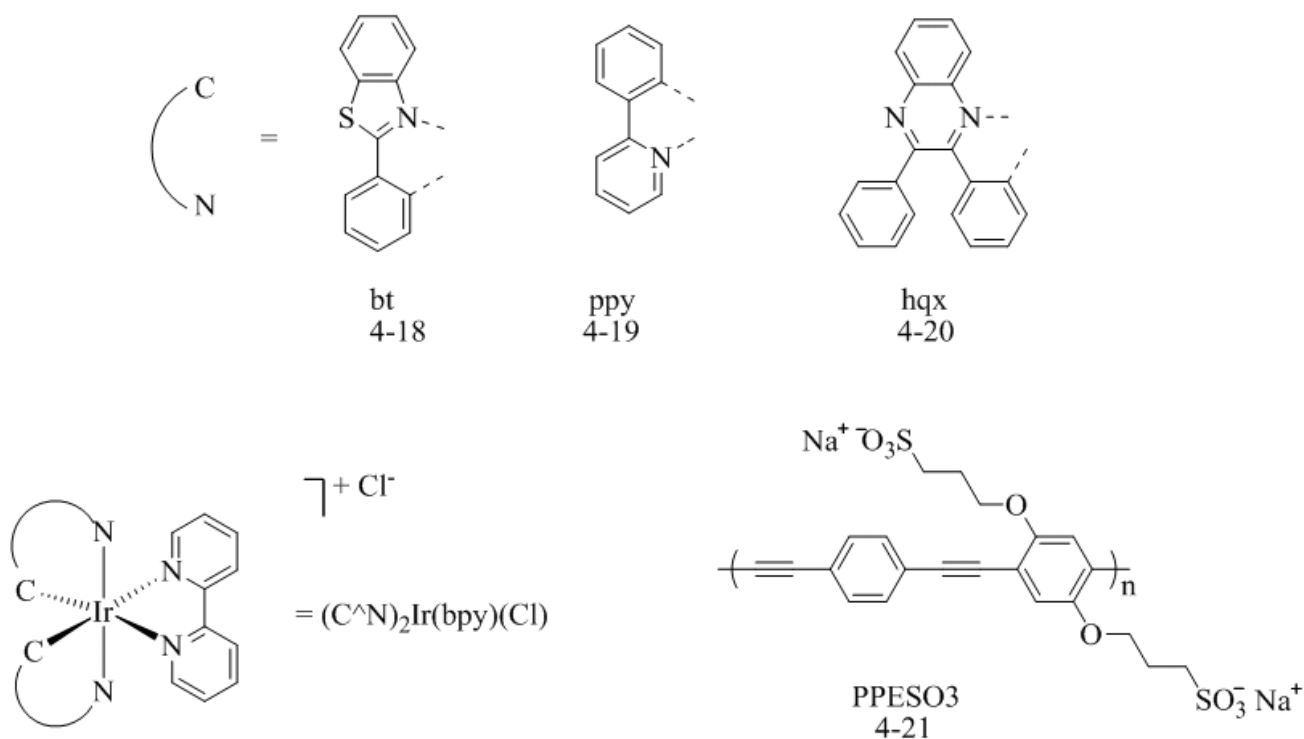


Figure 4-4. The cationic iridium dyes and anionic polymer to be used in this study: bt, 2-phenylbenzothiazole; ppy, 2-phenylpyridine; hqx, 2,3-diphenylquinoxaline; PPESO3, poly(phenylene ethynylene sulfonate).

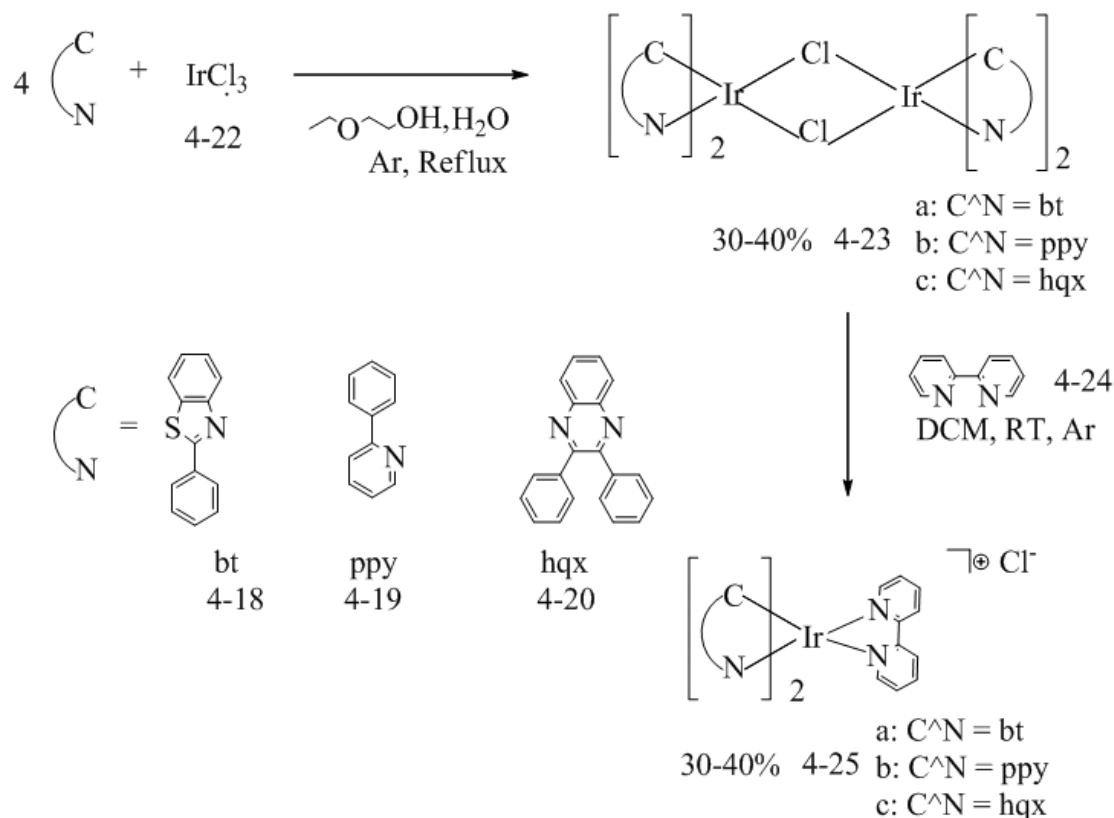


Figure 4-5. The synthesis of the cationic iridium dyes.^{44,163,166}

Synthesis and Characterization

The bipyridyl iridium (III) complexes containing 2-phenylbenzothiazole (bt) **4-18**, 2-phenylpyridine (ppy) **4-19** or 2,3-diphenylquinoxaline (hqx) **4-20** as ligands were synthesized according to the route outlined in Figure 4-5. Four equivalents of the ligands (abbreviated as C^N) were refluxed with iridium (III) chloride overnight in a 3:1 mixture of 2-ethoxyethanol and water, resulting in the chloro-bridged dimeric complexes **4-23a-c**.^{44,163,164,166} The dimer was cleaved through room temperature reaction with 2,2'-bipyridine (bpy) **4-24** to afford the iridium (III) complexes **4-25a-c** as the chloride salt. The ppy complex is known to the literature.¹⁶⁶ Although the acetylacetonate (acac) iridium (III) complexes of **4-18**, **4-19**, and **4-20** have been extensively studied in the literature,^{44,163-167} the bpy salts were instead studied because their cationic nature enables them to form ion-pair complexes with PPESO₃, **4-21**. This is a necessary

requirement for LbL self assembly, but the electrostatic polymer-dye bond is also required to maximize the chances of singlet-triplet sensitization.⁷² If the dye was not capable of ion-pairing with PPESO3, the chances of polymer triplet sensitization would be low, as described in the discussion section.

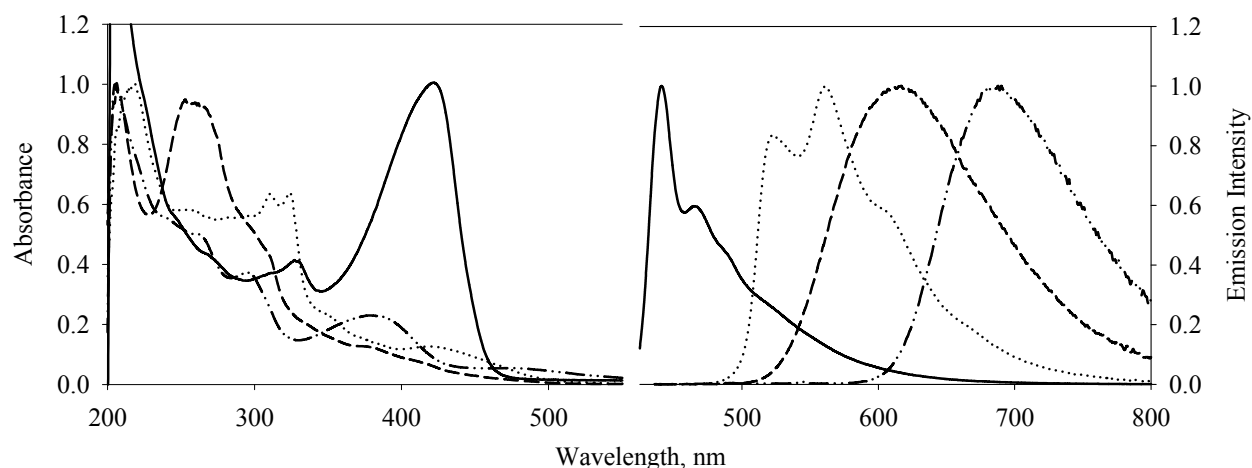


Figure 4-6. Absorption and emission spectra in methanol for PPESO3 and the iridium dyes in order of decreasing emission maximum: PPESO3, Ir(bt)₂(bpy)Cl, Ir(ppy)₂(bpy)Cl, Ir(hqx)₂(bpy)Cl.

The identities of the products were confirmed through nuclear magnetic resonance (NMR) and mass spectrometry, in addition to ultraviolet-visible absorption (UV-VIS), photoluminescence (PL) and transient absorption (TA) spectroscopies. Attempts were first made to acquire ¹H NMR spectra of the iridium dye's chloride salts in dimethylsulfoxide-d₆ (DMSO-d₆). For all three dyes, only peaks corresponding to the protonated solvent and water were observed. It was determined that the complexes were not completely dissolved in DMSO-d₆. Subsequent attempts at better dissolving the iridium dyes in DMSO succeeded only with Ir(hqx)₂(bpy)Cl. As a result, Ir(bt)₂(bpy)Cl and Ir(ppy)₂(bpy)Cl were metathesized to the hexafluorophosphate (PF₆) salt. Metathesis was achieved by dissolving the dyes in equal parts ethanol and water. Excess potassium hexafluorophosphate was then added and the neat products almost immediately precipitated. The salts, Ir(bt)₂(bpy)PF₆ and Ir(ppy)₂(bpy)PF₆, were readily

dissolved in acetonitrile-d₃ and gave clean ¹H NMR spectra. All three dyes exhibit complex, aromatic splitting patterns between 6.00 ppm and 9.00 ppm that correspond to the protons on the bpy and C^N moieties.

Table 4-2. Photophysical characteristics of the cationic iridium dyes in methanol.

Entry	Dye	$\lambda_{\text{max}}^{\text{A}}$, nm (ϵ , M ⁻¹ -cm ⁻¹)	E _T , eV	τ_{p} , μs	Φ_{p}
1	PPESO3	426 (57 000) ^a	2.81 ^b	0.447	0.78 ^b
2	Ir(bt) ₂ (bpy)Cl	213 (53 750), 257 (24 035), 313 (25 825), 325 (25 675), 418 (4 985)	2.36	2.17	0.32±0.06 ^c
3	Ir(ppy) ₂ (bpy)Cl	256 (40 020), 264 (39 430), 310 (18 260), 376 (5 248), 410 (3 293)	2.25	0.225 ^d	0.19±0.02 ^c
4	Ir(hqx) ₂ (bpy)Cl	260 (41 070), 296 (30 150), 381 (18 430), 469 (3 714)	1.96	0.645	0.77±0.1 ^e

Notes: ^a Value obtained from reference 71. ^b This data is for the S₁-S₀ transition. ^c Rose Bengal was used as a standard (Φ_{f} = 0.11 in EtOH+0.01 M KOH).¹⁶⁸ ^d The literature value is 0.337 μs .¹⁶⁶ ^e Rhodamine B was used as a standard (Φ_{f} = 0.69 in MeOH).¹⁶⁹

The UV-VIS and PL spectra of Ir(bt)₂(bpy)Cl, Ir(ppy)₂(bpy)Cl, Ir(hqx)₂(bpy)Cl and PPESO3 in methanol are given in Figure 4-6. The absorption spectra for the complexes are characterized by weak, low-energy metal-to-ligand charge transfer (MLCT) bands between 350-500 nm and strong, higher energy π - π^* bands between 200-350 nm. As discussed in Chapter 3, PPESO3 is characterized by a structured π - π^* absorption centered at 426 nm. The molar absorption coefficients for the Ir³⁺ complexes and for PPESO3 are given in Table 4-2. The emission spectra are also shown in Figure 4-6. The emission spectra of PPESO3 and Ir(bt)₂(bpy)Cl show well-defined vibronic peaks, whereas the phosphorescence spectra of the ppy and hxq complexes are featureless. As expected from their corresponding acac complexes,^{44,163} the phosphorescence maximum of each dye red-shifts, indicating that a range of sensitizer triplet energies has been obtained. The phosphorescence quantum efficiency of the

hqx complex is a relatively high 0.77, while the quantum efficiencies of the bt and ppy complexes are considerably lower (Table 4-2).

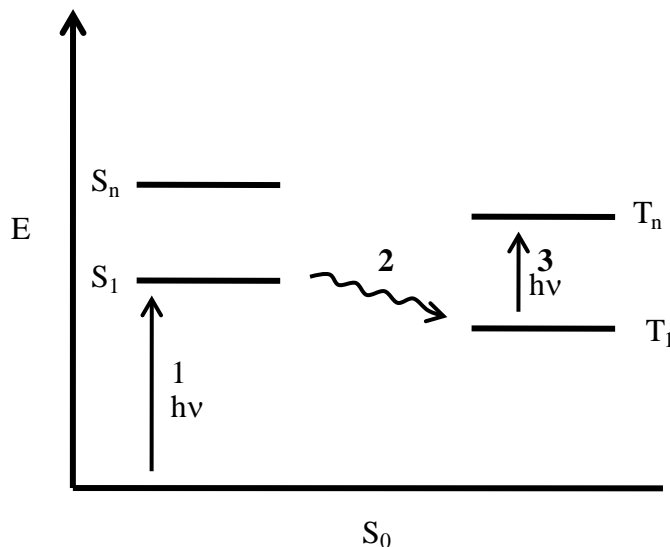


Figure 4-7. Simplified Jablonski diagram of the photophysical processes involved in triplet-triplet transient absorption. One, the pump; two, intersystem crossing; three, the probe.

Triplet-triplet transient absorption was used to estimate the phosphorescence lifetimes of PPESO3 and of each bpy complex. As discussed in Chapter 1, conjugated molecules have a singlet and triplet manifold, consisting of higher-energy singlet and triplet states. Transient absorption spectroscopy, described graphically in Figure 4-7, is a way of accessing the singlet and triplet manifolds of molecules. Using a monochromatic, pulsed laser (the “pump”), the molecule is excited to the first excited singlet state, S₁ (step 1). Assuming a fast rate of intersystem crossing, the S₁ state crosses to the first excited triplet state, T₁ (step 2). At this point, a polychromatic light source illuminates the molecule (the “probe,” step 3). The molecules, previously excited by the laser, are excited again by the probe, promoting the electrons from the molecule’s T₁ state to the higher triplet excited states, T_n. The result is an absorption spectrum of a molecule’s excited state. Furthermore, if several TA spectra are

acquired with different times between the pump and probe pulses, triplet lifetimes can be estimated.

The triplet-triplet TA spectra of iridium dyes **4-18**, **4-19** and **4-20** are given in Figure 4-8A-C, respectively. In agreement with the phosphorescence spectra (Figure 4-6), the triplet TA spectra for **4-18**, **4-19** and **4-20** feature a structured absorption that red-shifts as the dyes' triplet energies decrease. The triplet lifetimes estimated from the TA spectra are summarized in Table 4-2; for the most part, they are shorter than other triplet lifetimes of iridium (III) acac complexes (1.1 μ s to 14 μ s in 2-methyltetrahydrofuran).^{44,165,166}

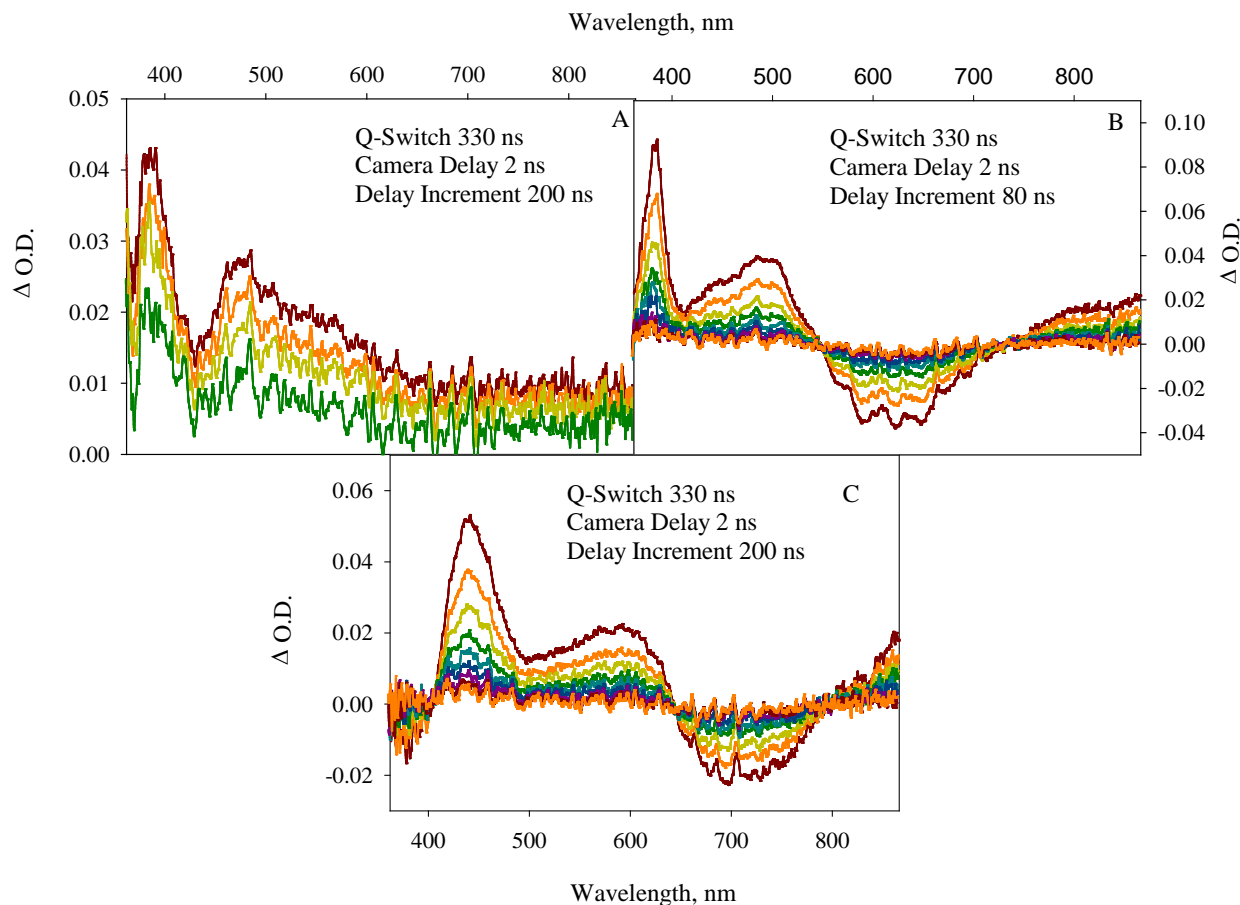


Figure 4-8. Triplet-triplet transient absorption spectra in methanol. A) Ir(bt)₂(bpy)Cl. B) Ir(ppy)₂(bpy)Cl. C) Ir(hqx)₂(bpy)Cl.

Results

To determine the ability of the cationic iridium dyes to sensitize PPESO3 triplets, each dye was used to spectrophotometrically titrate PPESO3 in methanol. In each experiment, an aliquot of PPESO3 was prepared, to which were added a series of iridium dye aliquots. Upon addition, the iridium dye diffused to the polymer, whereupon the cationic dye became electrostatically bound to the anionic sulfonate side chains of PPESO3. While coordinated, the dye quenched the PPESO3 singlet exciton, converting it into a dye-based triplet. Depending on the triplet energy of the dye, the triplet energy could be back-transferred to PPESO3, sensitizing the PPESO3 triplet. Fluorescence titrations of PPESO3 (concentration 4.61 μM) were carried out to determine the ability of the dye to quench singlet PPESO3 excitons, while triplet-triplet transient absorption titrations (PPESO3 concentration 17.4-19.1 μM) were performed to probe each dye's ability to sensitize PPESO3 triplets.

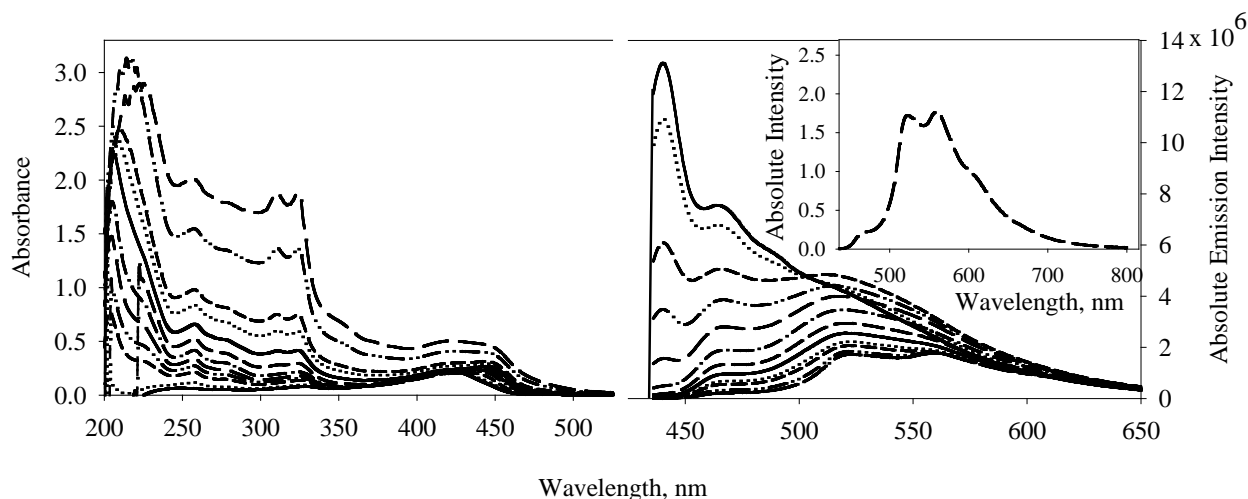


Figure 4-9. Absorption and emission spectra for the titration of a 4.61 μM solution of PPESO3 in methanol by $\text{Ir}(\text{bt})_2(\text{bpy})\text{Cl}$. The quencher concentrations are listed in order of decreasing PPESO3 fluorescence intensity: 0.0 μM , 2.23 μM , 4.45 μM , 6.68 μM , 8.90 μM , 16.7 μM , 19.8 μM , 24.7 μM , 29.8 μM , 35.1 μM , 57.5 μM , and 77.7 μM (inset).

Titration with Ir(bt)₂(bpy)Cl

With a triplet energy of 2.36 eV, Ir(bt)₂(bpy)Cl has the highest triplet energy of the dyes synthesized, so it will be considered to be a high-energy quencher. The results of a fluorescence titration of PPESO3 with this dye are given in Figure 4-9. When the solution is just PPESO3, the characteristic fluorescence of the polymer is observed to have a maximum at 441 nm. Upon addition of Ir(bt)₂(bpy)Cl, the fluorescence intensity of the polymer decreases, while a red-shifted, broad peak rises near 520 nm. This is possibly the formation of PPESO3 aggregates induced by the presence of the iridium dye. As more dye is added, the fluorescence intensity of the PPESO3 decreases and by a Ir(bt)₂(bpy)Cl concentration of ~78 μ M, only the phosphorescence of the dye can be seen, indicating quantitative quenching of the PPESO3 singlets has occurred.

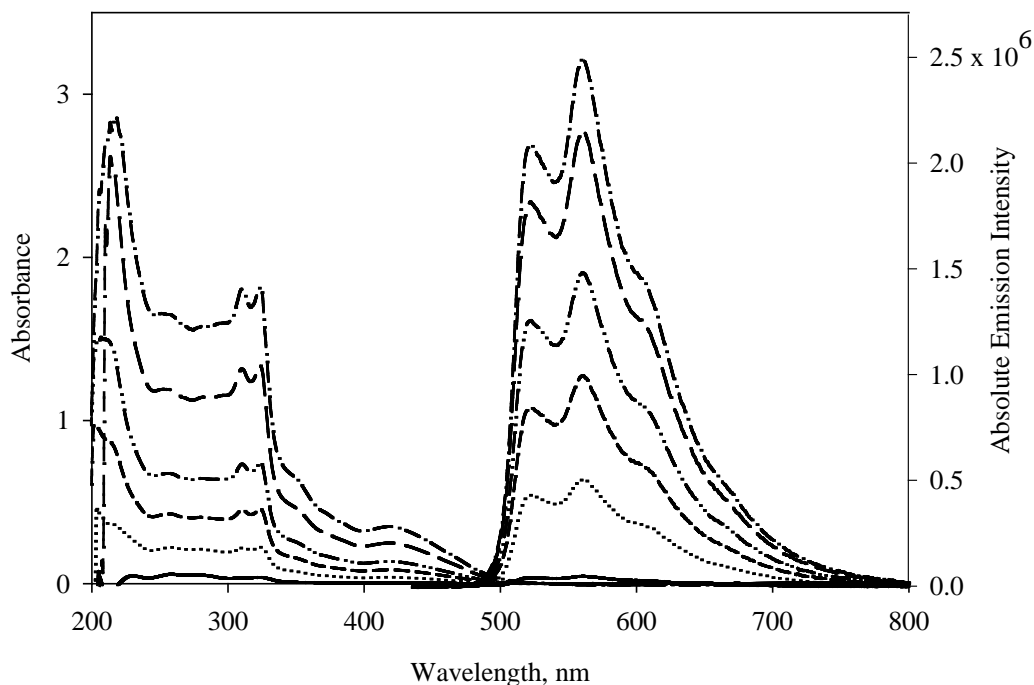


Figure 4-10. Absorption and emission spectra for the titration of Ir(bt)₂(bpy)Cl in methanol without PPESO3. The acceptor concentrations are listed in order of increasing phosphorescence intensity: 4.45 μ M, 6.68 μ M, 15.7 μ M, 26.2 μ M, 47.7 μ M, and 77.7 μ M.

The fluorescence quenching spectra were acquired at an excitation wavelength of 420 nm. At this wavelength, Ir(bt)₂(bpy)Cl itself absorbs (Figure 4-9). The emission observed at 78 μ M Ir(bt)₂(bpy)Cl during the PPESO3 titration is either due to the dye is being directly excited by the fluorimeter, or the dye is being excited by accepting energy from PPESO3. To determine which is the operative mechanism, a separate titration of only Ir(bt)₂(bpy)Cl was carried out using the same excitation wavelength and dye concentrations as in the titration of PPESO3, but without the polymer. Any emission thus observed can be attributed to direct excitation of Ir(bt)₂(bpy)Cl. The results are shown in Figure 4-10. In the absence of PPESO3, phosphorescence from the dye can be clearly seen at every concentration. Unfortunately, the aggregate emission of PPESO3 masks the dye's emission at the majority of concentrations; however, at a concentration of ~78 μ M, the emission intensity of the dye is stronger than when PPESO3 is present. This suggests that some of the excitation energy from Ir(bt)₂(bpy)Cl is being back-transferred to PPESO3, and that substantial direct excitation of the dye is occurring.

Triplet-triplet TA spectra confirmed the occurrence of triplet energy back-transfer. The TA spectrum of a 17.1 μ M solution of PPESO3 in methanol is shown in Figure 4-11A. There is a T₁-T_n feature centered at 734 nm, suggesting a triplet lifetime of 0.447 μ s (Table 4-2). Upon addition of 4 μ M Ir(bt)₂(bpy)Cl (Figure 4-11B), the strength of the signal doubles, indicating a substantial increase in the triplet population of PPESO3 excitons. As evident in Figure 4-8A, Ir(bt)₂(bpy)Cl does not exhibit a TA signal at 734 nm, so the intensity increase of this peak can be only due to the dye sensitizing PPESO3 triplets. When the change transient absorption signal is monitored at 734 nm and analyzed as a function of iridium dye concentration, the results of Figure 4-12 are obtained. As more Ir(bt)₂(bpy)Cl is titrated into the 17.4 μ M PPESO3 solution, the intensity of the triplet exciton decay rises. Eventually doubling in intensity, the change in

optical density stabilizes by a dye concentration of $\sim 8 \mu\text{M}$. As indicated by Figures 4-9 and 4-10, $8 \mu\text{M Ir(bt)}_2(\text{bpy})\text{Cl}$ has a very small absorption at the pump wavelength of 355 nm, suggesting that direct excitation of the sensitizer is minimal: the majority of the dye triplets produced in the TA experiment are the result of the transfer of excitation energy from PPESO3 to the dye. Together with the fluorescence titration, this suggests that the $\text{Ir(bt)}_2(\text{bpy})\text{Cl}$ quenches the PPESO3 singlet, converting it into a dye-based triplet which is then back-transferred to the PPESO3, forming a PPESO3 triplet exciton.

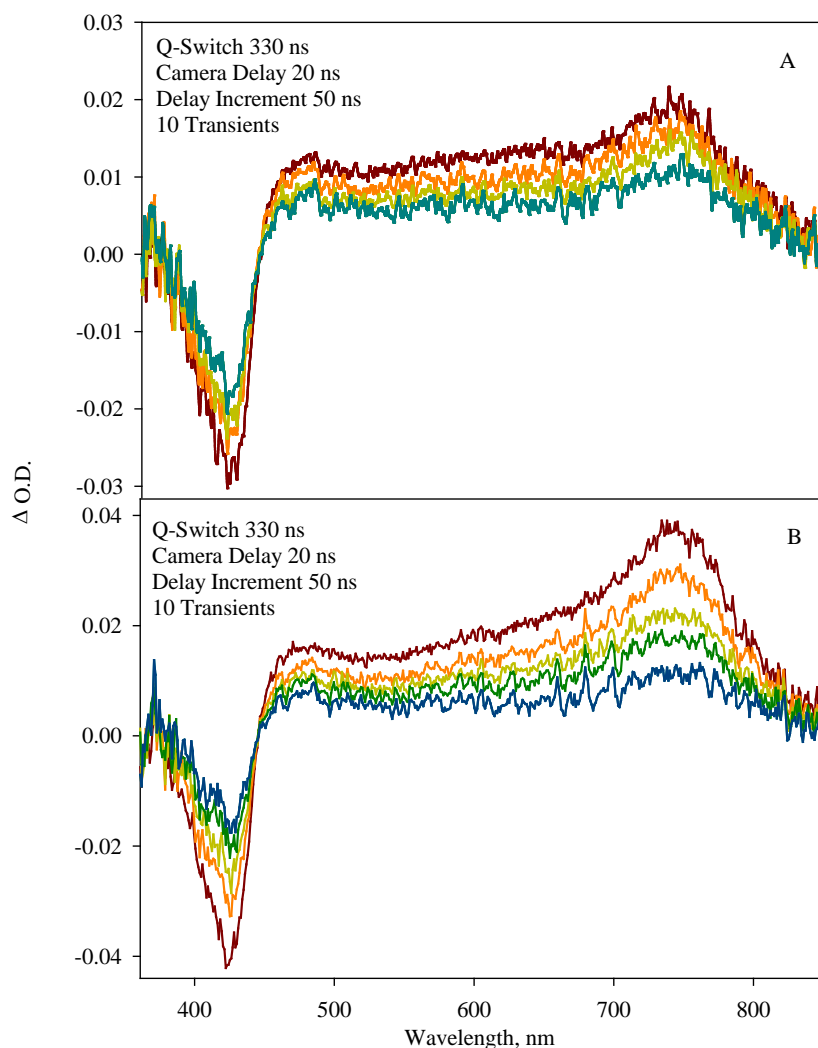


Figure 4-11. Triplet-triplet transient absorption spectra in methanol. A) $17.4 \mu\text{M PPESO3}$. B) $4.0 \mu\text{M Ir(bt)}_2(\text{bpy})\text{Cl}$ in $17.4 \mu\text{M PPESO3}$.

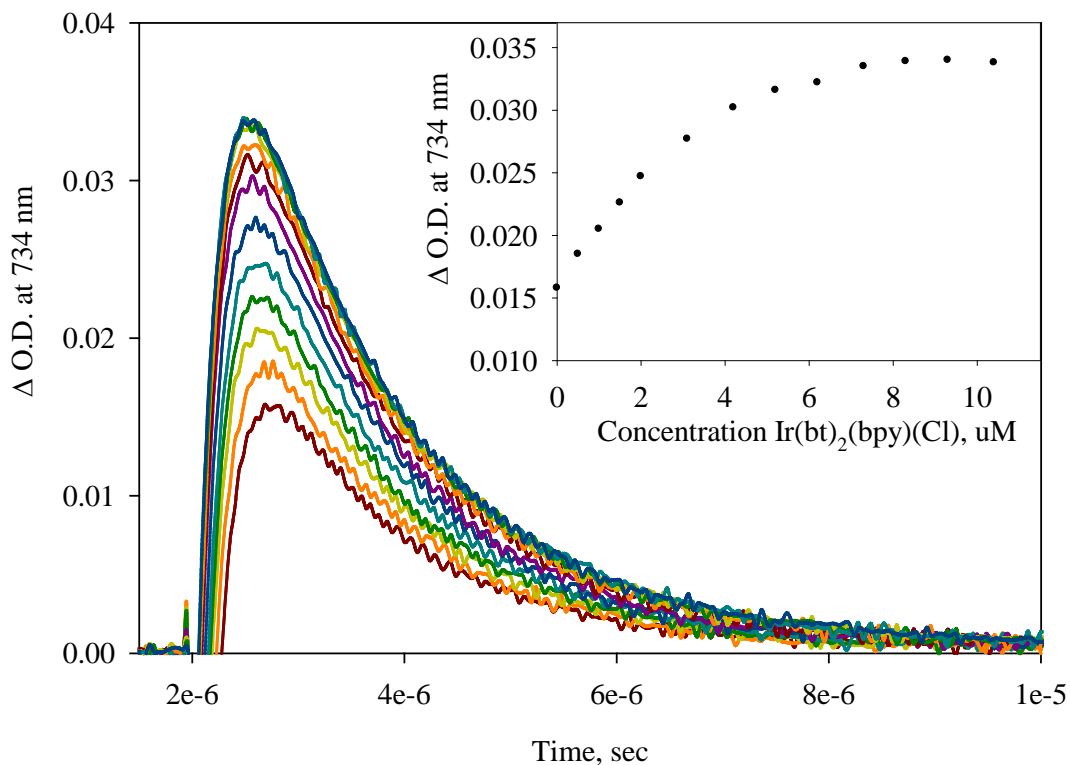


Figure 4-12. Triplet-triplet transient decay at 734 nm for 17.4 μM PPESO3 in methanol titrated by $\text{Ir}(\text{bt})_2(\text{bpy})\text{Cl}$. In order of increasing transient signal, the quencher concentrations are 0.0 μM , 0.5 μM , 1.0 μM , 1.5 μM , 2.0 μM , 3.1 μM , 4.2 μM , 5.2 μM , 6.2 μM , 7.3 μM , 8.3 μM , 9.3 μM , and 10.4 μM . The inset shows the change in the transient signal as a function of quencher concentration. All decays were obtained using a pump energy of 2.5 mJ.

Titration with $\text{Ir}(\text{ppy})_2(\text{bpy})\text{Cl}$

With a triplet energy of 2.25 eV, between that of $\text{Ir}(\text{bt})_2(\text{bpy})\text{Cl}$ and $\text{Ir}(\text{hqx})_2(\text{bpy})\text{Cl}$, $\text{Ir}(\text{ppy})_2(\text{bpy})\text{Cl}$ is a medium-energy quencher. When a fluorescence titration of PPESO3 with $\text{Ir}(\text{ppy})_2(\text{bpy})\text{Cl}$ is performed, Figure 4-13 is obtained. Initially, the characteristic fluorescence of PPESO3 is observed, but as the concentration of $\text{Ir}(\text{ppy})_2(\text{bpy})\text{Cl}$ increases from 0.0 μM to 64.1 μM , the fluorescence intensity of the polymer decreases. Unlike the titration with $\text{Ir}(\text{bt})_2(\text{bpy})\text{Cl}$, the ppy dye does not seem to induce any significant aggregation of PPESO3; instead, $\text{Ir}(\text{ppy})_2(\text{bpy})\text{Cl}$ phosphorescence is clearly seen at a concentration of 38 μM , compared to almost 80 μM for the bt dye.

A comparison of the PL titrations involving $\text{Ir(ppy)}_2(\text{bpy})\text{Cl}$ with (Figure 4-13) and without PPESO3 (Figure 4-14) reveal that the medium energy dye could also be sensitizing the formation of PPESO3 triplets. Using the same excitation wavelength and quencher concentrations as the PPESO3 titrations, the contribution of direct excitation of the ppy dye to the phosphorescence intensities is obtained and shown in Figure 4-14. In the absence of PPESO3, the phosphorescence intensity of $\text{Ir(ppy)}_2(\text{bpy})\text{Cl}$ is higher than when PPESO3 is present, suggesting that triplet energy transfer from the dye to PPESO3 is occurring.

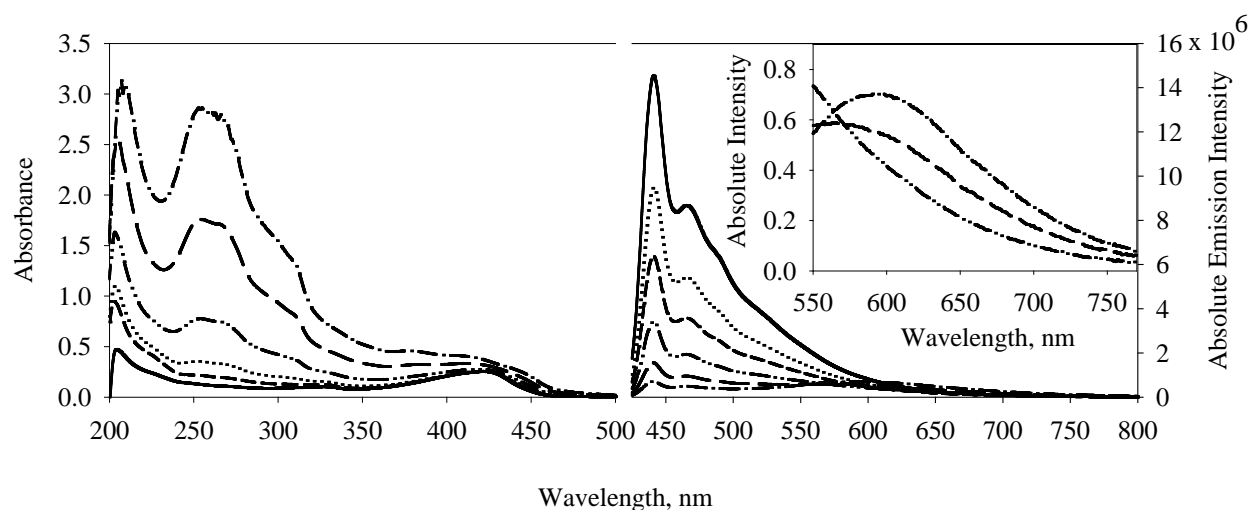


Figure 4-13. Absorption and emission spectra for the titration of a 4.61 μM solution of PPESO3 in methanol by $\text{Ir(ppy)}_2(\text{bpy})\text{Cl}$. The quencher concentrations are listed in order of decreasing PPESO3 fluorescence intensity: 0.0 μM , 2.14 μM , 5.33 μM , 16.1 μM , 37.6 μM , and 64.1 μM . The inset shows the rise of $\text{Ir(ppy)}_2(\text{bpy})\text{Cl}$ phosphorescence from 16.1 μM -64.1 μM .

Triplet energy back-transfer was confirmed by a transient absorption titration of PPESO3 with $\text{Ir(ppy)}_2(\text{bpy})\text{Cl}$, as shown in Figure 4-15. The triplet decay of PPESO3 observed at 734 nm, the maximum TA wavelength of PPESO3, is exponential and suggests a PPESO3 triplet lifetime of 0.447 μs . As the concentration of the ppy dye increases to $\sim 7.5 \mu\text{M}$, the intensity of the TA signal doubles. This is consistent with the doubling of signal strength observed during the titration of PPESO3 by $\text{Ir(bt)}_2(\text{bpy})\text{Cl}$ (Figures 4-11 and 4-12). As Figure 4-8B indicates, the

transient absorption of only $\text{Ir(ppy)}_2(\text{bpy})\text{Cl}$ does not feature any appreciable signal at 734 nm.

This suggests that the rise in TA signal during the PPESO3 titration is due to an increase of PPESO3 triplets caused by triplet back-energy transfer from the iridium dye.

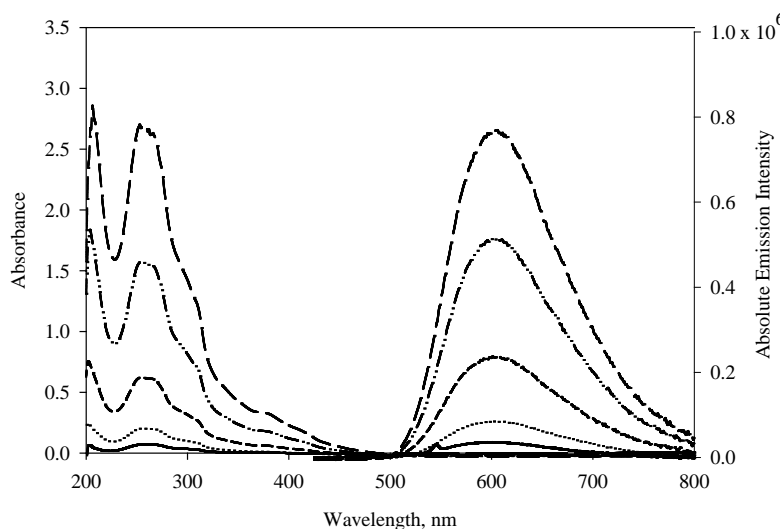


Figure 4-14. Absorption and emission spectra for the titration of $\text{Ir(ppy)}_2(\text{bpy})\text{Cl}$ in methanol without PPESO3. The acceptor concentrations are listed in order of increasing phosphorescence intensity: 2.14 μM , 5.33 μM , 16.1 μM , 37.6 μM , 64.1 μM .

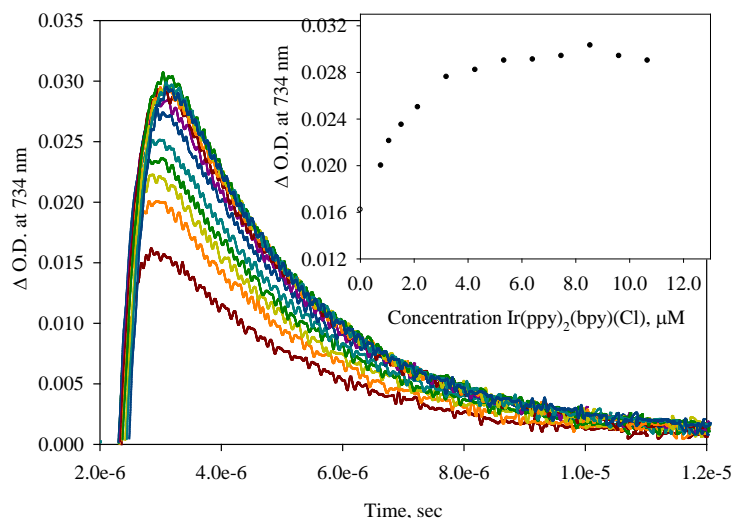


Figure 4-15. Triplet-triplet transient decay at 734 nm for 17.4 μM PPESO3 in methanol titrated by $\text{Ir(ppy)}_2(\text{bpy})\text{Cl}$. In order of increasing transient signal, the quencher concentrations are 0.0 μM , 0.769 μM , 1.07 μM , 1.53 μM , 2.14 μM , 3.20 μM , 4.27 μM , 5.34 μM , 6.41 μM , 7.47 μM , 8.54 μM , 9.61 μM , and 10.7 μM . The inset shows the change in the transient signal as a function of quencher concentration. All decays were obtained using a pump energy of 2.5 mJ.

Titration with Ir(hqx)₂(bpy)Cl

Having the lowest triplet energy, 1.96 eV, Ir(hqx)₂(bpy)Cl can be thought of as a low-energy quencher. When this dye is used in the fluorescence titration of a 4.61 μM solution of PPESO3 in methanol, Figure 4-16 is obtained. The fluorescence intensity of PPESO3 was observed to continually decrease as the dye was added, indicating singlet energy transfer from polymer to dye was occurring. Unlike the titrations involving the bt and ppy dyes, the fluorescence intensity of PPESO3 is extremely sensitive to Ir(hqx)₂(bpy)Cl concentration; near-quantitative quenching was obtained with a dye concentration of $\sim 10\ \mu\text{M}$, compared to concentrations greater than 60 μM for the high- and medium-energy quenchers. Also unique to the titration of PPESO3 by the hqx dye is the observation of dye phosphorescence at $\sim 0.90\ \mu\text{M}$ Ir(hqx)₂(bpy)Cl. Such a rapid onset of dye phosphorescence could indicate that the triplet energy of the hqx dye is lower than the triplet energy of PPESO3, preventing triplet back-energy transfer from occurring.

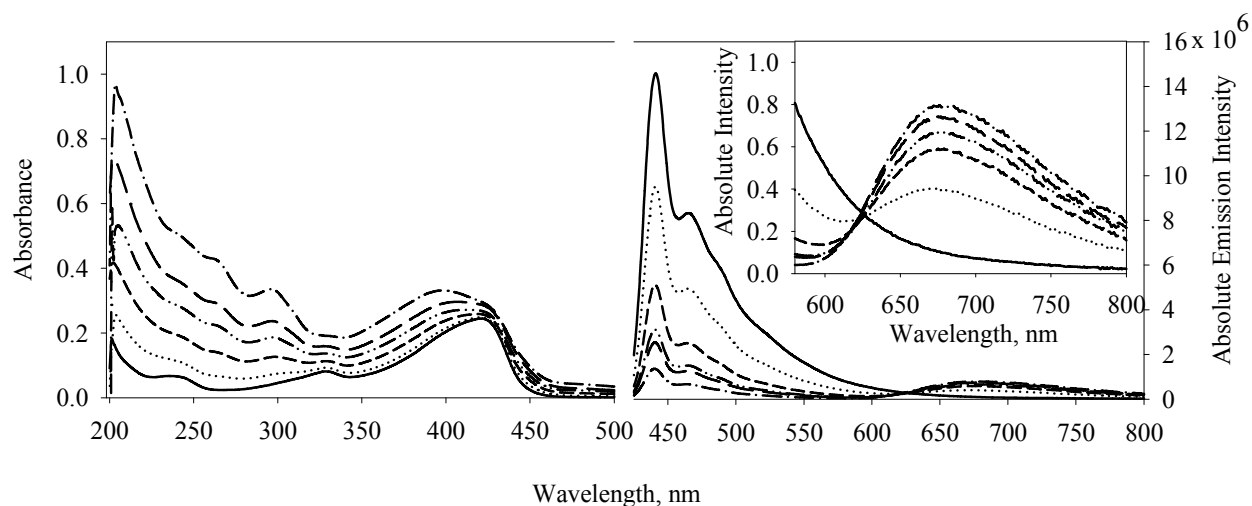


Figure 4-16. Absorption and emission spectra for the titration of a 4.61 μM solution of PPESO3 in methanol by Ir(hqx)₂(bpy)Cl. The quencher concentrations are listed in order of decreasing PPESO3 fluorescence intensity: 0.0 μM , 0.898 μM , 2.69 μM , 4.49 μM , 6.28 μM , and 9.87 μM . The inset shows the rise of Ir(hqx)₂(bpy)Cl phosphorescence from 0.00 μM -9.87 μM .

When $\text{Ir}(\text{hqx})_2(\text{bpy})\text{Cl}$ is titrated in the absence of PPESO3, using the same excitation wavelength and dye concentrations, Figure 4-17 is obtained. At every concentration employed, the phosphorescence intensity of $\text{Ir}(\text{hqx})_2(\text{bpy})\text{Cl}$ is higher in the presence of PPESO3. For dyes that are able to sensitize PPESO3 triplets, the phosphorescence intensity of the dye is always lower in the presence of PPESO3; since the opposite trend was observed for $\text{Ir}(\text{hqx})_2(\text{bpy})\text{Cl}$, the possibility exists that the triplet energy of the hqx dye is lower than the triplet energy of PPESO3. When the hqx dye quenches PPESO3 singlets *via* energy transfer, its excitation energy can only be released through the natural decay modes of $\text{Ir}(\text{hqx})_2(\text{bpy})\text{Cl}$, increasing the phosphorescence intensity of the dye.

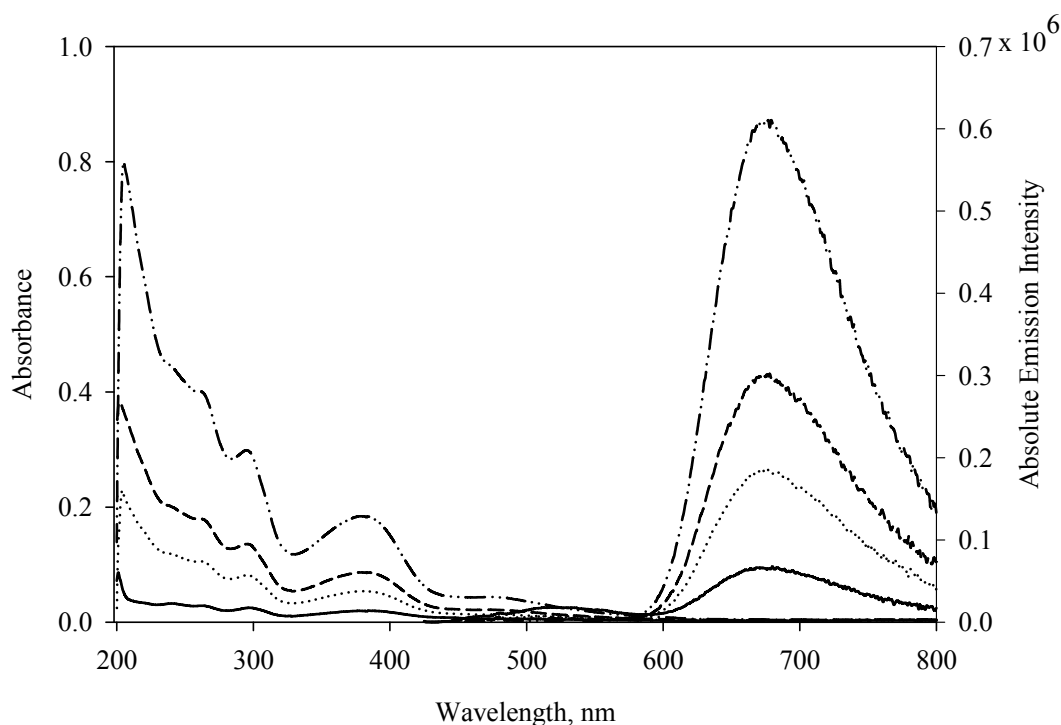


Figure 4-17. Absorption and emission spectra for the titration of $\text{Ir}(\text{hqx})_2(\text{bpy})\text{Cl}$ in methanol without PPESO3. The acceptor concentrations are listed in order of increasing phosphorescence intensity: 0.898 μM , 2.69 μM , 4.49 μM , and 9.87 μM .

A triplet-triplet TA titration of PPESO3 by $\text{Ir}(\text{hqx})_2(\text{bpy})\text{Cl}$ confirms the dye's inability to sensitize the formation of PPESO3 triplets (Figure 4-18). Resembling an exponential decay

pattern, the TA signal of PPESO3 monitored at 734 nm continually decreases with each addition of Ir(hqx)₂(bpy)Cl, ultimately approaching zero around a concentration of 4 μM. When the hqx dye is added, it quenches both PPESO3 singlets and naturally formed triplets. Since the triplet population of the sample decreases with the amount of quencher added, the TA signal will be observed to decrease. The continual reduction of the PPESO3 TA signal suggests that the triplet energy of Ir(hqx)₂(bpy)Cl is too low to sensitize the formation of PPESO3 triplets.

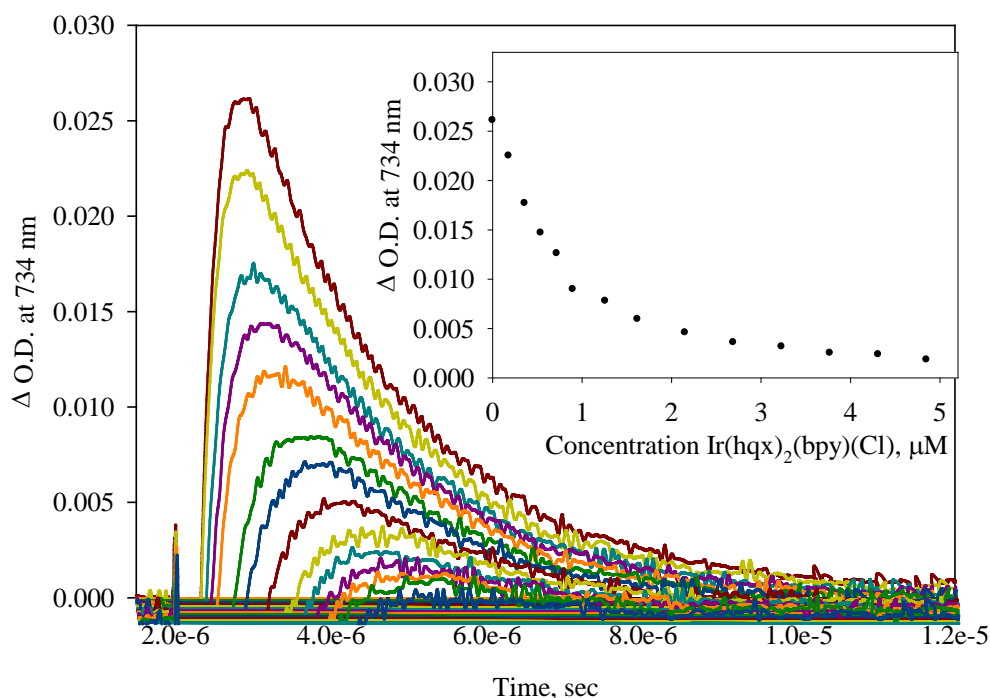


Figure 4-18. Triplet-triplet transient decay at 734 nm for 19.1 μM PPESO3 in methanol titrated by Ir(hqx)₂(bpy)Cl. In order of decreasing transient signal, the quencher concentrations are 0.0 μM, 0.180 μM, 0.359 μM, 0.539 μM, 0.718 μM, 0.898 μM, 1.26 μM, 1.62 μM, 2.15 μM, 2.69 μM, 3.23 μM, 3.77 μM, 4.31 μM, 4.85 μM. The inset shows the change in the transient signal as a function of quencher concentration. All decays were obtained using a pump energy of 2.5 mJ.

Discussion

Quenching Efficiency

When a series of variable triplet energy dyes, Ir(bt)₂(bpy)Cl, Ir(ppy)₂(bpy)Cl, and Ir(hqx)₂(bpy)Cl, were used to titrate PPESO3 during fluorescence measurements, a systematic

reduction in the fluorescence intensity of PPESO3 was observed. Titration experiments using transient absorption measurements indicated that depending on the triplet energy level of the quencher, an increase in the triplet PPESO3 population was observed. This was attributed to back-energy transfer of triplet excitation energy from the dye to the polymer. When the cationic quencher is initially added to the anionic polymer solution, the quencher diffuses to the polymer, whereupon an ion-pair complex is formed. The quencher accepts singlet excitation energy from PPESO3, ultimately converting this energy to a dye-based triplet exciton. Because an ion-pair complex has been formed between the polymer and quencher, the intermolecular distance is small enough to enable Dexter transfer of the triplet energy from the dye back to the polymer, thereby sensitizing the formation of PPESO3 triplets. Triplet back energy transfer is also allowed because the electrostatic complex prevents diffusion of the donor and acceptor away from each other after singlet quenching has occurred.

Because PPESO3 forms an ion-pair complex with quencher molecules, the quenching mechanism is said to be static; that is, the rate of exciton quenching can be expected to exceed the rate of molecular diffusion in solution, typically $10^{10} \text{ M}^{-1}\text{-s}^{-1}$.¹³⁸ The Stern-Volmer model, Equation 2-5, has been used to calculate the rate constant of exciton quenching for electrostatic complexes of polymers and quenchers.^{138,170}

$$\frac{I_0}{I} = 1 + K_{SV}[Q] \quad (2-5)$$

In this equation, I_0 and I represent the emission intensity of the donor in the absence and presence of quencher, Q , respectively, while K_{SV} is the Stern-Volmer constant, equation 2-6.

$$K_{SV} = k_q \tau \quad (2-6)$$

The Stern-Volmer constant is a product of the unquenched donor lifetime, τ , and the quenching rate constant, k_q . Traditionally, the Stern-Volmer relationship has been used to describe

situations where the donor and acceptor diffuse together, the acceptor quenches the donor, and the two diffuse apart.⁷² Different researchers^{138,170} have shown this model to be applicable in cases of static quenching as well. When a purely diffusional quenching mechanism operates, k_q cannot exceed the rate of molecular diffusion in solution, about $10^{10} \text{ M}^{-1}\text{-s}^{-1}$: diffusion of the acceptor to the donor, not exciton quenching, becomes the rate limiting step.¹³⁸ Assuming an average iridium dye lifetime of $1.00 \mu\text{s}$, it follows from Equation 2-6 that the diffusion-limited Stern-Volmer constant would have a maximum value of 10^4 M^{-1} . If a static quenching mechanism dominates a system, the Stern-Volmer and quenching constants will exceed the maximum limits imposed by diffusion. As long as a plot of I_0/I versus quencher concentration is linear, the Stern-Volmer model can be used to calculate the quenching rate constant for a donor-acceptor system, as k_q determines the magnitude of I_0/I .^{138,170}

Stern-Volmer analyses of PPESO3 quenching by the low-, medium-, and high-energy quenchers can be found in Figure 4-19. Static quenching of conjugated polymers can often exhibit Stern-Volmer plots such as Figure 4-19D, where the plot is initially linear, then begins to curve upward in a non-linear fashion.^{138,170} It should be noted that all three iridium dyes produced non-linear Stern-Volmer plots similar in shape to Figure 4-19D, but for clarity, the nonlinear portions of Figures 4-19A-C have been omitted. The nonlinear Stern-Volmer plot has been attributed to exciton diffusion along the polymer backbone and dye-induced polymer aggregation.¹³⁸ Once bound to the polymer, the dye can quench excitons produced directly on the repeat unit it is bound to. In addition, PPESO3 is a conjugated polymer, enabling other excitons on the polymer to intramolecularly diffuse to the quenching site. The cationic quencher can also induce aggregation of the anionic polymer; in this aggregate, excitons can hop from one polymer chain to another. When these two processes combine, they greatly increase the potency

of the quencher. As more quencher is added, the effects increase, resulting in a nonlinear Stern-Volmer plot at “high” quencher concentrations.¹³⁸ This is graphically depicted in Figure 4-20.

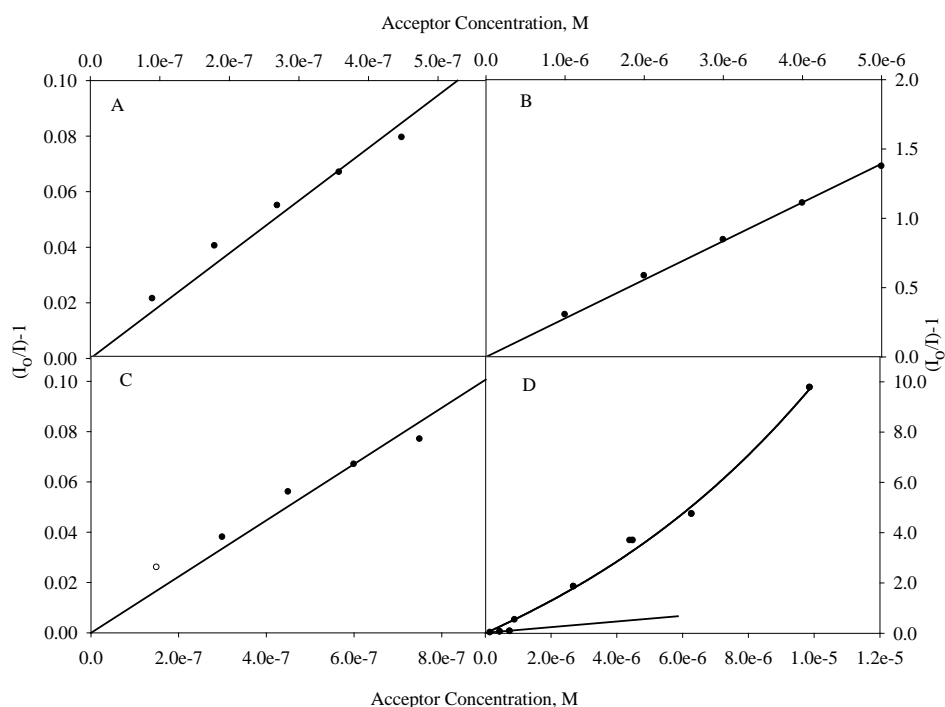


Figure 4-19. Stern-Volmer plots for 4.61 μM PPESO3 titrated in methanol. A) Ir(bt)₂(bpy)Cl titration. B) Ir(ppy)₂(bpy)Cl titration. C) Ir(hqx)₂(bpy)Cl titration. D) Titration with Ir(hqx)₂(bpy)Cl showing the nonlinear Stern-Volmer plot. In plot D, the fits are produced using a linear fit and a non-linear fit of the data. The linear fit is an extrapolation of the first three data points, showing the expected linearity of the data. The nonlinear fit shows the observed non-linearity of the data. The nonlinear portions of A-C have been omitted for clarity.

The propensity for conjugated polymer donor-acceptor complexes to exhibit nonlinear Stern-Volmer plots has led to the practice of using very low, often submicromolar, concentrations of acceptor to achieve a linear Stern-Volmer plot from which K_{sv} and k_q can be determined.^{138,170} The values of these constants for the bt, ppy, and hxq quenching of PPESO3 can be found in Table 4-3. The Stern-Volmer and quenching rate constants for all the systems are considerably greater than the limiting values imposed by diffusion, indicating the quenching mechanism is indeed static. The onset of nonlinearity in a Stern-Volmer plot can vary with each

quencher; to provide a better comparison of quenching efficiency for the various acceptors used, Q_{90} values are also listed in Table 4-3. These values are extracted from the Stern-Volmer plot when the dye is 90% quenched, corresponding to an I_0/I value of 10.¹³⁸ For the $\text{Ir}(\text{bt})_2(\text{bpy})\text{Cl}$ and $\text{Ir}(\text{ppy})_2(\text{bpy})\text{Cl}$ dyes, the Q_{90} values are $\sim 48 \mu\text{M}$ and $38 \mu\text{M}$, respectively, compared to a value of $\sim 12 \mu\text{M}$ for $\text{Ir}(\text{hqx})_2(\text{bpy})\text{Cl}$. The lower Q_{90} value for the hqx/low-energy dye suggests this is the most efficient quencher of the three. It has been suggested¹³⁸ that the association constant for the donor-acceptor complex is responsible for varying values of Q_{90} . In particular, $\text{Ir}(\text{hqx})_2(\text{bpy})\text{Cl}$ has the largest available area among the three dyes for π -stacking. The association constant for the $\text{PPESO-Ir}(\text{hqx})_2(\text{bpy})\text{Cl}$ complex could be higher than the other dyes because of the greater ability of $\text{Ir}(\text{hqx})_2(\text{bpy})\text{Cl}$ to undergo π -stacking with the donor, resulting in a stronger donor-acceptor complex. This would increase the efficiency of the dye to quench PPESO3 excitons, requiring less dye to reach the same amount of quenching.

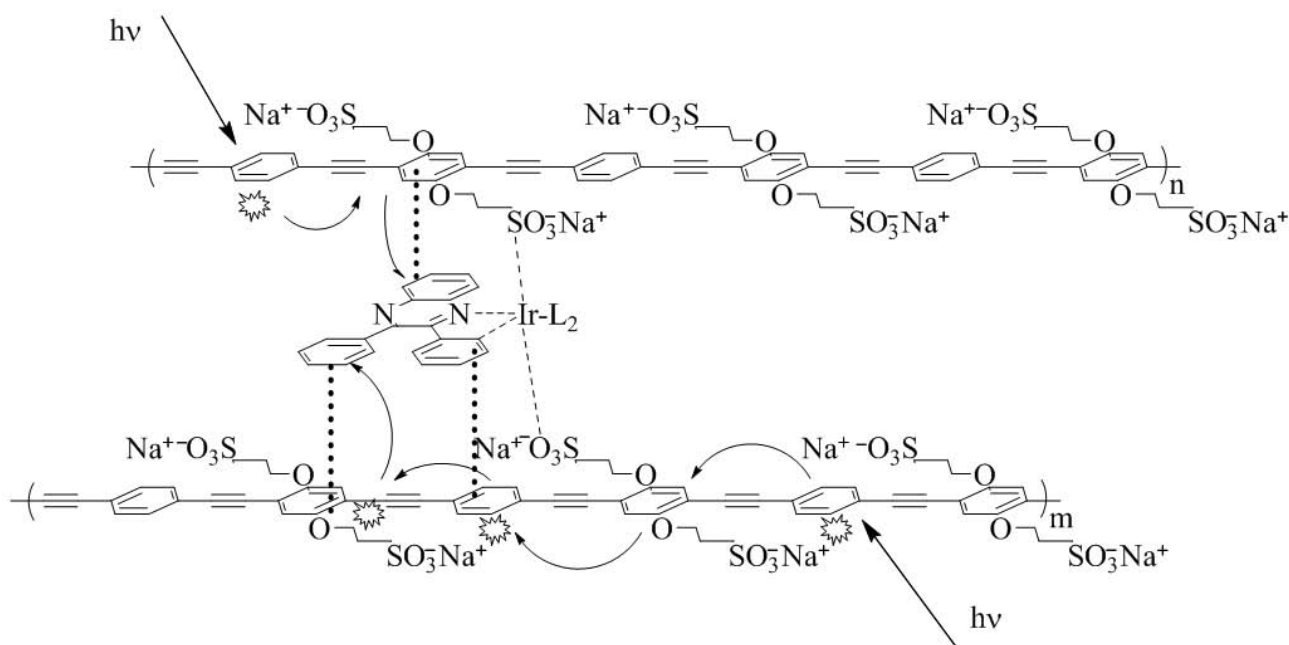


Figure 4-20. Schematic depiction of the origin of nonlinear Stern-Volmer plots with statically-quenched PPESO3. Adapted from Schanze *et.al.*¹³⁸ Represents a singlet exciton; represents exciton delocalization and transfer; represents π - π stacking; represents electrostatic attraction. The example quencher is $\text{Ir}(\text{hqx})_2(\text{bpy})\text{Cl}$.

Table 4-3. Summary of the PPESO3 quenching data by (C^N)₂Ir(bpy)Cl dyes in methanol solution.

Entry	C ^N	$K_{sv} \times 10^5, M^{-1}$	$k_q \times 10^{14}, M^{-1} \cdot s^{-1}$ ^a	$Q_{90}, \mu M$
1	bt	1.87±0.05	4.07±0.1	47.5±10
2	ppy	2.73±0.03	5.93±0.08	37.6±10
3	hqx	1.01±0.06	2.20±0.1	12.3±10

Notes: ^a $\tau_f = 0.46$ ns was assumed for PPESO3.⁷¹

Triplet Sensitization

Transient absorption provided a way of probing the relative number of triplet excited states in PPESO3. By comparing the intensity of the transient absorption signal before and after the addition of an iridium dye, the ability of the dye to influence the number of PPESO3 triplet excitons can be ascertained. Using this technique, it was determined that addition of Ir(bt)₂(bpy)Cl and Ir(ppy)₂(bpy)Cl increased the transient absorption signal, indicating a rise in PPESO3 triplet population. By contrast, addition of Ir(hqx)₂(bpy)Cl decreased the TA signal, indicating that no additional PPESO3 triplets could be formed by this donor-acceptor complex.

After the iridium dye is added to the PPESO3 solution, the polymer and metal complex. When the PPESO3 is photoexcited, the exciton diffuses along the polymer backbone to the iridium dye, whereupon the excitation energy is transferred from the polymer to the dye and the polymer fluorescence is quenched. The dye then becomes excited, ultimately forming a dye-based triplet. For Ir(bt)₂(bpy)Cl [$E_T = 2.36$ eV] and Ir(ppy)₂(bpy)Cl [$E_T = 2.25$ eV] complexes with PPESO3, the triplet energy of the dye lies above the triplet energy level of the polymer, as shown in Figure 4-21. The dye returns to its electronic ground state by transferring its triplet energy back to PPESO3, sensitizing the polymer triplet. Because an electrostatic donor-acceptor complex is formed, the dye is not able to diffuse away from the polymer, making triplet sensitization possible. However, when Ir(hqx)₂(bpy)Cl [$E_T = 1.96$ eV] complexes with PPESO3, no triplet sensitization occurs because the triplet energy of this dye lies below the triplet energy

of the polymer. This makes triplet back energy transfer energetically disfavored, causing the dye to phosphoresce. Indeed, a dye phosphorescence increase at every quencher concentration was only observed for the PPESO3-Ir(hqx)₂(bpy)Cl system, indicating that no triplet excitation energy from the dye could be back-transferred to the polymer. Armed with these results, the triplet energy of PPESO3 can be estimated to lie between 1.96-2.25 eV. A similar polymer, **4-26**, was estimated to have a triplet energy of 2.22 eV. This polymer is similar in structure to PPESO3, so the estimated triplet energy range of PPESO3 is not entirely unexpected.¹⁷¹

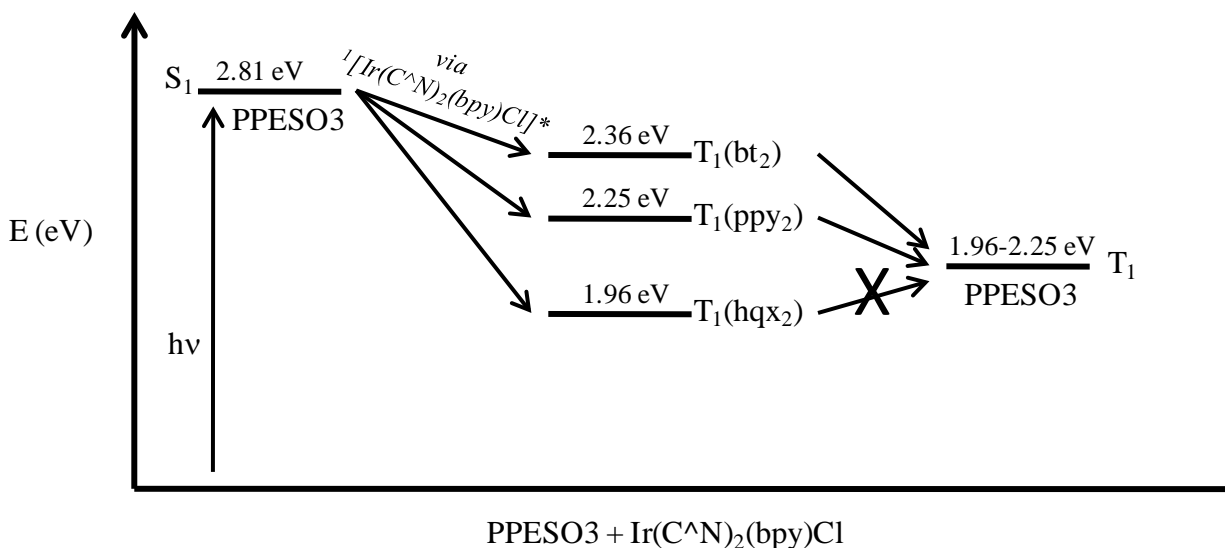


Figure 4-21. Energy level diagram depicting the triplet sensitization of PPESO3 by Ir(bt)₂(bpy)Cl, Ir(ppy)₂(bpy)Cl, and Ir(hqx)₂(bpy)Cl.

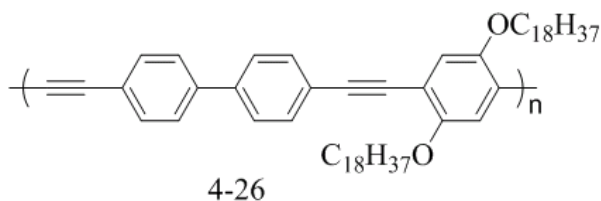


Figure 4-22. Structure of BP-PPE-C₁₈.¹⁷¹

Application to LbL Films

The purpose of this study was to probe the feasibility of incorporating a triplet sensitizer in LbL films of PPESO3 to improve the exciton diffusion length for these films. Studies by multiple researchers have indicated that incorporating triplet sensitizers in thin organic films can enhance the length of exciton diffusion.¹⁶⁰⁻¹⁶² As discussed in Chapter 2, triplet excitons generally have exciton diffusion lengths significantly greater than those of singlets. The exciton diffusion studies in Chapter 3 determined that aggregation of PPESO3 in LbL films, in addition to the short exciton lifetime, significantly decreases its singlet exciton diffusion length. Although the presence of aggregates in LbL films will always have an impact on the ability of excitons to diffuse, the increase in exciton lifetime afforded by triplet sensitization will undoubtedly increase the exciton diffusion length in these films.

There are several ways to incorporate the iridium dyes into LbL films. For discussion purposes, it is assumed that all of the following films are built on glass using PPESO3 as a polyanion and one of the iridium dyes **4-18** or **4-19** as a cation. The simplest experiment would involve films of the structure glass|ITO|[sensitizer/PPESO3]_n, where ITO acts as an electron accepting quencher for the sensitized triplet excitons and n is the number of bilayers. These films will more than likely feature complete fluorescence quenching of the PPESO3 by the sensitizer; combined with the fact that phosphorescence of PPESO3 was not observed in the titration emission spectra in this chapter (Figures 4-10, 4-13, and 4-16), transient absorption would have to be used to probe the triplet population of PPESO3 as a function of total film thickness. The change in triplet optical density for unquenched, sensitized, n bilayer PPESO3 films on glass could be compared to the change in triplet optical density for an equal number of sensitized PPESO3 bilayers on ITO. Equation 2-12 would then be applied to the data, affording the triplet exciton length of diffusion. Although film aggregation will still decrease the exciton

length of diffusion, this effect should be partially offset by the increase in the exciton lifetime afforded by the triplet sensitization. Because the pump and probe energies can be irreproducible between measurements, it will be necessary to perform multiple repeats of the experiment to generate average values of exciton quenching.

Another architecture affords an experiment not easily performed with solutions: the interplay of fluorescence quenching and triplet sensitization. These films would have the architecture substrate|sensitizer|[PMA/PAH]_n|PPESO3.¹³¹ The triplet sensitizer would be separated by a poly(methacrylate)/poly(allylamine hydrochloride) spacing layer *n* bilayers thick. In a fluorescence experiment, the PPESO3 would be photoexcited. The excitation energy would then be transferred through space to the sensitizer, quenching PPESO3's fluorescence. A variation of spacing layer thickness would result in a variation in fluorescence quenching, as a thicker spacer layer would allow fewer PPESO3 singlets to be quenched by the sensitizer. If the spacing layer is thick enough, no fluorescence quenching should occur. Once a set of films is identified as having varying amounts of fluorescence quenching, triplet-triplet transient absorption would be used to examine the ability of the sensitizer to induce formation of PPESO3 triplets. Because triplet sensitization occurs by short-range Dexter transfer and fluorescence quenching occurs through long-range Förster transfer, the film thicknesses at which the fluorescence quenching and triplet sensitization cease to become effective should be very different. Such an experiment is of interest concerning the fundamental photophysics of triplet sensitization, allowing for an estimation of the maximum distance over which triplet sensitization and fluorescence quenching can occur for the sensitizer/PPESO3 systems studied in this chapter.

Experimental

Materials

Iridium (III) chloride hydrate was purchased from Strem and used as received. The bpy, bt, ppy, and hqx ligands were purchased from Acros, while all other materials were purchased from Aldrich. Methanol used for spectrophotometry was of HPLC grade. Mass spectrometry was performed by the University of Florida Department of Chemistry Mass Spectrometry Services. The mass spectrograms can be found in Appendix B. ^1H NMR spectra are referenced with respect to the protonated solvent peak and can be found in Appendix C. The chloro-bridged dimers of bt $[\text{Ir}(\text{bt})_2\text{Cl}]_2$, ppy $[\text{Ir}(\text{ppy})_2\text{Cl}]_2$, and hqx $[\text{Ir}(\text{hqx})_2\text{Cl}]_2$, were prepared according to the literature procedures.^{44,163,166} Abigail Shelton synthesized $[\text{Ir}(\text{bt})_2\text{Cl}]_2$. Dichloromethane was distilled over calcium hydride before use.

Synthesis

Iridium (III) bis(2-phenylbenzothiazolato- $\text{N},\text{C}^{2'}$) bipyridyl chloride $[\text{Ir}(\text{bt})_2(\text{bpy})\text{Cl}]$, 4-18]. $[\text{Ir}(\text{bt})_2\text{Cl}]_2$ (75.3 mg, 0.058 mmol) and 2,2'-bipyridine (22.3 mg, 0.145 mmol) were suspended in 7 mL of methylene chloride. The reaction was allowed to stir overnight under argon at room temperature, after which time the reaction became a dark red-orange color that had a sandy-textured precipitate. Silica gel TLC (methylene chloride) was used to follow the reaction progress. After about 20 hr, TLC indicated consumption of $[\text{Ir}(\text{bt})_2\text{Cl}]_2$. When nitrogen was blown over the reaction spot while the TLC plate was being irradiated with UV light, there was an intense yellow spot observed at the origin corresponding to the product. The reaction was filtered and painstakingly recrystallized in toluene, affording the product as an orange powder (22 mg, 48%). MS (APCI-TOF) m/z : expected M^+ for $\text{C}_{36}\text{H}_{24}\text{IrN}_4\text{S}_2$, 769.1065; found 769.1057. ^1H NMR (CD_3CN , 300 MHz) 6.22 (m, 2H), 6.40 (d, 1H), 6.70 (dt, 2 H), 6.90 (m, 3

H), 7.13 (t, 2H), 7.40 (t, 2H), 7.58 (q, 2H), 7.68 (t, 2H), 7.76 (m, 1 H), 7.93 (d, 1H), 8.03 (d, 1H), 8.14 (m, 2H), 8.21 (d, 1H), 8.40 (d, 1H), 8.50 (d, 1H).

Iridium (III) bis(2-phenylpyridinato-N,C^{2'}) bipyridyl chloride [Ir(ppy)₂(bpy)Cl, 4-19]. [Ir(ppy)₂Cl]₂ (75.3 mg, 0.070 mmol) and 2,2'-bipyridine (26.8 mg, 0.175 mmol) were suspended in 7 mL of methylene chloride. The reaction was stirred under argon overnight at room temperature, after which time a dark orange solution had developed. Using a procedure similar to **4-18**, silica gel TLC (tetrahydrofuran) indicated complete consumption of the starting material and formation of the product (bright yellow-orange emission) after about 22 hr. A few milliliters of toluene were added to the reaction to precipitate the product. The orange colored, chunky precipitate was filtered, washed with toluene and recrystallized in a methylene chloride/toluene mixture, affording the product as a yellow powder (20 mg, 37%). MS (ESI-TOF) *m/z*: expected M⁺ for C₃₂H₂₄IrN₄, 657.1626; found 657.1646. ¹H NMR (CD₃CN-DMSO-d₆, 300 MHz) 6.30 (d, 2H), 6.91 (t, 2H), 7.24 (q, 4H), 7.50 (t, 2H), 7.60 (d, 2H), 7.82 (m, 4H), 8.00 (m, 2H), 8.10 (m, 4H), 8.51 (m, 2H).

Iridium (III) bis(2,3-diphenylquinoxaline-N,C^{2'}) bipyridyl chloride [Ir(hqx)₂(bpy)Cl, 4-20]. [Ir(hqx)₂Cl]₂ (75.0 mg, 0.047 mmol) and 2,2'-bipyridyl (18.4 mg, 0.118 mmol) were suspended in 6 mL of methylene chloride. The reaction was stirred at room temperature overnight and under argon, after which time the reaction became a red-brown color with a fine suspended particulate. After 29 hours, the silica gel TLC (methylene chloride) procedure of **4-18** indicated complete consumption of the starting material and formation of the product (bright red-orange emission). The reaction was filtered and washed with toluene. The filtrate was recrystallized in a mixture of methylene chloride and hexanes to afford a red, shiny, crystalline product (17 mg, 38%). MS (ESI-TOF) *m/z*: expected M⁺ for C₅₀H₃₄IrN₆, 911.2472; found

911.2495. ^1H NMR (CD_3CN , 300 MHz) 6.55 (d, 2H), 6.73 (dt, 4H), 7.09 (d, 2H), 7.27 (t, 2H), 7.38 (d, 2H), 7.70 (m, 8H), 7.91 (brs, 4H), 8.10 (d, 2H), 8.11 (t, 2H), 8.23 (t, 2H), 8.50 (d, 2H), 8.78 (d, 2H).

Optical Titrations

Ultraviolet-visible absorption measurements were performed on a Varian-Carey 50 Bio spectrophotometer. Photoluminescence measurements were obtained using a Jobin-Yvon Fluorolog-3 fluorimeter. Both measurements were obtained in a 1 cm^2 long neck emission cell. Transient absorption measurements were performed on previously described instrumentation in a 1 cm path-length flow cell.^{172,173} The general procedure for optical titrations of PPESO3 is as follows. All donor and acceptor aliquots were delivered using precision glass syringes purged three times with argon. An argon line was purged with a slow stream of argon for sixty minutes before use. Methanol (3.0 mL for photoluminescence, 10.0 mL for TA) was added to the cell and purged with argon for twenty minutes. An aliquot of PPESO3 was added to the methanol to give a concentration of $4.61\text{ }\mu\text{M}$ for photoluminescence measurements or $17.4\text{ }\mu\text{M}$ for TA titrations involving $\text{Ir}(\text{bt})_2(\text{bpy})\text{Cl}$ and $\text{Ir}(\text{ppy})_2(\text{bpy})\text{Cl}$. For TA titrations involving $\text{Ir}(\text{hqx})_2(\text{bpy})\text{Cl}$, a PPESO3 concentration of $19.1\text{ }\mu\text{M}$ was used so that the greatest range of quencher concentrations could be studied. In all cases, no further degassing of the PPESO3 solution was done after addition of the donor. The quenchers were dissolved in methanol and separately outgassed with argon for twenty minutes before use. To ensure quenching reproducibility, no acceptor aliquots less than $15\text{ }\mu\text{L}$ were added to the PPESO3 solutions. All TA titrations were monitored at a single wavelength, 734 nm , which corresponds to the maximum of the PPESO3 $\text{T}_1\text{-T}_n$ absorption. The optical power of the TA laser was held constant

at approximately 2.5 mJ; the pump's power was measured before the addition of each dye aliquot and adjusted as necessary.

Triplet lifetimes were estimated from the full transient absorption spectrum for each compound using SpecFit software. The global first order rate of decay was estimated; the inverse of this value afforded the triplet lifetime. Phosphorescence quantum yields were measured using relative actinometry. For Ir(bt)₂(bpy)Cl and Ir(ppy)₂(bpy)Cl, Rose Bengal ($\Phi_f = 0.11$ in 0.01 M KOH in absolute ethanol) was used as the actinometer¹⁶⁸ while for Ir(hqx)₂(bpy)Cl, Rhodamine B was used ($\Phi_f = 0.69$ in methanol).¹⁶⁹

CHAPTER 5

CONCLUSION

The previous chapters detailed the investigations into the ability of polymer-based excitons to diffuse in thin films of conjugated polymers. A new model of calculating the exciton diffusion coefficient, from which the length of diffusion can be derived, was validated against those values obtained using standard time-of-flight exciton diffusion measurements. Triplet exciton diffusion was studied using a series of platinum-acetylide thin films built from pPtPh, whereas singlet exciton diffusion was examined with layer-by-layer self assembled thin films using a poly(phenylene ethynylene) derivative, PPESO3. It was found that LbL films of conjugated polyelectrolytes such as PPESO3 tend to aggregate when formed, so a model of film aggregation was developed. As a way to improve upon the singlet exciton length of diffusion in LbL films, a series of cationic iridium dyes were developed to sensitize triplet formation in PPESO3. The ability of the dyes to sensitize PPESO3 triplets was confirmed using photoluminescence and transient absorption measurements.

Triplet Exciton Diffusion in Platinum Acetylide Thin Films

Although the literature is filled with various techniques to calculate exciton diffusion coefficients and lengths of diffusion, most require sophisticated instrumentation and complex mathematical modeling. For this reason, a new model of exciton diffusion was developed. This model assumes that acceptor molecules are molecularly dissolved, and uniformly dispersed in, spin-coated polymer films. Using an accurate method of estimating the polymer density, the concentration of acceptor molecules in the film can be calculated. Because the acceptor concentration is known, the Hindered Access model, a standard exciton quenching model, can be used along with exciton quenching measurements to determine the quenching rate constant. An equation derived from Fick's Law of Diffusion was then used to relate the quenching rate

constant to the coefficient of exciton diffusion. Using this model, the coefficient of triplet exciton diffusion for pPtPh films was calculated to be $4.59\text{--}4.96 \times 10^{-6} \text{ cm}^2\text{--s}^{-1}$, while the length of diffusion was estimated to be 22.2 - 23.5 nm, depending if PCBM or PtTPP was used as the acceptor. These results were confirmed using standard, literature-based time-of-flight measurements involving layered pPtPh|(C60 or PtTPP) films. Analysis of the available literature data revealed that a polymer-based triplet exciton can diffuse substantially more effectively than can a small molecule based triplet. This was attributed to the ability of a polymer-based exciton to diffuse intramolecularly *via* delocalization, and intermolecularly by exciton hopping.

There are several future experiments suggested by this work. Because of the obvious applications to organic solar cells, it would be interesting to relate the length of exciton diffusion to the photocurrent generated in a photovoltaic cell. The thiophene analogue of pPtPh, pPtTh, has been previously used to construct solar cells.⁹⁸ To eliminate the possibility of backbone defects, this polymer should be synthesized according to the AB asymmetric polymerization procedure outlined in Figure 2-5. Next, the coefficient and length of exciton diffusion would be calculated for pPtTh using the new exciton quenching model, with PCBM as the acceptor. A series of solar cells containing variable thickness pPtTh layers would be created, on top of which fullerene would be thermally evaporated. The thicknesses of the polymer layers should be incrementally adjusted to lie between half the exciton length of diffusion and a few times greater than the exciton length of diffusion. In this way, the photocurrent can be compared to the film thickness. This method would allow the researcher to determine the film thickness where the effects of optical absorption and film thickness combine to produce an optimal photocurrent.

Singlet Exciton Diffusion in LbL Thin Films

The mechanism by which layer-by-layer self assembled thin films are formed from conjugated polyelectrolytes was studied and the singlet exciton length of diffusion in an example

film was calculated. Two typical conjugated polyelectrolytes, the conformationally locked PPESO3 and conformationally flexible pFI, were used in conjunction with PDDA to build electrostatic LbL films. Through fluorescence measurements and atomic force microscopy imaging, it was found that the films tend to be aggregated. When LbL films were constructed using a variety of polyelectrolytes, deposition solvents, and substrates, the aggregation was found to persist. Experimentation revealed that the polyelectrolytes mainly aggregate after they are deposited onto the film, regardless of the deposition solvent used. A model of LbL film aggregation employing conjugated polyelectrolytes was proposed to account for these observations.

The effects of polyelectrolyte aggregation on the singlet exciton length of diffusion for PPESO3 were determined using time-of-flight studies. Films using PPESO3 and PDDA polyelectrolytes were built onto an ITO-coated substrate. Using the one-dimensional continuity model, the singlet exciton length of diffusion was found to be 2.12 nm (5.0 bilayers), significantly lower than most other singlet lengths of diffusion found in the literature. This low value was attributed to film aggregation. It was suggested that the aggregates common to LbL films act as exciton traps, preventing efficient exciton diffusion. One possibility of enhancing the length of exciton diffusion, triplet sensitization of PPESO3, was suggested.

The propensity for LbL films of conjugated polyelectrolytes to aggregate suggests a potential avenue for future research. One promising way of disrupting aggregation in LbL films is through the use of layered double hydroxides.¹⁴⁴⁻¹⁴⁷ These inorganic complexes are typically made by refluxing cationic metals, such as magnesium and aluminum ions, in water along with select counter-ions. The metals self-assemble into very rigid and very large molecular sheets and precipitate from solution as the sheets are formed. The assemblies are then suspended in water

and the LbL process carried out. The layered double hydroxides act as the cationic electrolyte, while a conjugated anionic polyelectrolyte is also used. Once deposited onto the conjugated polymer, the double hydroxides are so large, rigid, and immovable that they prevent the conjugated polymers from aggregating. This effect was exemplified by the work of Lu and Evans.¹⁴⁴ When they constructed LbL films from poly(*para*-phenylene) and a Mg-Al layered double hydroxide, the fluorescence intensity was found to increase with the number of bilayers, contrary to most literature examples of LbL films built from conjugated polyelectrolytes. This Mg-Al layered double hydroxide should be synthesized and used as the counter-ion for LbL films built from PPESO3 or pFl. If the fluorescence spectra of these films confirms Lu's and Evan's findings, atomic force microscopy and x-ray reflectivity measurements can be used to conclusively probe the unaggregated nature of these films.

Triplet Sensitization of PPESO3

Owing to the ability of polyelectrolytes in LbL films to aggregate, a series of triplet sensitizers for PPESO3 were developed. In theory, the increased lifetime of a triplet PPESO3 exciton should partially offset the effects of film aggregation on the ability of excitons to diffuse within these films. Phosphorescent, cationic iridium dyes, Ir(bt)₂(bpy)Cl, Ir(ppy)₂(bpy)Cl, and Ir(hqx)₂(bpy)Cl, were synthesized and their ability to sensitize PPESO3 triplet excitons was studied using photoluminescence and transient absorption spectroscopies. In this model, the cationic iridium dye was assumed to electrostatically bind with the anionic PPESO3. When the PPESO3 was photoexcited, it was determined that the singlet excitation energy was transferred *via* Förster transfer to the iridium dye. The dye then converted the singlet excitation into a dye-based triplet. Depending on the triplet energy of the iridium dye, the triplet energy was then back-transferred to the PPESO3, sensitizing the polymer-based triplet exciton. It was determined through fluorescence measurements that all three dyes can accept PPESO3 excitation energy, but

only Ir(bt)₂(bpy)Cl and Ir(ppy)₂(bpy)Cl have the ability to sensitize PPESO3 triplets, as suggested by triplet-triplet transient absorption experiments. The energy of the PPESO3 triplet exciton was estimated to be 1.96-2.25 eV. All three dyes were found to have Stern-Volmer and quenching rate constants of 10⁵ M⁻¹ and 10¹⁴ M⁻¹-s⁻¹, respectively. These values far exceeded those imposed by the diffusion-controlled limits. This suggests a super-quenching mechanism is operative, whereby one quencher molecule can accept energy from multiple repeat units and polymer chains.

The Ir(bt)₂(bpy)Cl and Ir(ppy)₂(bpy)Cl dyes were found to have the ability to sensitize PPESO3 triplets, enabling their use as counterions for PPESO3 in electrostatic LbL films. One possible experiment is to determine the triplet exciton diffusion coefficient for PPESO3 excitons. Films of the architecture substrate|[sensitizer|PPESO3]_n would be constructed, where n represents the number of bilayers. Essentially a repeat of the singlet exciton diffusion studies of Chapter 3, multilayer films using these electrolytes would be deposited from methanol onto glass, a non-quenching substrate, and onto ITO, a quenching substrate for PPESO3 excitons. Because the induced phosphorescence of PPESO3 is not visible in normal photoluminescence measurements, thin film transient absorption would have to be used to determine the relative amount of triplet exciton quenching. The transient signal of films with equal numbers of bilayers built on glass and ITO would be compared and the exciton diffusion parameters calculated. Since the optical power of light pulses in transient absorption experiments varies with each measurement, it is likely that the optical power would have to be carefully monitored and that several different batches of films would have to be made in order to obtain an average exciton quenching value for each film thickness.

APPENDIX A EXAMPLE CALCULATIONS FROM CHAPTER 2

Polymer Density

The density of a polymer, ρ , can be accurately calculated using the procedure of Albert and Malone,¹⁰⁸ Equation A-1, where a_1 is a constant, M_{ru} is the repeat unit molar mass, and P_{ru} is the parachor of the repeat unit. In the following example, the density of pPtPh will be calculated.

$$\rho = a_1 \frac{M_{ru}}{P_{ru}} \quad (A-1)$$

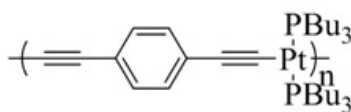


Figure A-1. Chemical structure of the pPtPh repeat unit.

The parachor, P , of an atom is given by Equation A-2, where V_m is the molar volume of the molten element and γ is the liquid surface tension.¹⁰⁹

$$P = V_m \sqrt[4]{\gamma} \quad (A-2)$$

Using the experimentally determined molar volume for molten platinum, $V_m = 9.09 \text{ cm}^3 \cdot \text{mol}^{-1}$,¹¹² and the surface tension of molten platinum, $\gamma = 1869 \times 10^{-3} \text{ N} \cdot \text{m}^{-1}$,¹¹³ Equation A-2 can be used to calculate the parachor for platinum.

$$P_{Pt} = 9.09 \frac{\text{cm}^3}{\text{mol}} \sqrt[4]{1869 \times 10^{-3} \frac{\text{N}}{\text{m}}} \quad (A-3)$$

$$P_{Pt} = 10.628 \frac{\text{cm}^3}{\text{mol}} \frac{\text{N}}{\text{m}} \quad (A-4)$$

The parachor of an element contains the parachor of one-half a single bond; the only time the parachor of a bond must be used is when multiple bonds are present. Note that rings also have their own parachors. The value of P_{ru} is calculated using group increments. For the polymer of interest, the number, x , of all rings, different atoms, and multiple bonds must be

ascertained. This data, along with the parachor, P_x , of each ring, bond, and atom type are then used in Equation A-5. The Mumford and Phillips parachors for bonds, rings, and atoms common to organic systems have been summarized by Quale, and are considered to be the most widely used values.¹⁰⁹

$$P_{ru} = \sum_x^n n_x P_x \quad (A-5)$$

This process is exemplified by Equation A-6, which depicts the parachor calculation for pPtPh, whose repeat unit formula is $C_{34}H_{58}P_2Pt$; also present in pPtPh are three double bonds (benzene), two triple bonds (acetylene) and one six-membered ring (benzene).

$$P_{pPtPh} = [C] \ 34(9.20) \frac{\text{cm}^3}{\text{mol}} \frac{N}{m} + [H] \ 58(15.4) \frac{\text{cm}^3}{\text{mol}} \frac{N}{m} + [P] \ 2(37.7) \frac{\text{cm}^3}{\text{mol}} \frac{N}{m} + \quad (A-6)$$

$$[Pt] \ 1(10.6) \frac{\text{cm}^3}{\text{mol}} \frac{N}{m} + [C=C] \ 3(19.0) \frac{\text{cm}^3}{\text{mol}} \frac{N}{m} + [C \equiv C] \ 2(38.0) \frac{\text{cm}^3}{\text{mol}} \frac{N}{m} +$$

$$[6 \text{ membered ring}] \ 1(0.8) \frac{\text{cm}^3}{\text{mol}} \frac{N}{m}$$

$$P_{pPtPh} = 1425.8 \frac{\text{cm}^3}{\text{mol}} \frac{N}{m} \quad (A-7)$$

The molar volume, V_m , of the repeat unit is calculated in a similar manner using group increment methods. Durchschalg and Zipper compiled a list of molar volumes for a variety of atoms and groups, but neglected to include the increments for carbon-carbon multiple bonds. When validated against the experimentally determined molar volumes of a variety of molecules, this method was found to be reasonably accurate.¹¹¹ Using their values, V_m for the pPtPh repeat unit can be calculated (Equation A-8). Note that the molar volume for Pt is taken from the literature.¹¹²

$$V_{m,pPtPh} = [C] 34(9.9) \frac{\text{cm}^3}{\text{mol}} + [H] 58(3.1) \frac{\text{cm}^3}{\text{mol}} + [P] 2(17.0) \frac{\text{cm}^3}{\text{mol}} + \quad (\text{A-8})$$

$$[Pt] 1(9.09) \frac{\text{cm}^3}{\text{mol}} + [6 \text{ membered ring}] 1(8.1) \frac{\text{cm}^3}{\text{mol}}$$

$$V_{m,pPtPh} = 567.59 \frac{\text{cm}^3}{\text{mol}} \quad (\text{A-9})$$

The a_1 constant can be obtained by dividing the repeat unit parachor by the molar volume, as shown in Equation A-10.

$$a_1 = \frac{P_{ru}}{V_{m,ru}} \quad (\text{A-10})$$

$$a_{1,pPtPh} = \frac{1425.8 \frac{\text{cm}^3}{\text{mol}} \frac{\text{N}}{\text{m}}}{567.59 \frac{\text{cm}^3}{\text{mol}}} \quad (\text{A-11})$$

$$a_{1,pPtPh} = 2.5120 \frac{\text{N}}{\text{m}} \quad (\text{A-12})$$

The polymer density can now be calculated using Equation A-1.

$$\rho = a_1 \frac{M_{ru}}{P_{ru}} \quad (\text{A-1})$$

$$\rho_{pPtPh} = 2.5210 \frac{\text{N}}{\text{m}} \frac{723.86 \frac{\text{g}}{\text{mol}}}{1425.8 \frac{\text{cm}^3}{\text{mol}} \frac{\text{N}}{\text{m}}} \quad (\text{A-13})$$

$$\rho_{pPtPh} = 1.28 \frac{\text{g}}{\text{cm}^3} \quad (\text{A-14})$$

Thin-Film Acceptor Concentration

The following example assumes that 20 μL of a 20.2 $\text{g}\cdot\text{L}^{-1}$ pPtPh donor solution and 0.179 μg of PtTPP were spin-coated onto a substrate. From the volume of the donor solution used and its concentration, 0.404 mg of pPtPh has been spin-coated with 0.179 μg (2.22×10^{-10}

mol) of PtTPP. The density of pPtPh can be used to calculate the volume of pPtPh used (Equation A-15).

$$v = \frac{\text{mass}}{\text{density}} \quad (\text{A-15})$$

$$v_{\text{pPtPh}} = \frac{4.04 \times 10^{-4} \text{ g pPtPh}}{1.28 \frac{\text{g}}{\text{cm}^3}} \times \frac{1 \text{ dm}^3}{1000 \text{ cm}^3} \quad (\text{A-16})$$

$$v_{\text{pPtPh}} = 3.16 \times 10^{-7} \text{ dm}^3 \quad (\text{A-17})$$

Assuming the ratio of donor-to-acceptor remains unchanged during spin-coating, it follows that the molar concentration of PtTPP in pPtPh can be calculated using Equation A-18, where C is the molar concentration of a known solute mass, m, in a known volume, v, of solvent.

$$C = \frac{m}{v} \quad (\text{A-18})$$

$$C_{\text{PtTPP}} = \frac{2.22 \times 10^{-10} \text{ mol PtTPP}}{3.16 \times 10^{-7} \text{ dm}^3 \text{ pPtPh}} \quad (\text{A-19})$$

$$C_{\text{PtTPP}} = 0.703 \times 10^{-3} \text{ M} \quad (\text{A-20})$$

Concentration-Based Exciton Diffusion Coefficient

After applying the Hindered-Access model to a series of pPtPh/PtTPP films, it was found that the quenching rate constant has the value $k_q = 1.39 \times 10^9 \text{ M}^{-1}\text{-s}^{-1}$. Details of the Hindered-Access model can be found elsewhere and will not be discussed here.¹⁰² From Fick's Law of Diffusion, Benson derived the collision frequency (Equation A-21), Z'_{AB} , of species A colliding with species B, where r_{AB} is the reactive radius of the two species (assumed to be 4 Å for Dexter transfer), D_{AB} is the diffusion coefficient, and N_{AV} is Avogadro's number.¹¹⁵

$$Z'_{AB} \left(\frac{1}{\text{M s}} \right) = \frac{4\pi r_{AB} (\text{cm}) D_{AB} \left(\frac{\text{cm}^2}{\text{s}} \right) N_{AV} (\text{mol}^{-1})}{1000 \frac{\text{cm}^3}{\text{dm}^3}} \quad (\text{A-21})$$

As discussed in Chapter 2, it is reasonable to assume that $k_q = Z'_{AB}$. By rearranging Equation A-21 for D_{AB} , the diffusion coefficient for the pPtPh/PtTPP system can be calculated (Equation A-22).

$$D_{AB} \left(\frac{\text{cm}^2}{\text{s}} \right) = \frac{k_q \left(\frac{1}{\text{M s}} \right) 1000 \left(\frac{\text{cm}^3}{\text{dm}^3} \right)}{4\pi r_{AB} (\text{cm}) N_{AV} (\text{mol}^{-1})} \quad (\text{A-22})$$

$$D_{\text{pPtPh}} = \frac{1.39 \times 10^9 \frac{1}{\text{M s}} \left(1000 \frac{\text{cm}^3}{\text{dm}^3} \right)}{4\pi (4 \times 10^{-8} \text{ cm}) 6.02 \times 10^{23} \text{ mol}^{-1}} \quad (\text{A-23})$$

$$D_{\text{pPtPh}} = 4.59 \times 10^{-6} \frac{\text{cm}^2}{\text{s}} \quad (\text{A-24})$$

Assuming that the pPtPh triplet exciton has a lifetime of $\tau = 1.2 \times 10^{-6} \text{ s}$, the exciton length of diffusion, L_D , can now be calculated using Equation A-25.⁸⁴

$$L_D (\text{m}) = \sqrt{D_{AB} \left(\frac{\text{cm}^2}{\text{s}} \right) \tau (\text{s})} \times \frac{0.01 \text{ m}}{\text{cm}} \quad (\text{A-25})$$

$$L_{D,\text{pPtPh}} = \sqrt{\left(4.59 \times 10^{-6} \frac{\text{cm}^2}{\text{s}} \right) (1.2 \times 10^{-6} \text{ s})} \times \frac{0.01 \text{ m}}{\text{cm}} \quad (\text{A-26})$$

$$L_{D,\text{pPtPh}} = 23.5 \times 10^{-9} \text{ m} \quad (\text{A-27})$$

APPENDIX B
MASS SPECTRA OF CATIONIC IRIIDIUM DYES

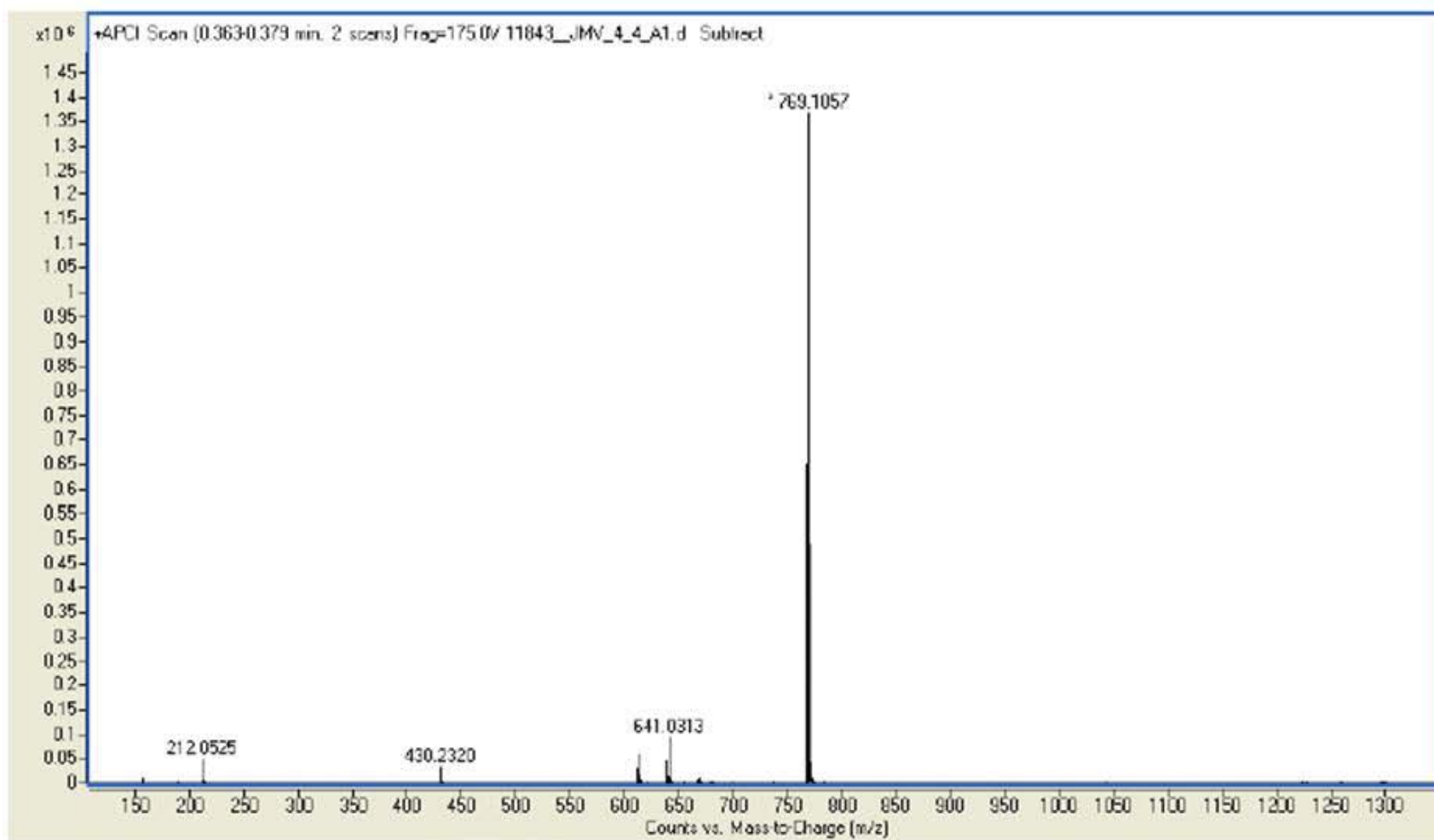


Figure B-1. Full APCI-TOF mass spectrum of $\text{Ir}(\text{bt})_2(\text{bpy})^+$.

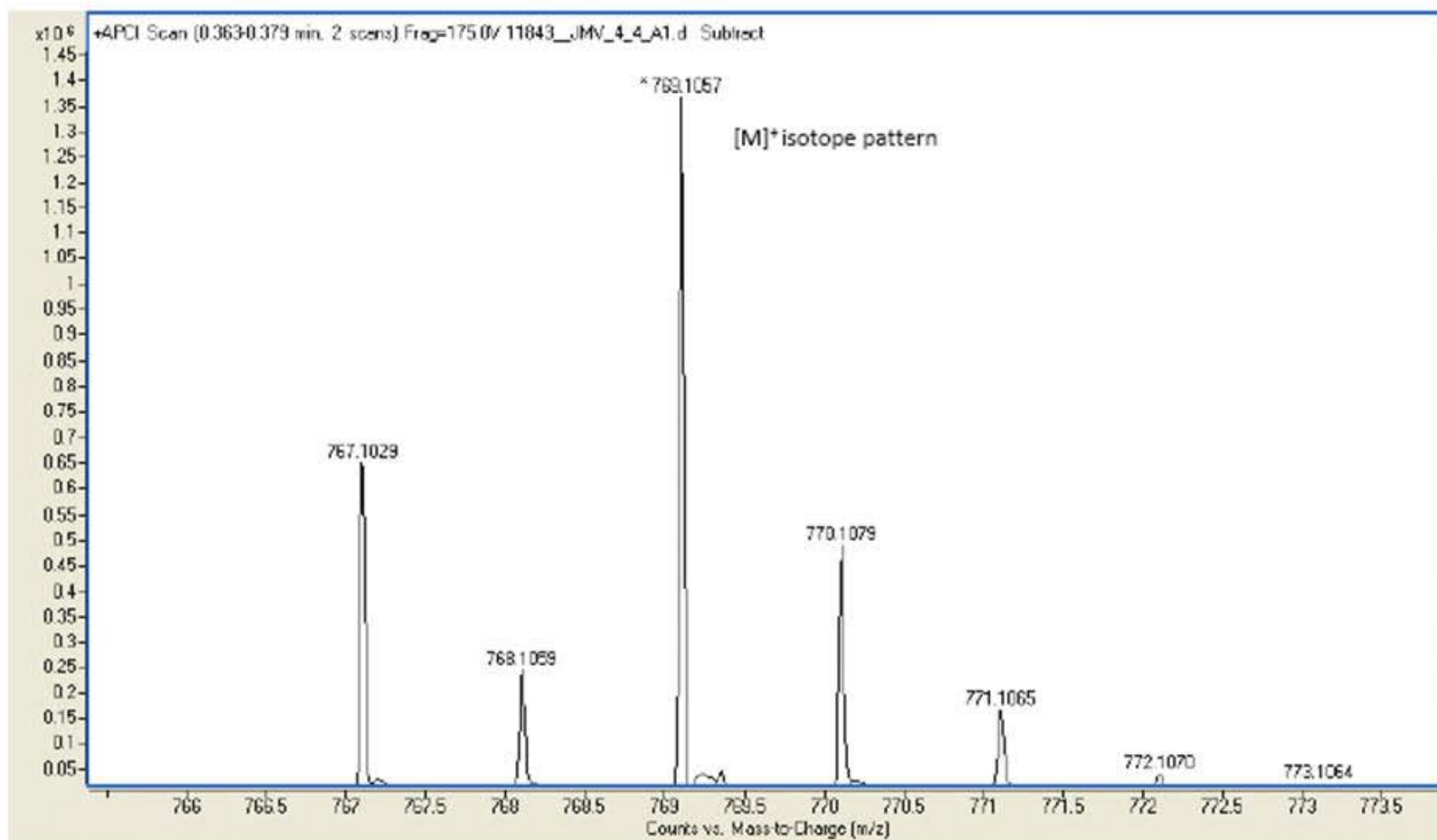


Figure B-2. Close-up view of the M^+ peak in the APCI-TOF mass spectrum of $\text{Ir}(\text{bt})_2(\text{bpy})^+$.

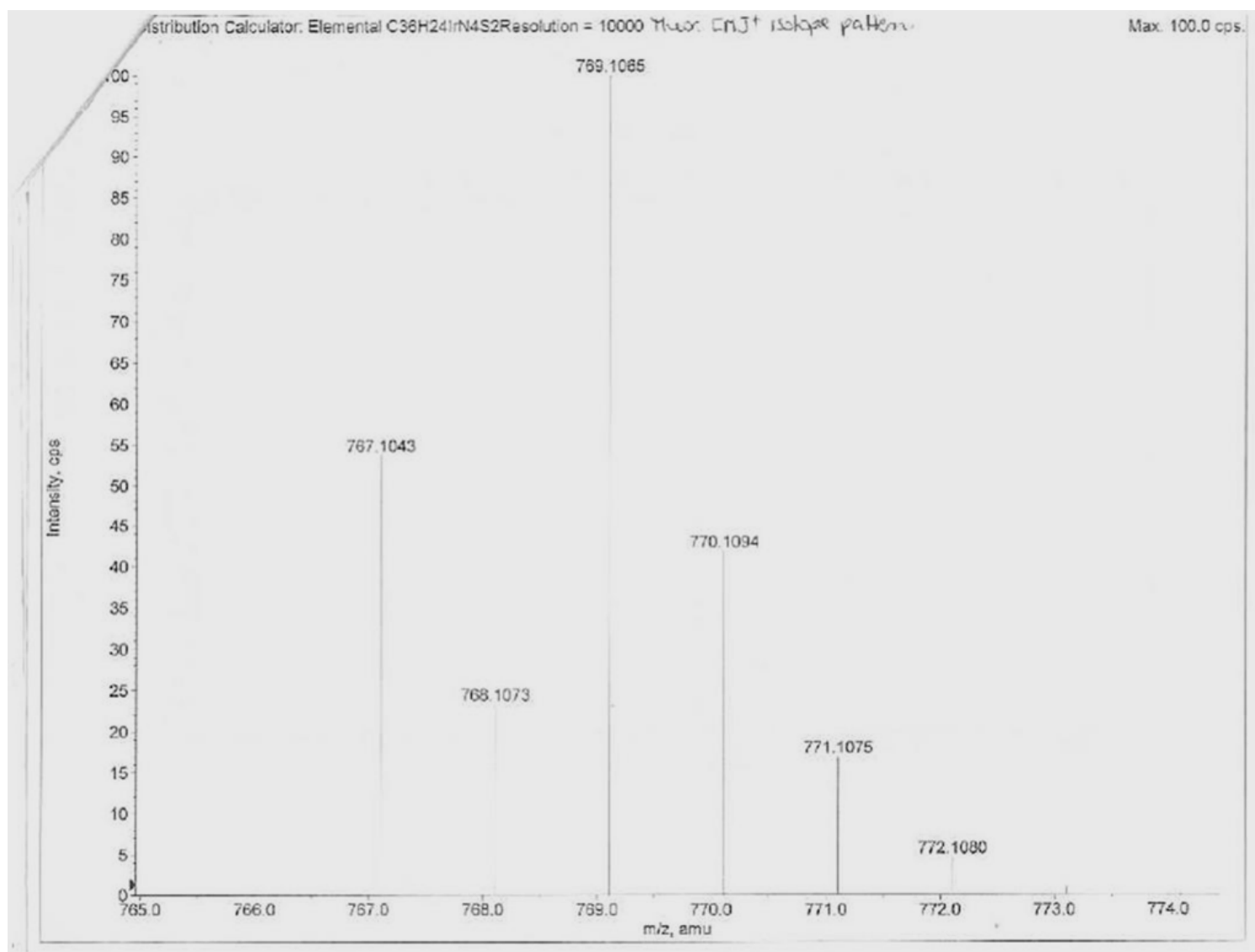


Figure B-3. Theoretical M^+ pattern for $\text{Ir}(\text{bt})_2(\text{bpy})^+$.

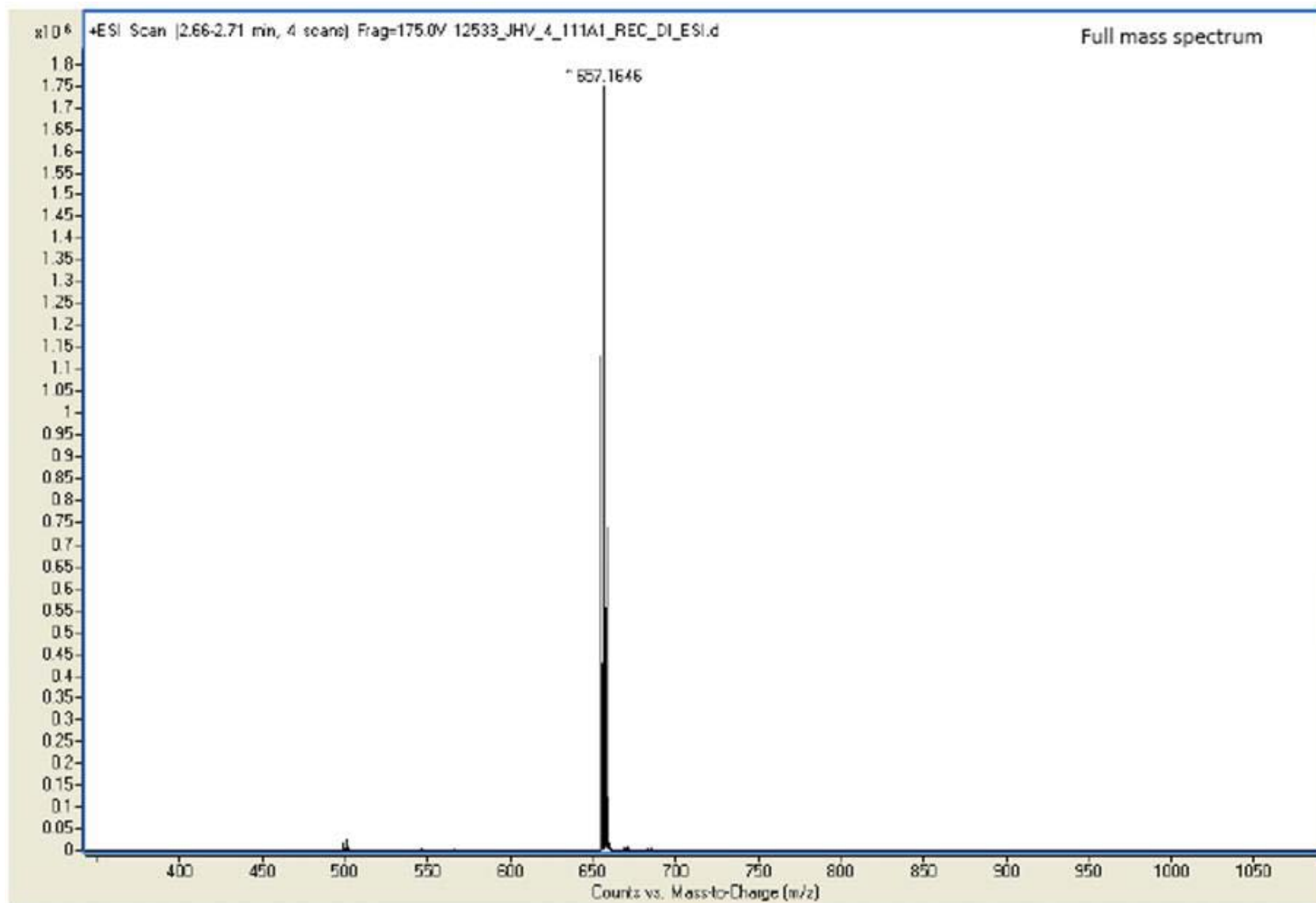


Figure B-4. Full ESI-TOF mass spectrum of Ir(ppy)₂(bpy)⁺.

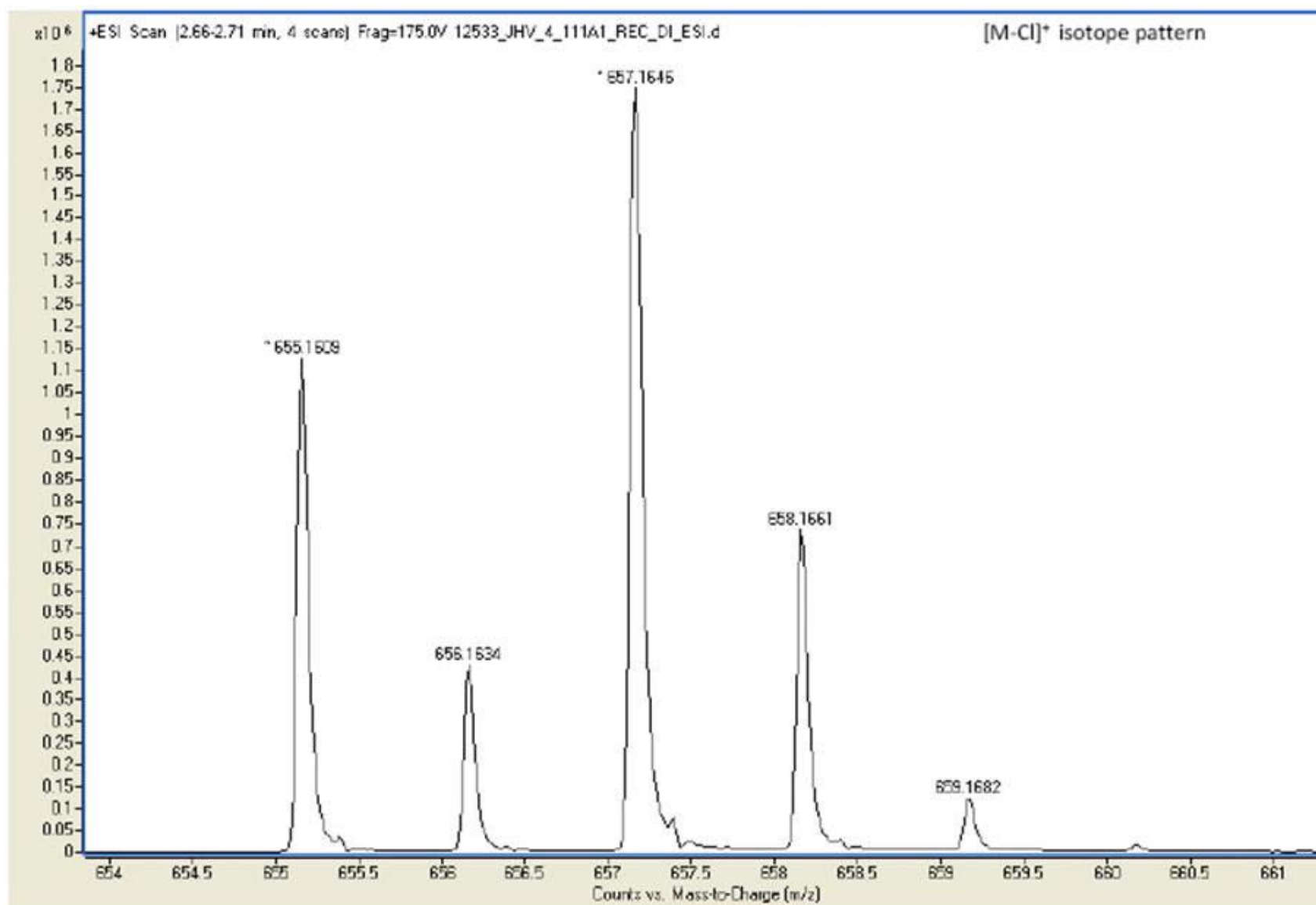


Figure B-5. Close-up view of the M^+ peak in the ESI-TOF mass spectrum of $\text{Ir}(\text{ppy})_2(\text{bpy})^+$.

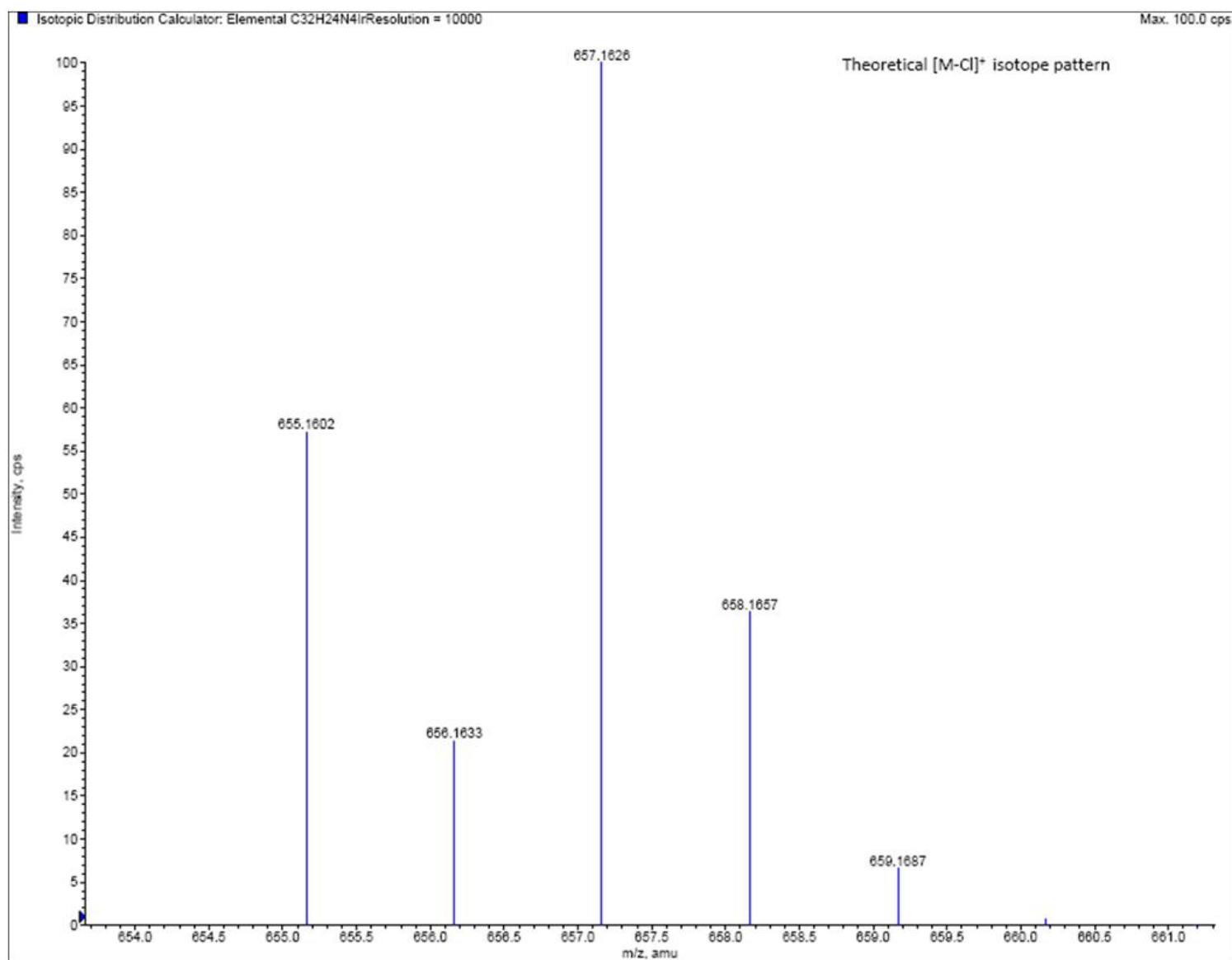


Figure B-6. Theoretical M⁺ pattern for Ir(ppy)₂(bpy)⁺.

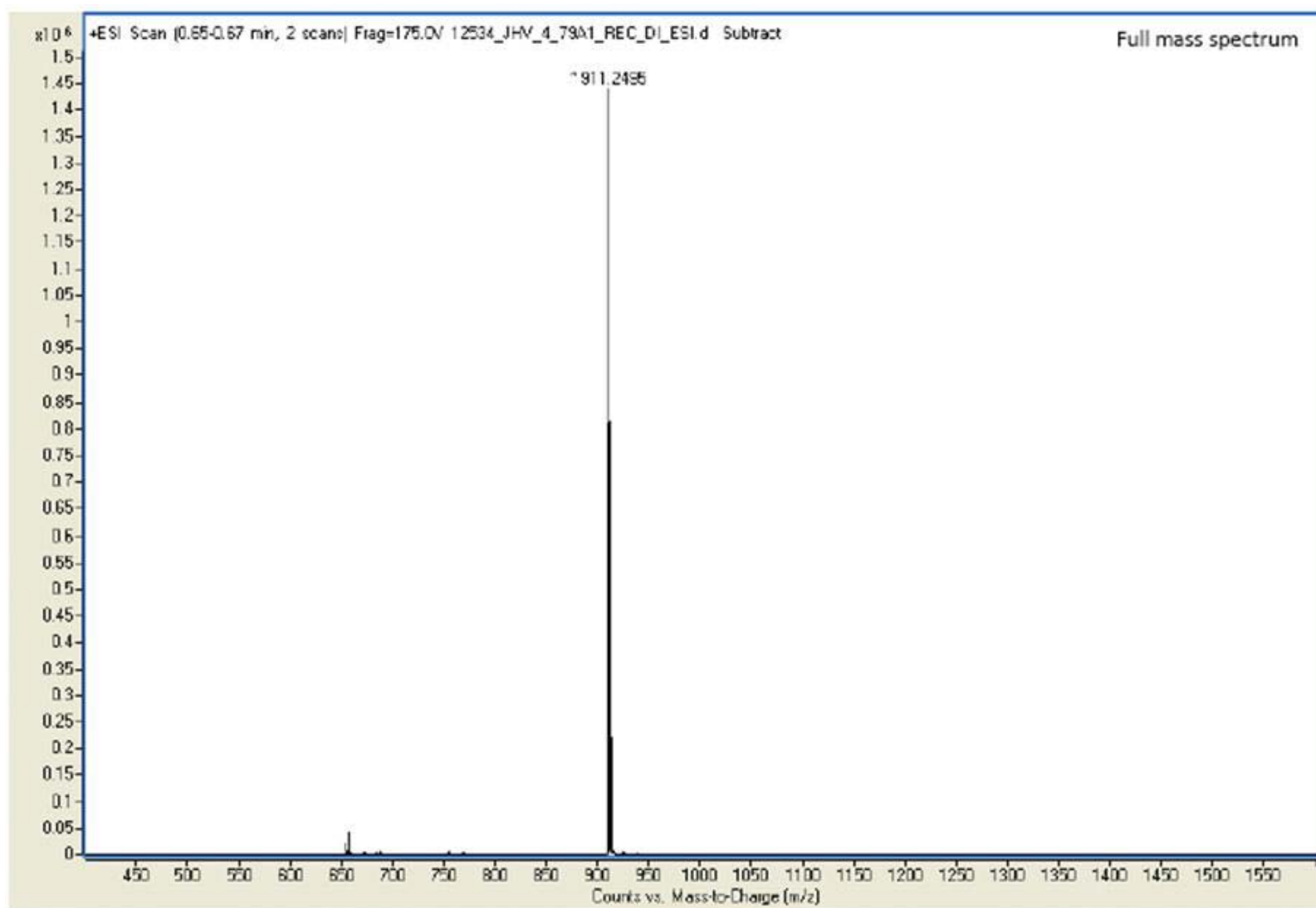


Figure B-7. Full ESI-TOF mass spectrum of $\text{Ir}(\text{hqx})_2(\text{bpy})^+$.

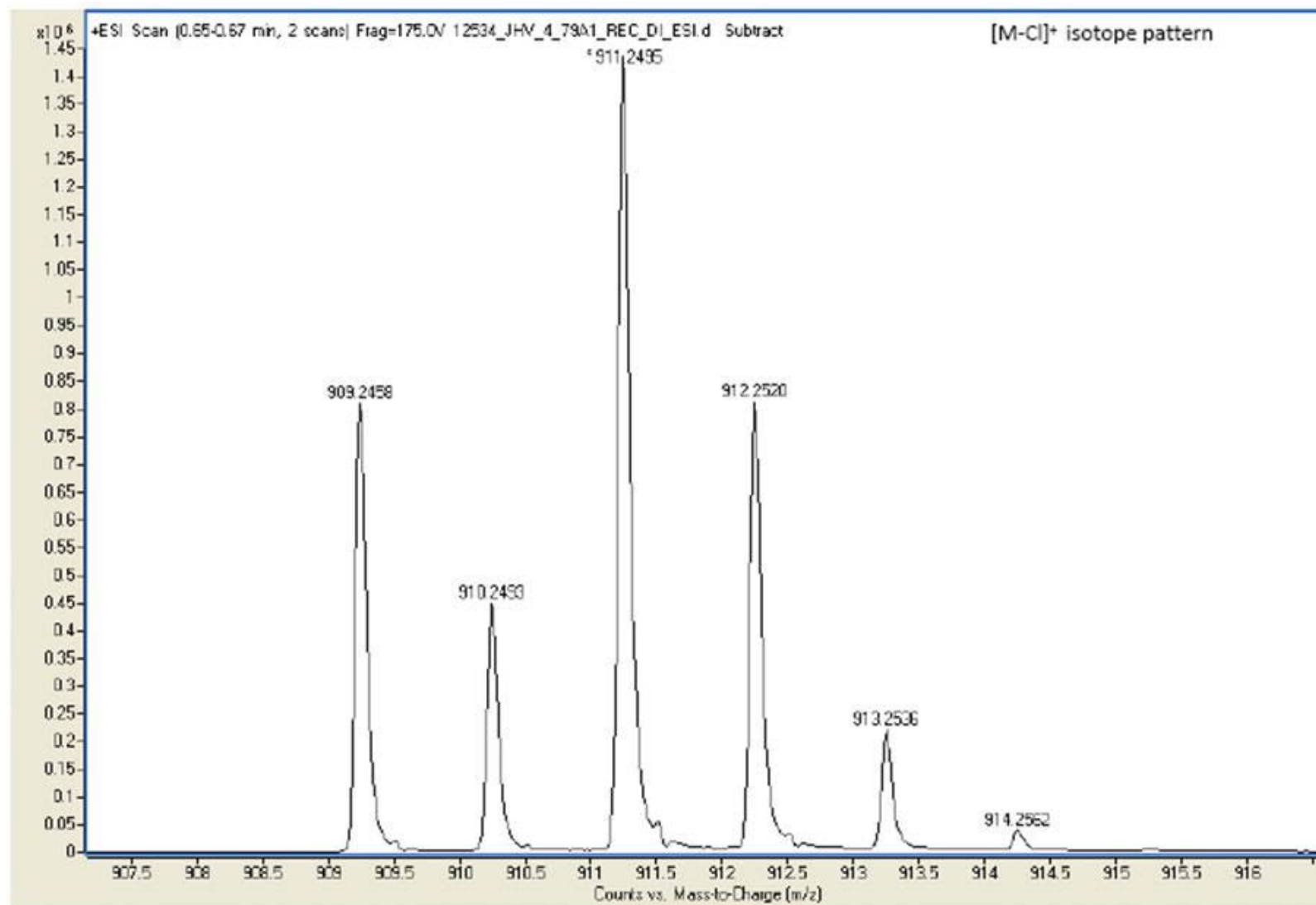


Figure B-8. Close-up view of the M^+ peak in the ESI-TOF mass spectrum of $\text{Ir}(\text{hqx})_2(\text{bpy})^+$.

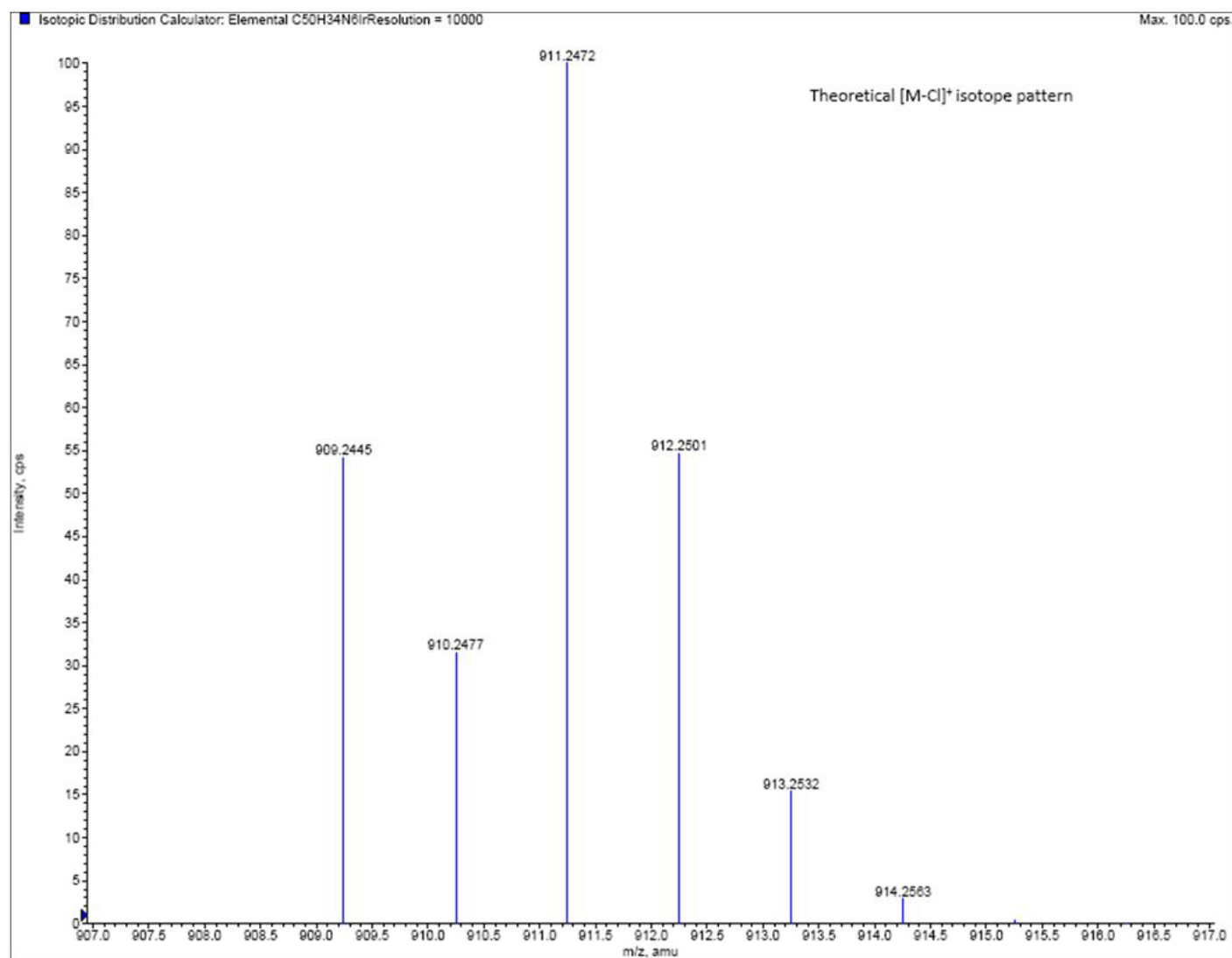


Figure B-9. Theoretical M⁺ pattern for Ir(hqx)₂(bpy)⁺.

APPENDIX C
NMR SPECTRA OF CATIONIC IRIDIUM DYES

VXR-300 stdpar pw array vxr5mm Mar-07-2006
PFI0H = 18.25 uS @ 55 dB
Maximized @ 9uS
Varian 5mm H/X Probe

Pulse Sequence: s2pul

Solvent: CD3CN
Ambient temperature
VXR-300S "vcr300"

PULSE SEQUENCE

Pulse 41.5 degrees
Acq. time 4.000 sec
Width 4887.6 Hz
516 repetitions

OBSERVE H1, 299.9614737 MHz

DATA PROCESSING

Gauss apodization 2.228 sec
FT size 65536
Total time 53 min, 28 sec

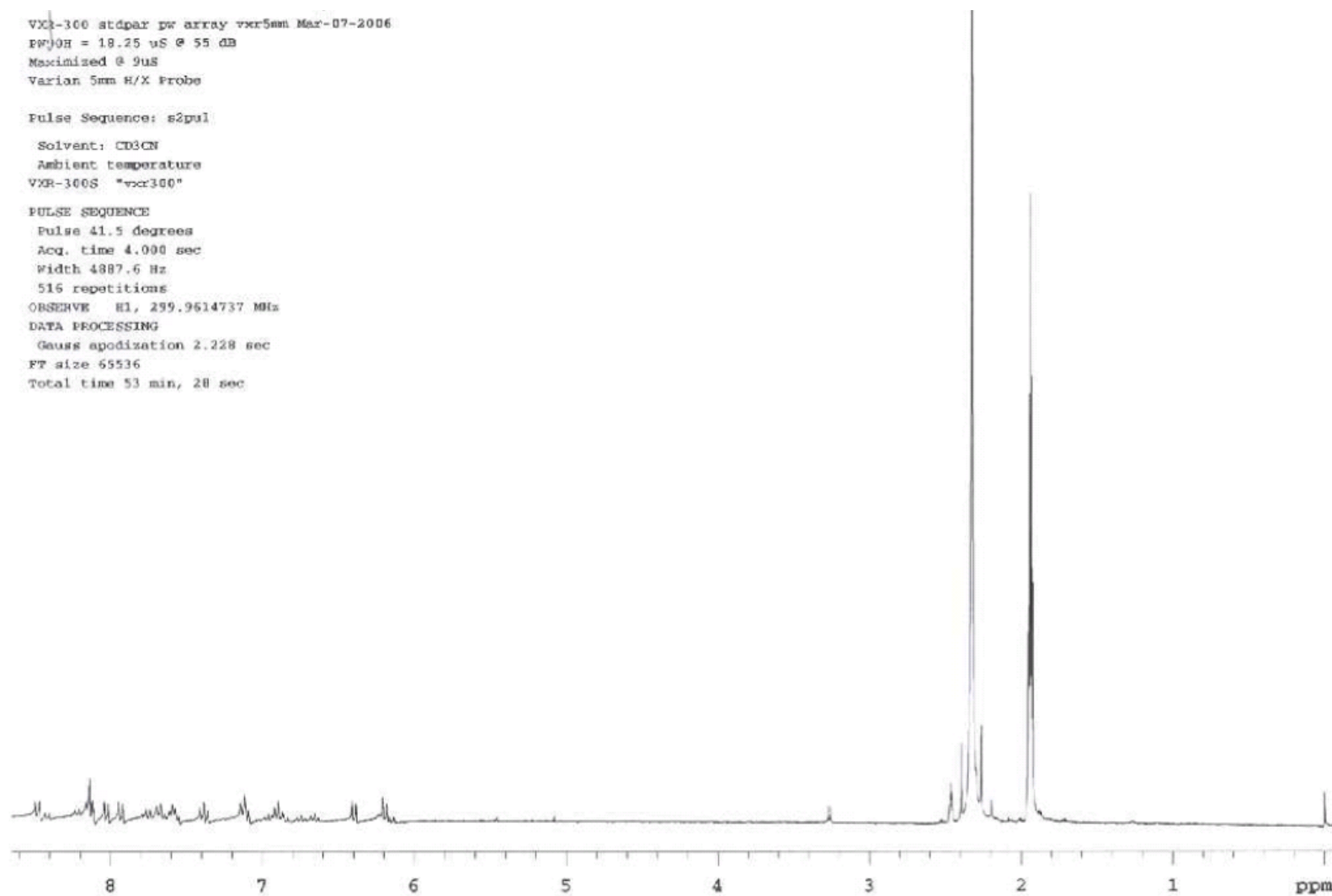


Figure C-1. ¹H NMR spectrum for Ir(bt)₂(bpy)PF₆ in acetonitrile-d₃ and dimethylsulfoxide-d₆.

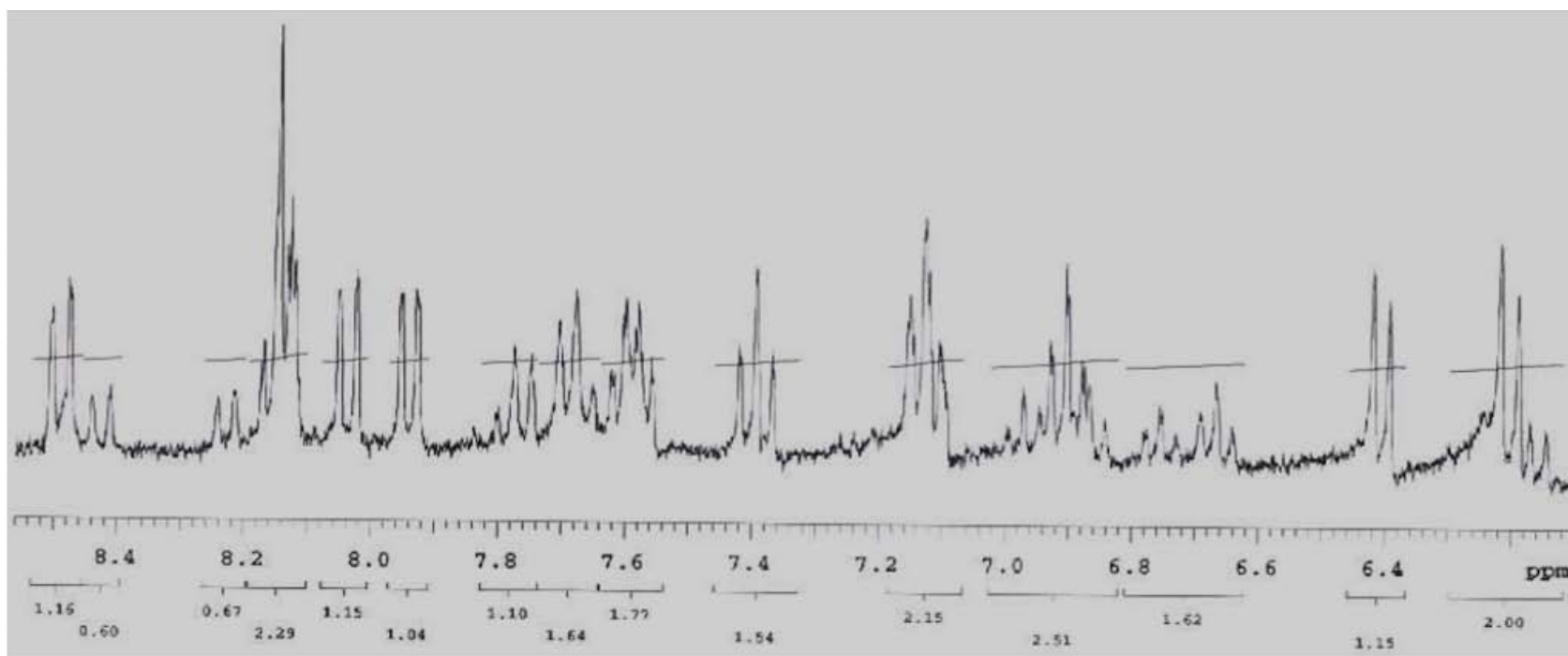


Figure C-2. Expansion of the ^1H NMR spectrum for $\text{Ir}(\text{bt})_2(\text{bpy})\text{PF}_6$ in acetonitrile-d_3 and $\text{dimethylsulfoxide-d}_6$.

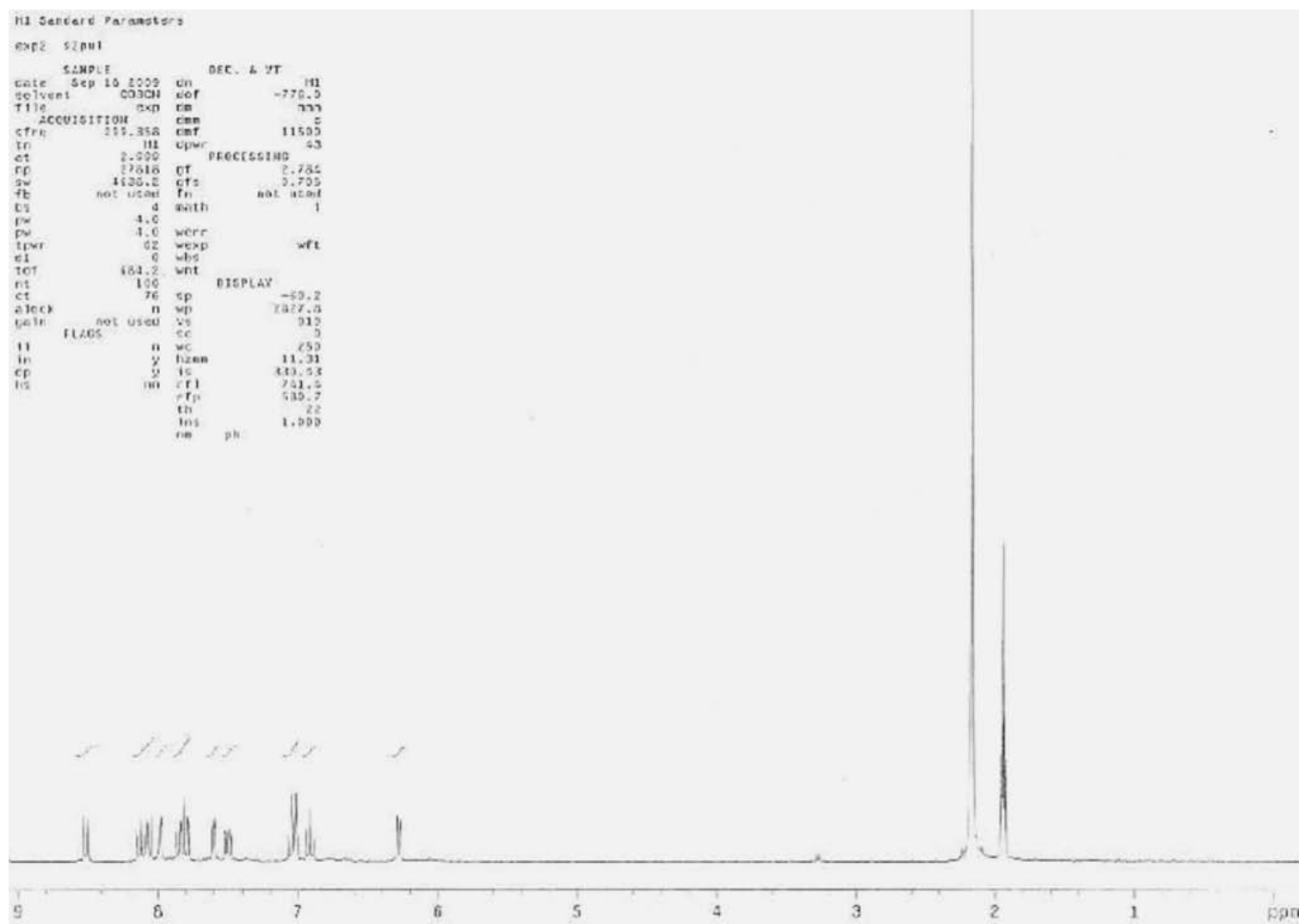


Figure C-3. ^1H NMR spectrum for $\text{Ir}(\text{ppy})_2(\text{bpy})\text{PF}_6$ in acetonitrile- d_3 .

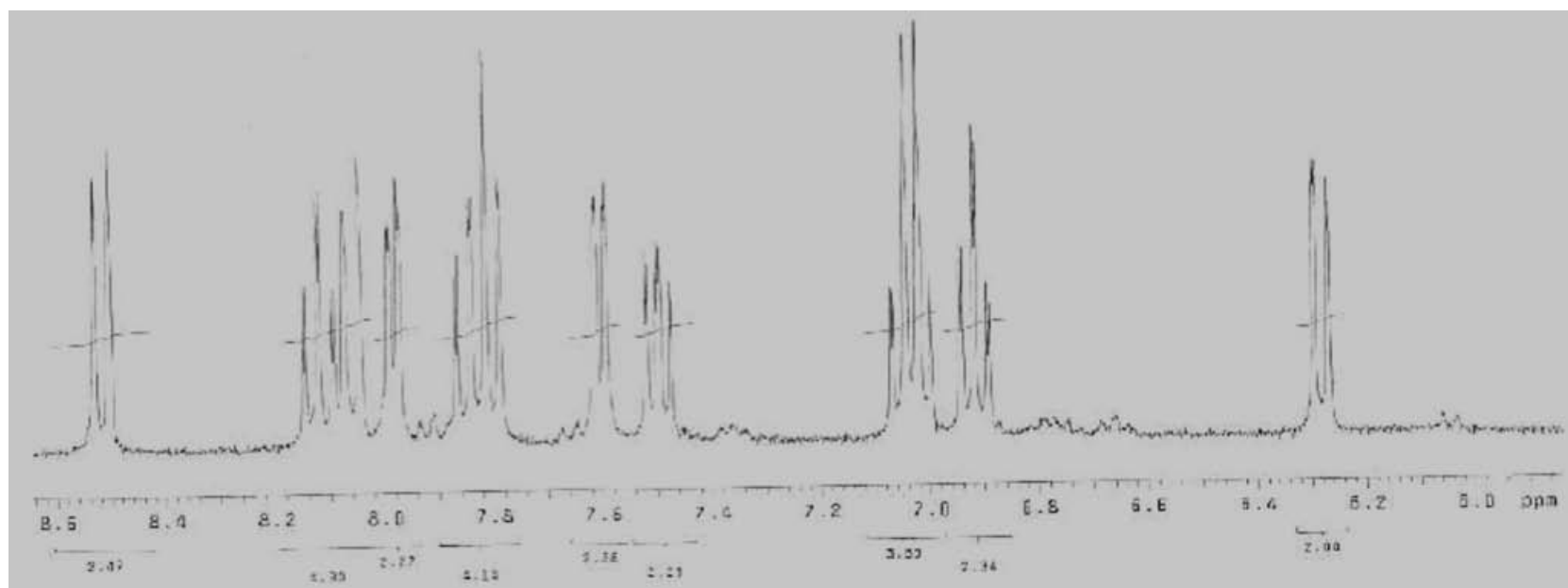


Figure C-4. Expansion of the ^1H NMR spectrum for $\text{Ir}(\text{ppy})_2(\text{bpy})\text{PF}_6$ in acetonitrile-d_3 .

Pulse Sequence: s2pul
Solvent: CDCl3
Ambient temperature
VXR-300S "vnr300"

PULSE SEQUENCE
Pulse 41.5 degrees
Acq. time 4.000 sec
Width 4887.6 Hz
16 repetitions
OBSERVE H1, 299.9612959 MHz
DATA PROCESSING
Gauss apodization 2.228 sec
FT size 65536
Total time 1 min, 4 sec

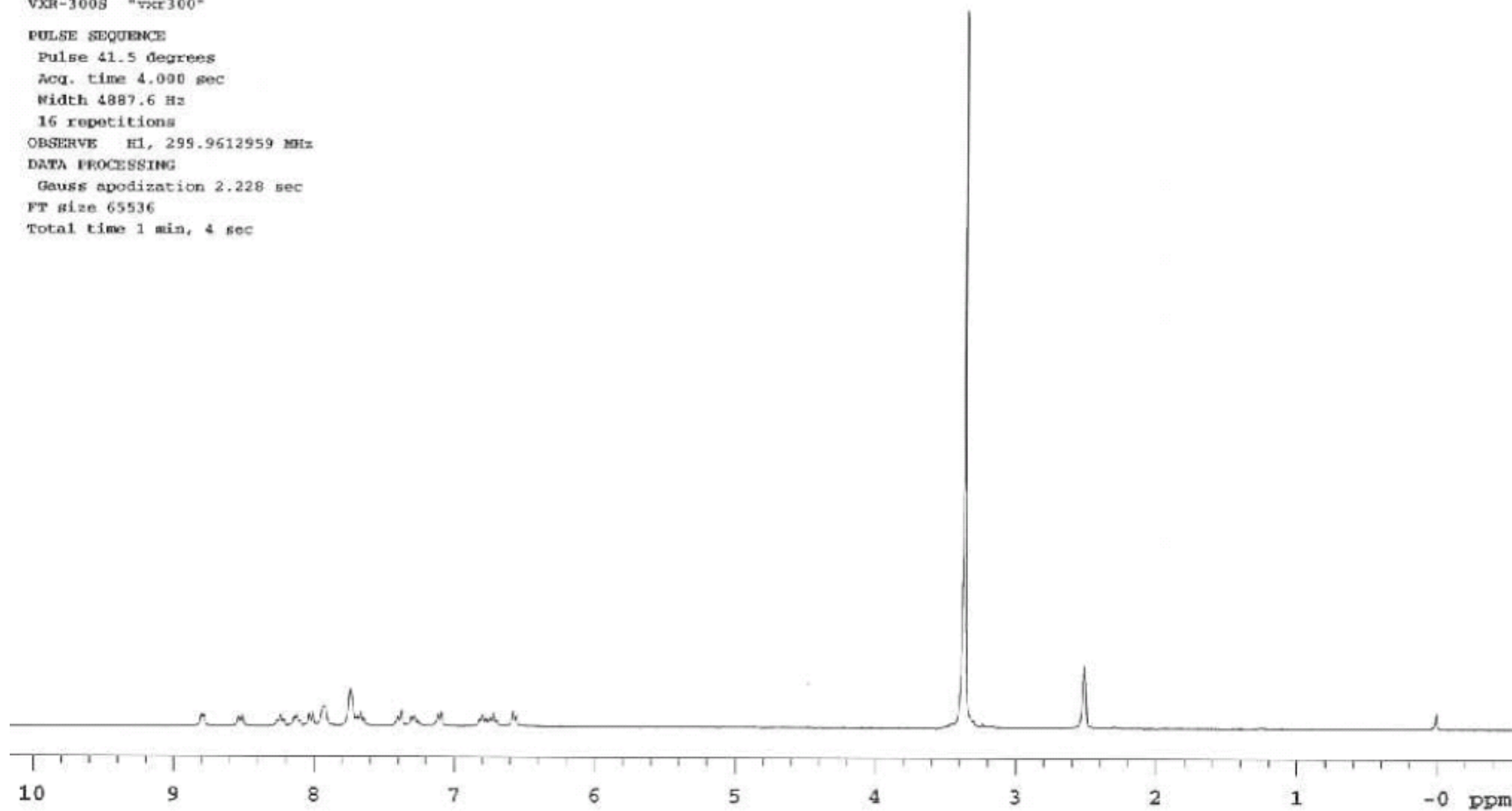


Figure C-5. ¹H NMR spectrum for Ir(hqx)₂(bpy)Cl in dimethylsulfoxide-d₆.

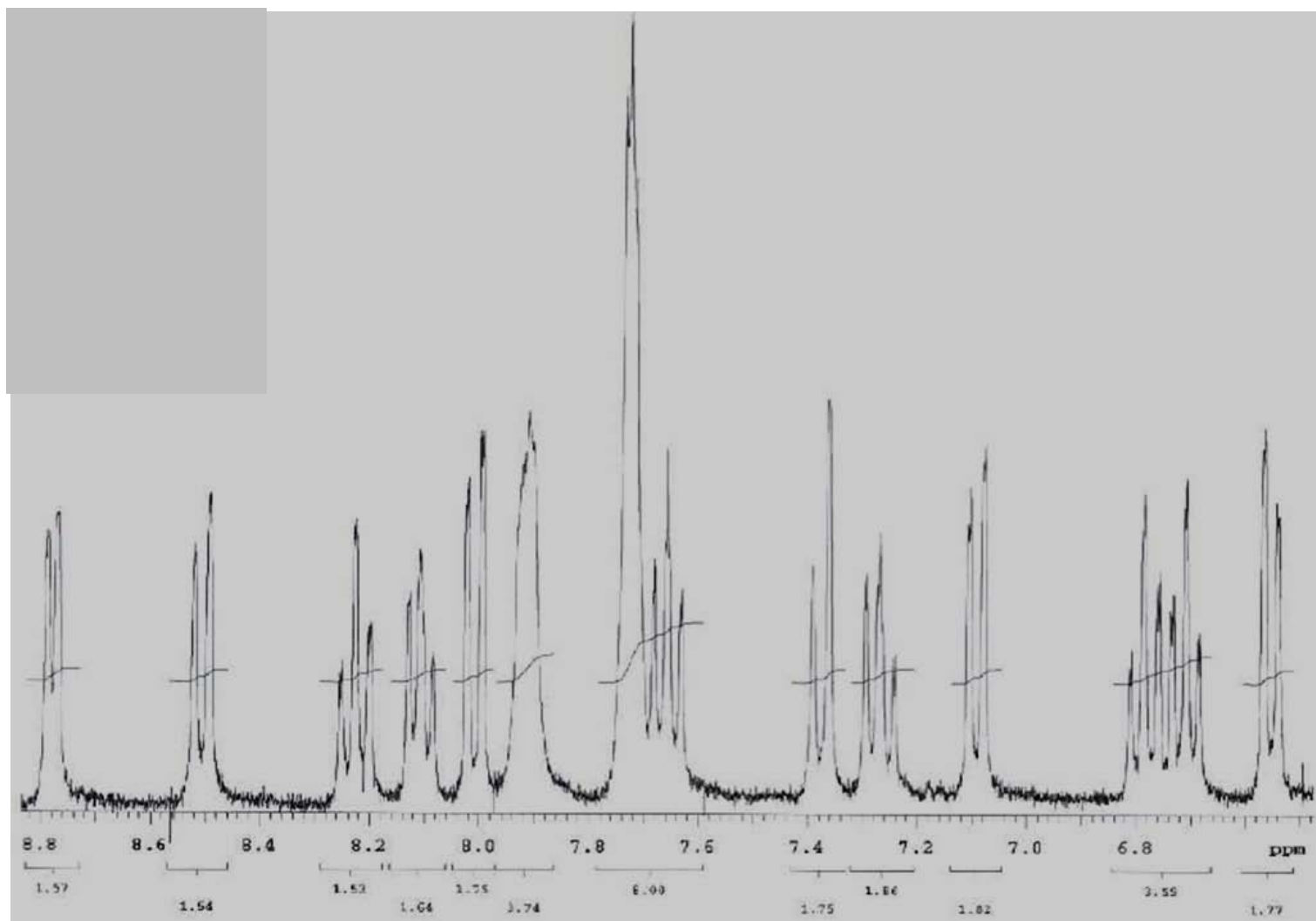


Figure C-6. Expansion of the ^1H NMR spectrum for $\text{Ir}(\text{hqx})_2(\text{bpy})\text{Cl}$ in $\text{dimethylsulfoxide-d}_6$.

APPENDIX D
REPRESENTATIVE DECAYS OF pPtPh FILMS

PCBM Blends

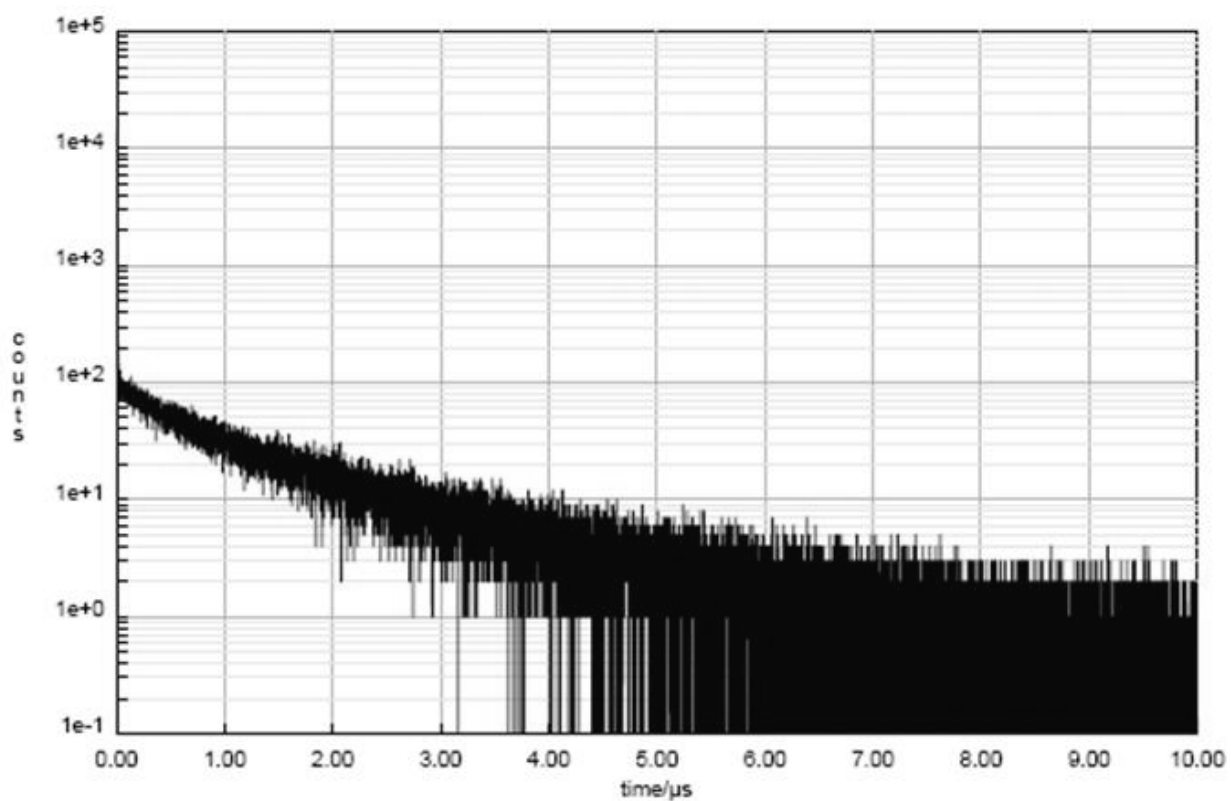


Figure D-1. TCSPC decay of a pristine pPtPh film (y-axis units in $\log(\text{counts per second})$).

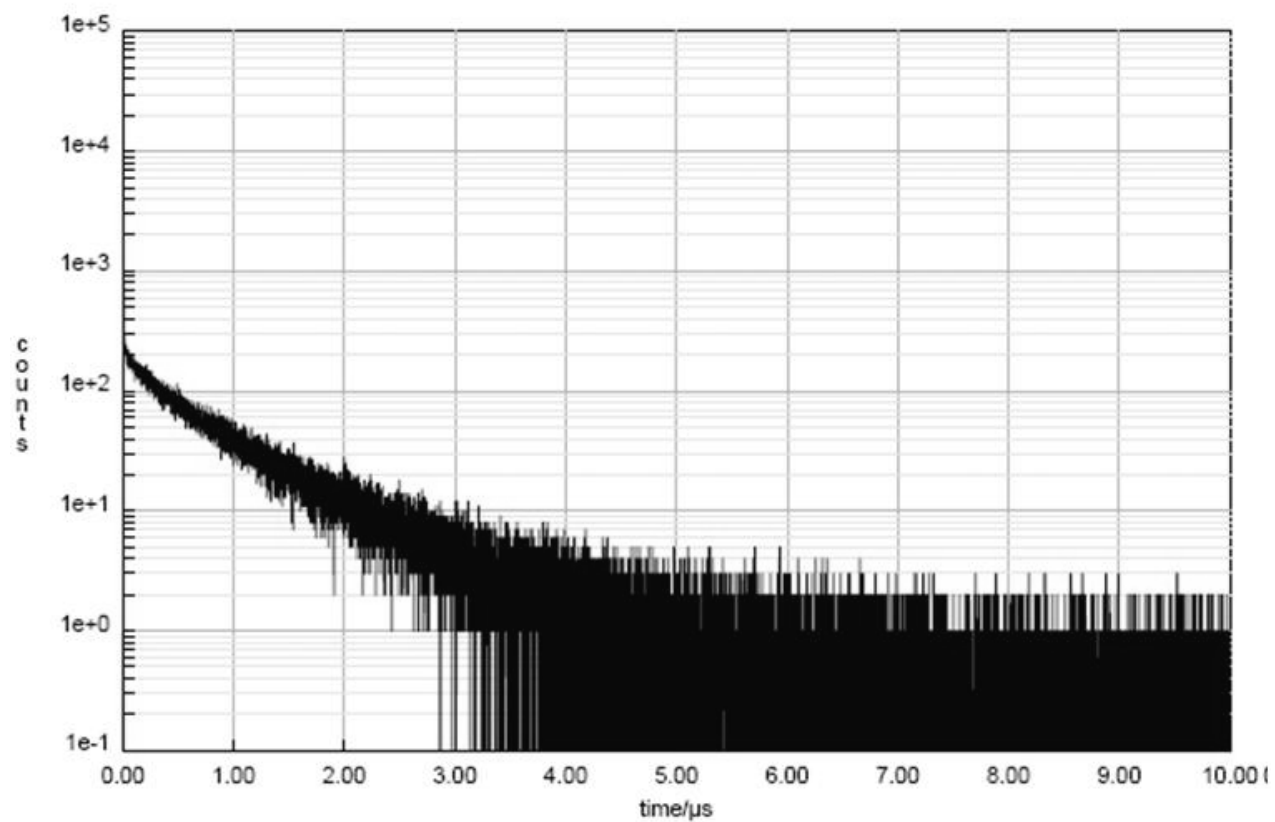


Figure D-2. TCSPC decay for a 0.025 wt% (0.351 mM) PCBM/pPtPh film.

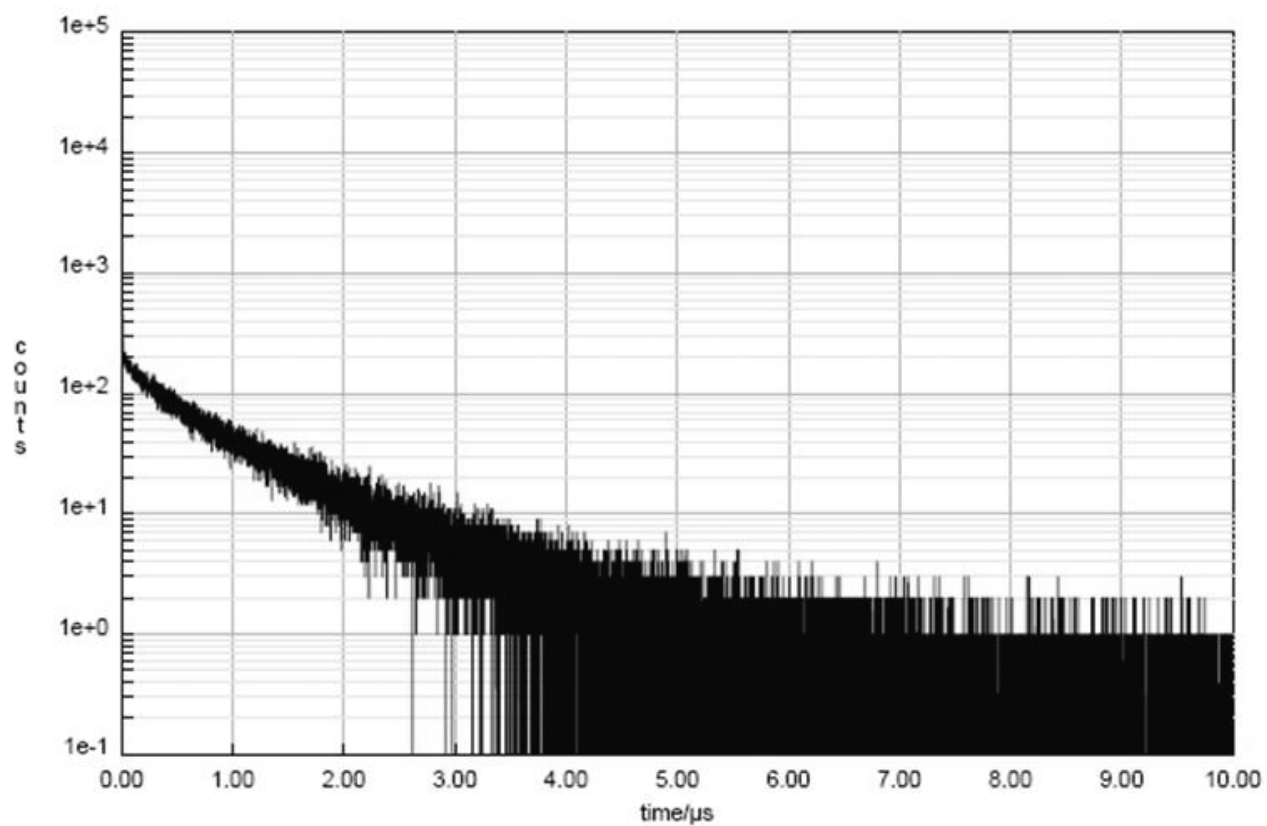


Figure D-3. TCSPC decay for a 0.050 wt% (0.703 mM) PCBM/pPtPh film.

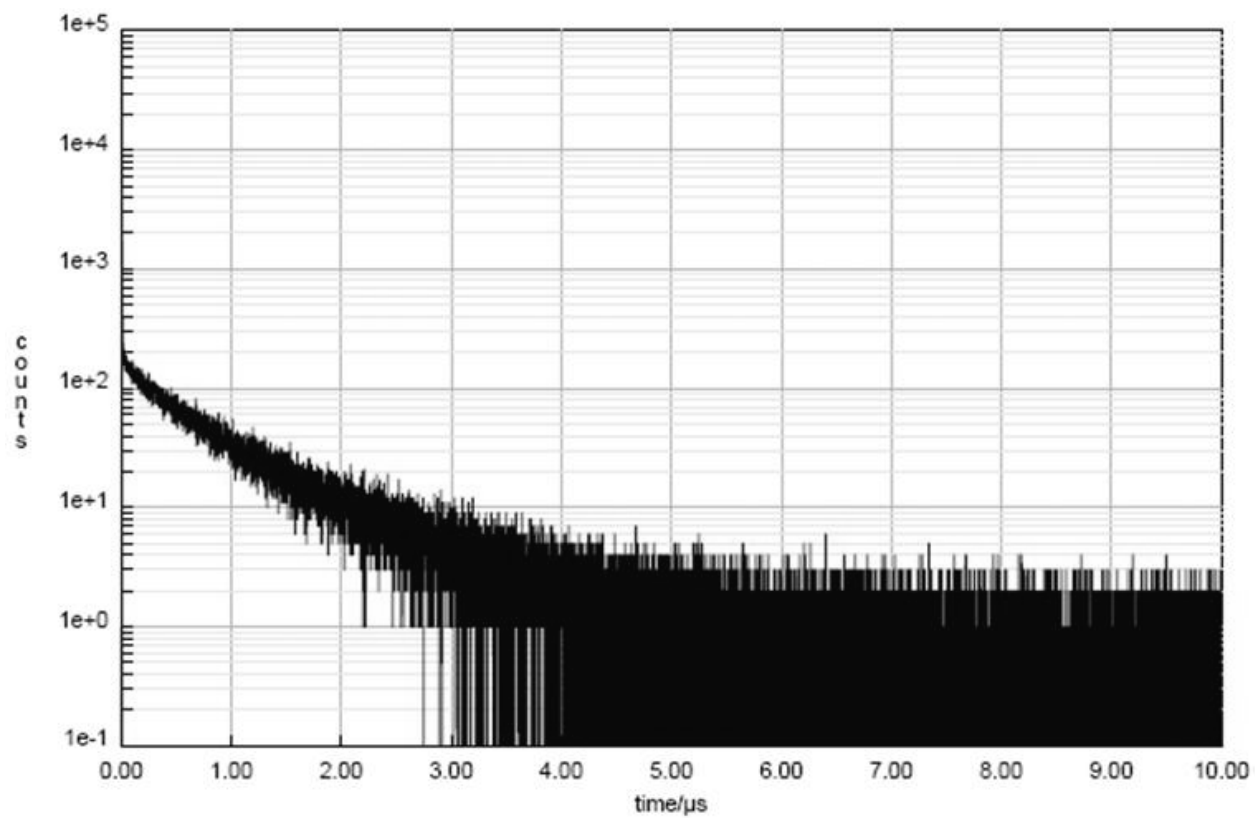


Figure D-4. TCSPC decay for a 0.075 wt% (1.05 mM) PCBM/pPtPh film.

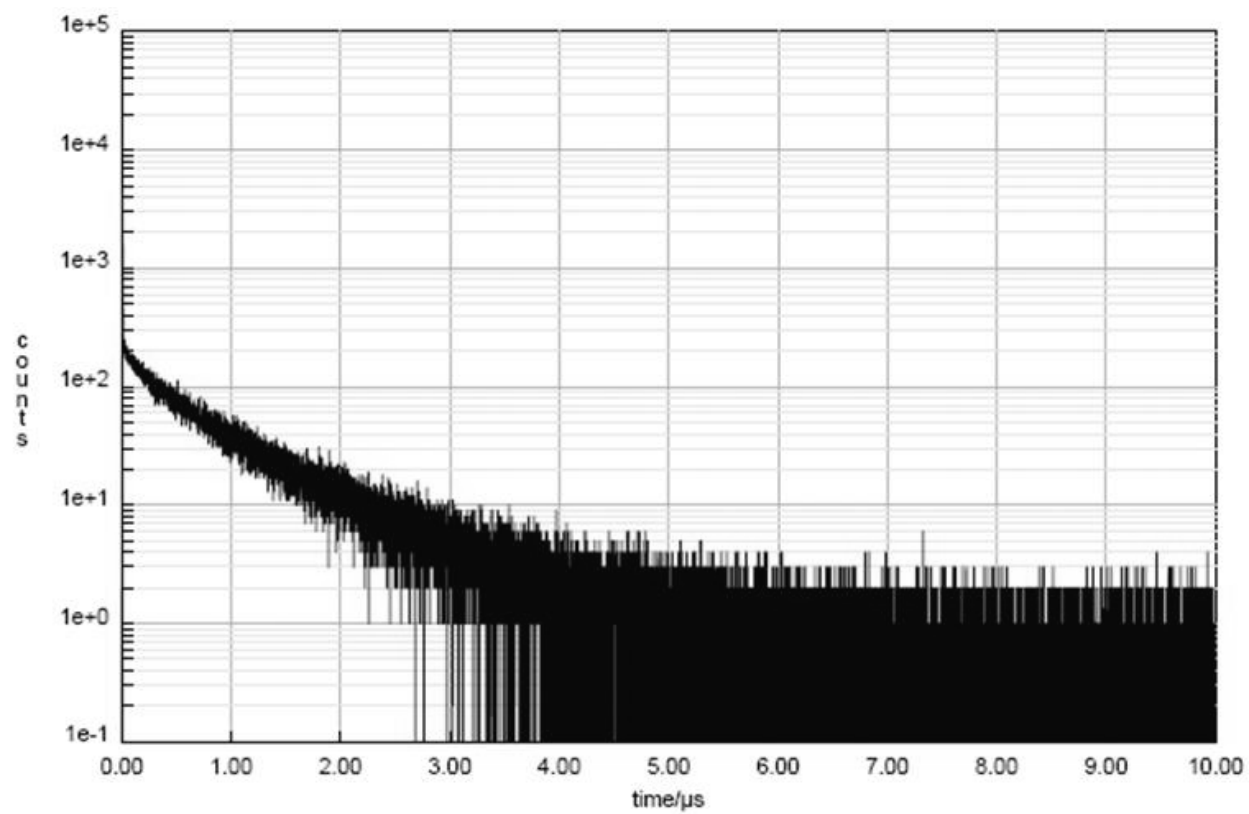


Figure D-5. TCSPC decay for a 0.100 wt% (1.41 mM) PCBM/pPtPh film.

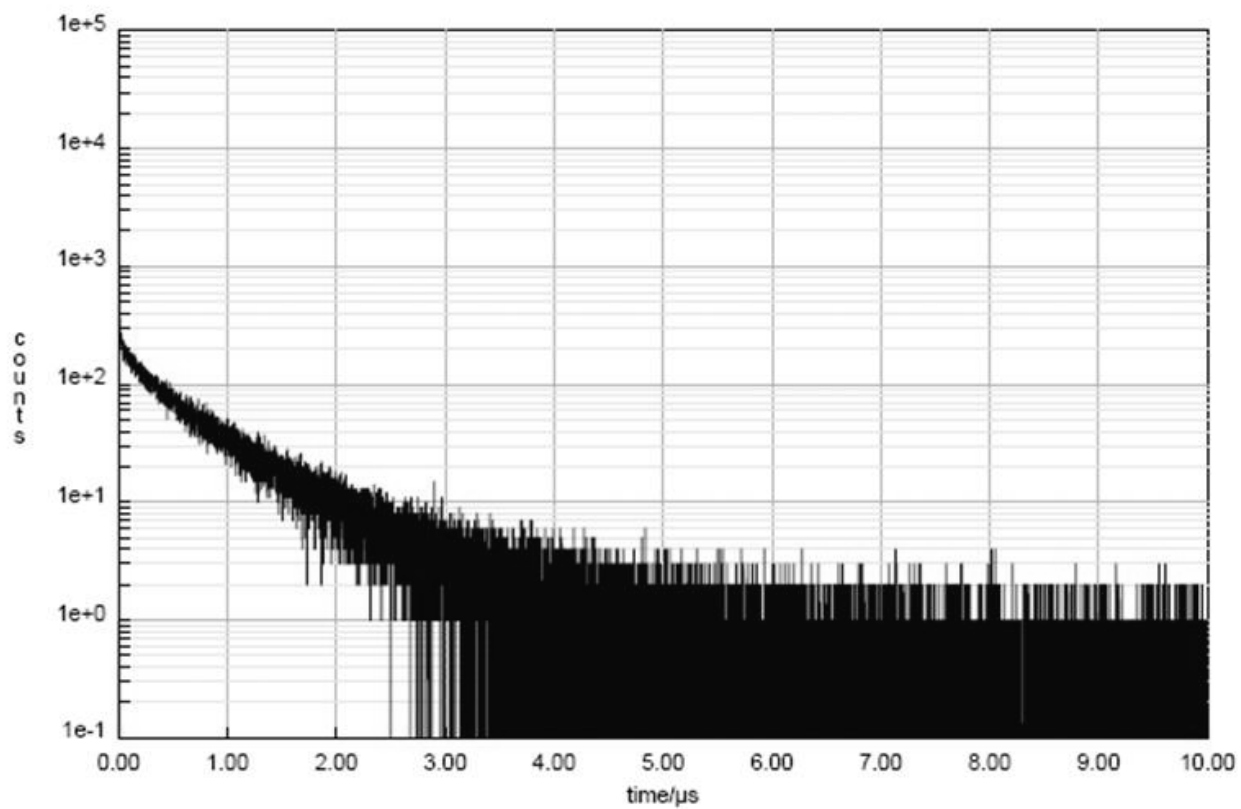


Figure D-6. TCSPC decay for a 0.125 wt% (1.76 mM) PCBM/pPtPh film.

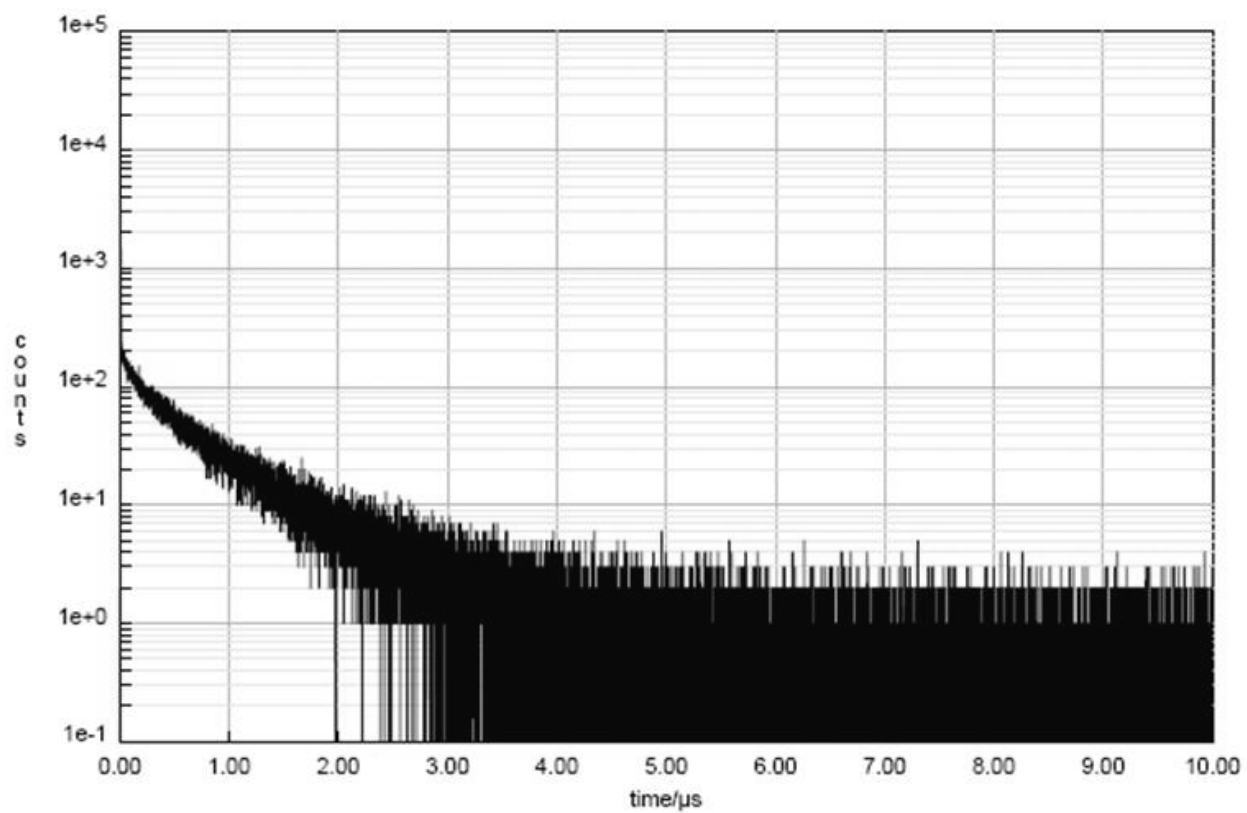


Figure D-7. TCSPC decay for a 0.225 wt% (3.17 mM) PCBM/pPtPh film.

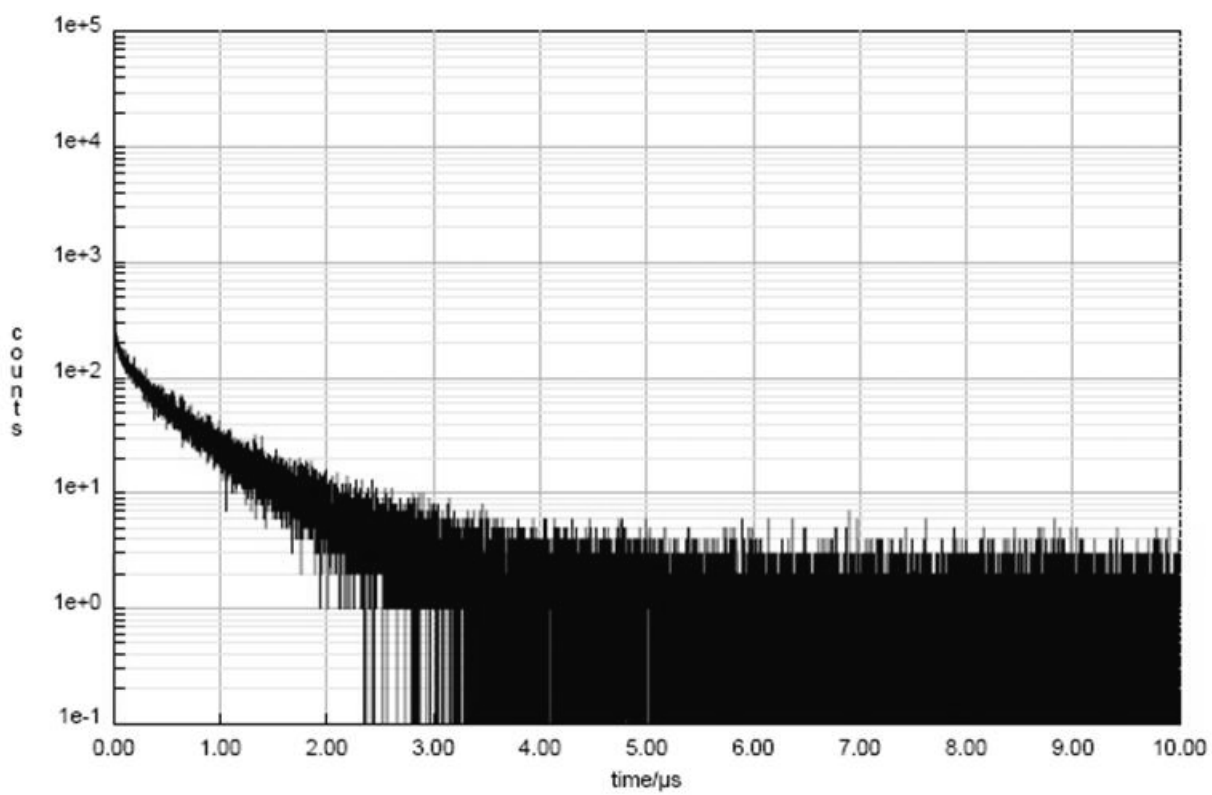


Figure D-8. TCSPC decay for a 0.325 wt% (4.58 mM) PCBM/pPtPh film.

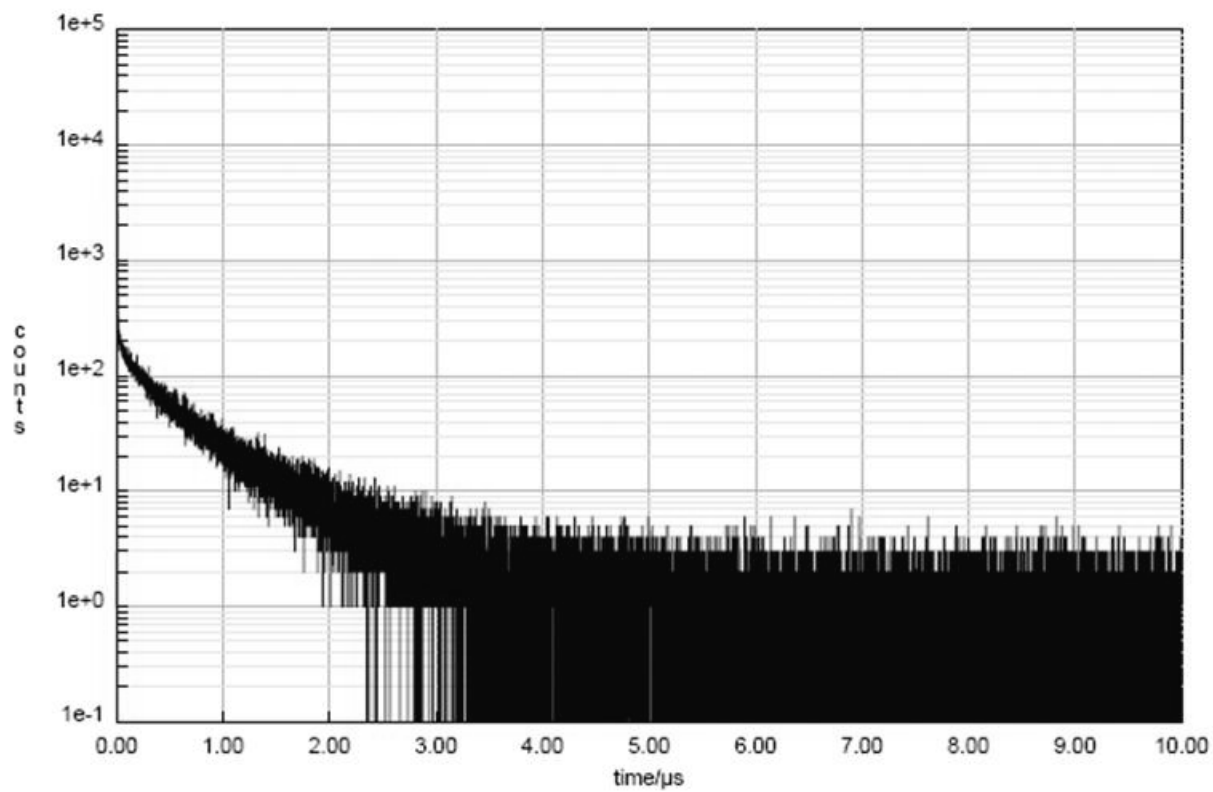


Figure D-9. TCSPC decay for a 0.425 wt% (5.97 mM) PCBM/pPtPh film.

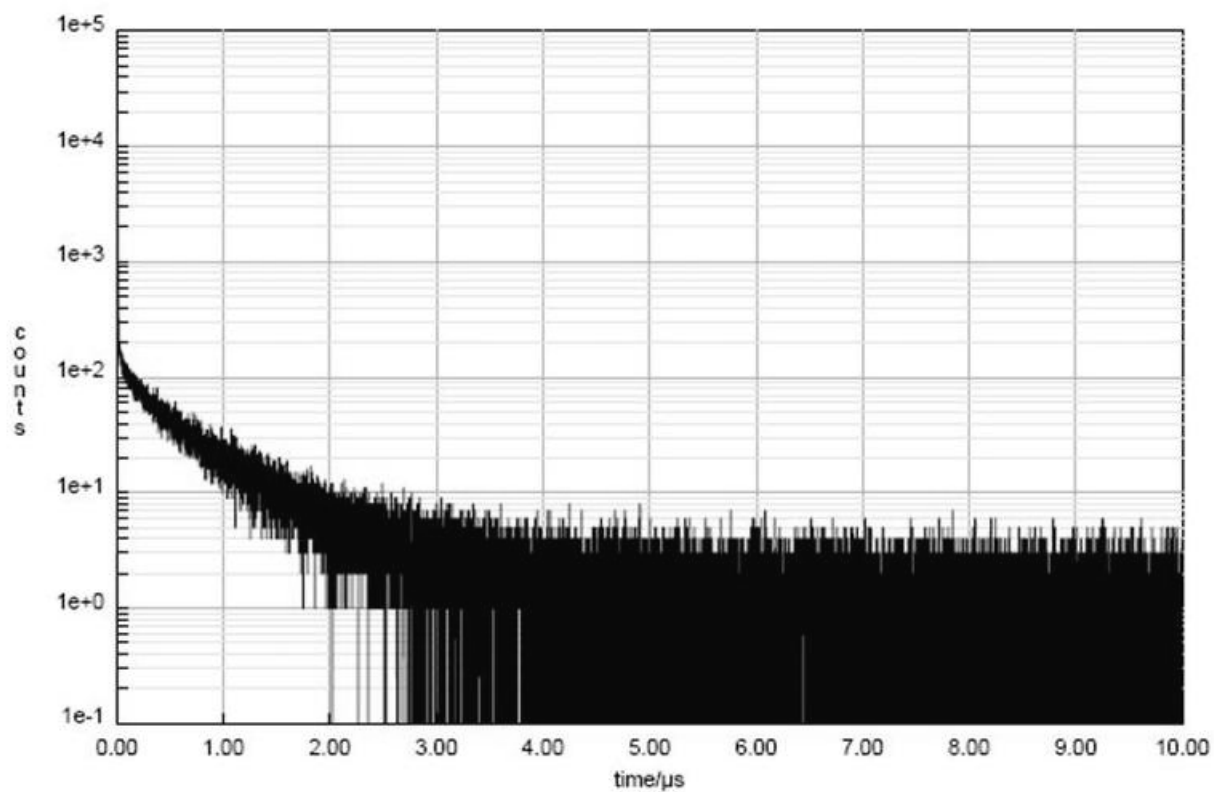


Figure D-10. TCSPC decay for a 0.525 wt% (7.37mM) PCBM/pPtPh film.

C60 Bilayer Films

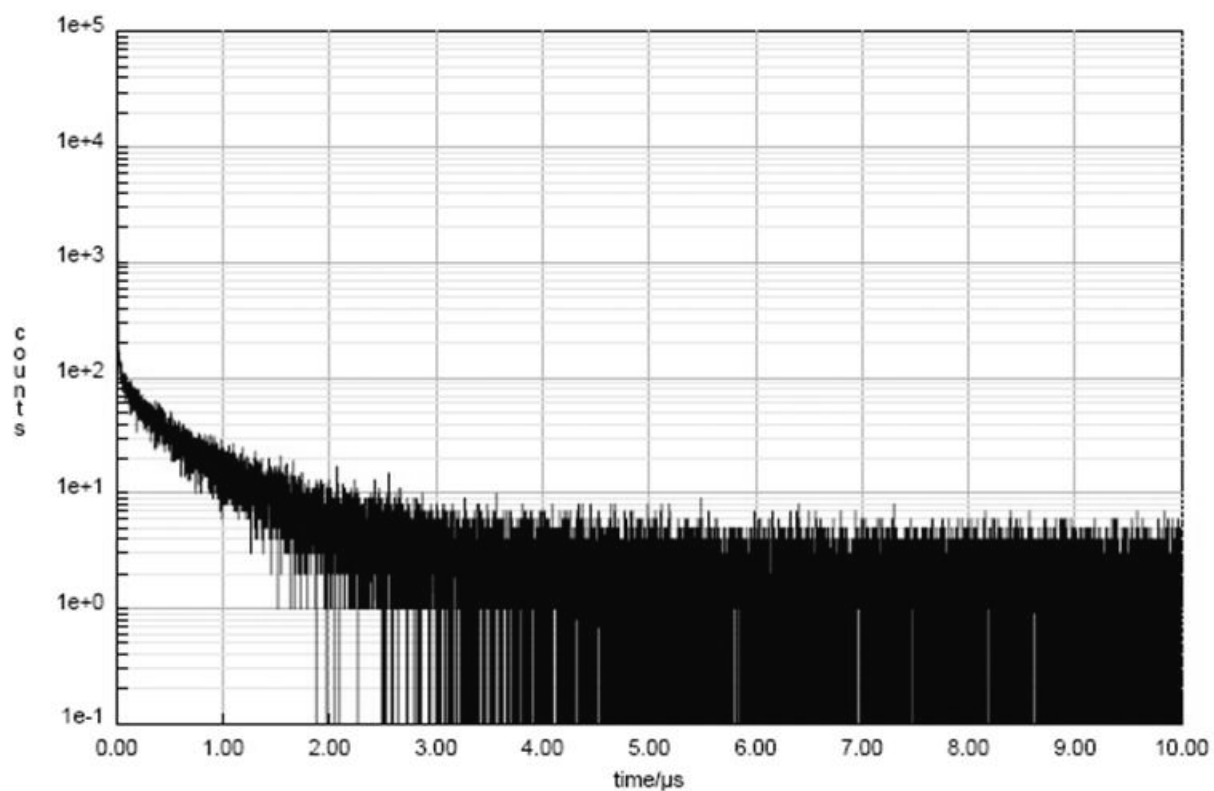


Figure D-11. TCSPC decay for C60 (40 nm)|pPtPh (31.7 nm) bilayer film. See Figure D-1 for the decay of an unquenched pPtPh film.

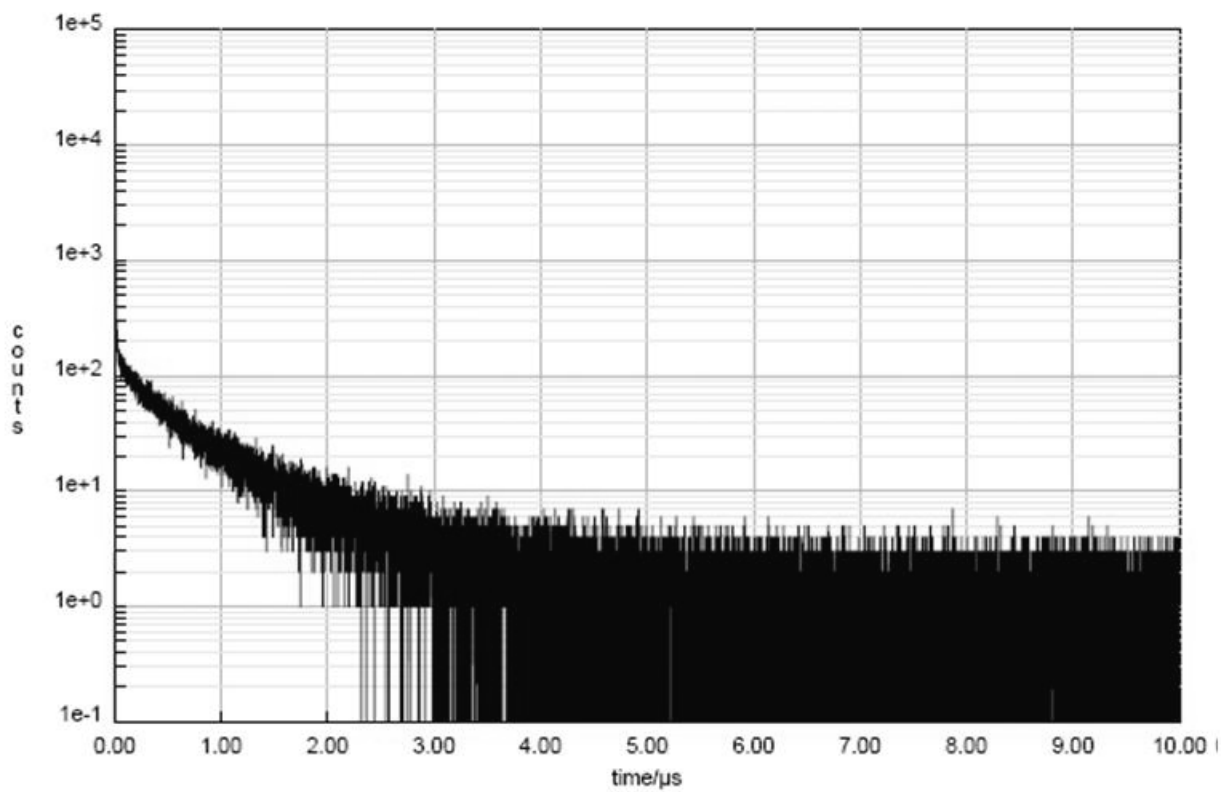


Figure D-12. TCSPC decay for C60 (40 nm)|pPtPh (43.2 nm) bilayer film.

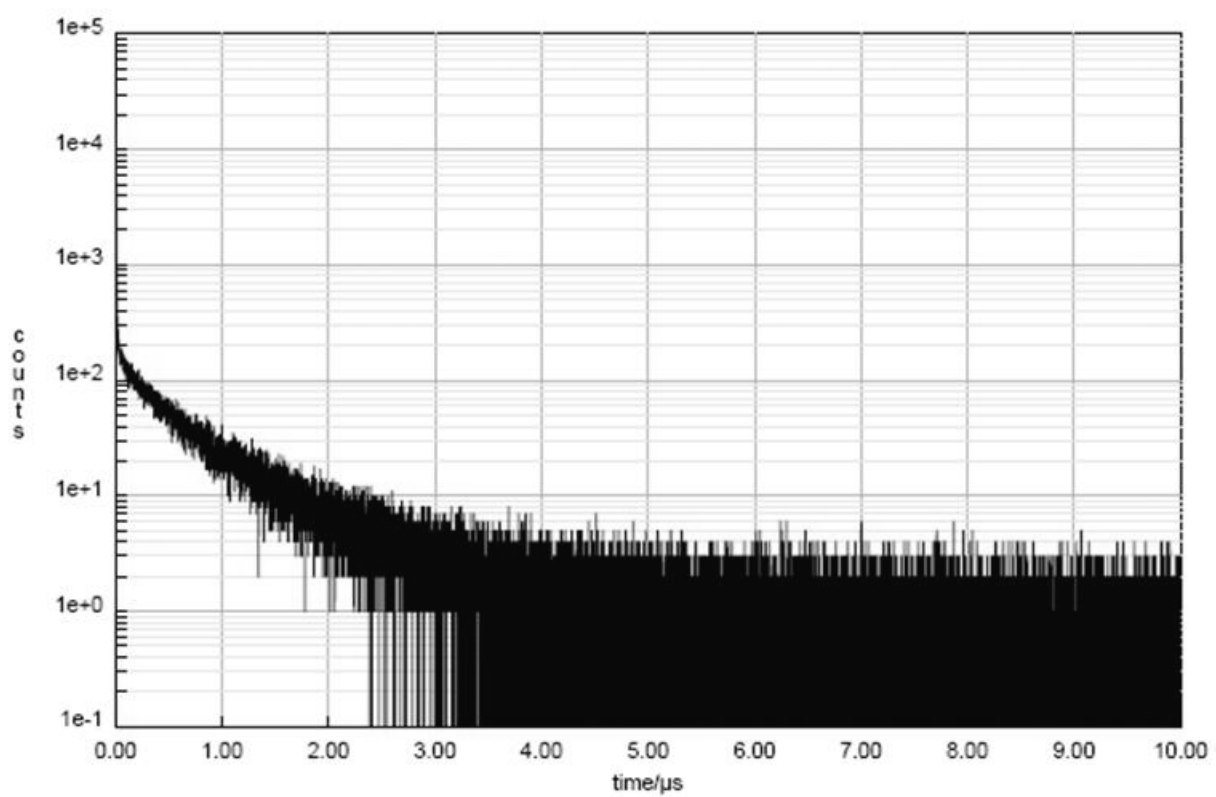


Figure D-13. TCSPC decay for C60 (40 nm)|pPtPh (48.5 nm) bilayer film.

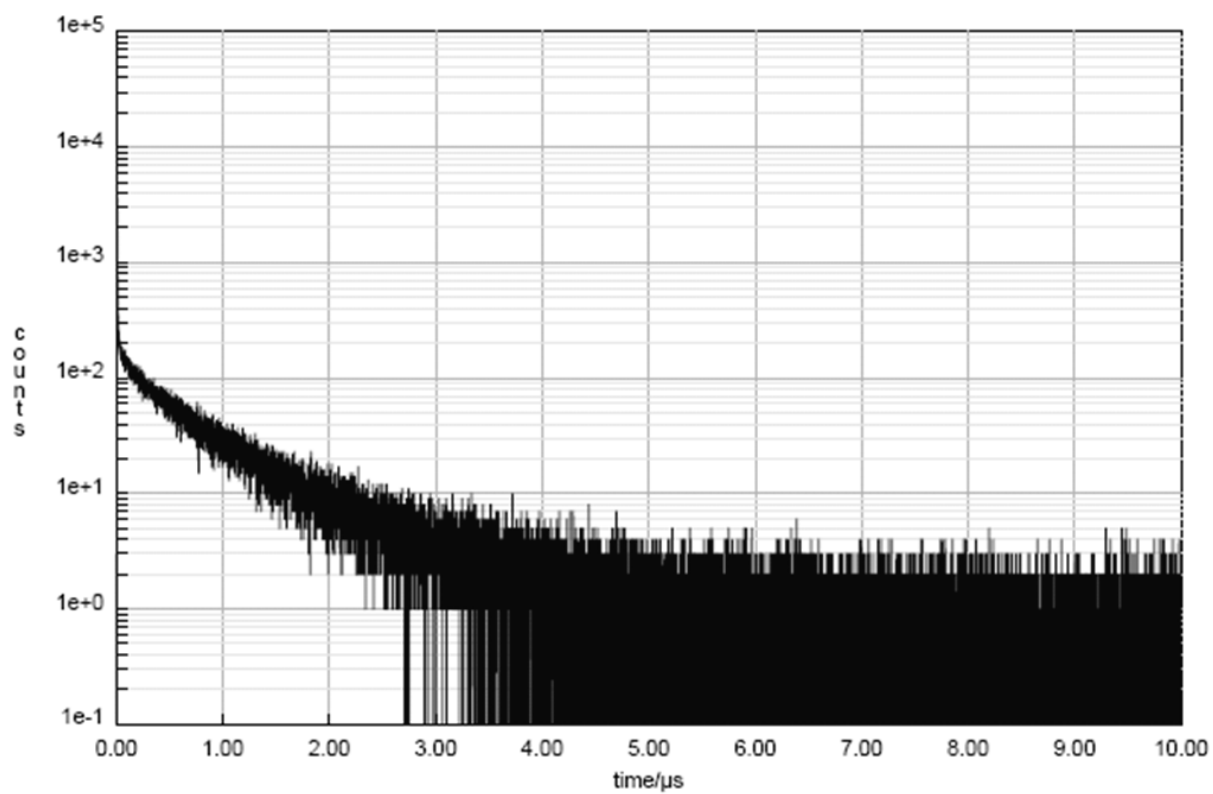


Figure D-14. TCSPC decay for C60 (40 nm)|pPtPh (75.2 nm) bilayer film.

PtTPP Blends

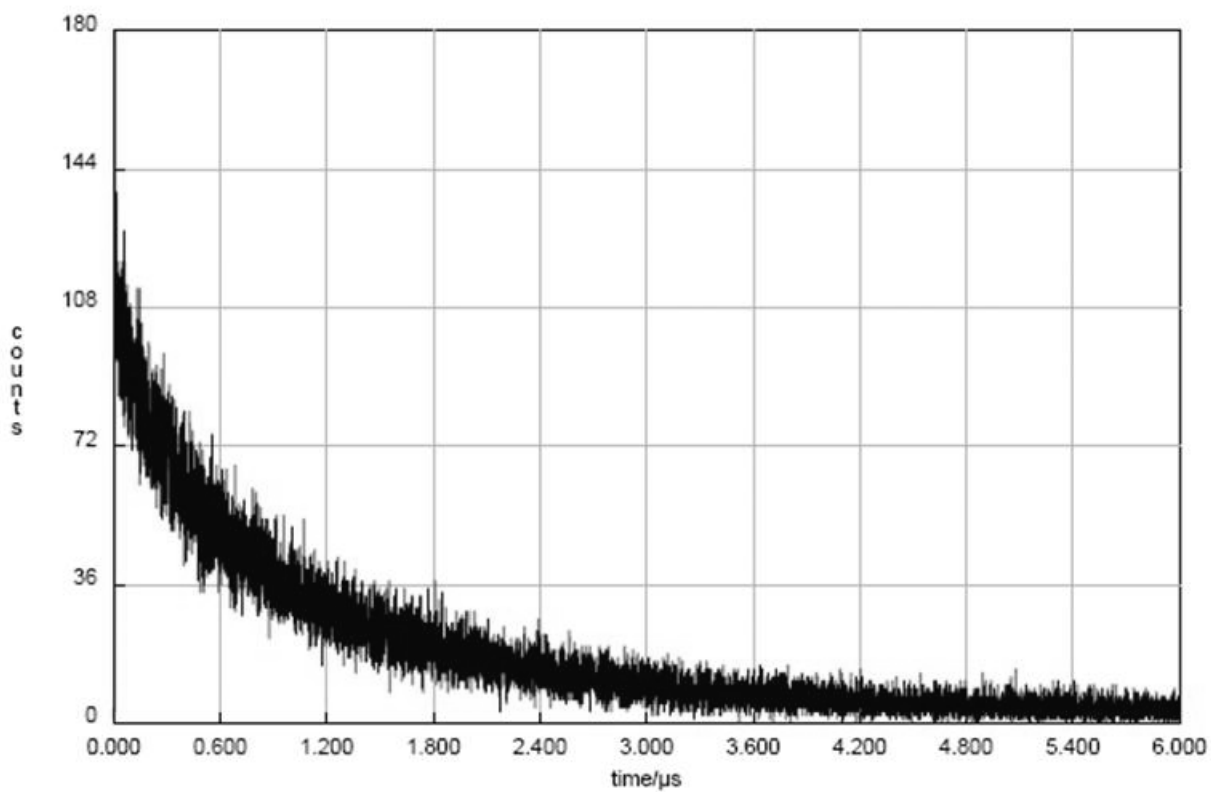


Figure D-15. TCSPC decay for a pristine pPtPh film (y-axis units in counts per second).

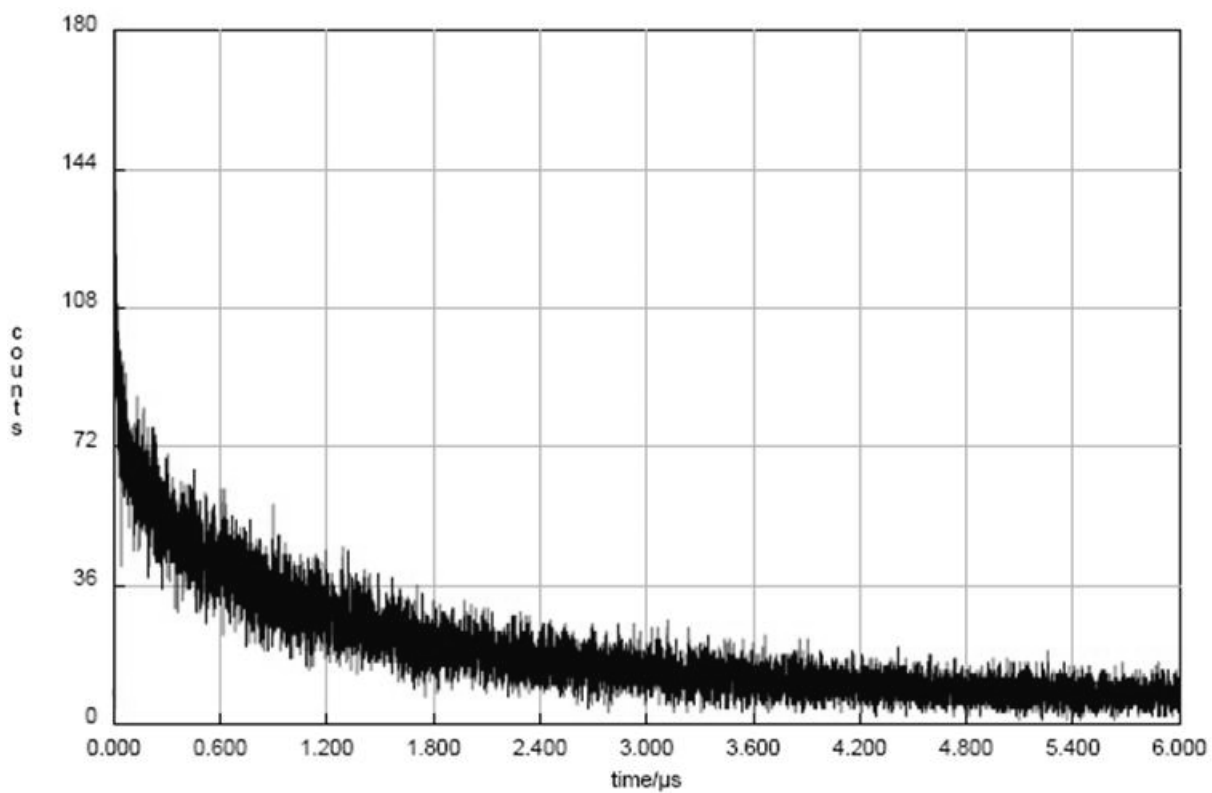


Figure D-16. TCSPC decay for a 0.022 wt% (0.351 mM) PtTPP/pPtPh film.

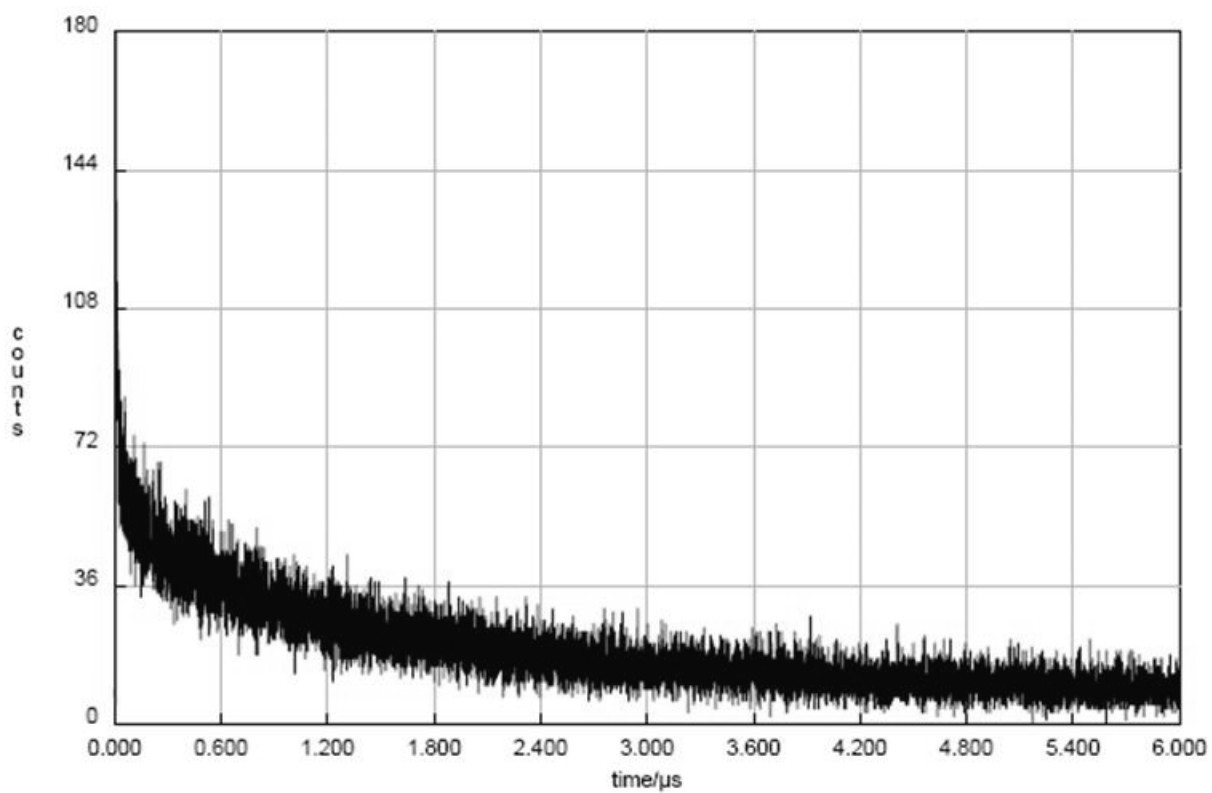


Figure D-17. TCSPC decay for a 0.044 wt% (0.703 mM) PtTPP/pPtPh film.

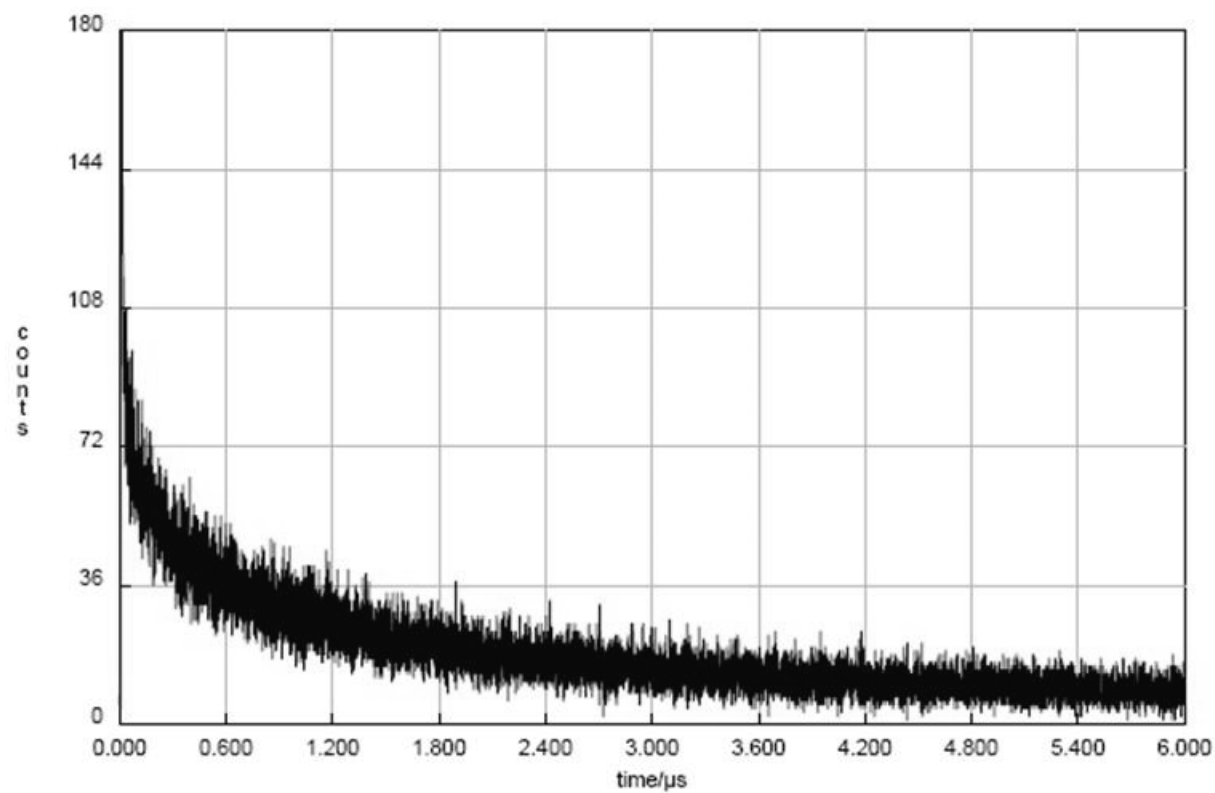


Figure D-18. TCSPC decay for a 0.11 wt% (1.76 mM) PtTPP/pPtPh film.

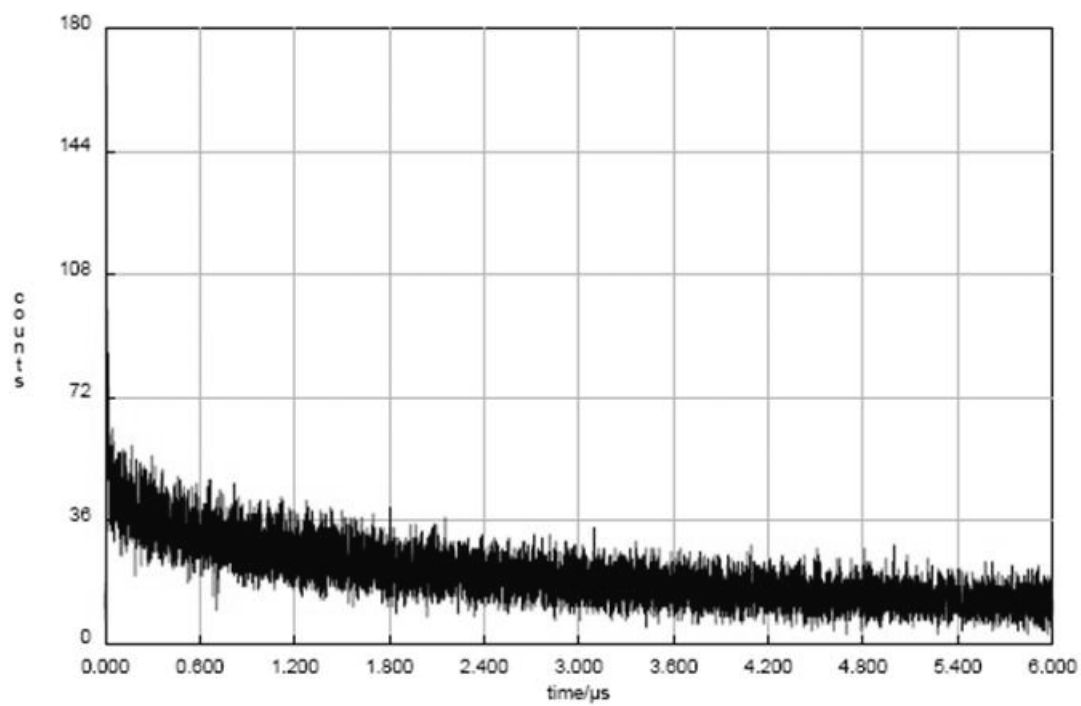


Figure D-19. TCSPC decay for a 0.20 wt% (3.17 mM) PtTPP/pPtPh film.

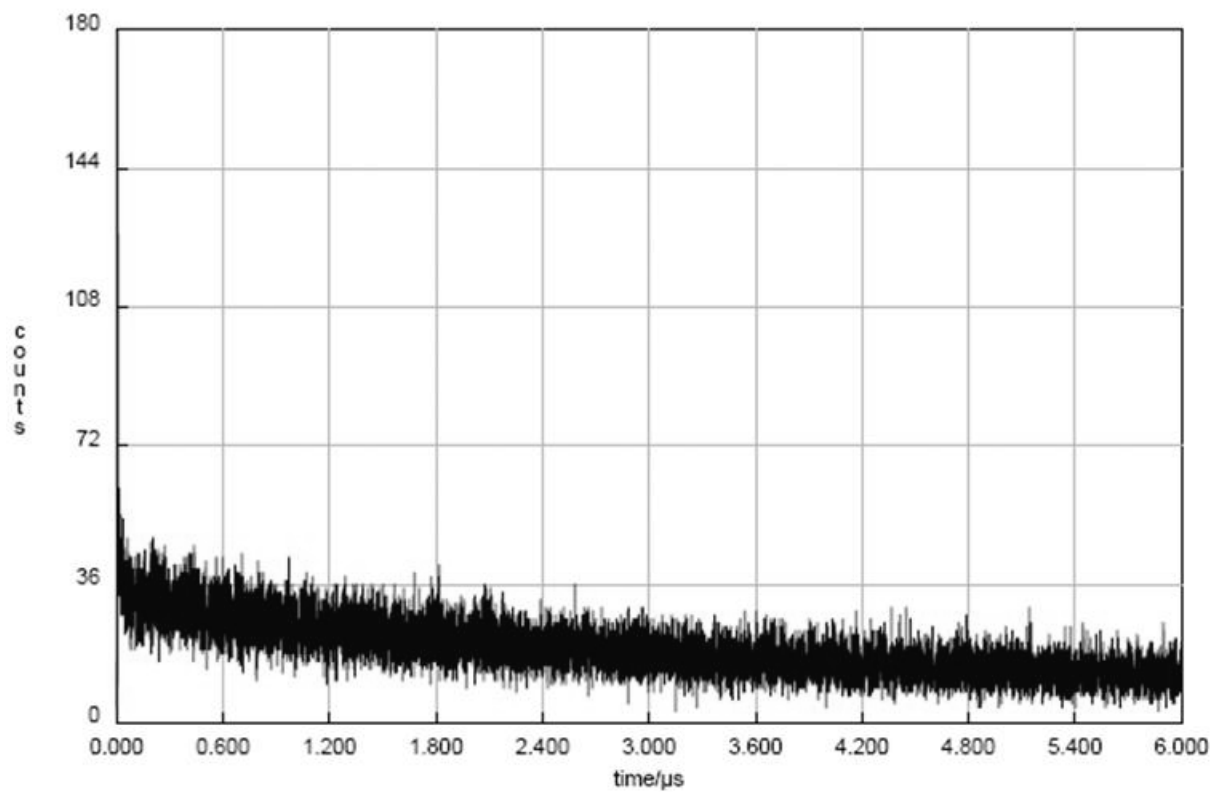


Figure D-20. TCSPC decay for a 0.29 wt% (4.58 mM) PtTPP/pPtPh film.

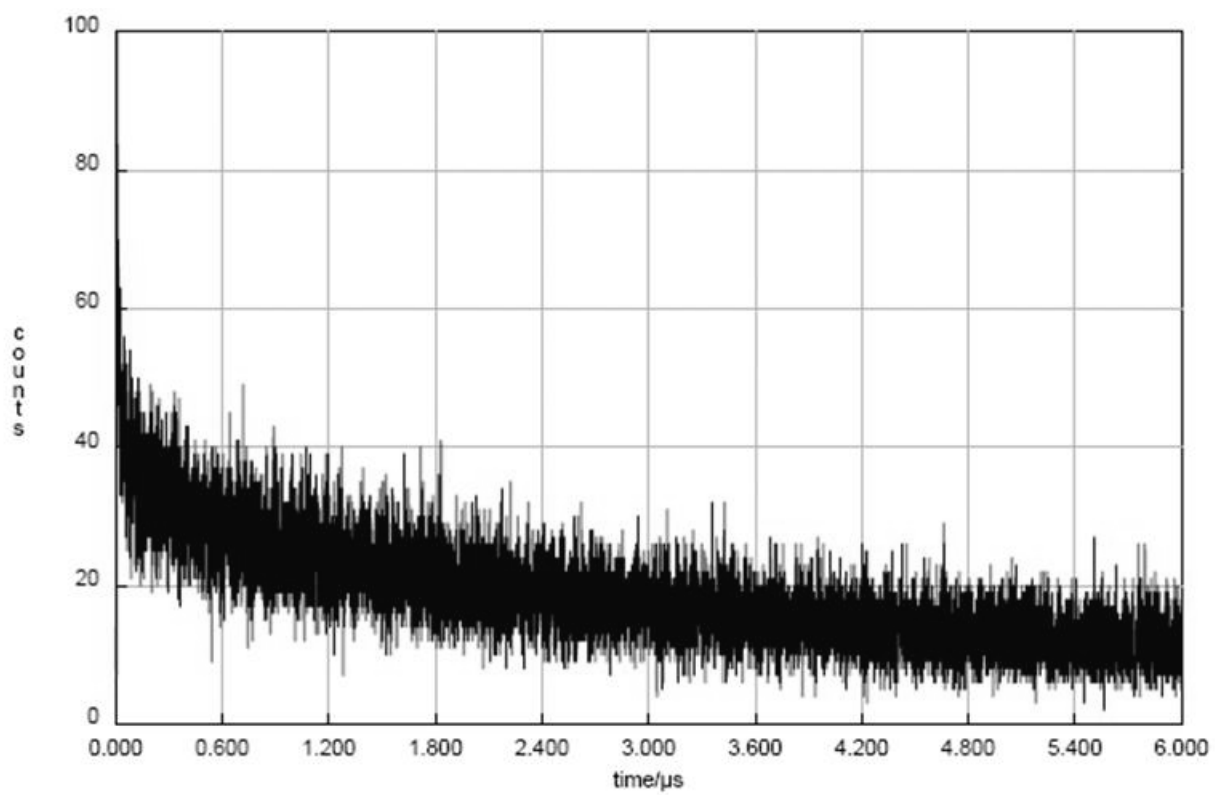


Figure D-21. TCSPC decay for a 0.38 wt% (5.97 mM) PtTPP/pPtPh film.

PtTPP Bilayer Films

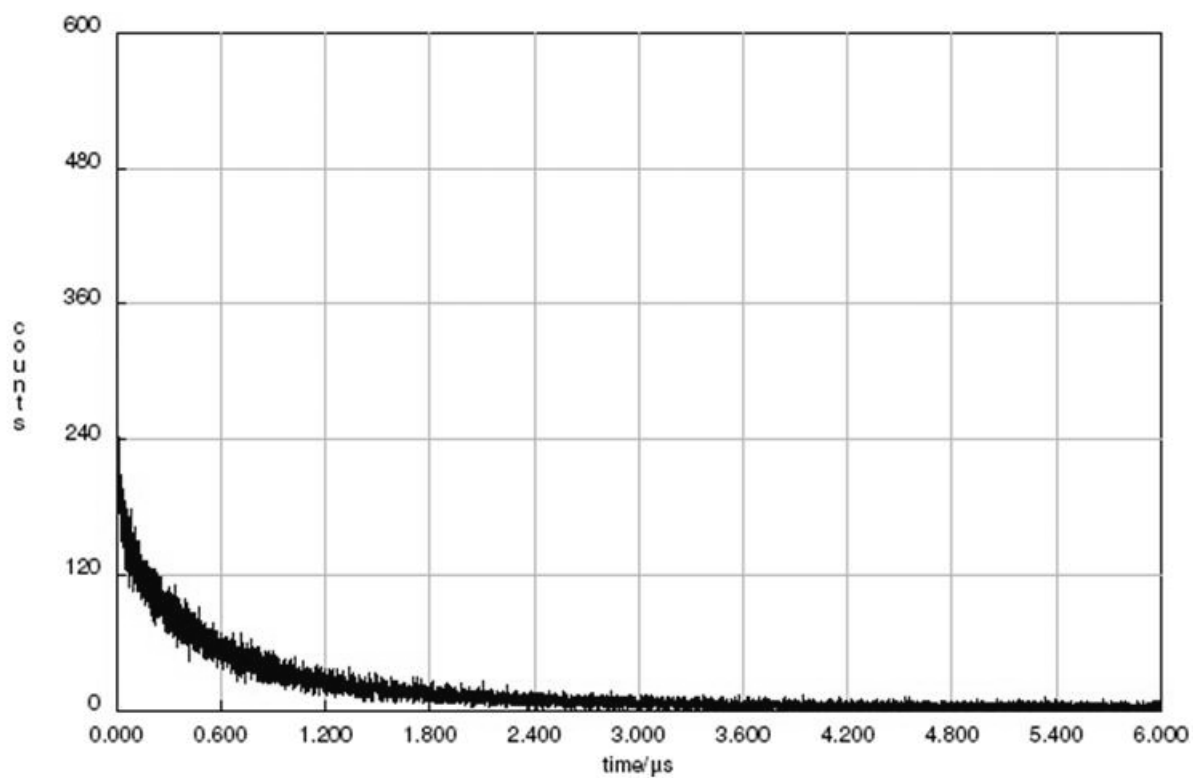


Figure D-22. TCSPC decay for PtTPP (40 nm)|pPtPh (22.7 nm) bilayer film.

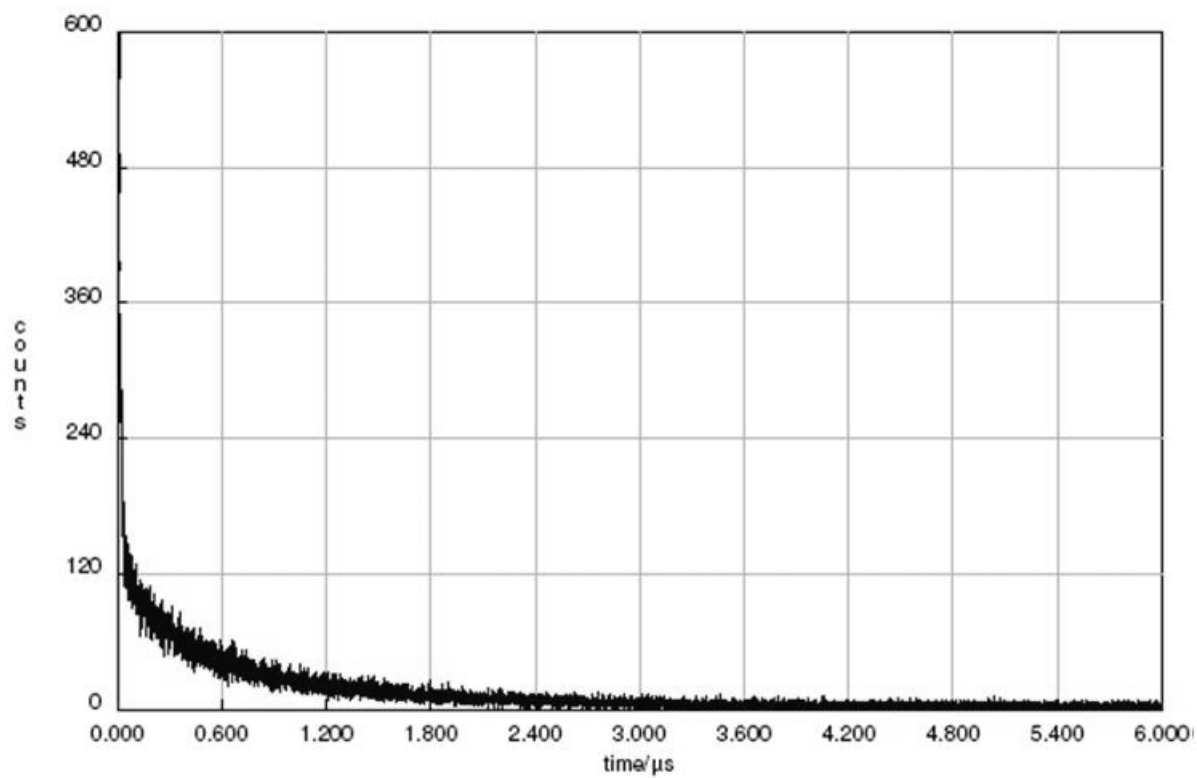


Figure D-23. TCSPC decay for PtTPP (40 nm)|pPtPh (24.3 nm) bilayer film.

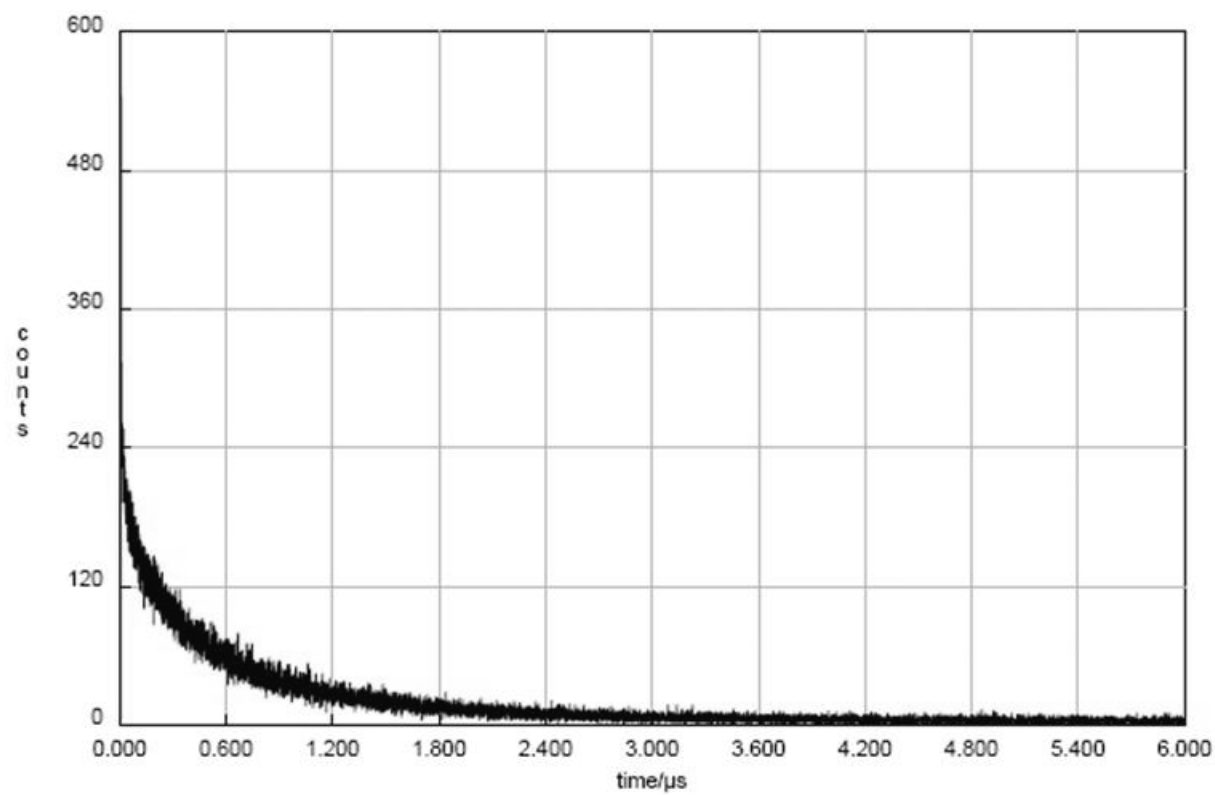


Figure D-24. TCSPC decay for PtTPP (40 nm)|pPtPh (31.7 nm) bilayer film.

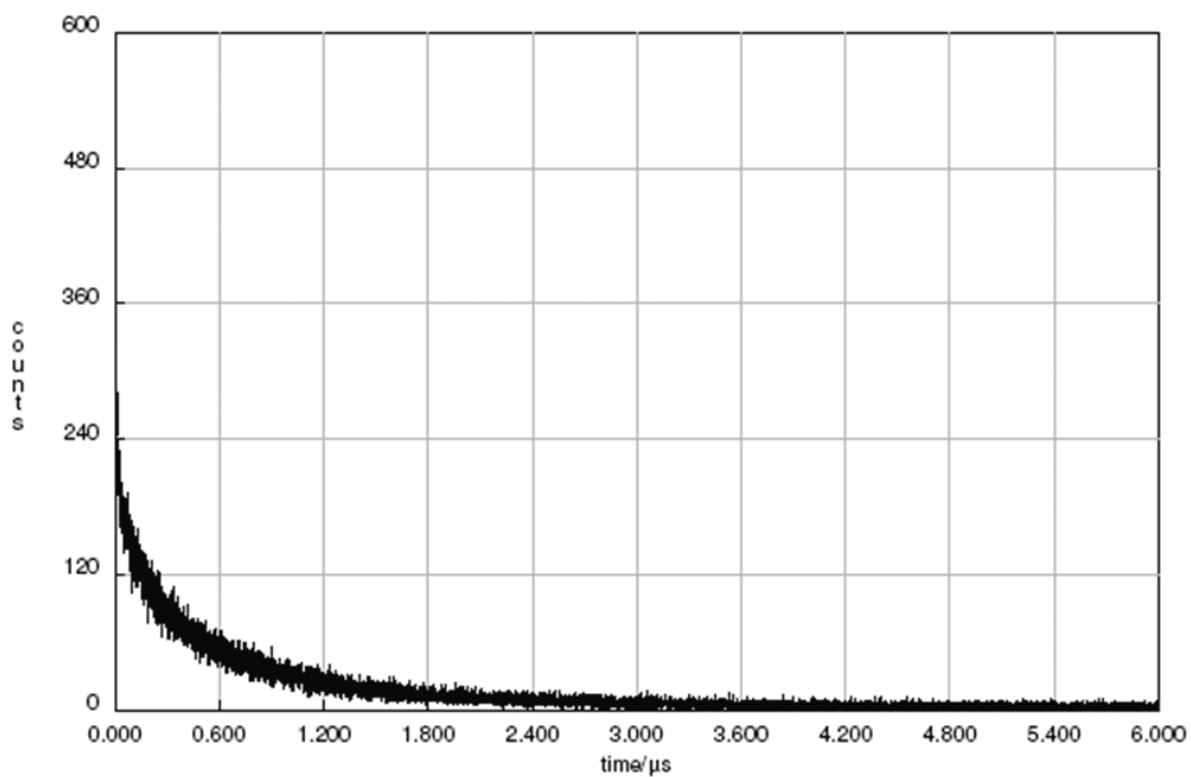


Figure D-25. TCSPC decay for PtTPP (40 nm)|pPtPh (46.7 nm) bilayer film.

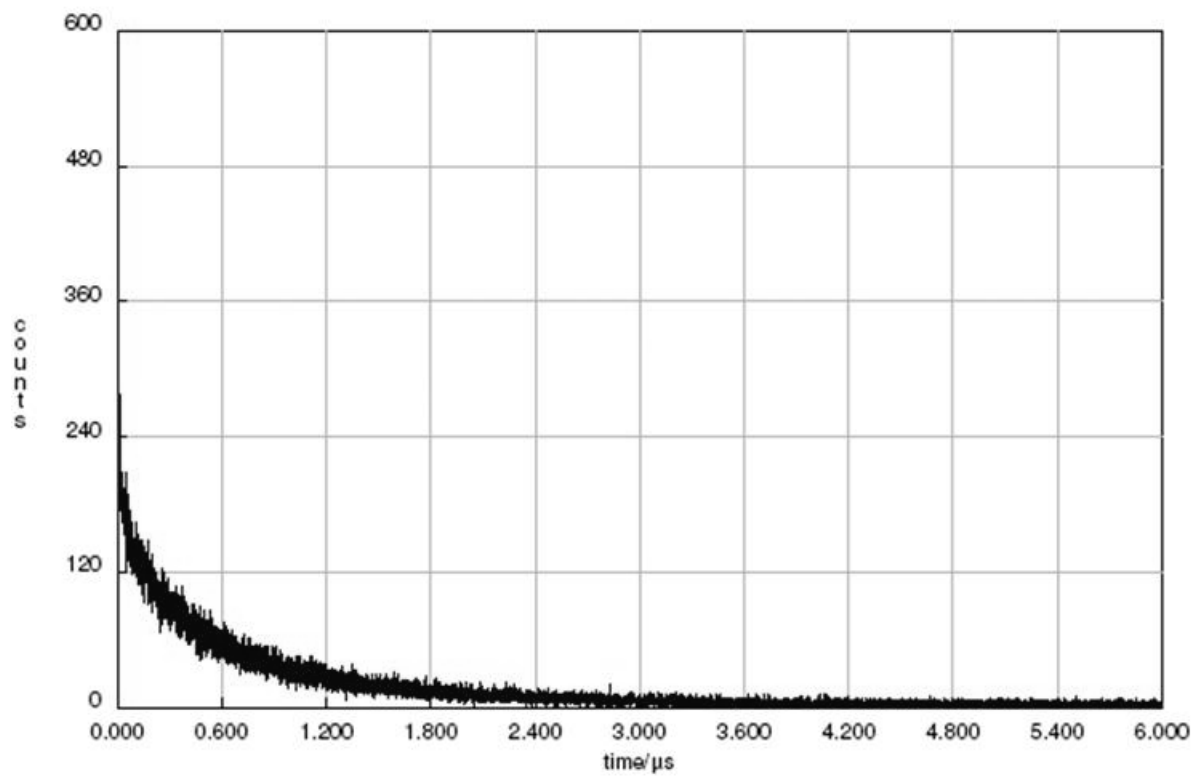


Figure D-26. TCSPC decay for PtTPP (40 nm)|pPtPh (55.0 nm) bilayer film.

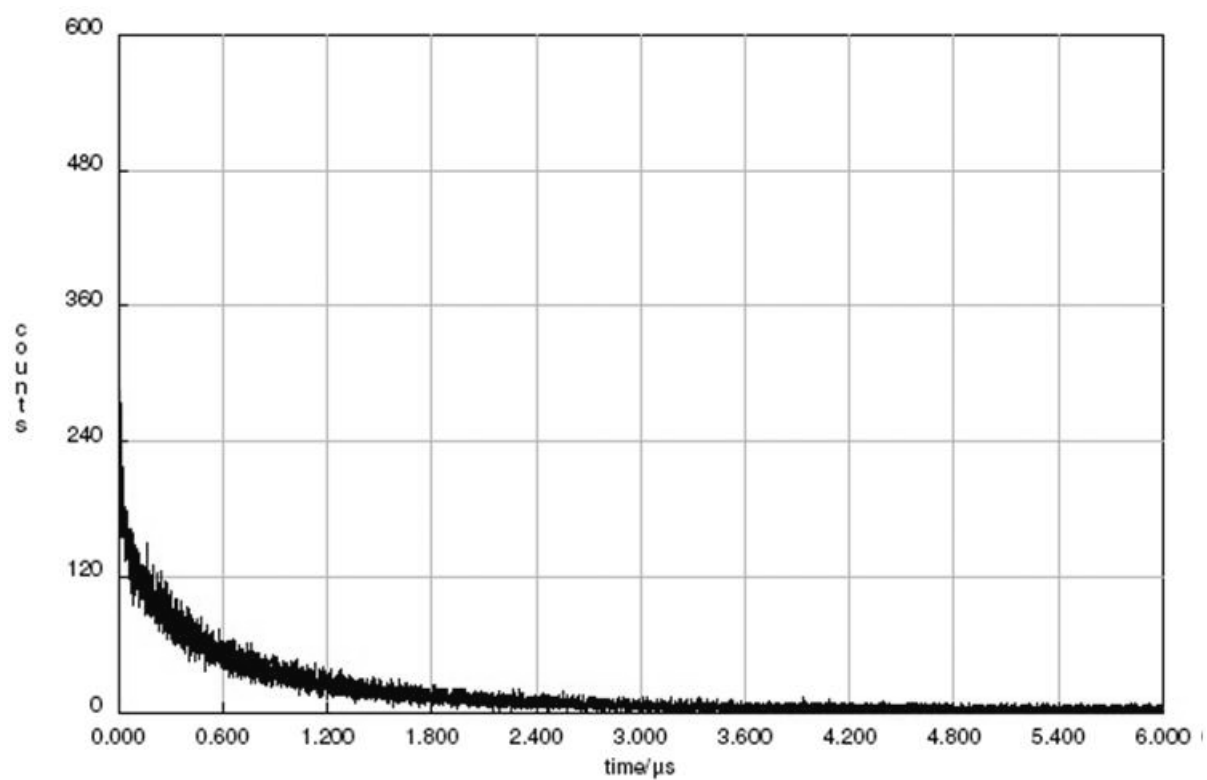


Figure D-27. TCSPC decay for PtTPP (40 nm)|pPtPh (65.0 nm) bilayer film.

LIST OF REFERENCES

1. Franklin, B.; Brownrigg, W.; Farish, M. *Philosophical Transactions (1683-1775)* **1774**, 64, 445.
2. Gaines, G. L. *Thin Solid Films* **1983**, 99, R9.
3. Blodgett, K. B. *J. Am. Chem. Soc.* **1935**, 57, 1007.
4. Chiarelli, P. A.; Liu, D. G.; Watkins, E. B.; Trouw, F. R.; Majewski, J.; Casson, J. L.; Tang, Z. X.; Johal, M. S.; Robinson, J. M.; Wang, H. L. *Thin Solid Films* **2009**, 517, 4638.
5. Talham, D. R.; Yamamoto, T.; Meisel, M. W. *J. Phys.: Condens. Matter* **2008**, 20, 184006.
6. Byrd, H.; Whipps, S.; Pike, J. K.; Ma, J. F.; Nagler, S. E.; Talham, D. R. *J. Am. Chem. Soc.* **1994**, 116, 295.
7. McCullough, D. H.; Regen, S. L. *Chem. Commun.* **2004**, 2787.
8. Perez-Morales, M.; de Miguel, G.; Bolink, H. J.; Martin-Romero, M. T.; Camacho, L. *J. Mater. Chem.* **2009**, 19, 4255.
9. Ashwell, G. J.; Sujka, M.; Green, A. *Faraday Discuss.* **2006**, 131, 23.
10. Ashwell, G. J.; Dawnay, E. J. C.; Kuczynski, A. P.; Szablewski, M.; Sandy, I. M.; Bryce, M. R.; Grainger, A. M.; Hasan, M. *J. Chem. Soc., Faraday Trans.* **1990**, 86, 1117.
11. Andreatta, G.; Benattar, J. J.; Petkova, R.; Wang, J. Y. J.; Tong, P.; Polidori, A.; Pucci, B. *Colloids. Surf., B: Physiochem. Eng. Aspects* **2008**, 321, 211.
12. Kozlovskaya, V.; Yakovlev, S.; Libera, M.; Sukhishvili, S. A. *Macromolecules* **2005**, 38, 4828.
13. Kharlampieva, E.; Sukhishvili, S. A. *Langmuir* **2004**, 20, 9677.
14. Stockton, W. B.; Rubner, M. F. *Macromolecules* **1997**, 30, 2717.
15. Mwaura, J. K.; Pinto, M. R.; Witker, D.; Ananthakrishnan, N.; Schanze, K. S.; Reynolds, J. R. *Langmuir* **2005**, 21, 10119.
16. Sasaki, T.; Ebina, Y.; Tanaka, T.; Harada, M.; Watanabe, M.; Decher, G. *Chem. Mater.* **2001**, 13, 4661.
17. Kim, B. S.; Park, S. W.; Hammond, P. T. *Acs Nano* **2008**, 2, 386.

18. Viinikanoja, A.; Areva, S.; Kocharova, N.; Aaritalo, T.; Vuorinen, M.; Savunen, A.; Kankare, J.; Lukkari, J. *Langmuir* **2006**, *22*, 6078.
19. Hoogeveen, N. G.; Stuart, M. A. C.; Fleeer, G. J.; Bohmer, M. R. *Langmuir* **1996**, *12*, 3675.
20. Pinto, M. R.; Kristal, B. M.; Schanze, K. S. *Langmuir* **2003**, *19*, 6523.
21. Jourdainne, L.; Lecuyer, S.; Arntz, Y.; Picart, C.; Schaaf, P.; Senger, B.; Voegel, J. C.; Lavalle, P.; Charitat, T. *Langmuir* **2008**, *24*, 7842.
22. Losche, M.; Schmitt, J.; Decher, G.; Bouwman, W. G.; Kjaer, K. *Macromolecules* **1998**, *31*, 8893.
23. Schmitt, J.; Grunewald, T.; Decher, G.; Pershan, P. S.; Kjaer, K.; Losche, M. *Macromolecules* **1993**, *26*, 7058.
24. Arys, X.; Laschewsky, A.; Jonas, A. M. *Macromolecules* **2001**, *34*, 3318.
25. Kharlampieva, E.; Kozlovskaya, V.; Ankner, J. F.; Sukhishvili, S. A. *Langmuir* **2008**, *24*, 11346.
26. Liang Hong; Steve Granick *J. Polym. Sci., Part B: Polym. Phys.* **2005**, *43*, 3497.
27. Schoeler, B.; Poptoshev, E.; Caruso, F. *Macromolecules* **2003**, *36*, 5258.
28. Salomaki, M.; Vinokurov, I. A.; Kankare, J. *Langmuir* **2005**, *21*, 11232.
29. Caruso, F.; Niikura, K.; Furlong, D. N.; Okahata, Y. *Langmuir* **1997**, *13*, 3422.
30. Ladam, G.; Schaad, P.; Voegel, J. C.; Schaaf, P.; Decher, G.; Cuisinier, F. *Langmuir* **2000**, *16*, 1249.
31. Kanaya, T.; Miyazaki, T.; Watanabe, H.; Nishida, K.; Yamana, H.; Tasaki, S.; Bucknall, D. B. *Polymer* **2003**, *44*, 3769.
32. Barbero, D. R.; Steiner, U. *Phys. Rev. Lett.* **2009**, *102*, 248303.
33. Daughton, W. J.; Givens, F. L. *J. Electrochem. Soc.* **1982**, *129*, 173.
34. Givens, F. L.; Daughton, W. J. *J. Electrochem. Soc.* **1979**, *126*, 269.
35. Lawrence, C. J. *Phys. Fluids* **1988**, *31*, 2786.
36. Kim, S.; Shin, D. H.; Kim, C. O.; Hwang, S. W.; Choi, S. H.; Ji, S.; Koo, J. Y. *Appl. Phys. Lett.* **2009**, *94*, 213113.

37. Motaung, D. E.; Malgas, G. F.; Arendse, C. J.; Mavundla, S. E.; Knoesen, D. *Mater. Chem. Phys.* **2009**, *116*, 279.
38. Müller-Buschbaum, P.; Hermsdorf, N.; Roth, S. V.; Wiedersich, J.; Cunis, S.; Gehrke, R. *Spectrochim. Acta, Part A* **2004**, *59*, 1789.
39. Shelke, V.; Sonawane, B. K.; Bhole, M. P.; Patil, D. S. *J. Non-Cryst. Solids* **2009**, *355*, 840.
40. Jaczewska, J.; Budkowski, A.; Bernasik, A.; Moons, E.; Rysz, J. *Macromolecules* **2008**, *41*, 4802.
41. Aal, A. A.; Mahmoud, S. A.; Aboul-Gheit, A. K. *Nanoscale Research Letters* **2009**, *4*, 627.
42. Kaul, A. R.; Gorbenko, O. Y.; Botev, A. N.; Burova, L. I. *Superlattices Microstruct.* **2005**, *38*, 272.
43. Videlot-Ackermann, C.; Brisset, H.; Zhang, J.; Ackermann, J.; Nenon, S.; Fages, F.; Marsal, P.; Tanisawa, T.; Yoshimoto, N. *J. Phys. Chem. C* **2009**, *113*, 1567.
44. Lamansky, S.; Djurovich, P.; Murphy, D.; Abdel-Razzaq, F.; Lee, H. E.; Adachi, C.; Burrows, P. E.; Forrest, S. R.; Thompson, M. E. *J. Am. Chem. Soc.* **2001**, *123*, 4304.
45. Izawa, T.; Mori, H.; Shinmura, Y.; Iwatani, M.; Miyazaki, E.; Takimiya, K.; Hung, H. W.; Yahiro, M.; Adachi, C. *Chem. Lett.* **2009**, *38*, 420.
46. El-Gendy, Y. A. *J. Phys. D: Appl. Phys.* **2009**, *42*, 115408.
47. Kowarik, S.; Gerlach, A.; Schreiber, F. *J. Phys.: Condens. Matter* **2008**, *20*, 184005.
48. Schreiber, F. *Physica Status Solidi a-Applied Research* **2004**, *201*, 1037.
49. Ruiz, R.; Choudhary, D.; Nickel, B.; Toccoli, T.; Chang, K. C.; Mayer, A. C.; Clancy, P.; Blakely, J. M.; Headrick, R. L.; Iannotta, S.; Malliaras, G. G. *Chem. Mater.* **2004**, *16*, 4497.
50. Mayer, A. C.; Ruiz, R.; Zhou, H.; Headrick, R. L.; Kazimirov, A.; Malliaras, G. G. *Phys. Rev. B.* **2006**, *73*, 205307.
51. Mayer, A. C.; Kazimirov, A.; Malliaras, G. G. *Phys. Rev. Lett.* **2006**, *97*, 105503.
52. Kowarik, S.; Gerlach, A.; Leitenberger, W.; Hu, J.; Witte, G.; Woll, C.; Pietsch, U.; Schreiber, F. *Thin Solid Films* **2007**, *515*, 5606.

53. Pratontep, S.; Brinkmann, M.; Nuesch, F.; Zuppiroli, L. *Phys. Rev. B.* **2004**, *69*, 165201.
54. Ruiz, R.; Mayer, A. C.; Malliaras, G. G.; Nickel, B.; Scoles, G.; Kazimirov, A.; Kim, H.; Headrick, R. L.; Islam, Z. *Appl. Phys. Lett.* **2004**, *85*, 4926.
55. Ruiz, R.; Nickel, B.; Koch, N.; Feldman, L. C.; Haglund, R. F.; Kahn, A.; Scoles, G. *Phys. Rev. B.* **2003**, *67*, 125406.
56. Bouchoms, I. P. M.; Schoonveld, W. A.; Vrijmoeth, J.; Klapwijk, T. M. *Synth. Met.* **1999**, *104*, 175.
57. Feldman, D. *Designed Monomers and Polymers* **2008**, *11*, 1.
58. Shirakawa, H.; Louis, E. J.; Macdiarmid, A. G.; Chiang, C. K.; Heeger, A. J. *J. Chem. Soc.-Chem. Commun.* **1977**, 578.
59. Hall, N. *Chem. Commun.* **2003**, 1.
60. Zhang, K.; Tao, Y. T.; Yang, C. L.; You, H.; Zou, Y.; Qin, J. G.; Ma, D. G. *Chem. Mater.* **2008**, *20*, 7324.
61. Tuladhar, S. M.; Sims, M.; Choulis, S. A.; Nielsen, C. B.; George, W. N.; Steinke, J. H. G.; Bradley, D. D. C.; Nelson, J. *Org. Electron.* **2009**, *10*, 562.
62. Odian, G. *Principles of Polymerization*, 4 ed.; John Wiley and Sons: Hoboken, New Jersey, USA, 2004.
63. Anslyn, E. V.; Dougherty, D. A. *Modern Physical Organic Chemistry*; University Science Books: Sausalito, California, USA, 2006.
64. Nambiar, R.; Woody, K. B.; Ochocki, J. D.; Brizius, G. L.; Collard, D. M. *Macromolecules* **2009**, *42*, 43.
65. Yu, J. M.; Chen, Y. *J. Polym. Sci., Part A: Polym Chem.* **2009**, *47*, 2985.
66. Sybert, P. D.; Beever, W. H.; Stille, J. K. *Macromolecules* **1981**, *14*, 493.
67. Miyake, J.; Tsuji, Y.; Nagai, A.; Chujo, Y. *Macromolecules* **2009**, *42*, 3463.
68. Huang, Y. Q.; Fan, Q. L.; Lu, X. M.; Fang, C.; Liu, S. J.; Yu-Wen, L. H.; Wang, L. H.; Huang, W. *J. Polym. Sci., Part A: Polym Chem.* **2006**, *44*, 5778.
69. Xue, C. H.; Cai, F. F.; Liu, H. Y. *Chem. Eur. J.* **2008**, *14*, 1648.
70. Smith, A. D.; Shen, C. K. F.; Roberts, S. T.; Helgeson, R.; Schwartz, B. J. *Res. Chem. Intermed.* **2007**, *33*, 125.

71. Zhao, X. Y.; Pinto, M. R.; Hardison, L. M.; Mwaura, J.; Muller, J.; Jiang, H.; Witker, D.; Kleiman, V. D.; Reynolds, J. R.; Schanze, K. S. *Macromolecules* **2006**, *39*, 6355.
72. Turro, N. J. *Modern Molecular Photochemistry*; University Science Books: Sausalito, California, USA, 1991.
73. Devi, L. S.; Al-Suti, M. K.; Zhang, N.; Teat, S. J.; Male, L.; Sparkes, H. A.; Raithby, P. R.; Khan, M. S.; Kohler, A. *Macromolecules* **2009**, *42*, 1131.
74. Schulz, G. L.; Holdcroft, S. *Chem. Mater.* **2008**, *20*, 5351.
75. Mei, J.; Ogawa, K.; Kim, Y. G.; Heston, N. C.; Arenas, D. J.; Nasrollahi, Z.; McCarley, T. D.; Tanner, D. B.; Reynolds, J. R.; Schanze, K. S. *ACS Appl. Mater. Interfaces* **2009**, *1*, 150.
76. Lunt, R. R.; Giebink, N. C.; Belak, A. A.; Benziger, J. B.; Forrest, S. R. *J. Appl. Phys.* **2009**, *105*.
77. Kurrle, D.; Pflaum, J. *Appl. Phys. Lett.* **2008**, *92*, 133306.
78. Ikeda, N.; Yoshimura, A.; Tsushima, M.; Ohno, T. *J. Phys. Chem. A* **2000**, *104*, 6158.
79. Marciniak, H.; Pugliesi, I.; Nickel, B.; Lochbrunner, S. *Phys. Rev. B* **2009**, *79*, 235318.
80. Tsuchida, A.; Yamamoto, M.; Liebe, W. R.; Burkhart, R. D.; Tsubakiyama, K. *Macromolecules* **1996**, *29*, 1589.
81. Black, M. R.; Chavez, C.; Brosha, E. *Org. Electron.* **2007**, *8*, 601.
82. Yang, C. L.; Tang, Z. K.; Ge, W. K.; Wang, J. N.; Zhang, Z. L.; Jian, X. Y. *Appl. Phys. Lett.* **2003**, *83*, 1737.
83. Giebink, N. C.; Sun, Y.; Forrest, S. R. *Org. Electron.* **2006**, *7*, 375.
84. Mikhnenko, O. V.; Cordella, F.; Sieval, A. B.; Hummelen, J. C.; Blom, P. W. M.; Loi, M. A. *J. Phys. Chem. B* **2009**, *113*, 9104.
85. Theander, M.; Yartsev, A.; Zigmantas, D.; Sundstrom, V.; Mammo, W.; Andersson, M. R.; Inganas, O. *Phys. Rev. B* **2000**, *61*, 12957.
86. Markov, D. E.; Hummelen, J. C.; Blom, P. W. M.; Sieval, A. B. *Phys. Rev. B* **2005**, *72*, 45216.
87. Kroeze, J. E.; Savenije, T. J.; Candeias, L. P.; Warman, J. M.; Siebbeles, L. D. A. *Sol. Energy Mater. Sol. Cells* **2005**, *85*, 189.

88. Wilson, J. S.; Kohler, A.; Friend, R. H.; Al-Suti, M. K.; Al-Mandhary, M. R. A.; Khan, M. S.; Raithby, P. R. *J. Chem. Phys.* **2000**, *113*, 7627.
89. Schanze, K. S.; Silverman, E. E.; Zhao, X. M. *J. Phys. Chem. B* **2005**, *109*, 18451.
90. Cardolaccia, T. Ph.D. Dissertation, University of Florida, 2005.
91. Zheng, Q. L.; Bohling, J. C.; Peters, T. B.; Frisch, A. C.; Hampel, F.; Gladysz, J. A. *Chem. Eur. J.* **2006**, *12*, 6486.
92. Farley, R. T.; Zheng, Q. L.; Gladysz, J. A.; Schanze, K. S. *Inorg. Chem.* **2008**, *47*, 2955.
93. de Quadras, L.; Shelton, A. H.; Kuhn, H.; Hampel, F.; Schanze, K. S.; Gladysz, J. A. *Organometallics* **2008**, *27*, 4979.
94. Beljonne, D.; Wittmann, H. F.; Kohler, A.; Graham, S.; Younus, M.; Lewis, J.; Raithby, P. R.; Khan, M. S.; Friend, R. H.; Bredas, J. L. *J. Chem. Phys.* **1996**, *105*, 3868.
95. Hummelen, J. C.; Knight, B. W.; Lepeq, F.; Wudl, F.; Yao, J.; Wilkins, C. L. *J. Org. Chem.* **1995**, *60*, 532.
96. KeshavarzK, M.; Knight, B.; Haddon, R. C.; Wudl, F. *Tetrahedron* **1996**, *52*, 5149.
97. Haddon, R. C. *Acc. Chem. Res.* **1992**, *25*, 127.
98. Guo, F. Q.; Kim, Y. G.; Reynolds, J. R.; Schanze, K. S. *Chem. Commun.* **2006**, 1887.
99. O'Connor, D. V.; Phillips, D. *Time-Correlated Single Photon Counting*; Academic Press: London, England, 1984.
100. Nguyen, L. H.; Hoppe, H.; Erb, T.; Gunes, S.; Gobsch, G.; Sariciftci, N. S. *Adv. Funct. Mater.* **2007**, *17*, 1071.
101. Wrobel, D.; Lukasiewicz, J.; Manikowski, H. *Dyes and Pigments* **2003**, *58*, 7.
102. Clements, J. H.; Webber, S. E. *J. Phys. Chem. A* **1999**, *103*, 2513.
103. Zhong, H. F.; Yang, X. N.; deWith, B.; Loos, J. *Macromolecules* **2006**, *39*, 218.
104. Bull, T. A.; Pingree, L. S. C.; Jenekhe, S. A.; Ginger, D. S.; Luscombe, C. K. *Acs Nano* **2009**, *3*, 627.
105. Keivanidis, P. E.; Howard, I. A.; Friend, R. H. *Adv. Funct. Mater.* **2008**, *18*, 3189.

106. Blondiaux, N.; Morgenthaler, S.; Pugin, R.; Spencer, N. D.; Liley, M. *Appl. Surf. Sci.* **2008**, 254, 6820.
107. Nilsson, S.; Bernasik, A.; Budkowski, A.; Moons, E. *Macromolecules* **2007**, 40, 8291.
108. Malone, W. M.; Albert, R. *J. Appl. Polym. Sci.* **1973**, 17, 2457.
109. Quayle, O. R. *Chem. Rev.* **1953**, 53, 439.
110. Edward, J. T. *Chem. Ind. (London)* **1956**, 52, 774.
111. Durchschlag, H.; Zipper, P. *Prog. Colloid Polym. Sci.* **1994**, 94, 20.
112. Lu, H. M.; Wen, Z.; Jiang, Q. *Colloids. Surf., A: Physiochem. Eng. Aspects* **2006**, 278, 160.
113. Ishikawa, T.; Paradis, P. F.; Koike, N. *Jpn. J. Appl. Phys., Part 1* **2006**, 45, 1719.
114. Ji, E. Doctoral Dissertation, University of Florida, 2009.
115. Benson, S. W. *The Foundations of Chemical Kinetics*; McGraw-Hill: New York, 1960.
116. Tan, C. Y.; Pinto, M. R.; Schanze, K. S. *Chem. Commun.* **2002**, 446.
117. Gulbinas, V.; Mineviciute, I.; Hertel, D.; Wellander, R.; Yartsev, A.; Sundstrom, V. *J. Chem. Phys.* **2007**, 127.
118. Huijser, A.; Savenije, T. J.; Meskers, S. C. J.; Vermeulen, M. J. W.; Siebbeles, L. D. A. *J. Am. Chem. Soc.* **2008**, 130, 12496.
119. Sokolik, I.; Walser, A. D.; Priestley, R.; Tang, C. W.; Dorsinville, R. *Synth. Met.* **1997**, 84, 921.
120. Baldo, M. A.; Forrest, S. R. *Phys. Rev. B.* **2000**, 62, 10958.
121. Bulovic, V.; Forrest, S. R. *Chem. Phys.* **1996**, 210, 13.
122. Namdas, E. B.; Ruseckas, A.; Samuel, I. D. W.; Lo, S. C.; Burn, P. L. *Appl. Phys. Lett.* **2005**, 86, 91104.
123. Anon. *FluoFit User's Manual and Technical Data*; 4.2 ed.; PicoQuant GmbH: Berlin, Germany.
124. Ariga, K.; Hill, J. P.; Ji, Q. M. *Phys. Chem. Chem. Phys.* **2007**, 9, 2319.

125. Geffroy, C.; Labeau, M. P.; Wong, K.; Cabane, B.; Stuart, M. A. C. *Colloids. Surf., A: Physiochem. Eng. Aspects* **2000**, *172*, 47.
126. Buron, C. C.; Filiatre, C.; Membrey, F.; Bainier, C.; Charraut, D.; Foissy, A. *J. Colloid Interface Sci.* **2007**, *314*, 358.
127. Dejeu, J.; Buisson, L.; Guth, M. C.; Roidor, C.; Membrey, F.; Charraut, D.; Foissy, A. *Colloids. Surf., A: Physiochem. Eng. Aspects* **2006**, *288*, 26.
128. Liu, G. M.; Zhao, J. P.; Sun, Q. Y.; Zhang, G. Z. *J. Phys. Chem. B* **2008**, *112*, 3333.
129. Maier, A.; Rabindranath, R.; Tieke, B. *Adv. Mater.* **2009**, *21*, 959.
130. Jomaa, H. W.; Schlenoff, J. B. *Macromolecules* **2005**, *38*, 8473.
131. Baur, J. W.; Rubner, M. F.; Reynolds, J. R.; Kim, S. *Langmuir* **1999**, *15*, 6460.
132. Lodi, A.; Caselli, M.; Zanfognini, B.; Cagnoli, R.; Mucci, A.; Parenti, F.; Schenetti, L.; Ponterini, G. *Thin Solid Films* **2008**, *516*, 8731.
133. Yu, D. B.; Zhang, C. Z.; Wang, X.; Jiang, C. X.; Xiong, T.; Meng, W. Q.; Liu, C.; Chen, D.; Zhong, A. Y. *J. Appl. Polym. Sci.* **2008**, *110*, 124.
134. Priefer, R.; Leach, K. E.; Krauss, T. D.; Drapo, J. R.; Ingalsbe, M. L.; van Dongen, M. A.; Cadwalader, J. C.; Baumler, M. A.; Pinto, M. S. *Surface & Coatings Technology* **2008**, *202*, 6109.
135. Zhao, X. Y.; Jiang, H.; Schanze, K. S. *Macromolecules* **2008**, *41*, 3422.
136. Brookins, B. Doctoral Dissertation, University of Florida, 2008.
137. Zhang, T.; Fan, H. L.; Zhou, J. G.; Liu, G. L.; Feng, G. D.; Jin, Q. H. *Macromolecules* **2006**, *39*, 7839.
138. Tan, C. Y.; Atas, E.; Muller, J. G.; Pinto, M. R.; Kleiman, V. D.; Schanze, K. S. *J. Am. Chem. Soc.* **2004**, *126*, 13685.
139. Knaapila, M.; Garamus, V. M.; Dias, F. B.; Almasy, L.; Galbrecht, F.; Charas, A.; Morgado, J.; Burrows, H. D.; Scherf, U.; Monkman, A. P. *Macromolecules* **2006**, *39*, 6505.
140. Rahman, M. H.; Chen, C. Y.; Liao, S. C.; Chen, H. L.; Tsao, C. S.; Chen, J. H.; Liao, J. L.; Ivanov, V. A.; Chen, S. A. *Macromolecules* **2007**, *40*, 6572.
141. Lane, T. J.; Fletcher, W. R.; Gormally, M. V.; Johal, M. S. *Langmuir* **2008**, *24*, 10633.

142. Swint, A. L.; Bohn, P. W. *Appl. Phys. Lett.* **2004**, *84*, 61.
143. Nuesch, F.; Rothberg, L. J.; Forsythe, E. W.; Le, Q. T.; Gao, Y. L. *Appl. Phys. Lett.* **1999**, *74*, 880.
144. Yan, D. P.; Lu, J.; Wei, M.; Han, J. B.; Ma, J.; Li, F.; Evans, D. G.; Duan, X. *Angew. Chem. Int. Ed.* **2009**, *48*, 3073.
145. Szekeres, M.; Szechenyi, A.; Stepan, K.; Haraszti, T.; Dekany, I. *Colloid. Polym. Sci.* **2005**, *283*, 937.
146. Chen, X.; Lei, Y.; Yang, W. S. *Chem. Lett.* **2008**, *37*, 1050.
147. Altuntasoglu, O.; Unal, U.; Ida, S.; Goto, M.; Matsumoto, Y. *J. Solid State Chem.* **2008**, *181*, 3257.
148. Bergstedt, T. S. Doctoral Dissertation, University of Florida, 1999.
149. Hammond, G. S.; Turro, N. J.; Wyatt, P.; Deboer, C. D. *J. Am. Chem. Soc.* **1964**, *86*, 2532.
150. Mizuno, K.; Sugita, H.; Hirai, T.; Maeda, H. *Chem. Lett.* **2000**, 1144.
151. Haneline, M. R.; Tsunoda, M.; Gabbai, F. P. *J. Am. Chem. Soc.* **2002**, *124*, 3737.
152. Saltiel, J.; Hammond, G. S. *J. Am. Chem. Soc.* **1963**, *85*, 2515.
153. Ikezawa, H.; Kutal, C.; Yasufuku, K.; Yamazaki, H. *J. Am. Chem. Soc.* **1986**, *108*, 1589.
154. Klima, R. F.; Gudmundsdottir, A. D. *J. Photochem. Photobiol. A-Chem.* **2004**, *162*, 239.
155. Nielsen, B. R.; Jorgensen, K.; Skibsted, L. H. *J. Photochem. Photobiol. A-Chem.* **1998**, *112*, 127.
156. Mizuno, K.; Ichinose, N.; Otsuji, Y.; Caldwell, R. A. *J. Am. Chem. Soc.* **1985**, *107*, 5797.
157. Barwise, A. J. G.; Gorman, A. A.; Leyland, R. L.; Smith, P. G.; Rodgers, M. A. J. *J. Am. Chem. Soc.* **1978**, *100*, 1814.
158. Ramamurthy, V.; Eaton, D. F.; Caspar, J. V. *Acc. Chem. Res.* **1992**, *25*, 299.
159. Omary, M. A.; Elbjeirami, O.; Gamage, C. S. P.; Sherman, K. M.; Dias, H. V. R. *Inorg. Chem.* **2009**, *48*, 1784.
160. Luhman, W. A.; Holmes, R. J. *Appl. Phys. Lett.* **2009**, *94*, 153304.

161. Adachi, C.; Kwong, R. C.; Djurovich, P.; Adamovich, V.; Baldo, M. A.; Thompson, M. E.; Forrest, S. R. *Appl. Phys. Lett.* **2001**, *79*, 2082.
162. Goushi, K.; Kwong, R.; Brown, J. J.; Sasabe, H.; Adachi, C. *J. Appl. Phys.* **2004**, *95*, 7798.
163. Tani, K.; Fujii, H.; Mao, L.; Sakurai, H.; Hirao, T. *Bull. Chem. Soc. Jpn.* **2007**, *80*, 783.
164. Chen, H. Y.; Yang, C. H.; Chi, Y.; Cheng, Y. M.; Yeh, Y. S.; Chou, P. T.; Hsieh, H. Y.; Liu, C. S.; Peng, S. M.; Lee, G. H. *Can. J. Chem.* **2006**, *84*, 309.
165. Lamansky, S.; Djurovich, P.; Murphy, D.; Abdel-Razzaq, F.; Kwong, R.; Tsyba, I.; Bortz, M.; Mui, B.; Bau, R.; Thompson, M. E. *Inorg. Chem.* **2001**, *40*, 1704.
166. Ohsawa, Y.; Sprouse, S.; King, K. A.; Dearmond, M. K.; Hanck, K. W.; Watts, R. J. *J. Phys. Chem.* **1987**, *91*, 1047.
167. Sprouse, S.; King, K. A.; Spellane, P. J.; Watts, R. J. *J. Am. Chem. Soc.* **1984**, *106*, 6647.
168. Seybold, P. G.; Gouterma, M.; Callis, J. *Photochem. Photobiol.* **1969**, *9*, 229.
169. Velapoldi, R. A.; Tonnesen, H. H. *J. Fluorescence* **2004**, *14*, 465.
170. Chen, L. H.; McBranch, D. W.; Wang, H. L.; Helgeson, R.; Wudl, F.; Whitten, D. G. *Proc. Natl. Acad. Sci. U. S. A.* **1999**, *96*, 12287.
171. Walters, K. A.; Ley, K. D.; Schanze, K. S. *Chem. Commun.* **1998**, 1115.
172. Wang, Y. S.; Schanze, K. S. *Chem. Phys.* **1993**, *176*, 305.
173. Farely, R. Ph.D. Dissertation, University of Florida, 2007.

BIOGRAPHICAL SKETCH

Jarrett H. Vella, Jr. was born in Beaufort, South Carolina and grew up in Charleston, South Carolina. In May of 2005, he graduated *magna cum laude* from the College of Charleston with a B.S. in chemistry. While at the College, he worked with Professor Charles. F. Beam studying multiple anion condensations. During this time, his interest in organic chemistry began to develop. Opting to attend the University of Florida for his graduate studies, Jarrett decided to obtain his Ph.D. in organic chemistry with Professor Kirk S. Schanze and eventually concentrated on physical organic chemistry.